

Sustainable Civil Infrastructures

Wynand JvdM Steyn
Zhixin Wang
Glynn Holleran *Editors*

Transportation Infrastructure Engineering, Materials, Behavior and Performance

Proceedings of the 6th GeoChina
International Conference on Civil &
Transportation Infrastructures: From
Engineering to Smart & Green Life Cycle
Solutions – Nanchang, China, 2021



 Springer

Sustainable Civil Infrastructures

Editor-in-Chief

Hany Farouk Shehata, SSIGE, Soil-Interaction Group in Egypt SSIGE, Cairo, Egypt

Advisory Editors

Khalid M. ElZahaby, Housing and Building National Research Center, Giza, Egypt

Dar Hao Chen, Austin, TX, USA

Sustainable Civil Infrastructures (SUCI) is a series of peer-reviewed books and proceedings based on the best studies on emerging research from all fields related to sustainable infrastructures and aiming at improving our well-being and day-to-day lives. The infrastructures we are building today will shape our lives tomorrow. The complex and diverse nature of the impacts due to weather extremes on transportation and civil infrastructures can be seen in our roadways, bridges, and buildings. Extreme summer temperatures, droughts, flash floods, and rising numbers of freeze-thaw cycles pose challenges for civil infrastructure and can endanger public safety. We constantly hear how civil infrastructures need constant attention, preservation, and upgrading. Such improvements and developments would obviously benefit from our desired book series that provide sustainable engineering materials and designs. The economic impact is huge and much research has been conducted worldwide. The future holds many opportunities, not only for researchers in a given country, but also for the worldwide field engineers who apply and implement these technologies. We believe that no approach can succeed if it does not unite the efforts of various engineering disciplines from all over the world under one umbrella to offer a beacon of modern solutions to the global infrastructure. Experts from the various engineering disciplines around the globe will participate in this series, including: Geotechnical, Geological, Geoscience, Petroleum, Structural, Transportation, Bridge, Infrastructure, Energy, Architectural, Chemical and Materials, and other related Engineering disciplines.

**SUCI series is now indexed in SCOPUS
and EI Compendex.**

More information about this series at <http://www.springer.com/series/15140>


Wynand JvdM Steyn · Zhixin Wang ·
Glynn Holleran
Editors

Transportation Infrastructure Engineering, Materials, Behavior and Performance

Proceedings of the 6th GeoChina International
Conference on Civil & Transportation
Infrastructures: From Engineering
to Smart & Green Life Cycle
Solutions – Nanchang, China, 2021

 Springer

Editors

Wynand JvdM Steyn 
Civil Engineering
University of Pretoria
Pretoria, Gauteng, South Africa

Zhixin Wang
Hainan Province Hydrogeological
Engineering Geological Survey Institute
Haikou, China

Glynn Holleran
University Of Auckland
Auckland, New Zealand

ISSN 2366-3405

Sustainable Civil Infrastructures

ISBN 978-3-030-79856-7

<https://doi.org/10.1007/978-3-030-79857-4>

ISSN 2366-3413 (electronic)

ISBN 978-3-030-79857-4 (eBook)

© The Editor(s) (if applicable) and The Author(s), under exclusive license
to Springer Nature Switzerland AG 2021

This work is subject to copyright. All rights are solely and exclusively licensed by the Publisher, whether the whole or part of the material is concerned, specifically the rights of translation, reprinting, reuse of illustrations, recitation, broadcasting, reproduction on microfilms or in any other physical way, and transmission or information storage and retrieval, electronic adaptation, computer software, or by similar or dissimilar methodology now known or hereafter developed.

The use of general descriptive names, registered names, trademarks, service marks, etc. in this publication does not imply, even in the absence of a specific statement, that such names are exempt from the relevant protective laws and regulations and therefore free for general use.

The publisher, the authors and the editors are safe to assume that the advice and information in this book are believed to be true and accurate at the date of publication. Neither the publisher nor the authors or the editors give a warranty, expressed or implied, with respect to the material contained herein or for any errors or omissions that may have been made. The publisher remains neutral with regard to jurisdictional claims in published maps and institutional affiliations.

This Springer imprint is published by the registered company Springer Nature Switzerland AG
The registered company address is: Gewerbestrasse 11, 6330 Cham, Switzerland

Introduction

This volume contains 13 papers that were accepted and presented at the GeoChina International Conference 2021 on Civil & Transportation Infrastructures: From Engineering to Smart & Green Life Cycle Solutions, held in Nanchang, China, September 18–19, 2021. It contains research data, discussions and conclusions focusing on pavement materials and engineering. Topics include issues related to general road construction, bituminous material and granular material reuse and improvements, and rail ballast stabilization. As society needs to travel to engage in productive and effective commerce, social, educational and related activities, the efficiency of travel needs to be improved. This is founded on an operational transport infrastructure system that is well designed, engineered, constructed and maintained. This volume intends to share some of the latest innovations and thoughts in the areas of pavement infrastructure materials, behavior and performance. Access to this volume should enable the reader to gain an understanding of such novel information that should support improvements in the provision of an effective road transportation system for the benefit of the greater society served by the road network.

Contents

Conservation Planning of Road Construction Raw Materials - Satara a Case Study	1
Anand B. Tapase, Sabir S. Sayyed, Nagendra Patil, Digvijay Kadam, Ajay Shelar, and Ravindra P. Patil	
Critical Pavement Response Analysis Under Overloading for Design of Low Volume Rural Roads	25
Omkar D. Patil, Piyush G. Chandak, Anand B. Tapase, Ravindra P. Patil, and Nanasaheb E. Patil	
Impulse Compaction	41
Bißmann Michael	
A Preliminary Laboratory Study of Fatigue Performance of Geogrid-Reinforced Asphalt Beam	67
Tom Darzins, Hangyu Qiu, and Jianfeng Xue	
Low Temperature Crack Resistance of Recycled Asphalt Mixture with Waste Frying Oil Based on Semi-circular Bending Test	78
Yingbiao Wu, Jinjin Shi, Yu Zhang, and Jinyan Liu	
Viability Assessment of the Use of Ground Tire Rubber (GTR) as a Modifier in Asphalt Binders	89
Zahid Hossain, Biswajit Bairgi, Musharraf Zaman, and Edgar O’Rear	
Role of Graphene Oxide Nanosheet on Mixing and Compacting Temperature of Bitumen	110
Hillol Chakravarty, Sanjeev Sinha, Pramanand Kumar, and Subrata Das	
Performance Evaluation of Fiber-Reinforced Expansive Subgrade Soil Stabilized with Alkali Activated Binder, Lime, and Cement: A Comparative Study	118
Mazhar Syed, Anasua GuhaRay, and Ankit Garg	

Assessing a Sand Clay Liner Material for Protecting Highways and Road Shoulders	140
Muawia Dafalla, Abdullah Shaker, and Abdul Naser Abdul Ghani	
The Thermo-mechanical Behaviour of Clay in Different Stress and Temperature Paths	150
Kuanjun Wang, Zhigang Shan, Kanmin Shen, Mingyuan Wang, Wenbo Du, and Boyu Mao	
Assessment of the Pavement Subgrade Using Different In-situ Testing Methods	166
Kasun Wimalasena, Chaminda Gallage, Jianfeng Xue, and Jeffry Lee	
Investigation of the Effect of Compaction Density on the Deformation Characteristics of Type 2.3 Granular Material	176
C. P. G. Jayalath and Chaminda Gallage	
Investigation on the Performance of Railway Ballast Track Stabilized by Cement Asphalt Mortar	187
Tri Ho Minh Le, Seong-Hyeok Lee, Dae-Wook Park, and Jung-Woo Seo	
Author Index	199

About the Editors

Prof. Wynand JvdM Steyn is Head of Department, Professor of the Department of Civil Engineering and Chair of the School of Engineering at the University of Pretoria. He is a professionally registered pavement engineer with a research interest in vehicle–pavement interaction, accelerated pavement testing, pavement engineering, pavement materials, civiltronics and instrumentation. He completed both his undergraduate and graduate studies at the University of Pretoria, South Africa. He has authored, co-authored and edited 41 journal papers, 21 chapters (author/co-author/editor) and 109 conference papers. He is Associate Editor of the International Journal for Pavement Engineering and the International Journal of Pavement Research and Technology, and has a B3 National Research Foundation (NRF) rating. He is Fellow of the South African Institution of Civil Engineers, Fellow of the South African Academy of Engineering (SAAE) and Adjunct Professor at the Chang’an University in Xian and the Shandong Jianzhu University in Jinan, China.

Dr. Zhixin Wang Ph.D., PE is Senior Engineer of Hainan Province Hydrogeological Engineering Geological Survey Institute. He is also Member of National First-Class Construction Engineers in construction engineering and Member of Registered Civil Engineers in the geotechnical field. He engages mainly in geotechnical engineering survey design and construction, geological disaster assessment and construction, underground engineering, marine geotechnical engineering, water and soil conservation and other engineering and research work. He has supervised and led over five National Natural Science Foundation and Provincial Natural Science Foundation projects, as well as more than ten provincial key engineering projects. He has published more than ten papers.

Glynn Holleran is Research Fellow at the University of Auckland in the Civil and Environmental Engineering Department. He is Managing Director of Advanced Asphalt Technologies, New Zealand, Registered Engineer of Engineering New Zealand, Chartered Chemist of the Royal Australian Chemical Institute and American Chemical Society. He is Life Member of the association of Asphalt

Pavement Technologists USA. He has worked in materials science and engineering since 1977 in all continents, including Eastern Europe, Asia, China, Middle East, Africa, North America, South America and Australasia, and he has many published journal and conference papers. His specialty is polymer chemistry and rheology and performance asphalt mix design, pavement design, bitumen chemistry (former bitumen consultant to Mobil oil international) and refining. He has been associated with FHWA projects in the USA and government projects in New Zealand. He is currently working on an MBIE government project on electric vehicle charging. Current interests are pavement preservation and toll roads in India and work with Texas A&M in Qatar. He is a reviewer for several ASCE and other international journals. He has had several patents with Mobil Oil, and a current patent in polymer science in India is under review.



Conservation Planning of Road Construction Raw Materials - Satara a Case Study

Anand B. Tapase¹✉, Sabir S. Sayyed², Nagendra Patil¹, Digvijay Kadam¹,
Ajay Shelar¹, and Ravindra P. Patil³

¹ Department of Civil Engineering, Rayat Shikshan Sanstha's, Karmaveer Bhaurao Patil
College of Engineering, Satara, India

{nagendra.patil, digvijay.kadam, ajay.shelar}@kbpcoes.edu.in

² Visvesvaraya Technological University, Belagavi, India

³ Jain AGMIT, Jamkhandi, India

Abstract. Due to uneven climatic and overloading conditions, reducing pavement life is the major area in front of researchers. Several steps have already been taken to extend the life of the pavement and improve the design of bituminous mixture which may be costly or may not suitable for every area due to variation in the number of parameters. Other part leads the researcher to think about the exhausting conventional materials and waste disposal problems which are gradually becoming a challenge for sustainability. The present experimental and analytical investigation proposes a cost-effective and eco-friendly approach towards sustainable construction of road network and to mitigate the early deterioration of roads. The investigation discusses the experimental and analytical investigation of the use of different waste materials like RAP and waste plastic etc. in different layers of flexible pavement. The results reveal that the waste materials having somehow similar properties to that with conventional materials can be used partially in place of conventional materials. Application of optimum use of waste materials together with analytical investigation satisfying the minimum criteria's allow to use waste materials in different layers of pavement. The further investigation about the local field condition present in the study area together with the outcome of analytical and experimental investigation supports to propose design charts for different subgrade soil conditions. The use of waste material in road construction not only mitigate with waste disposal problem but also shows improvements in governing parameters.

Keywords: Ecofriendly · Cost-effective · Sustainable

1 Introduction

Due to tremendous growth in various sectors including industrial sectors in developing countries like India are producing various types of wastes to a very large extent in day to day life which causes the severe problem of their treatment and disposal. Many developed countries like United States, UK, etc., had made advancements in the recycling of waste materials and developed guidelines for using these waste materials like Reclaimed

asphalt pavement (RAP), waste plastic (WP) etc. in different layers of pavement. But the developing country like India is not that much aware to use these different waste due to lack of investigation for their local environment [16].

Due to disposal problem of these non-degradable types of waste creating very severe effect on environment and creates a need to find the solution to deal with this critical issue. Most of developed nations has already done remarkable research work about the use of the different non-degradable wastes in different construction amenities while the under developing countries like India has not established the advanced methodology and guidelines about the use of this waste materials. As India is developing country to boost the economic growth of country the up gradation of infrastructure facilities has given prime importance in its few of the recent five year development plans. Around 90% of pavements constructed in India are of flexible pavement structures categorized in different classes like national highways, state highways and rural roads. Due to rapid increase in the automobile sector around 250 million registered vehicles has already registered in last three years, Also two wheeler production sector puts the country on number one position across the globe in the year 2019 onwards. This increased traffic intensity on roads are creating very serious issue regarding traffic jams, delay in traffic movements which ultimately leading to more number of accidents with continue increment in number of injured persons and fatalities in last several years. To deal with this problem India is adding 40 Kms of newly constructed pavements every day to its existing road networks [23]. The excavation carried out for the construction of new roads or for expansion of existing road network produces huge amount of Reclaimed asphalt pavement (RAP) material throughout the country and leftovers or landfilled aside of these newly constructed pavements as it is for many years. During the production of Hot Mix Asphalt (HMA) for heating and drying of 1 ton of aggregates around 6 to 7 L of fuel is required while lakh of tons of aggregates are produced every day for the construction of new pavements in India. Also vast amount of harmful gases are emitted during heating of binders and aggregates for HMA production. The scarcity of good quality aggregates near the construction site necessitates the hauling of aggregates from quarry sites causes the emission due to hauling vehicles which is also makes the pavement construction uneconomical. So by the use of alternative materials for aggregates and binders the extracted waste materials like RAP, waste plastic (WP) etc. can save the environment and also economy can be achieved [12].

To address this issue together with an eco-friendly and environmental approach, the present study focuses to check the suitability of various locally available waste materials that can be used in pavement construction. (e.g. aggregates, RAP binder, WP, etc.). The objective of the study is to examine the effect of RAP aggregates and WP modified bitumen together by varying its proportions to know their optimum combination to satisfy pavement performance in terms of fatigue and rutting life of pavement experimentally and analytically. The stretch of National Highway 4 (NH-4 Pune Bengaluru) passing across Satara district is getting deteriorated at several location much earlier than its design life and requires maintenance within few years after opening to traffic Fig. 2, 3. The present study focusses to address this issue with sustainable development approach by the use of waste materials produced in the vicinity of project area. Pavement renovation with the use of locally available non degradable waste materials by checking its suitability

from both field and laboratory assessment is the thrust area where most of developments are taking place in recent years. The use of waste plastic in road construction saves the environment by reducing the amount of emissions produced at the time of preparation of bituminous mixes [31].

2 Literature Survey

Fazanah et al. [15] uses the natural and recycled aggregates in different bituminous mixes to study different physical and mechanical properties, the study finds that the mix with higher proportion of recycled aggregates improves the workability, compaction and deformation resistance compared to mix prepared with natural aggregates. Helwany et al. [22] recommended the need of a finite element model to assess the performance of pavement under application of variable load when different materials are used in different layers of pavement. Chandak et al. [10] reported the necessity of such a finite element model which can assess the performance of pavement by considering the combined effect of various parameters like tyre pressure, loading, temperature conditions etc. for their local field conditions. Ripunjoy et al. [28] et al. proposed that rutting distress in pavement progressed by fatigue distress in its early stage of their commencement but later remains constant after originating the fatigue cracking.

Tahan et al. [11] investigated the effect on bituminous mix prepared by replacing the aggregates by recycled aggregates from two sources i.e. demolished concrete from old structure and the other from recently casted concrete cubes. HMA with recycled aggregates from fresh concrete cubes showing better results for stress concentration, contact properties of aggregates and rutting values as compared to mix prepared with aggregates from old concrete structures. Farooq et al. [14] studied the different approaches for the use of RAP in WMA pavements to highlight its advantages, limitations with environmental and economic approach.

Ranadive et al. [27] recommended the usefulness of 2 D finite element analysis to assess the performance of pavement for the use of different material properties in different layers of pavement sections with varying thicknesses. Sabir et al. [29] informed the effectiveness of finite element method for optimum design of pavement section undergoing varying temperature gradient from top to bottom layer of pavement. The study illustrates that structural capacity reduces at high temperature for pavement constructed with soft bituminous mix, while the pavement experiences the cracking even at low temperature for hard bituminous mix. The effectiveness of analysis by Finite element method, for different waste materials to be used in different pavement layers are demonstrated by Sinha et al. [1]. R. Izaks et al. [26] concludes that bituminous mixtures with high percentage of RAP mixtures fulfills the performance specifications of pavement for local environmental conditions. S. L. Hake et al. [13] reported that use of plastic in bituminous mix up to 15% enhances the different required properties of the mix. Ankit et al. [2] proposed the improved guidelines for wet mix asphalt by the use of RAP and reclaimed asphalt shingles. The study reported that the use of RAP up to 70% offers acceptable outcome in terms of pavement performance. Pakhar et al. [25] reported that tropical countries like India where the mean temperature is exceeding 40 °C in several parts of country can achieve the economy in road construction by saving rupees 45,000 per kilometer by the use of plastic up to 10% in wearing course of pavement.

3 Field and Laboratory Investigation

3.1 Collection of Waste and Conservative Materials from the Study Area

The VG 30 bitumen binder with penetration grade value of 60/70 which is used as paving material for Bengaluru-Pune NH-4 project passing across Satara district is considered for the present work analysis. The natural aggregates derived from parental rock basalt which is available throughout the district of Satara is tested for various properties like durability, hardness, strength etc. to check their suitability as pavement construction material.

RAP aggregates were acquired from the demolished pavement stored aside NH-4 from four locations after its up gradation from 2 lane to 4 lane (Fig. 1). The corresponding traffic data about the project were extracted from the records of National Highway Authority of India (NHAI) and the codes issued by Indian Road Congress (IRC). Before the use of collected RAP samples in bituminous mix it undergoes the procedure same that as of natural aggregates i.e. crushing, screening and separating for same size to use as replacement to natural aggregates in the proportion of 50%, 75%, and 100%.

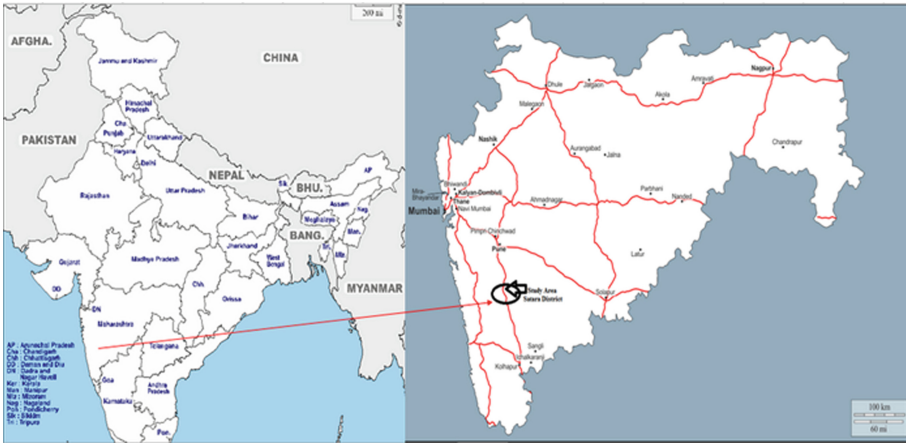


Fig. 1. Location map of study area

3.2 Experimental Setup and Laboratory Investigation

In the present investigation along with conventional materials like bitumen and aggregate, the effect of partial replacement of conventional materials by waste materials like WP and RAP aggregates is elaborated. The present work exploration was carried out on conservative materials like conventional aggregates and bitumen along with its replacement by different waste materials like RAP aggregates and WP is described. The results obtained from physical test carried out for the bitumen and aggregates according to the procedure as per the Indian and ASTM Standards [3–9] are presented in Table 1 and Table 2.



Fig. 2. Rutting failure on NH-4 Near Satara



Fig. 3. Fatigue failure on NH-4 Near Satara

Table 1. Conventional test properties of Bitumen

Test name	CB	CB + WP	Minimum requirements	Testing method [17, 19]	Standards [3, 5, 7, 8]
Elastic recovery, @ 25 °C,%	34	35	Min.35	IRC-SP 53:2010	ASTM-D6084
Ductility, @ 25 °C, mm	92	83	Min. 80	IS 1208: 1978	ASTM-D113
The softening point, °C	50	51	Min. 55	IS 1205: 1978	ASTM-D36
A penetration test, @25 °C, 100 g,5 s	65	40	Max.60	IS 1203: 1978	ASTM-D5

Table 2. Test results for aggregate

Test name	Conventional aggregate	RAP aggregates	MORT&H V th (Revision 6)	Reference [21]
Specific gravity	2.67	2.34	Min. 2.5	IS: 2386 (Part 3)
Los Angeles abrasion value	16.70%	20.40%	Max. 40%	IS: 2386 (Part 5)
Impact value	12.60%	16.90%	Max. 30%	IS: 2386 (Part 4)
Water absorption	1.58%	1.75%	Max. 2%	IS: 2386 (Part 3)
Crushing strength	16.70%	18.20%	Max. 30%	IS: 2386 (Part 4)
Flakiness	13%	10%	Max. 35%	IS: 2386 (Part 1)
Elongation	15%	13%	Max. 35%	IS: 2386 (Part 1)
Coating & Stripping of Bitumen aggregate mixture	Retained 98%	Retained 98%	Min. retained coating 90%	---

The hardness and consistency of conventional bitumen samples were tested by a penetration test conducted at 25 °C. The viscous transition of binders is evaluated after testing the samples by softening test as per the standards of ASTM D36 [5]. The ductile nature of binders to check its ability to form thin film around the surface of aggregates were tested by ductility test [3]. The test for Elastic recovery was conducted at 25 °C as per the guidelines of [8] ASTM D6084 (Table 3).

Table 3. Tensile strength ratio (%) [9]

Binder type	Avg. tensile strength (Conditioned sample)	Avg. tensile strength (Unconditioned sample)	TSR
VG 30	0.790	0.890	88.76%
C.B. + 2.5% WP	0.830	0.950	87.36%
C.B. + 5% WP	0.835	0.990	83%
C.B. + 7.5% WP	0.905	1.10	82.27%
C.B. + 10% WP	0.96	1.25	76.8%

To simulate the field conditions the detailed investigation is carried out on the procedure recommended for the Marshall Stability test as per ASTM D 1559 [4]. The gradations adopted for laboratory specimen mix preparation are taken as specified by the Ministry of Road Transport and Highways [21]. Here blending percentage for aggregate is taken as 20 mm size aggregate 25% of the total aggregate mix, 12.5 mm, 10 mm, 6 mm each 10%, and grit as 45% as per mix design prepared for Bituminous Layer (BL) of flexible pavement. Initially different percentages of bitumen content varying between

4.5% to 6.0% with an increment of 0.5% for each trial is taken for getting the optimum bitumen content for the conventional mix. In the detailed investigation, optimum bitumen content was evaluated from the control mix, followed by partial replacement of bitumen in various percentages of WP and RAP aggregates were mixed before partially replacing the conventional aggregates. The percentage of waste plastic varies between 2.5%, 5%, 7.5%, and 10% to replace conventional bitumen by its weight is trailed to find the optimum percentage of waste plastic that can be used in bituminous mix. To achieve more accurate results three samples were tested for each trailed percentage [20]. The specimens for Marshall Stability test were prepared by following gradation accepted, weighing, heating, mixing and finally placing in the mould as shown in Fig. 4. Tensile strength ratio of modified mix for varying binder content was determined by indirect tensile strength performed as per ASTM D 6931-12 [9]. Tensile strength ratio is one of the important test as it defines the moisture resistance of aggregate coating, as per the limits specified by code of practice [17, 18] the strength of dry and wet specimens should not be less than 225 kPa and 100 kPa respectively [6].

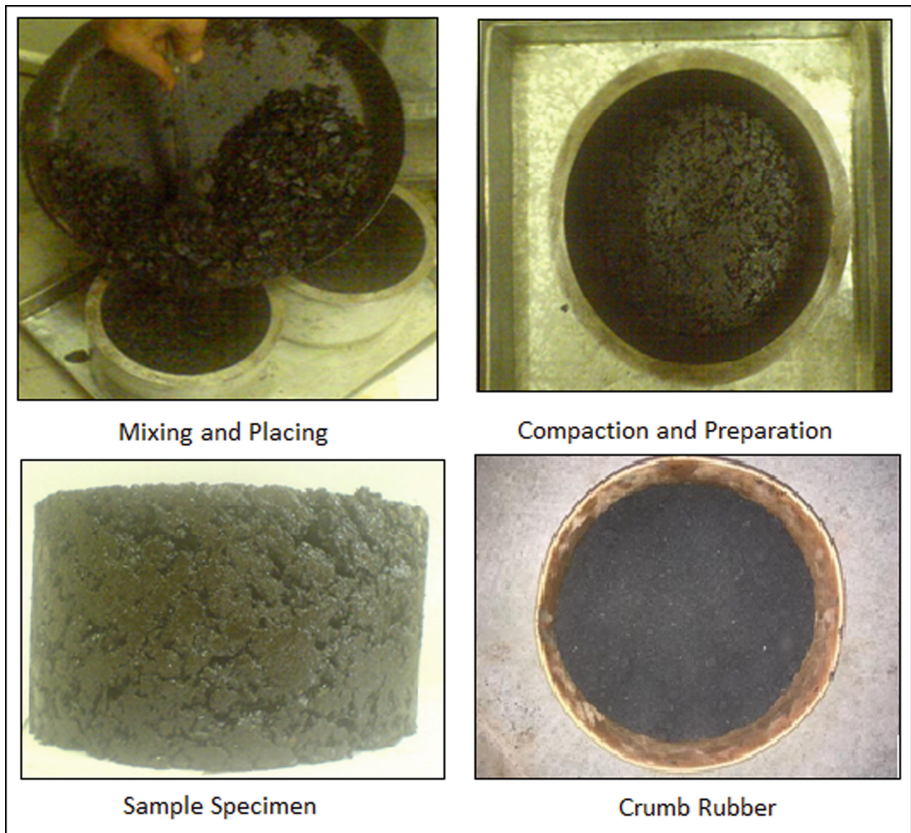


Fig. 4. Specimen preparation

4 Analytical Investigations

During the analytical investigation, the methodology adopted is in the line with respect to the consideration of various parameters and procedures suggested by different pavement design guidelines proposed by the Indian Roads Congress (IRC) and AASHTO. The present work is extended to study the use of available waste material (RAP and WP) for replacement of exhausting conventional materials by the analytical investigation. To get design charts for various subgrade conditions in Satara district from the selected cases and hypothetical sections two-dimensional axisymmetric finite element analysis is done using a program coded in FORTRAN. Figure 15 summarizes various finite element parameters including the idealization and hypothetical section and should be a reference throughout the paper. Fatigue cracking of pavement is caused due to the excessive horizontal tensile strain at the bottom of the bituminous layer and rutting undulations are due to the vertical compressive strain on top of the subgrade. The critical points are highlighted in Fig. 15 on which the critical parameters are evaluated for every assumed case for the study.

The work is an extension of earlier reported work wherein the methodology is validated with the reported case studies and closed-form solutions Tapase et al. [30]. The Idealization as shown in Fig. 15, formation, and solution for prevailing equations of the considered structure by a finite element model is prepared for assessment and evaluation of the design processes. The idealization and solution of two-dimensional analysis were carried out by considering four noded quadrilateral elements for a mesh consist of 880 quadrilateral elements and 958 nodes. The horizontal extent of the pavement is considered 3 times the pavement width which is around 1050 mm which denotes an indefinite horizontal extent (Fig. 15). The nodes on the centerline of the road along the loading line and vertical faces i.e. 1050 mm from the centerline are free to move in the axial direction while restrained the movement along the radial direction. The nodes lying at bottom of the subgrade are restricted for movement in both axial and radial directions.

The data collected for loading and type of subgrade soil for a particular highway stretch of NH-4 passing through the study area (Satara District), decides the minimum and maximum range of trial thicknesses for various pavement layers from available design codes in India. The bituminous layer (BL) which is composed of bituminous concrete (BC) and dense bituminous macadam (DBM) has depth variation between 125 mm to 200 mm for different combinations of traffic conditions and material properties for which design charts are proposed in different plates suggested by IRC 37-2012. The values of resilient modulus (E) were extracted from available design codes, which is an outcome of rigorous field and experimental tests carried out in various parts of the country. The upper layer of pavement which is known as Bituminous layer (BL) is varying in the range of 100 mm to 175 mm with an interval of 25 mm with a modulus value of $E_1 = 2000$ MPa, 1600 MPa, and 800 MPa for bituminous mix VG 30, modified bitumen and RAP in bituminous layer respectively. The layer next to BL is the base layer varying its thicknesses 100 mm, 150 mm and 200 mm with modulus value $E_2 = 800$ MPa for base treated with RAP. The thickness of sub base layer is kept constant at 250 mm with modulus value determined based on the type of subgrade soil based on the guidelines provided by code of practice IRC 37-2012 [30]. For the third combination i.e. modified bitumen with cemented sub base the modulus value for BL and base layer is

$E_1 = 1600$ MPa and $E_2 = 800$ MPa and the modulus of cemented sub base is considered as $E_3 = 600$ MPa for all the trailed cases under this combination. The variation for the depth of pavement layer remains same as that of earlier two combination.

The different values of the modulus of the granular layer are shown in Fig. 15. In the present study, a uniform tyre pressure of 0.575 MPa with a 40 KN wheel load by a single axle is applied as shown in Fig. 15. The design of pavement section for considered trials is checked for selected modified subgrade soil of $E_5 = 66$ MPa (8% C. B. R.) which is the minimum C.B.R. value has to be attained for any modified subgrade of 500mm thickness as per the condition stated in the design manual of flexible pavement in India [30].

The study can be useful to give useful design charts for varying combinations of depths and materials as per the field conditions of subgrade soil for the use of waste materials like RAP, WP etc. in BL of pavement. [24]. The present study considers various types of subgrade soils (good and poor) available in different parts of the Satara district which shows the extreme variation in modulus values ranging between 10 MPa to 80 MPa as reported by Piyush et al. [31]. Considering these vast variations in the types of subgrade soil's in the Satara district soils are categorized into five types silt (5 MPa), silty sand (25 MPa), sandy clay (45 MPa), clay (80 Mpa), and gravel (100 MPa). To design field-specific beneficial design charts it is essential to do the investigation such that which involves laboratory testing followed by an analytical approach.

5 Results and Discussion

The current investigative study deals with the experiential and analytical investigations of reclaimed asphalt pavement aggregates partially substituted to traditional aggregates and WP substituted to content of bitumen. From the obtained results of physical properties of all these materials as stated in Table 1 and Table 2, it is concluded that these chosen materials for examination are apt for pavement construction. From the initial examination as described in Table 1, it is observed that ignoring the minor differences in the physical properties of waste plastic, not much change is seen.

The experiential work was conducted on the RAP samples obtained from numerous sites, from which the optimal partial substitution of traditional aggregates with RAP is assessed by means of the Marshall Stability test. Analogously, the optimal use of WP is checked experientially and methodically displaying notifiable enhancements in the results. Marshall Stability (KN), percentage air voids, bulk density (gm/cc), flow value (mm), and percentage V.M.A are experientially assessed from conducted laboratory tests to obtain optimal bitumen content, optimal waste plastic mix, and optimal RAP aggregate mix. The attained outcomes are understood and showcased in graphical form. Figure 5 represents the graphical explanation of attained results displaying content of bitumen variation to the bulk density for WP mix in line with that of the controlled mix. The values of Bulk density vary from 2.23 gm/cc to 2.35 gm/cc. It is seen that 7.5% WP mix demonstrates acceptable results with respect to Marshall Stability (kN), bulk density (gm/cc), percentage air voids, flow value (mm), and percentage V.M.A in comparison with controlled mix of 5.50% content of bitumen for all trials as stated in (Fig. 5, 6, 7, 8 and 9). It is determined that the optimal content of bitumen is at 5.50% and

bitumen can be substituted by WP by 7.5%. Likewise, from Figs. 10, 11, 12, 13 and 14 it is stated that RAP aggregates demonstrate results which are inside the allowed limits even at 100.00% substitution; ultimately highlighting the advantages of using RAP as aggregate in construction of road (Figs. 22, 23, 26, 27 and 28).

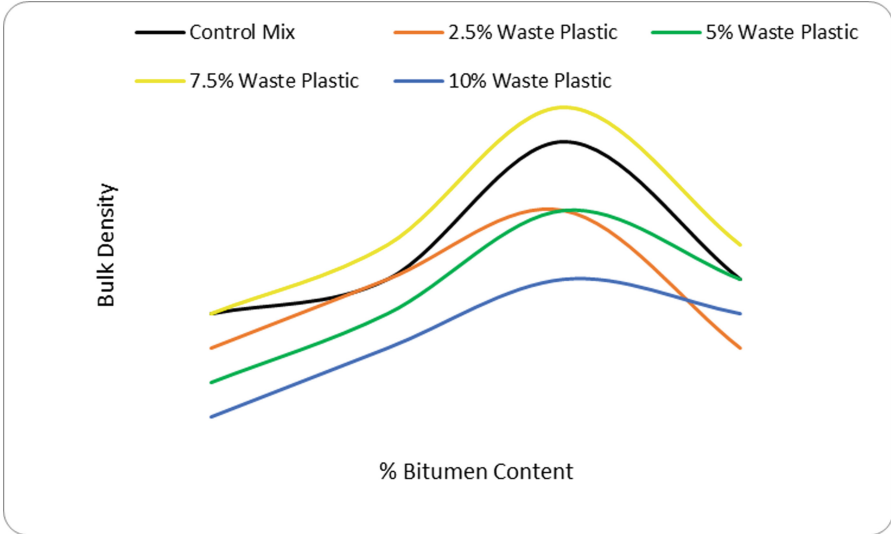


Fig. 5. Bulk density Vs. Percentage bitumen content for waste plastic mix

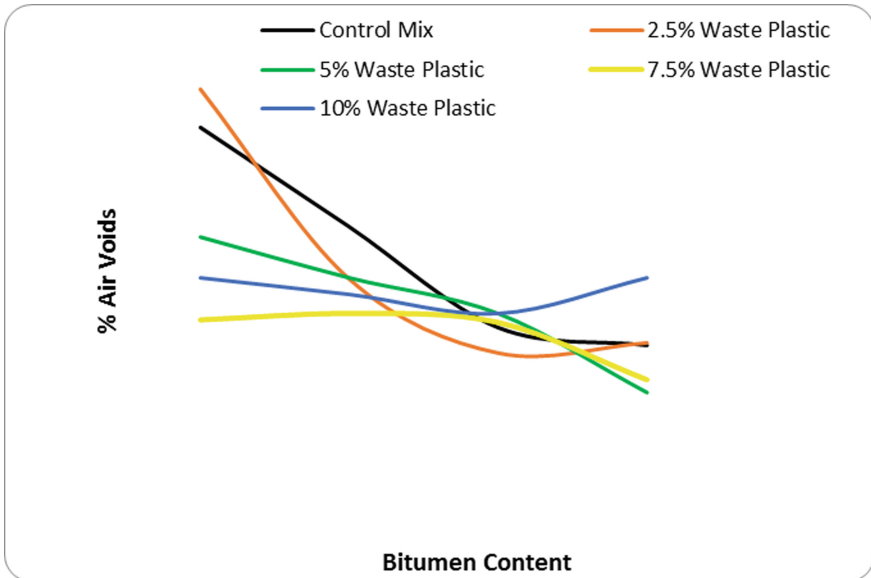


Fig. 6. % Air voids Vs. Percentage bitumen content for waste plastic mix

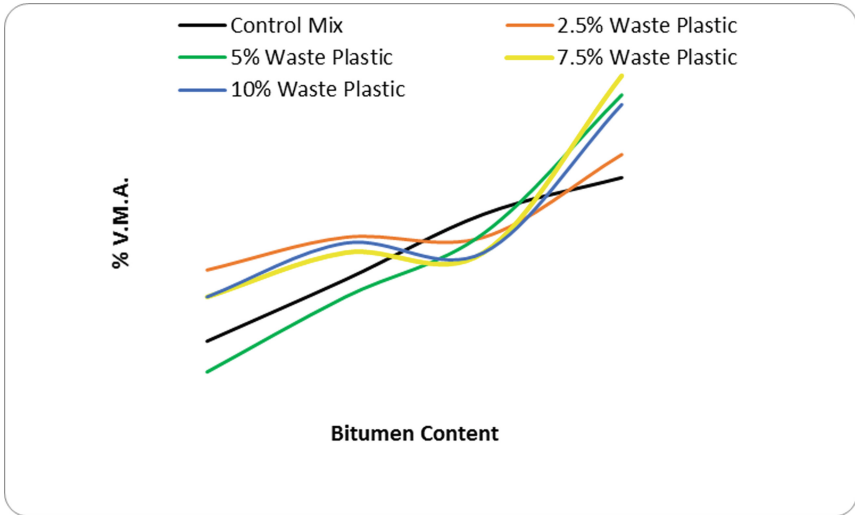


Fig. 7. % V.M.A. Vs. Percentage bitumen content for waste plastic mix

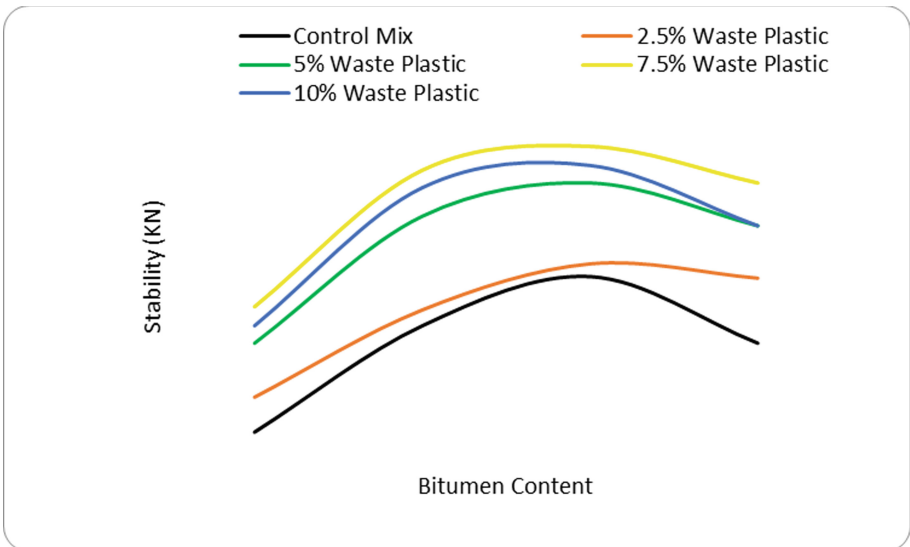


Fig. 8. Marshall stability (KN) Vs. Percentage bitumen content for waste plastic mix

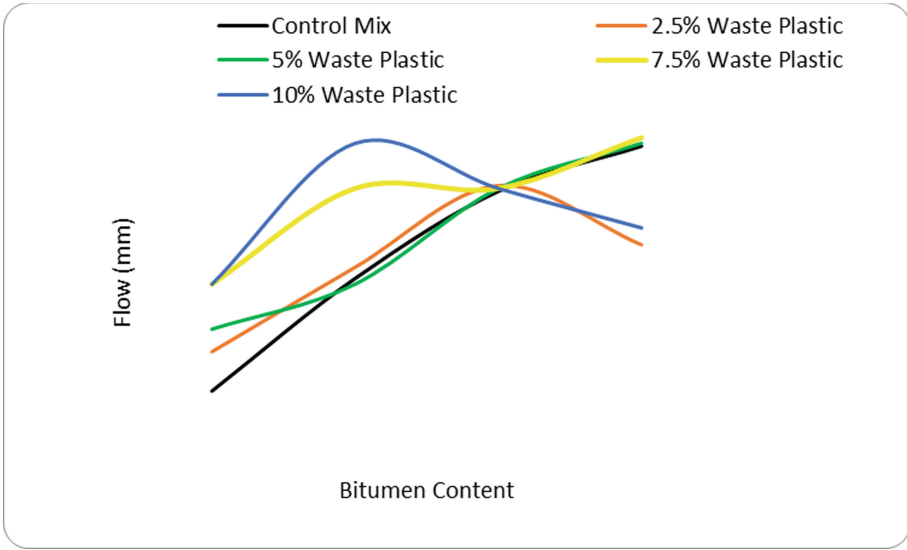


Fig. 9. Flow value (mm) Vs. Percentage bitumen content for waste plastic mix

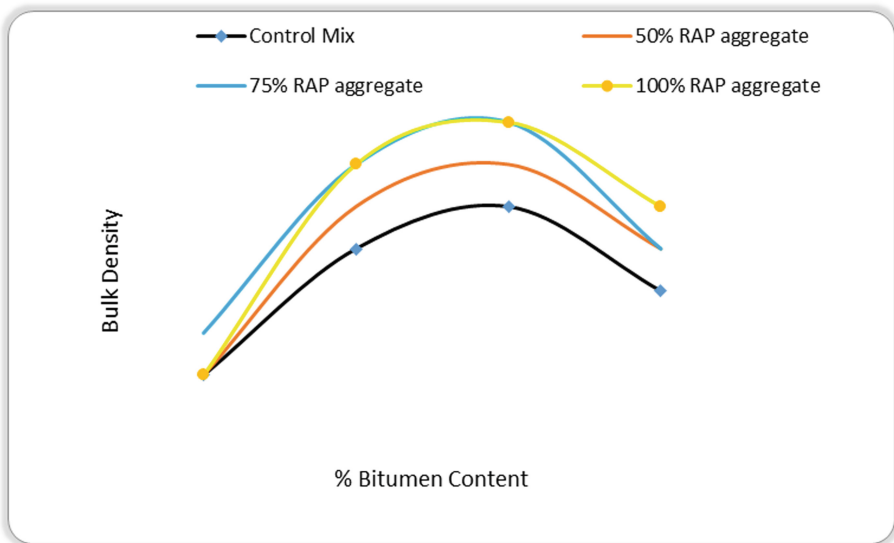


Fig. 10. Bulk density Vs. Percentage bitumen content for RAP aggregate

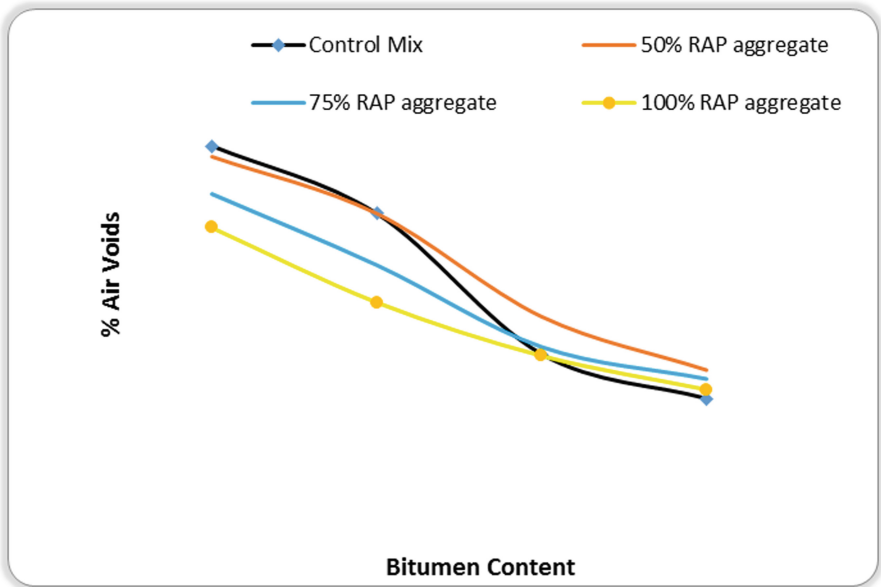


Fig. 11. % Air voids Vs. Percentage bitumen content for RAP aggregate

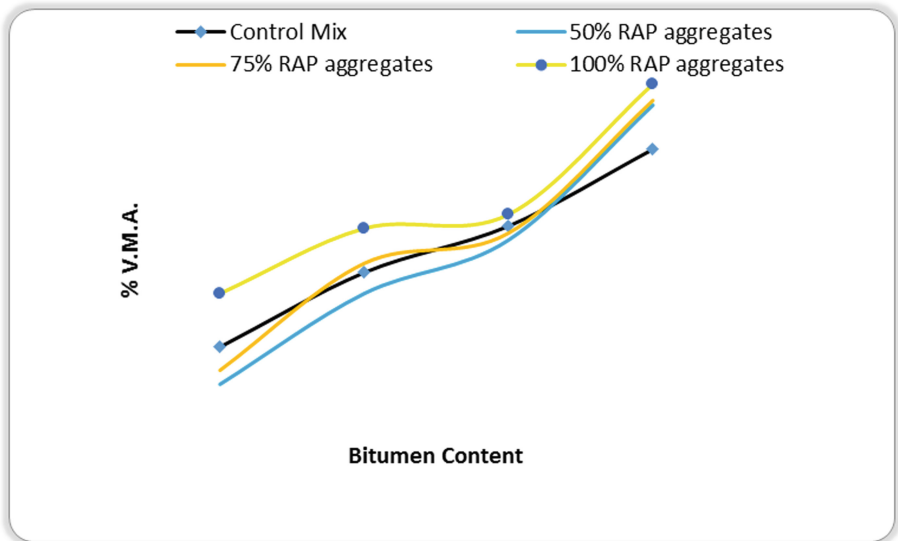


Fig. 12. % V.M.A. Vs. Percentage bitumen content for RAP aggregate

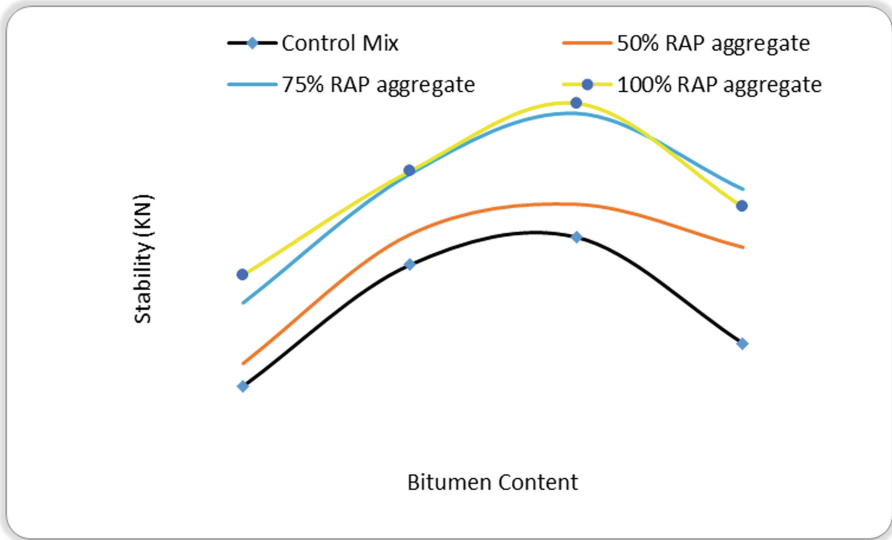


Fig. 13. Marshall stability (KN) Vs. Percentage bitumen content for RAP aggregate

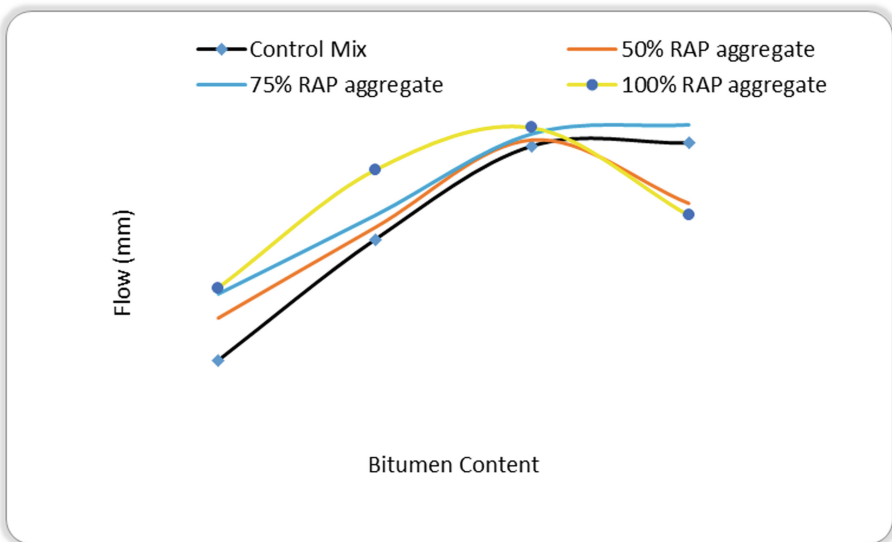


Fig. 14. Flow value (mm) Vs. Percentage bitumen content for RAP aggregate

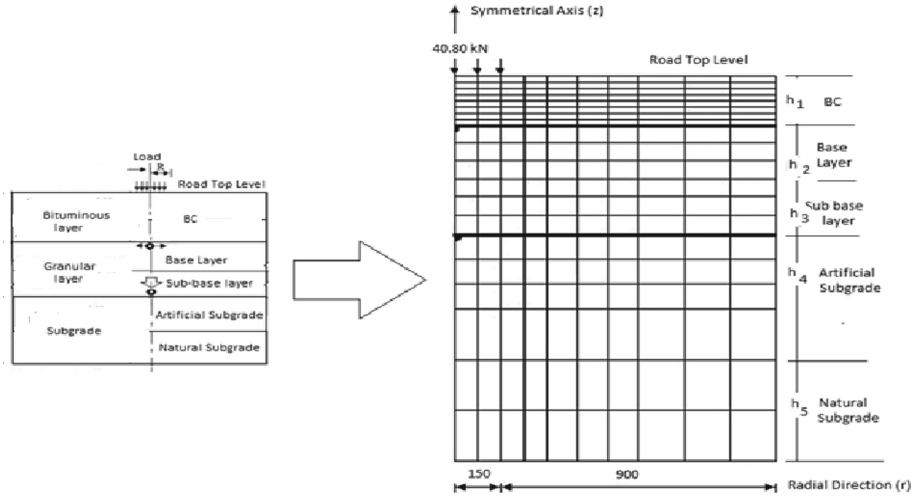


Fig.15. Pavement section and hypothetical idealization

To create design charts for numerous subgrade types in Satara district from the particular trials and theoretical sections; finite element analysis was performed by means of Fortran language. For the purpose of analytical study, the consequence of using WP mix and RAP aggregates on the critical factors namely, the horizontal tensile strains at the bottom of the bituminous layer (\mathcal{E}_t) and the vertical compressive strain at the top of the subgrade (\mathcal{E}_v) are calculated and construed by assuming 4 trial depths of BL in conjunction with 3 base layer depths (Figs. 16, 17, 18 and 19).

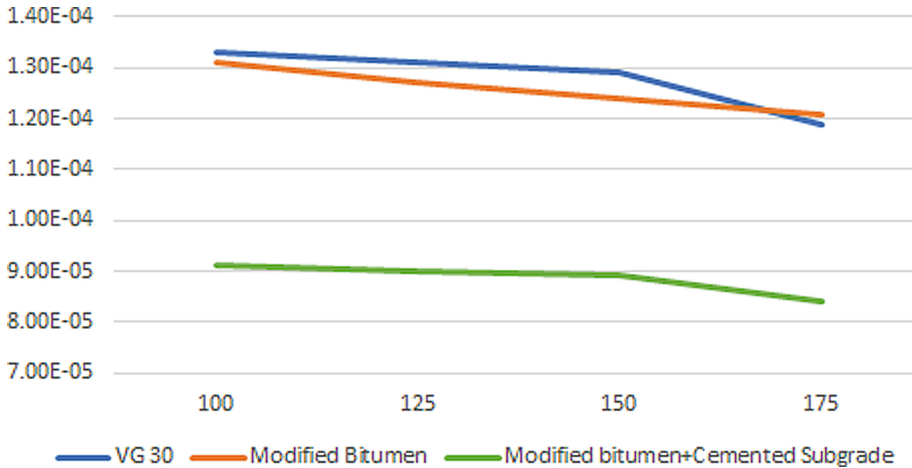


Fig. 16. The thickness of BL variation Vs. Horizontal tensile strain at bottom of BL

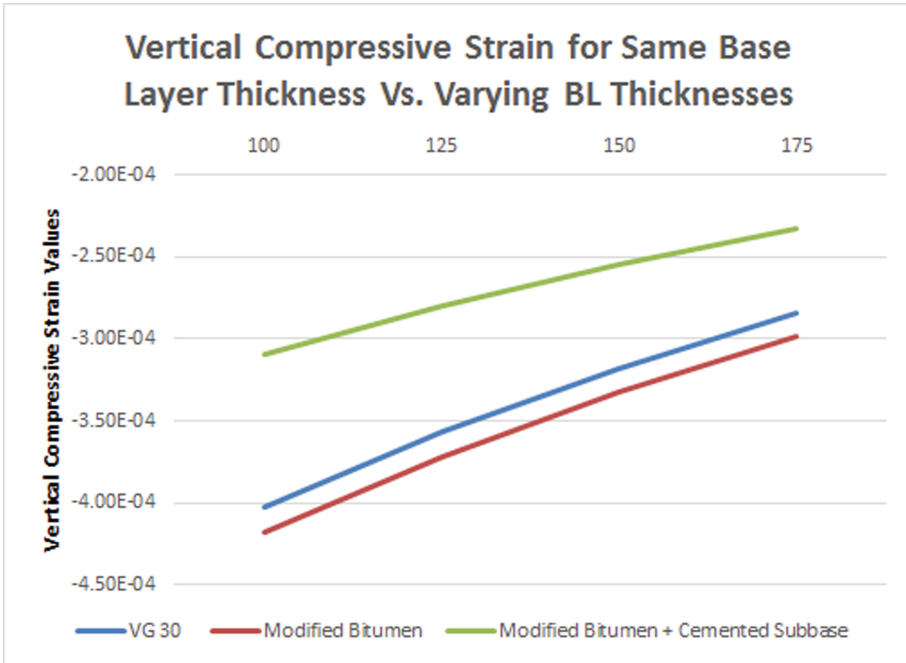


Fig. 17. Thickness of BL variation Vs. Vertical compressive strain at top of the subgrade

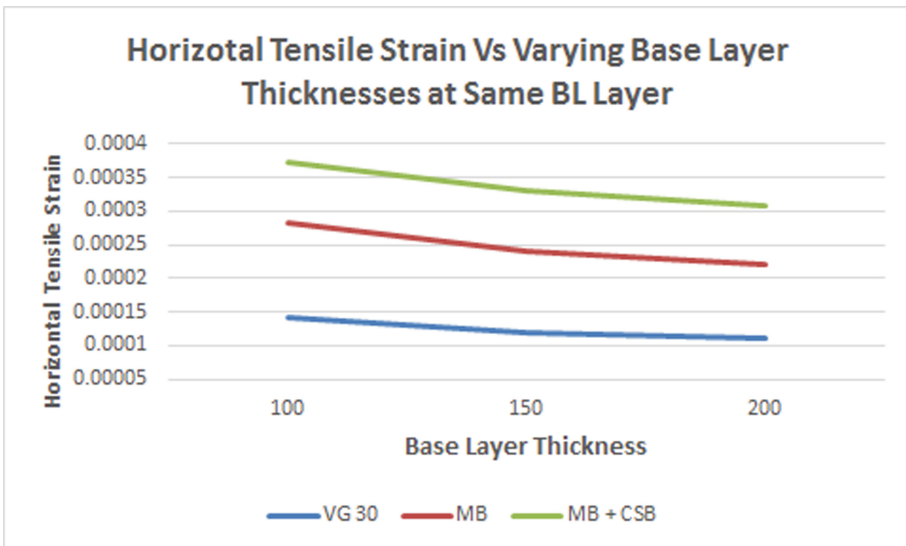


Fig. 18. Thickness of base layer variation Vs. Horizontal tensile strain at bottom of BL

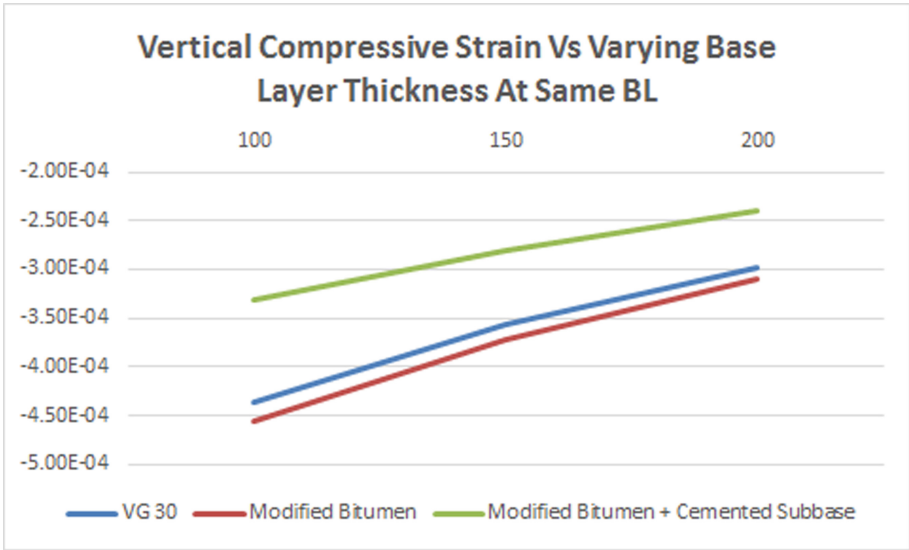


Fig. 19. Thickness of base layer variation Vs. Vertical compressive strain at top of the subgrade

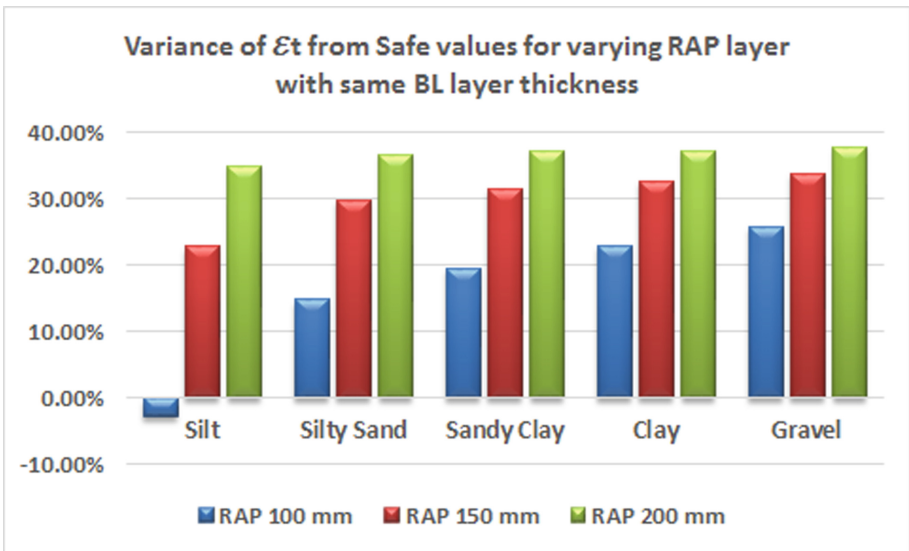


Fig. 20. Variance of ϵ_t from safe values for varying RAP layer with same BL layer thickness (VG 30)

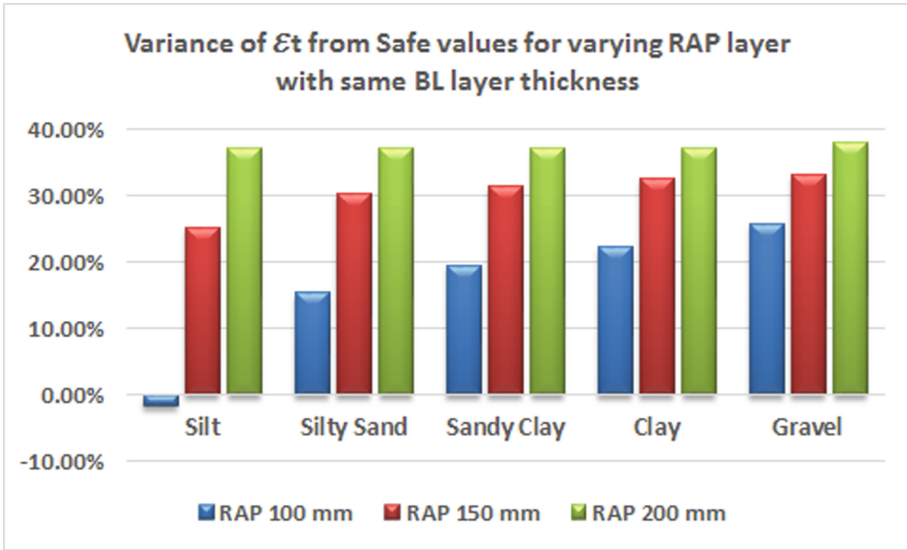


Fig. 21. Variance of ϵ_t from safe values for varying RAP layer with same BL layer thickness (Modified Bitumen)

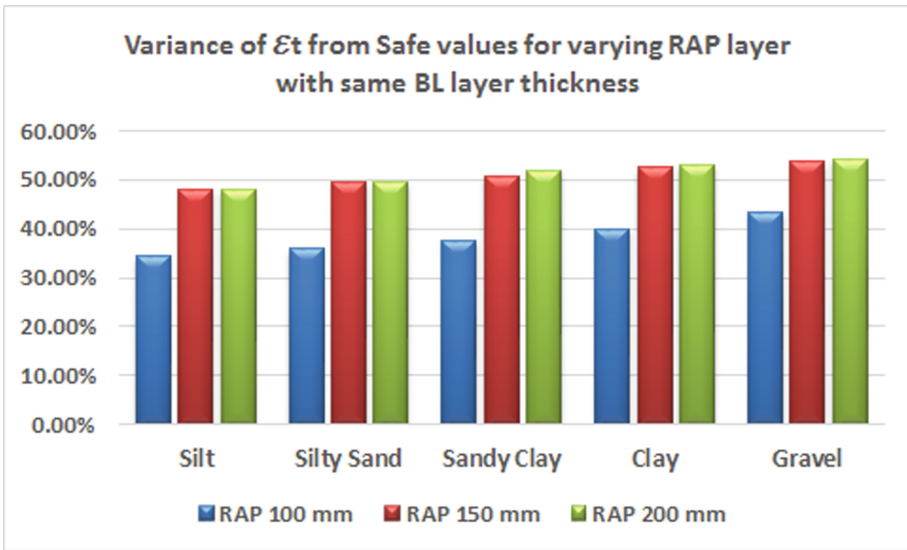


Fig. 22. Variance of ϵ_t from Safe values for varying RAP layer with same BL layer thickness (Modified Bitumen + Cemented sub base)

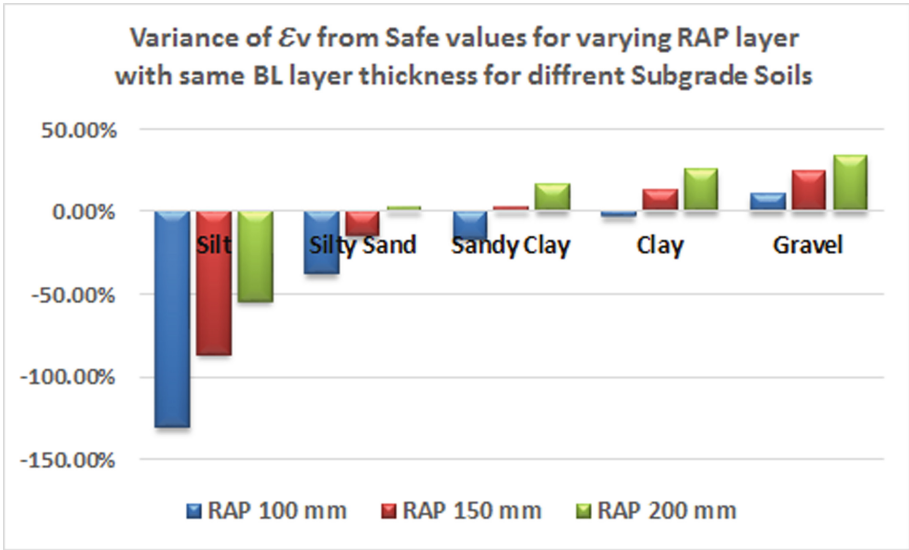


Fig. 23. Variance of ϵ_v from Safe values for varying RAP layer with same BL layer thickness (VG 30)

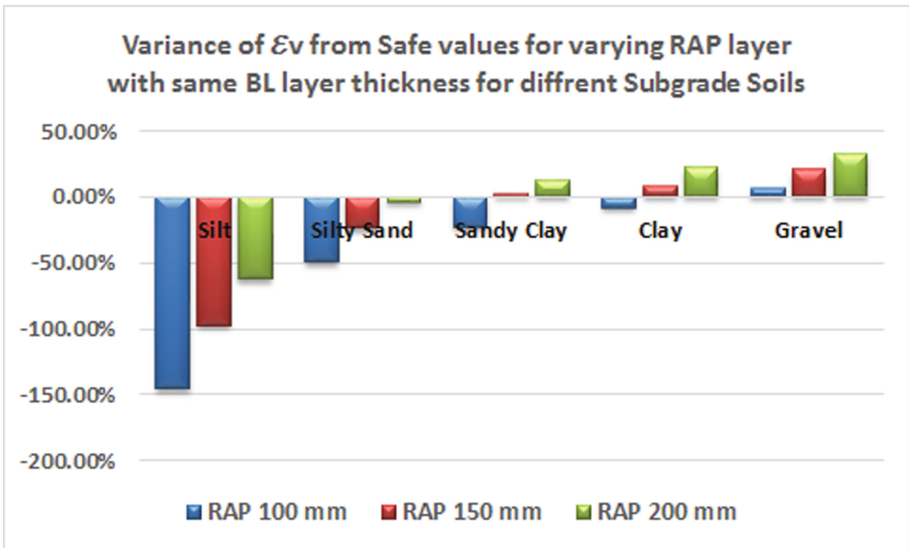


Fig. 24. Variance of ϵ_v from Safe values for varying RAP layer with same BL layer thickness (Modified Bitumen)

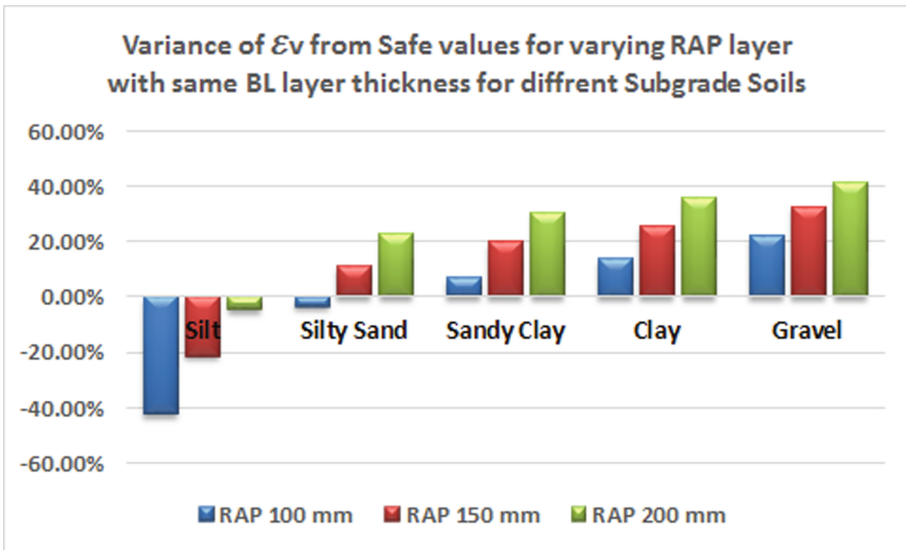


Fig. 25. Variance of ϵ_v from Safe values for varying RAP layer with same BL layer thickness (Modified Bitumen + Cemented sub base)

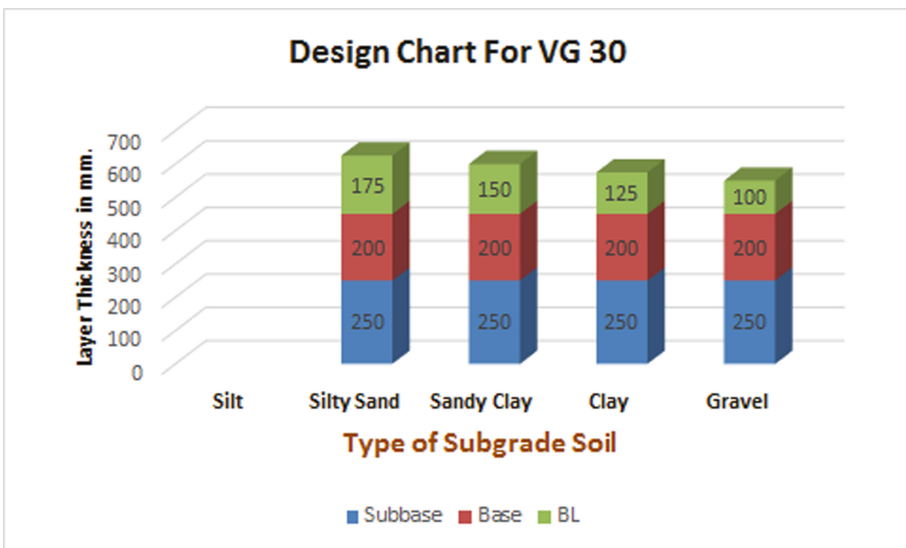


Fig. 26. Design chart for VG 30 Bitumen in BL

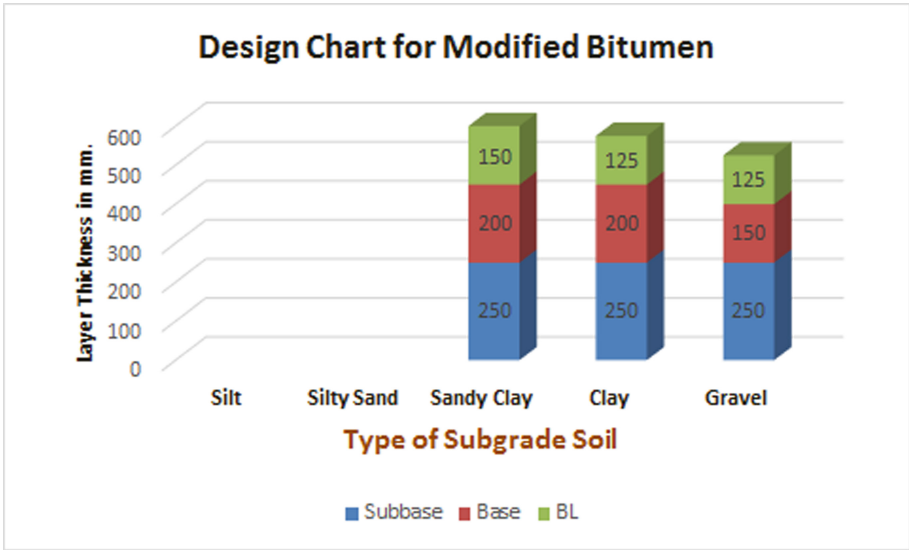


Fig. 27. Design chart for (RAP + WP) in BL

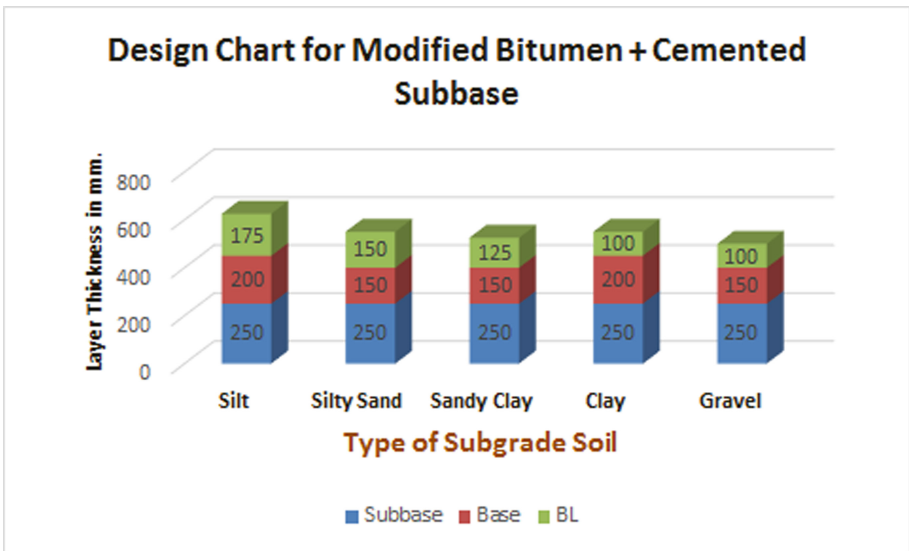


Fig. 28. Design chart for modified Bitumen + Cemented subbase in BL

The analysis for base layer with BM VG 30 highlighted that the horizontal tensile strain is within the allowed limit for fatigue criterion for same BL depth in conjunction with the base layer depths of 100mm, 150mm and 200mm (Fig. 20). Whereas the analysis for rutting criterion is not satisfying the values for the groupings of base layer depths for poor subgrade soils silt and silty sand (Fig. 21). Likewise, the analysis for modified

bitumen in conjunction with RAP in base layer displays that fatigue criterion values are well inside the safety values (Fig. 21) similarly the rutting criterion is not inside the safety values for the poor the subgrade soil silt, silty sand, sandy clay but on safer sides for good subgrade soils like clay and gravel. (Fig. 24). The analytical study performed for modified bitumen with cemented sub base for fatigue criterion are on the higher side than of safe values by about 50% and displays that rutting criteria also on safer side except the poor subgrade soil silt (Fig. 25).

6 Conclusions

The effect of waste materials independently and in groupings on physical properties such as rutting and fatigue by laboratory tests and the analytical examination is assessed. The viscous changeover temperature of binder mixtures is seen reduced when the WP is employed in the binder which is more vulnerable to hotter climate. The capability of the binder to produce a ductile thin layer around the aggregates is lessened, thereby increasing the stiffness of the binder. The hardness of the binder maybe helpful to reduce the rutting but might create a grave dent particularly in the cold climate zones regarding fatigue failure. From the experimental examination, it is understood that the rise in the percent values of WP in conventional bitumen creates a stiff mix. From the Tensile Strength Ratio (TSR), it is suggested to employ 7.5% WP in BL as the TSR value is close to 80.00% although further rise in WP percent values display the decrease in TSR values. RAP aggregates show substantial results even at 100.00% substitution of traditional aggregates. Hence, it is deduced that after crushing, screening, and separating in the equivalent sizes, the utilization of RAP aggregates for novel constructions is beneficial and shows to be a sustainable substitute for road construction projects. Upon increment of the percent values of WP and RAP, it is detected that the hardness of the binder upsurges and the capability of binder to create a ductile thin layer around the aggregates is also seen to be reducing thereby, creating the binder stiff and inconsistent. The RAP aggregates gotten from the old pavements is likely to be reutilized in the construction of newer pavements. Using the data obtained from the analytical examination, the pavement life is estimated for numerous hypothetical assumptions. It is detected that the use of WP has considerably augmented the numbers of rutting cycles however, decrease the fatigue cycles consequence in resistance to rutting but amounts to fatigue cracking. Additional increment in the percentage of WP results in failure of pavement in fatigue. It is inferred from the experiential and analytical examination that the percentage increment in WP may result to be helpful in controlling the rutting. For subgrade soils such as clay and gravel which are having good strength, least BL thickness of 125 mm with a least base layer depth of 150 mm placates the criterions of fatigue and rutting. For subgrade soils such as silt and silty sand which are having weak strength, it is very difficult to suggest a design chart based on the trialed combinations without performing any soil improvement technique. For the soils like clay and gravel, there is no necessity to provide additional thickness for base and BL but the minimum layer depths of 150 mm and 125 mm for the base and BL layer placates the criterions on safer sides. In conclusion, founded on the laboratory and analytical study, design charts are created which enhances the design methodology in cost saving and provide an eco-friendly substitute

to traditional materials. It is possible to use remnants of old pavement in the construction of new pavement with a sustainable method on the way to waste management and road construction.



References

1. Sinha, A.K., Chandra, S., Kumar, P.: Finite element analysis of flexible pavement with different subbase materials. *Indian Highways* **42**(2), 53–63 (2014)
2. Sharma, A., Kumar, P., Walia, A.: Use of recycled material in WMA- future of greener road construction. *Transp. Res. Procedia* **48**, 3770–3778 (2020)
3. ASTM D113. Standard test method for ductility of bituminous materials. USA: American Society for Testing and Materials (2007)
4. ASTM D1559 Standard Test Method for Marshall Stability for Bituminous Mixtures
5. ASTM D36/D36M. Standard test method for softening point of bitumen (ring and ball apparatus). Pennsylvania, USA: American Society for Testing and Materials (2012)
6. ASTM D4123 Standard Test Method for Indirect Tension Test for Resilient Modulus of Bituminous Mixtures
7. ASTM D5/D5M. Standard test method for penetration of bituminous materials. Pennsylvania, USA: American Society for Testing and Materials (2013)
8. ASTM D6084. Standard test method for elastic recovery of asphalt materials by Durometer. Pennsylvania, USA: American Society for Testing and Materials (2007)
9. ASTM D6931 Standard Test Method for Indirect Tensile (IDT) of Strength of Bituminous Mixtures
10. Chandak, P.G., Tapase, A.B., Sayyed, S.S., Attar, A.C.: A state-of-the-art review of different conditions influencing the behavioral aspects of flexible pavement. In: Mohammad, L. (ed.) *Advancement in the Design and Performance of Sustainable Asphalt Pavements*, pp. 300–312. Springer, Cham (2018). https://doi.org/10.1007/978-3-319-61908-8_22
11. El-Tahan, D., Gabr, A., El-Badawy, S., Shetawy, M.: Evaluation of recycled concrete aggregate in asphalt mixes Innovative. *Infrastruct. Solutions* **3**, 20 (2018) <https://doi.org/10.1007/s41062-018-0126-7>
12. Dombe, S., Tapase, A.B., Ghugal, Y.M., Konnur, B.A., Akshay, P.: Investigation on the use of e-waste and waste plastic in road construction. In: Badawy, S., Chen D.H., (eds.) *Recent Developments in Pavement Engineering. Geo-MEeast 2019. Sustainable Civil Infrastructures*, pp. 85–99, Springer, Cham (2020) https://doi.org/10.1007/978-3-030-34196-1_6
13. Hake, S.L., Damgir, R.M., Awsarmal, P.R.: Utilization of Plastic waste in Bitumen Mixes for Flexible Pavement920190. *World Conference on Transport Research – WCTR, Transportation Research Procedia*, vol. 48, pp. 3779–3785. Elsevier (2020) <https://doi.org/10.1016/j.trpro.2020.08.041>
14. Farooq, M.A., Mir, M.S.: Use of reclaimed asphalt pavement (RAP) in warm mix asphalt (WMA) pavements: a review. *Innovative Infrastruct. Solutions* **2**(1), 1–9 (2017). <https://doi.org/10.1007/s41062-017-0058-7>
15. Tahmoorian, F., Samali, B.: Laboratory investigations on the utilization of RCA in asphalt mixtures. *Int. J. Pavement Res. Technol.* **11**, 627–638 (2018). <https://doi.org/10.1016/j.ijprt.2018.05.002>
16. Gade, A., Kulkarni, S., Tapase, A., Bonde, S.: A cost-effective approach towards road construction—kondave a case study. In: Steyn, W., Holleran, I., Nam, B. (eds.) *Pavement Materials and Associated Geotechnical Aspects of Civil Infrastructures. Geo-China 2018. Sustainable Civil Infrastructures*, pp. 98–106. Springer, Cham (2019) https://doi.org/10.1007/978-3-319-95759-3_8

17. IRC SP 53–2010 Second Revision, Guidelines on Use of Modified Bitumen in Road Construction
18. IRC: 37–2012. Guidelines for the design of flexible pavements. Indian Roads Congress, New Delhi
19. IS (1201 to 1220): 1978 Indian standard methods for testing tar and bituminous materials
20. IS 15462: Polymer and Rubber Modified Bitumen, Bureau of Indian Standards
21. IS 2386 Part (1–5) Indian Standard Methods of Test for Aggregates
22. Ranadive, M.S., Tapase, A.B.: Parameter sensitive analysis of flexible pavement. *Int. J. Pavement Res. Technol.* **9**(6), 466–472 (2016). <https://doi.org/10.1016/j.ijprt.2016.12.001>
23. Ministry of Road Transport and Highways (MORT&H), Specifications for Roads and Bridge Works (Fifth Edition), Indian road Congress, New Delhi, India (2013)
24. Chandak, P.G., Tapase, A.B., Patil, R.P., Sayyed, S.S.: Design charts for black cotton subgrade soil in karad taluka: a case study. *Innovative Infrastruct. Solutions* **6**(1), 1–13 (2020). <https://doi.org/10.1007/s41062-020-00372-1>
25. Duggal, P., Shisodia, A.S., Havelia, S., Jolly, K.: Use of waste plastic in wearing course of flexible pavement. In: Adhikari, S., Bhattacharjee, B., Bhattacharjee, J. (eds.) *Advances in Structural Engineering and Rehabilitation*, pp. 176–187. Springer, Singapore (2020) https://doi.org/10.1007/978-981-13-7615-3_16
26. Izaksa, R., Haritonovsb, V., Klasac, I., Zaumanisd, M.: Hot mix asphalt with high RAP content, institute of science and innovation in mechanical and industrial engineering. *Procedia Eng.* **114**, 676–684 (2015) <https://doi.org/10.1016/j.proeng.2015.08.009>
27. Ranadive, M.S., Tapase, A.: Pavement performance evaluation for different combinations of temperature conditions and bituminous mixes. *Innovative Infrastruct Solutions* **1**(1), 1–5 (2016). <https://doi.org/10.1007/s41062-016-0040-9>
28. Gogoi, R., Das, A., Chakraborty, P.: Are fatigue and rutting distress modes related? *Int. J. Pavement Res. Technol.* **6**(4), 269–273 (2013) [https://doi.org/10.6135/ijprt.org.tw/2013.6\(4\).269](https://doi.org/10.6135/ijprt.org.tw/2013.6(4).269)
29. Sayyed S.S., Patil R.P., Tapase A., Attar A.C., Chandak P.G. Review and Assessment of Flexible Pavement. In: Chen, D., Kim, S., Tapase, A. (eds.) *Advancements on Sustainable Civil Infrastructures. Geo-China 2018. Sustainable Civil Infrastructures*, pp. 139–149. Springer, Cham (2019) ISBN: 978-3-319-96241-2. https://doi.org/10.1007/978-3-319-96241-2_12
30. Tapase, A.B., Randive, M.S.: Predicting Performance of Flexible Pavement using finite element method. In: Mohammad, L. (eds.) *Advancement in the Design and Performance of Sustainable Asphalt Pavements, Sustainable Civil Infrastructures, GeoMEast 2017*, pp. 137–146. Springer, Cham (2018). https://doi.org/10.1007/978-3-319-61908-8_11
31. Menaria, Y., Sankhla, R.: Use of waste plastic in flexible pavements-green roads. *J. Civil Eng.* **5**, 299–311 (2015) <https://doi.org/10.4236/ojce.2015.53030>



Critical Pavement Response Analysis Under Overloading for Design of Low Volume Rural Roads

Omkar D. Patil¹✉, Piyush G. Chandak^{1,2} , Anand B. Tapase³ , Ravindra P. Patil⁴, and Nanasaheb E. Patil¹

¹ Annasaheb Dange College of Engineering and Technology, Ashta, India
pgc_civil@adcet.in

² Visvesvaraya Technological University, Belagavi, India

³ Rayat Shikshan Sanstha's, Karmaveer Bhaurao Patil College of Engineering, Satara, India

⁴ Jain AGMIT, Jamkhandi, India

Abstract. This study is focused on analyzing the effects of overloaded vehicles on low volume roads and their comparison with standard axle load of 81.60 kN. The overloads assumed are 1.25 times, 1.50 times and 2.0 times the standard axle load. The main objective of this research is to check the trends in the values of tensile strain, vertical strain and vertical surface deflections in pavement with respect to subgrade modulus and high pressure intensities. Results indicate that the effect of overloading and varying pressure intensities is significant on compressive strain; however effect on tensile strain is comparatively insignificant. The compressive strains increase by almost 95% when overloading is increased by 2 times the standard axle load while a significant rise of almost 50% is also seen when overloading is increased by 1.25 times the standard axle load. When the overloading is 2 times the standard axle load, it has been observed that fatigue cycles decrease by almost 40% while varying the subgrade modulus. Also, for the same condition of 2 times overloading, the fatigue cycles decrease by almost 70% while varying the pressure intensities. Further analysis reveals that the cumulative cycles reduce by almost 95% for both the cases and hence, highlights the importance of overloading in design criteria. The allowable overload limit in India is 1.25 times the standard axle load and hence, design charts are created for overloading phenomena by using 1.25 times the standard axle load as the ultimate load to create realistic and long-lasting design of low volume roads.

Keywords: Overloading · Low volume roads · Fatigue · Rutting

1 Introduction

Good quality roads are essential for the growth of the country, as they are the only medium to reach out to every corner of the country and open many backward and remote areas and bring them to the mainstream. According to the Economic Survey in the year 2017–2018, road transport has a 3.06% contribution in Gross value addition. For financial

years 2020–2025, it is said that the Indian Government is planning to invest Rs. 102 lakh crore in infrastructure, out of which 19 percent of share has been kept for road network [1]. India has a road network of more than 59 lakh km² in which about 80% of the road network consists of Low Volume Roads (LVRs). LVRs act as agents increasing growth rate and help to change the social and economic attitude of people.

Design guidelines for flexible pavements are based on California Bearing Ratio (CBR) method and were first brought into use in 1970. In the last few decades traffic patterns, traffic volume, and technology have made considerable development and there is a need for a more holistic design method, which will consider the phenomena of overloading vehicles using LVRs and not relying on the use of standard axle load of 81.60 kN for the design purpose. As per the IRC 37: 2012, rutting occurs due to compressive strain exceeding allowed values and acting at the top of the subgrade, and fatigue which occurs due to tensile strain at the bottom of the bituminous exceeding allowed values are the two main failure criteria.

The present research methodology has been focused on showcasing the effects of overloaded vehicles using LVRs and the detrimental effects on various parameters such as tensile strains, compressive strains, and surface deflections. In this study, IITPave software has been used, which has an inbuilt function of the linear elastic program. The said software has been used by all the design guidelines of the Indian Roads Congress and many researchers all over the world. The input parameters for the study taken into consideration are material properties of different layers of LVRs, Poisson's ratio, tyre pressure intensity, wheel load, and the thickness of the bitumen and aggregate layer. These parameters help in analyzing the road pavement with greater accuracy. In this study, rutting and fatigue are considered as the main failure criteria for the analysis of LVRs.

2 Literature Review

Chandak et al. [2] observed in the state of the art research paper covering the different aspects related to the LVRs and questions the reliability of the conventional design methods used for the design of LVRs. It discusses the reasons for the failure of roads and probable solutions to prevent it. It is necessary to consider some of the key factors such as different material properties, climatic changes, and change of traffic volume over the period, the thickness of the different layers of the pavement, etc. The current design guidelines do not consider the overloading effect, which fails pavement much before its design life since the use of LVRs by heavy vehicles is common in most parts of the country. Therefore, it is suggested that design will be more economical and efficient if roads are designed using with due consideration to overloading phenomena.

Suleiman and Varma [3] stated that with time, the usage by heavy vehicles on LVRs has increased manifold. The study was focused in North Dakota, USA. The authors stated that the LVRs in North Dakota were not designed for heavy overloading. The study also considers the effect of change in seasons such as spring and summer. The study considers the truck damage factors, steering axle-dual tyres, tandem axle, and tridem axle. The study suggests that the steering axles are capable to do immense damage to the pavement whereas on the other hand tridem axles are friendlier to the pavement. This study further

studies the effect of seasonal variation on the pavement. Sahoo et al. [4] stated that it is crucial to collect data on rural roads for a long time to develop a logical or rational pavement design system, while also the collected data will be helpful in the maintenance of pavements. The research study collects data under different circumstances considering the different subgrade, climatic and traffic conditions. The research was focused on the study of granular pavements that are used in LVRs. Since the study has been conducted in India, the researchers state that the roads under the “Pradhan Mantri Gram Sadak Yojana” scheme which are designed as granular pavements with a thin bitumen layer at the top, do not refer to any documented performance data, and hence it is suggested to use an alternate more economical and efficient method which will be more rational design. For this study, roughness and permanent deformation under the wheels, that is rutting, are considered the main failure criterion.

Tapase et al. [5] observed the premature failure of the LVRs is due to heavily overloaded vehicles using the LVRs to refrain from paying the fees of toll booths situated on highways. The research was focused on the impact of overloading on LVRs and its direct connection to the failure of the LVR. This study gives considerable proof and results showing the factors like temperature, seepage, climatic changes affect the road pavements greatly. Even if the pavement is designed following all the guidelines and theoretical values, it needs redesigning as per the site conditions and hence site testing should be given utmost importance while designing. The design needs to be wholesome and should be focused on trying various parameters while designing such roads. Ranadive and Tapase [6] stated the importance of different parameters on road pavement using the finite element method. The study gives the importance of both theoretical knowledge and the results obtained from the actual site in the design of roads. Furthermore, it has been seen that the increase in the thickness of the bituminous layer affected both rutting as well as fatigue. However, the increase in the thickness of the base layer majorly affected the rutting cycles and showed very less effect on fatigue. Gupta et al. [7] observed that safety and economical design has always been the ultimate goal of road design and due to change in trends special attention must be given to the design of LVRs. These roads are key elements and play a vital role in the development of the rural areas. The study aims for a more logical or sensible method to design the LVRs. In this study, rutting has been considered as the main failure criterion and changes in a granular layer have been taken into account. The author has used the finite element method for the calculation of the failure strains and stresses in the pavement. Resilient modulus has been considered in this study as it defines the strength of subgrade under dynamic loading more accurately. The design charts obtained from the study are applied to the pavement designed for traffic up to 1 million standard axles (msa) and subgrade modulus has been varied from 20 MPa to 250 MPa.

Gupta and Kumar [8] observed that the rutting is one of the main contributors to the failure of the flexible pavement of LVRs and hence needs to be examined thoroughly. Such failures can seriously affect vehicle steering and may cause many traffic hazards. The study attempts a detailed study on the structural analysis of pavements using the finite element method and testing the effect of different moduli on vertical deflections. For this study, ANSYS and KENLAYER software have been used. The purpose of the study was to learn the sensitivity of variables such as stress, strain, and deflection in reducing

the vertical surface deflection. The study was further focused to find an alternate way to reduce the vertical deflections by varying different values of the elasticity modulus of the component layers of flexible pavement.

Morton et al. [9] observed the combined effect of various tyre pressures and axle loads on the flexible pavement. The advancement in technology in recent years such as the automobile industry and tyre industry affects the design of flexible pavement tremendously. The increase in the tyre pressure is observed and it has reached up to 1 MPa which is more than the usual reading of 0.7 MPa. This puts more pressure on roads, which are not designed for these changes. The heavy vehicle industry has modified itself and therefore the ability to carry load increased. For the pavement design, a more holistic approach is needed especially since these new advancements are needed to be considered and modification of rules and regulations is required.

3 Methodology

A flexible pavement consists of four layers namely a bituminous layer, base course, subbase course, and subgrade. Subbase and base courses are together considered as a granular layer or aggregate layer as shown below in Fig. 1. It has low or negligible flexural strength. Also, the flexible pavement has the unique property of transferring deflection from layer to layer. For the design of flexible pavement IRC: 37 [10] design code is used.

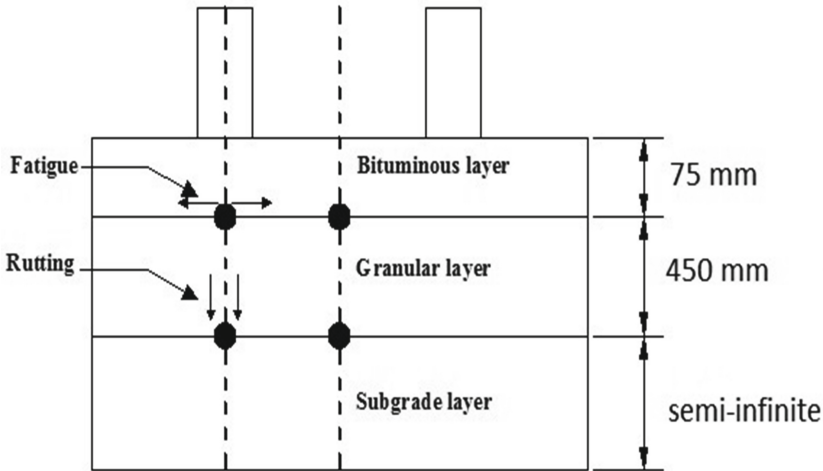


Fig. 1. Location of critical points in flexible pavement

When vehicles start passing on roads, due to the heavy stress on the pavement a permanent vertical deformation occurs in one or multiple pavement layers in longitudinal direction under the wheels, called ruts. Shallow ruts can also be formed due to the consolidation or by secondary compaction and also by the shear deformation. Some of

the important causes of rutting are repetitive loading, heavy vehicles using the road, low compaction, or poor compaction of layers of pavements, or inadequate design of layers. It greatly affects the steering ability of the drivers and might lead to tragic accidents. Rutting occurs at the top of the subgrade layer and transfers to the surface layer with time. Rutting model is created by the IRC [9] gives equation as follows:

$$N = 4.1656 \times 10^{-8} \times \left(\frac{1}{\varepsilon_v} \right)^{4.5337} \quad (1)$$

Where, N = Number of cumulative standard axles, ε_v = maximum compressive strain at the top of the subgrade.

Fatigue occurs due to the creation of the horizontal tensile stresses at the bottom of the surface of the bituminous layer. Cycling loading develops the minute cracks in layers, which with time and further loading widens and expands until cracks appear on the surface. The fatigue model or equation by IRC is given below which is obtained from the Marshall Method [10]:

$$N_f = 2.2 \times 10^{-4} \times \left(\frac{1}{\varepsilon_t} \right)^{3.89} \times \left(\frac{1}{M_r} \right)^{0.854} \quad (2)$$

Where, N_f = fatigue life in several standard axles, ε_t = maximum tensile strain at the bottom of the bituminous layer, and M_r = elasticity modulus of bituminous layer [10].

3.1 Field Investigation Survey

To understand and study the areas affected by overloading phenomena and observe its implication on rural roads, a field investigation survey was carried out in Satara District, Maharashtra State, India. The investigation was conducted for three months between October 2019 to December 2019. In India, agriculture and its allied products are one of the primary occupations of the people. In the district of Satara, two major sugar production factories require the delivery of sugarcanes from heavy and medium commercial vehicles (HCV and MCV). The field study was also focused on three areas in the district which employ windmills for the generation of electricity. These windmill fields are situated on high terrain areas such as ridges and small hills. The routes to these hills are through many villages and internal low volume rural roads which are subjected to tandem-axle vehicles carrying the heavy parts of the windmills. One more area for study is the low volume rural roads adjacent to the mainstream highways installed with toll gathering booths. Many HCV and MCV try to evade these toll fees and use these adjacent LVRs, exerting uncalculated and unprecedented loads on such roads.

A questionnaire was prepared and a survey conducted to understand how many vehicles utilize these roads, the reasons for using such roads, and the tentative amount of overloads employed in these heavy vehicles. The data was collected during peak hours of day and evening timings. The targeted audiences were local authorities from villages, managers from factories, drivers of the vehicles, and workers from toll booths, and people from its nearby areas. The survey from a sugar production factory revealed that the MCV and HCV are overloaded by the vehicle owners by almost 1.5 times to 2.0

times its actual carrying capacity. This practice by the owners is to gain more profit and avoid transportation costs. The data collected from the local authorities and drivers of vehicles carrying parts of the windmill revealed that the load exerted by such vehicles is tremendous with very high tyre pressure intensities as well. The local authorities reported that due to these vehicles the roads deteriorate very early and high annual repairs and maintenance are required after the monsoon season. The study also revealed that almost 2 to 3 vehicles per 10 heavy vehicles use adjacent LVRs to the toll booths. This increases the unprecedented numbers of heavy vehicles using these roads reducing the design life while also consuming fatigue and cumulative lives.

3.2 Input Parameters for Varying Subgrade

The traffic category for the study is assumed as 2 msa. As per the IRC guidelines, the standard axle load is taken as 81.60 kN for the analysis. The wheel load on a single wheel is hence calculated as 20 kN. The tyre pressure intensity is assumed as 0.70 MPa. The granular layer has been assumed constant at 450 mm with a bituminous layer of 75 mm consisting of open-graded Bituminous Macadam lying above it. The resilient modulus of the granular layer has been assumed as $E_2 = 200$ MPa and for Bituminous layer $E_1 = 700$ MPa with Poisson's ratio for both assumed as $\mu = 0.35$. Clay, Loess, Sand, Gravel, and Silt are some of the soil types and their modulus of elasticity (MOE) varies from 10–200 MPa [11]. For this study, the MOE of the subgrade is varied using representative soil sampling depending on soil type and nature. The values of modulus of elasticity in the study area of the Satara district also vary between 10 MPa to 120 MPa [12, 17]. Hence, representative subgrade soils have been assumed for this study as 30, 60, 90, and 120 MPa [13]. The Poisson's ratio for subgrade has been assumed as $\mu = 0.45$. Such soil sampling will enable the study to analyze the effects of overloading on different types of subgrade materials [10].

As per Boussinesq's theory, as the distance between the point of observation and the point where the load is acting increases the stress decreases. Therefore, while designing a pavement; critical points where exerted stress is the maximum is important and necessary, as it will ultimately result in safety for all the rest of the points. Therefore, four critical points are considered for study as shown in Fig. 1; the two critical points at the bottom of the bituminous layer for horizontal tensile stress analysis for fatigue failure and two at the top of the subgrade layer for the analysis of vertical plastic deflection, namely rutting. The horizontal distance between the two wheels is assumed as 160 mm center to center for all the trials. To consider the effect of overloading, hypothetical conditions are assumed wherein, the overloading condition of 1.5 times (120 kN) and 2 times (160 kN) of the standard axle load is taken for the study. The legal axle load permitted in India of 1.25 times the standard axle load as 102 kN [14, 18–22] has also been taken into consideration for the study. The tyre pressure of the vehicle is kept constant as 0.70 MPa. As per IRC guidelines, the MOE of the bituminous layer is kept constant at 700 MPa [11] and that of the aggregate layer is kept at 200 MPa for all the trials [10].

3.3 Input Parameters for Varying Pressure Intensities

For this analysis, the subgrade of elasticity modulus is kept constant at 60 MPa, which refers to the fair strength of subgrade [15] with Poisson's ratio of 0.45. The granular layer is assumed constant with thickness 450 mm and elasticity modulus at 200 MPa. The usual tyre pressure intensity for standard axle loads vary in between 0.56 MPa to 0.70 MPa [16]. Although with high overloads, the tyre pressure intensities also increase manifold. Hence, the four loading conditions of 81.60 kN, 102 kN, 120 kN, and 160 kN have each been varied with high tyre pressure intensities of 0.70 MPa, 0.84 MPa, and 0.98 MPa [14, 18–22]. The variations in compressive strain, vertical strain, and surface deflections have been noted and analyzed. For analysis, IITPave software was deployed for all the trials mentioned above. IITPave is the after version of the software FPave. In IRC:37-2012 IITPave is used for the analysis of the pavement [10]. All the above inputs are required in the software for the analysis purpose except the subgrade thickness, which is considered as semi-infinite by the software itself.

3.4 Creating Design Charts

To create more reliable and long-lasting design charts that are subjected to heavy overloading; tyre pressure has been assumed to be more than regular tyre pressure of 0.70 MPa and in between 0.70 MPa and 0.98 MPa. Hence, for this purpose, the tyre pressure is assumed and kept constant at 0.84 MPa for all trials with the ultimate load considered as 1.25 times the standard axle load. Hence, the legal axle load of 102 kN permitted in India has been assumed for this purpose. The design thickness charts are created for the assumed subgrade values. The bituminous layer is varied between 50 mm and 100 mm consisting of bituminous macadam. The granular layer has been varied between 300 mm to 600 mm with equal increments of 75 mm for each trial [17–22]. The modulus of elasticity has been assumed as 200 MPa for all trials. For subgrade with poor strength such as 30 MPa; a modified subgrade has been suggested with 200 mm thickness and is kept constant for all trials.

4 Results and Discussion

4.1 Analysis of Varying Subgrade

For the study, the granular layer thickness is kept constant at 450 mm and the bituminous layer at 75 mm. The trends in changes in compressive strain, tensile strain, and displacements are calculated. Also, fatigue and rutting lives in terms of the number of standard axles are calculated. In Fig. 2, the vertical compressive strains are calculated concerning every assumed subgrade modulus of elasticity. It is seen from Fig. 3 that as the elasticity modulus of subgrade increases for every loading condition, the vertical strain values go on decreasing. However, for a particular elasticity modulus of subgrade, there is a considerable increase in vertical strains as loading conditions are varied from 81.60 kN to 160 kN. Almost 20% increase is observed in vertical strain for every trial increase when loading condition is increased from 81.60 kN. While almost 95% increase is observed when loading is varied from 81.60 kN to 160 kN. The percentage variation concerning the loading condition is almost the same for every MOE of subgrade.

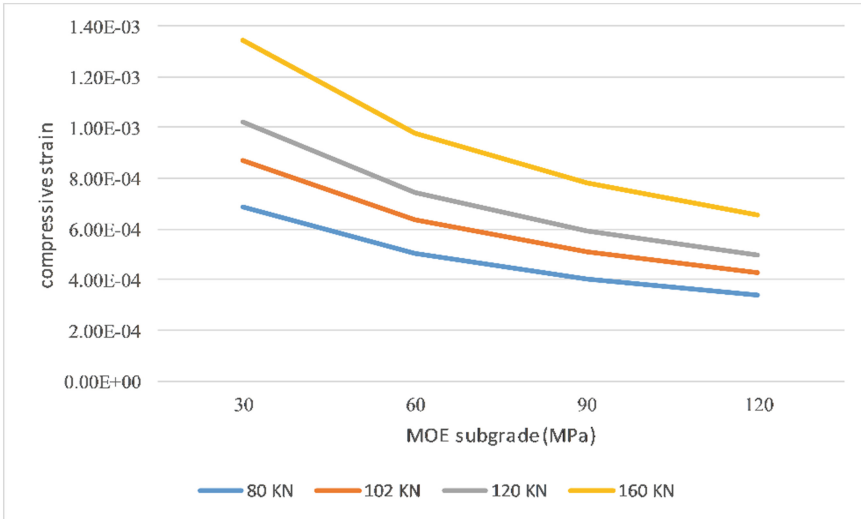


Fig. 2. Vertical compressive strain with respect to subgrade and overloading

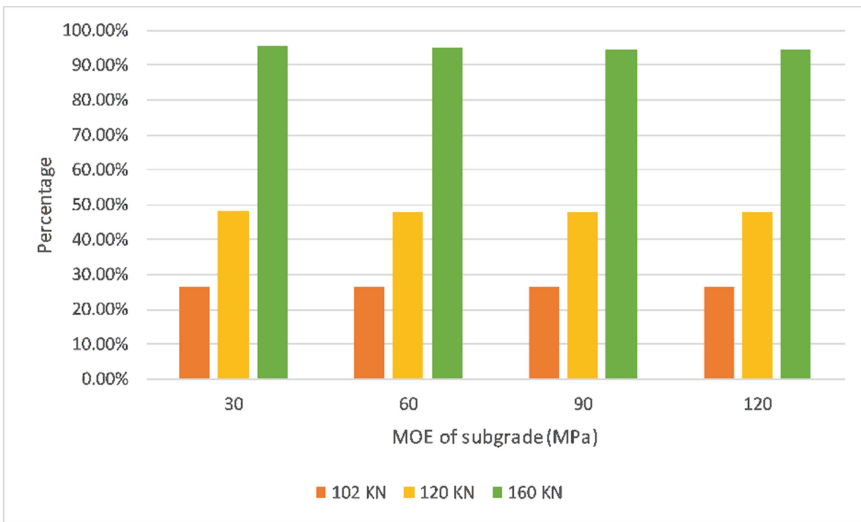


Fig. 3. Percentage Variation in vertical compressive strain with respect to subgrade and overloading

From Fig. 4 and Fig. 5, it is observed that there is a gradual decrease in tensile strain concerning an increase in MOE of subgrade. The percentage variation in tensile strain is observed to be increasing with every trial for MOE of subgrade and change in loading conditions as well. An almost 18% increase is seen when loading condition is varied from 81.60 kN to 160 kN for 30 MPa subgrade modulus. This percentage variation

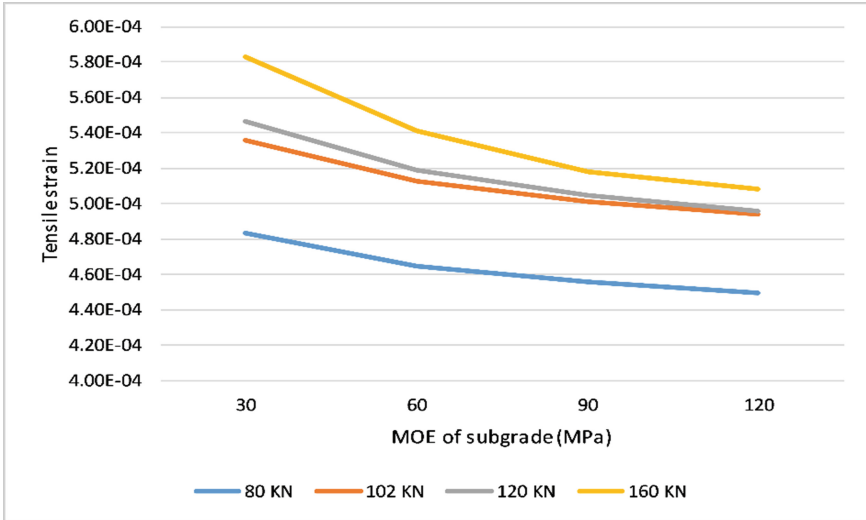


Fig. 4. Tensile strain with respect to subgrade and overloading

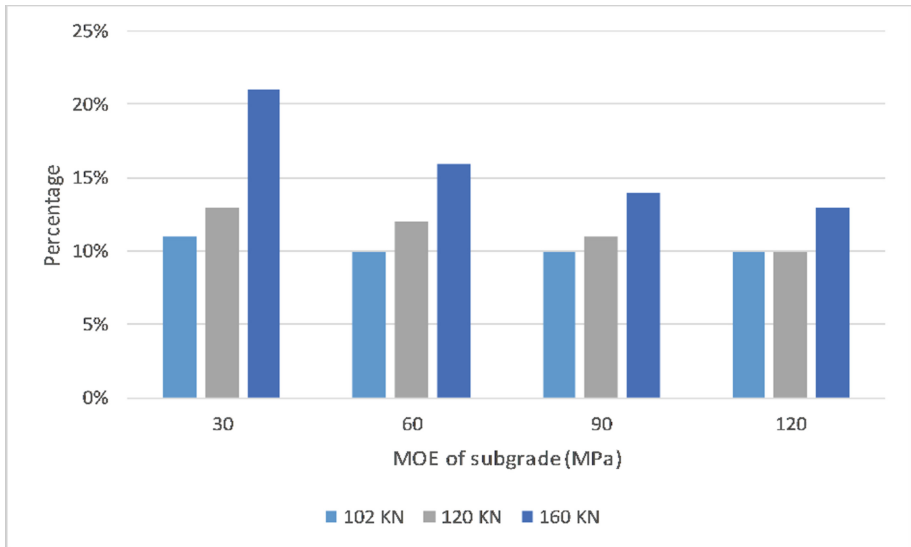


Fig. 5. Percentage variation in tensile strain with respect to subgrade and overloading

decreases as the subgrade modulus is increased. Hence, for good strength of subgrade, there is not much effect on tensile strain due to overloading.

From Fig. 6, it is seen that surface displacement decrease with an increase in MOE of subgrade but increases with increments in the loading conditions while keeping subgrade constant. For every increase in loading condition, while keeping subgrade constant, surface displacements increase by almost 25%.

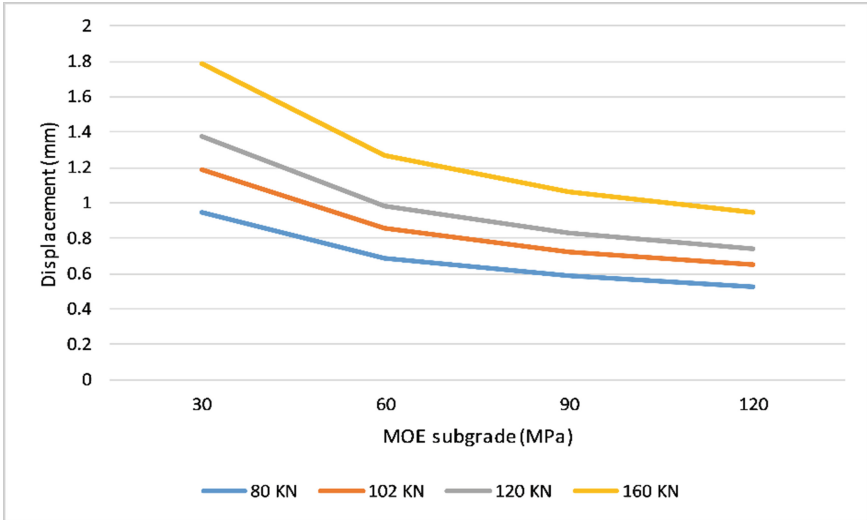


Fig. 6. Surface displacements with respect to subgrade and overloading

The fatigue life and cumulative life are calculated in terms of the number of standard axles. From Table 1, a reduction in life is observed as the load increases. When the load is 2 times the standard axle the reduction observed in fatigue life is almost 40% on average and the reduction in cumulative life is 95% that is, the life reduces to half when the load gets doubled. When the legal axle load is applied, the reduction in cumulative life is observed to be 66% concerning standard axle load.

Table 1. Fatigue life and number of cumulative standard axles for varying subgrade

MOE subgrade(MPa)	Load (kN)	Fatigue life (Nf)	Number of cumulative std. axles (N)	Nf (% variation) (w.r.t. 81.60 kN)	N (% variation) (w.r.t. 81.60 kN)
30	81.60	6.49E+06	9.01E+06	–	–
	102	4.33E+06	3.08E+06	33%	66%
	120	4.03E+06	1.51E+06	38%	83%
	160	3.12E+06	4.32E+05	52%	95%
60	81.60	7.52E+06	3.74E+07	–	–
	102	5.13E+06	1.29E+07	32%	66%
	120	4.91E+06	6.33E+06	35%	83%
	160	4.17E+06	1.82E+06	45%	95%

(continued)

Table 1. (continued)

MOE subgrade(MPa)	Load (kN)	Fatigue life (Nf)	Number of cumulative std. axles (N)	Nf (% variation) (w.r.t. 81.60 kN)	N (% variation) (w.r.t. 81.60 kN)
90	81.60	8.12E+06	1.03E+08	–	–
	102	5.63E+06	3.56E+07	31%	66%
	120	5.46E+06	1.75E+07	33%	83%
	160	4.94E+06	5.06E+06	39%	95%
120	81.60	8.55E+06	2.33E+08	–	–
	102	5.94E+06	8.01E+07	30%	66%
	120	5.85E+06	3.95E+07	32%	83%
	160	5.33E+06	1.14E+07	38%	95%

4.2 Analysis for Varying Pressure Intensities

From Table 2 and Fig. 7, it is seen that compressive strains increase by almost 26% when loading is increased from 81.60 kN to 102 kN, while increases by almost 94% when compared between 81.60 kN and 160 kN. However, for every loading condition, the percentage variation remains constant when pressure intensities are varied from 0.7 MPa to 0.98 MPa. Hence, the change in pressure intensities affects compressive strain significantly.

Table 2. Compressive strain with respect to pressure intensities and overloading

MOE subgrade (MPa)	Pressure intensity (MPa)	Load (kN)			
		81.60 kN	102 kN	120 kN	160 kN
60	0.7	5.031 E-04	6.368 E-04	7.447 E-04	9.800 E-04
	0.84	5.053 E-04	6.403 E-04	7.496 E-04	9.886 E-04
	0.98	5.069 E-04	6.429 E-04	7.532 E-04	9.948 E-04

From Table 3 and Fig. 8, it is seen that tensile strains increase by about 10–18% when loading is increased from 81.60 kN to 102 kN while increases by almost 37% when compared between 81.60 kN and 160 kN. However, for every increment in loading conditions, the percentage variation reduces when pressure intensities are varied from 0.7 MPa to 0.98 MPa. Hence, change in pressure intensities does not affect tensile strain significantly.

The fatigue life and cumulative life are calculated in terms of the number of standard axles. From Table 4a and Table 4b, a reduction in life is observed as the load increases. When the load is two times the standard axle the average reduction observed in fatigue

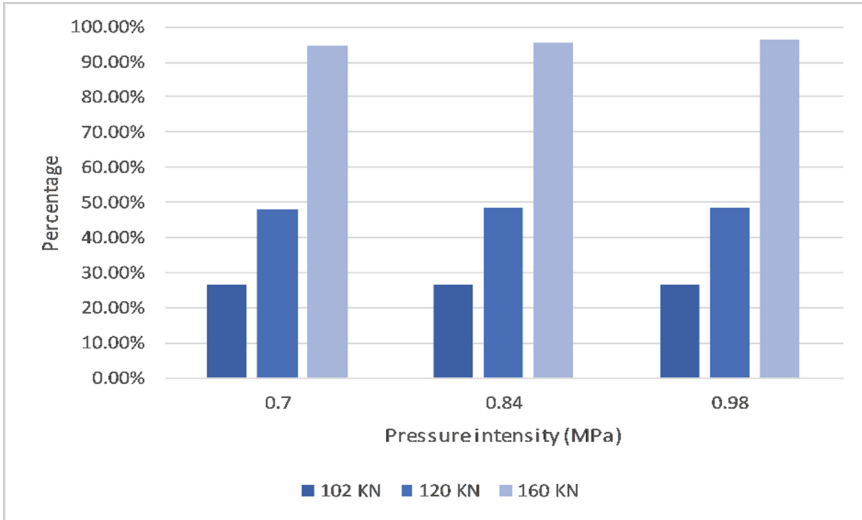


Fig. 7. Percentage variation in compressive strain with respect to pressure intensities and overloading

Table 3. Tensile strain with respect to pressure intensities and overloading

MOE subgrade (MPa)	Pressure intensity (MPa)	Load (kN)			
		81.60 kN	102 kN	120 kN	160 kN
60	0.7	4.649 E-04	5.129 E-04	5.19 E-04	5.408 E-04
	0.84	4.994 E-04	5.753 E-04	6.124 E-04	6.745 E-04
	0.98	5.226 E-04	6.167 E-04	6.739 E-04	7.284 E-04

life is 70% and the reduction in cumulative life is 95% that is, the reduction in life. When the legal axle load is applied, the reduction in cumulative life is observed to be 66% whereas the average reduction in fatigue life is observed to be 41% concerning standard axle load.

4.3 Design Charts

Based on the analysis conducted for varying subgrade and tyre pressure intensities; design thickness charts have been created using input parameters as stated in Sect. 3.4. These charts are assuming higher axle load and tyre pressure intensity exerted on it. Hence, the overall pavement depth increases but these charts will prove more beneficial and will not deteriorate early in the design life of low volume roads. Figure 9 depicts the design thickness chart created for the assumed subgrade values. The 50 mm depth of BM seems to be insufficient to deal with heavy overloads and tyre pressure intensities. Although most of the values at 100 mm BM are well inside the allowed limits; 75 mm of

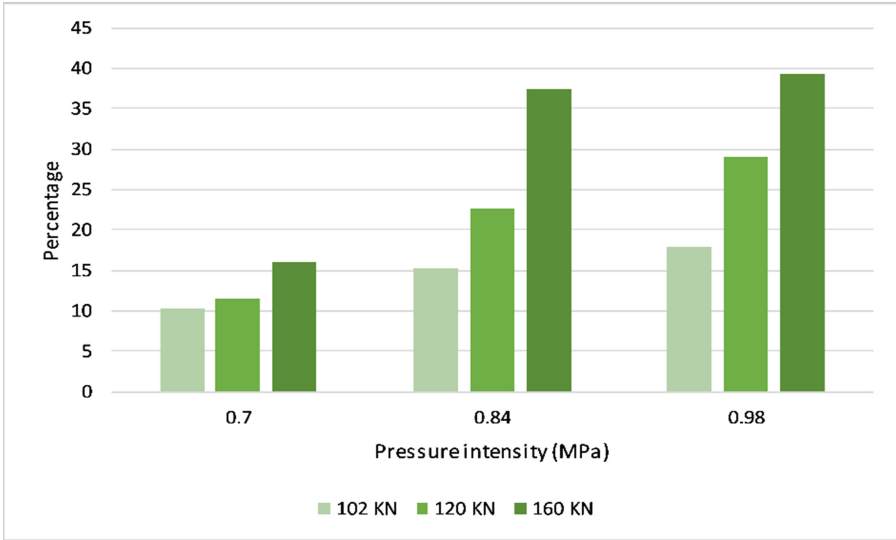


Fig. 8. Percentage variation in tensile strain with respect to pressure intensities and overloading

Table 4. (a) Fatigue lives with respect to pressure intensities and overloading

MOE of subgrade (MPa)	Pressure intensity (MPa)	Load (kN)			
		81.60 kN	102 kN	120 kN	160 kN
60	0.7	7.53E+06	5.14E+06	4.91E+06	2.19E+06
	0.84	5.70E+06	3.29E+06	2.58E+06	1.77E+06
	0.98	4.78E+06	2.51E+06	1.78E+06	1.31E+06

Table 4. (b) Cumulative lives with respect to pressure intensities and overloading

MOE of subgrade (MPa)	Pressure intensity (MPa)	Load (kN)			
		81.60 kN	102 kN	120 kN	160 kN
60	0.7	3.74E+07	1.29E+07	6.33E+06	1.82E+06
	0.84	3.67E+07	1.25E+07	6.14E+06	1.75E+06
	0.98	3.62E+07	1.23E+07	6.01E+06	1.70E+06

BL has been suggested considering the economical aspect and optimum combination. The granular layer depth of LVRs goes on decreasing as the modulus of elasticity of subgrade goes on increasing. The suggested new design charts vary significantly from those suggested by the design guidelines [15] in India.

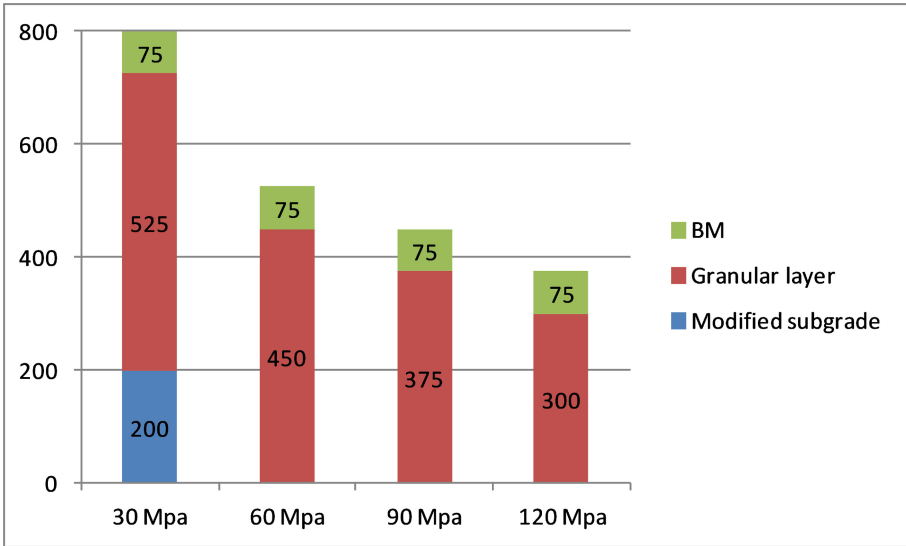


Fig. 9. Design thickness charts based on overloading phenomena

5 Conclusions

From the detailed analysis, it can be easily deduced that the overloading phenomena affect the low volume roads quite significantly. One of the primary reasons for early failure of low volume roads can be easily attributed to such overloading phenomena. These loads reduce the design life of the LVRs and hence, repairs and maintenance are required very early into the life of LVRs [18]. In some of the circumstances where the LVRs are expected to bear the overloaded vehicles running over them, it is necessary to take into consideration such type of analysis for better design of the pavements. The detailed field investigation survey was also helpful to understand the actual scenarios and conditions of the overloading phenomena on the low volume rural roads. This data proved to be beneficial while designing the thickness charts based on the overloaded conditions.

For subgrades with poor strength such as 30 MPa soil, the results of overloading can be drastic and will reduce the life of the pavement considerably. For low volume roads, rutting is assumed as the primary failure criteria and from the analysis, it is seen that for varying subgrade values with overloading phenomena, there is an almost 95% increase in compressive strain values from 81.60 kN to 160 kN and only 18% increase in tensile strain for the same assumed conditions. The surface displacements are also hugely affected by overloading conditions. In terms of the cumulative life of the LVRs, there is a huge decrement in the number of axles by almost 66% when loading is increased from 81.60 kN to 102 kN. When the subgrade modulus is varied, it has been observed that fatigue cycles and cumulative standard cycles for loading of 160 kN concerning 81.60 kN decrease by almost 40% and 95% respectively.

The analysis for varying high-pressure intensities and constant subgrade modulus, the results of overloading can be radical and will diminish the life of the pavement

noticeably. For low volume roads, rutting is assumed as the primary failure criteria and from the analysis, it is seen that for varying pressure intensities with constant subgrade, there is an almost 90% increase in compressive strain values from 81.60 kN to 160 kN and about 26% increase when loading condition is varied from 81.60 kN to 102 kN for the same assumed conditions. However, the variations in pressure intensities do not affect the tensile strain values significantly. In terms of fatigue life and cumulative life of the LVRs, there is a huge decrement in the number of axles by almost 41% and 66% respectively when loading is increased from 81.60 kN to 102 kN. When the pressure intensities are varied, it has been observed that fatigue cycles and cumulative standard cycles for loading of 160 kN with respect to 81.60 kN decrease by almost 70% and 95% respectively.

Based on such detailed analysis, it is suggested that the designing procedure of LVRs should not be completely dependent on the design guidelines and assuming thicknesses of different layers as stated by the code for various CBR values and traffic categories. It is imperative that a detailed survey of the traffic conditions, axle load survey, and type of vehicles using the LVRs needs to be considered and different designs for every condition are to be thought of. It is suggested that the LVRs subjected to heavy overloading are to be designed by using legal axle load as the ultimate load on the pavement rather than standard axle load with high-pressure intensity as input parameters; which might increase the thicknesses of component layers but will give a more long-lasting design chart and improve the performance and life of such LVRs. The 50 mm depth of the bituminous layer using bituminous macadam seems to be inadequate to deal with heavy overloads and tyre pressure intensities. Most of the values at 100 mm BL are well within the limits but considering economical aspect and optimum combination; 75 mm of BL has been suggested. The overall depth of pavement goes on reducing as the modulus of elasticity of subgrade is increased. The design thickness chart hence created using higher values of axle load and tyre pressure intensity will prove to be more realistic and long-lasting for subgrades subjected to overloading phenomena.

References

1. Government of India Ministry of Finance. Economic survey 2019–2020 (2019). https://www.indiabudget.gov.in/economicsurvey/doc/vol2chapter/echap08_vol2.pdf
2. Frikha, W., Kawamura, S., Liao, W.-C. (eds.): GeoChina 2018. SCI, Springer, Cham (2019). <https://doi.org/10.1007/978-3-319-95756-2>
3. Suleiman, N., Varma, A.: Modeling the response of paved low-volume roads under various traffic and seasonal conditions. *Transp. Res. Rec. J. Transp. Res. Board* **1989–2**, 230–236 (2007). <https://doi.org/10.3141/1989-68>
4. Sahoo, U., Ahmed, S., Reddy, K.S.: Long-term performance evaluation of rural road pavements in India. In: *Design, Analysis, and Asphalt Material Characterization for Road and Airfield Pavements*, American Society of Civil Engineers, Reston, VA, pp. 91–98 (2014). <https://doi.org/10.1061/9780784478462.012>
5. Tapase, A.B., Chandak, P.G., Patil, R.P., Attar, A.C., Sayyed, S.S.: Evaluation and remedial measures on premature failure of roads in India. *J. Perform. Constr. Facil.* **34** (2020). [https://doi.org/10.1061/\(ASCE\)CF.1943-5509.0001384](https://doi.org/10.1061/(ASCE)CF.1943-5509.0001384)
6. Ranadive, M.S., Tapase, A.B.: Parameter sensitive analysis of flexible pavement. *Int. J. Pavement Res. Technol.* **9**, 466–472 (2016). <https://doi.org/10.1016/j.ijprt.2016.12.001>

7. Gupta, A., Kumar, P., Rastogi, R.: A mechanistic-empirical approach for the design of low volume pavements. *Int. J. Pavement Eng.* **16**, 797–808 (2015). <https://doi.org/10.1080/10298436.2014.960999>
8. Gupta, A., Kumar, A.: Comparative structural analysis of flexible pavements using finite element method. *Int. J. Pavement Eng. Asph. Technol.* **15**, 11–19 (2014). <https://doi.org/10.2478/ijpeat-2013-0005>
9. Morton, B., Luttig, E., Horak, E., Visser, A.: The effect of axle load spectra and tyre inflation pressures on standard pavement design methods. In: 8th Conference of Asphalt Pavements South Africa (2004)
10. I.R. Congress, IRC 37: Guidelines for the design of flexible pavements, New Delhi, India (2012)
11. Punmia, B.C., Jain, A.K.: *Soil Mechanics and Foundations*, 16th edn. Laxmi publications (P) Ltd.
12. Chandak, P.G., Tapase, A.B., Patil, R.P., Sayyed, S.S., Attar, A.C.: Utilizing different wastes in rural roads of Karad, District – Satara, India. *Int. J. Innov. Technol. Exp. Eng.* **8** (2019). <https://doi.org/10.35940/ijitee.A4906.119119>
13. Zeeveart, L.: *Foundation engineering for difficult subsoil conditions* (1982). ISBN 10: 0442201699
14. Rao, S.K., Srinivasa Rao, D., Murthy, V.S.: Analysis of vehicle overloading from axle load surveys – case studies. *Indian High.* 25–31 (2010)
15. I.R. Congress, IRC: SP 72: Guidelines for the design of flexible pavements for low volume rural roads, New Delhi, India (2015)
16. Sinha, A.K., Chandra, S., Kumar, P.: Finite element analysis of flexible pavement with different subbase materials. *Indian Highw.* **42**(2), 53–63 (2014)
17. Chandak, P.G., Tapase, A.B., Patil, R.P., Sayyed, S.S.: Design charts for black cotton subgrade soil in Karad Taluka: a case study. *Innov. Infrastruct. Solut.* **6**(1), 1–13 (2020). <https://doi.org/10.1007/s41062-020-00372-1>
18. Ranadive, M.S., Tapase, A.B.: Investigation of behavioral aspects of flexible pavement under various conditions by finite element method. In: Yang, Q., Zhang, J.M., Zheng, H., Yao, Y. (eds.) *Constitutive Modeling of Geomaterials*. Springer Series in Geomechanics and Geoengineering. Springer, Heidelberg (2013). https://doi.org/10.1007/978-3-642-32814-5_100
19. Chandak, P.G., Tapase, A.B., Sayyed, S.S., Attar, A.C.: A state-of-the-art review of different conditions influencing the behavioral aspects of flexible pavement. In: Mohammad, L. (ed.) *GeoMEast 2017*. SCI, pp. 300–312. Springer, Cham (2018). https://doi.org/10.1007/978-3-319-61908-8_22
20. Tapase, A.B., Ranadive, M.S.: Predicting performance of flexible pavement using finite element method. In: Mohammad, L. (ed.) *GeoMEast 2017*. SCI, pp. 137–146. Springer, Cham (2018). https://doi.org/10.1007/978-3-319-61908-8_11
21. Sayyed, S.S., Patil, R.P., Tapase, A., Attar, A.C., Chandak, P.G.: Review and assessment of flexible pavement. In: Chen, D., Kim, S., Tapase, A. (eds.) *GeoChina 2018*. SCI, pp. 139–149. Springer, Cham (2019). https://doi.org/10.1007/978-3-319-96241-2_12
22. Tapase, A., Ranadive, M.: Performance evaluation of flexible pavement using finite element method. In: Chen, D., Lee, J., Steyn, W.J. (eds.) *ASCE GSP 266, GeoChina 2016: Material, Design, Construction, Maintenance, and Testing of Pavement*, pp. 9–17 (2016). <https://doi.org/10.1061/9780784480090.002>

Impulse Compaction

History, Technic, Examples

Bißmann Michael^(✉)

Terra-Mix Bodenstabilisierungs GmbH, Schönaich 96, 8521 Wettmannstätten, Austria
michael.bissmann@terra-mix.com

Abstract. Impulse Compaction is a relatively new method of soil improvement. In this paper, the origin, the historical roots, the current state of the art practice, and the various possibilities of Impulse Compaction use and application will be discussed. Furthermore, current documentation and quality assurance standards will be shown. Some selected projects will then underline the potential and attractiveness of Impulse Compaction.

1 Introduction

To improve the subsoil in terms of its load-bearing capacity, soil compaction is still the most economical method because, in general, little to no foreign material is added and instead the inherent load-bearing capacity of the soil material is stimulated and optimized. Stomping is the oldest type of compaction (Fig. 1): already in ancient times, people improved their soil with the help of muscle strength or with small falling weights creating dynamic soil compaction. The modern impulse compactor (Fig. 1) takes this old principle and adapts it to the demands of modern projects by being much more time efficient and providing better quality results.



Fig. 1. Compacting in the past, stomping (left), and now, impulse compactor (right)

Modern **Impulse Compaction**, also known as Rapid Impact Compaction (RIC), is the action of compacting the ground with a so-called impulse compactor, in which

a defined weight falls freely from a height of up to 1.2 m onto a steel plate that is resting on the ground. The dropped weight is hydraulically lifted and this can be done so quickly as to perform up to 60 blows per minute, while the steel plate, the so-called compactor foot, always remains in contact with the ground. Within the family of soil improvement methods, Impulse Compaction can be seen as the “missing link” between near-surface compaction (rolling) and deep compaction (vibro-compaction, dynamic deep compaction) (Fig. 2) [1, 2].

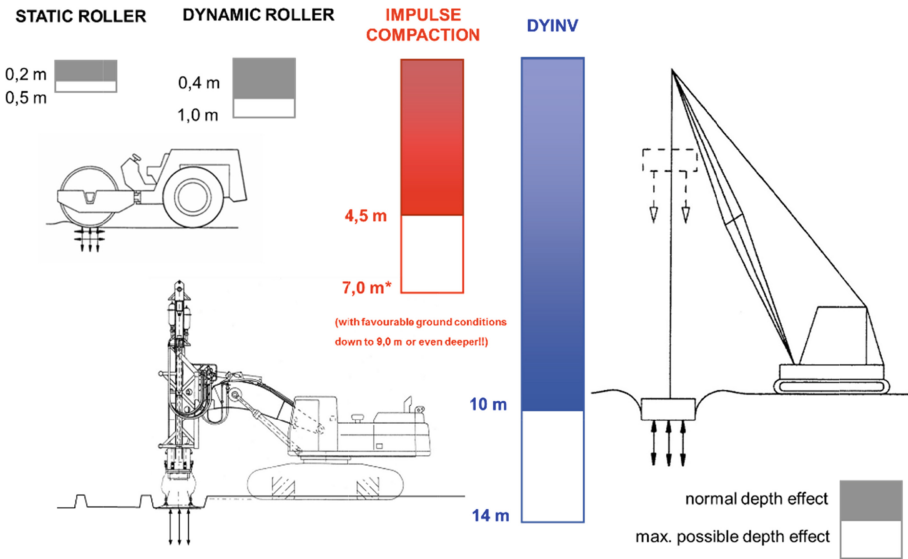


Fig. 2. Depth effect of various methods of subsoil improvement: near-surface, impulse and deep compactions

Impulse Compaction has many advantages when compared to the other compaction methods. Due to the fact that usually no or very little foreign material has to be introduced, Impulse Compaction is not only economically advantageous, it also generates by far the smallest carbon footprint compared to the other processes. Furthermore, compared to dynamic intensive compaction, Impulse Compaction generates far fewer vibrations, which may be of advantage in certain scenarios. However, in some urban settings, the vibrations from Impulse Compaction can still be too high. Some notes about the increased administrative and technical measurement effort required for soil improvement near existing buildings are described by Dobrzycki et al. in [6] and some interesting ideas for reducing vibration waves are described by Herbut in [7].

To the author’s knowledge, modern Impulse Compaction is only commercially done using freely falling weights: companies that use hydraulically accelerated hammers, as opposed to freely falling weights, only use them for driving piles of wood, steel or precast concrete and not for ground improvement as such. There have been attempts and considerations on the part of Terra-Mix to accelerate the falling weight by means of a

rocket propulsion system in order to reduce costs by reducing the weight, but these have not yet come to any useful results.

2 Historic Development of Impulse Compaction

“War is the father of all things” is an old German proverb which is, unfortunately, often the case. In the 1980’s, when the Falkland Islands conflict between Great Britain and Argentina escalated, the British Ministry of Defence looked for ways to remediate field damage such as repairing the bomb craters in the area of the runway as quickly as possible. Subsequently, the British company BSP developed the Rapid Runway Compactor (RRC) (Fig. 3 and 4) which eventually became the Rapid Impact Compactor (RIC) in the civil industry. Both the terms “RIC” and “Impulse Compaction” are used in English today, and the latter will be used in this paper [3].



Fig. 3. British Ministry of Defence DV104 compactor or rapid runway compactor

RIC was initially used on major projects outside of Europe, such as in the Middle East, South Africa [12], Japan, USA and Canada [8, 11]. Becker provides an interesting overview of the development of Impulse Compaction in [9]. In Europe, Impulse Compaction was first made “(industry) socially acceptable” by the Terra-Mix company of Austria, as it developed a complete documentation and quality assurance process for Impulse Compaction work in cooperation with the Technical Universities of Vienna and Innsbruck.



Fig. 4. Port Stanley on Falkland with (repaired) bomb craters (left) and the RRC at work (right) compacting the refilled craters [10].

3 Technical Description of Impulse Compaction

The impulse compactor is a dynamic compaction device based on a piling hammer technology and is used to increase the bearing capacity of soils through controlled impacts. A drop weight of 5 to 16 tonnes is dropped onto the compactor foot assembly 40–60 times a minute. The foot, which remains in contact with the ground at all times, has a diameter that can range from 80 cm to 2 m, but 1.5 m is common.

The compaction results in a rearrangement of the solid material in the soil, because as the water and air pores are displaced, the solid particles are brought into an even denser positioning. In coarse-grained or mixed-grain soils, water in the soil can be squeezed out of between the grains by pressing the grains together and creating a higher contact pressure. In cohesive soils, instead of reducing the soil volume by displacing pore spaces, the result of the mechanical compaction action is rather to have a constant displacement of the material, as the (almost) incompressible water pushes the impermeable grain material in front of it. This effect can also be seen occasionally when material bulges out laterally during Impulse Compaction. In such cohesive soil cases, a soil improvement with Impulse compaction can still be achieved by compacting in (time order) primary and secondary grid patterns or by including longer waiting times between the passes.

Due to the hammering action and the soil rearrangement below, the compactor foot can penetrate up to 1 m into the soil, and when using a special construction, it can penetrate even deeper (which is desired in that case). During the compaction process, each individual impact is measured and documented by a depth sensor. Data monitoring during the compaction process and the online monitoring display in the operator's cab enable the operator to have detailed compaction control. The total impact depth of the compactor foot, the number of blows, and the "Final Set" of the compactor foot (resulting settlement from each particular blow) all contribute to making the decision to stop a hole.

The resulting compaction craters (Fig. 5) are usually filled with the site material, and the process is repeated until a previously defined 'stop code' is reached. Alternatively, external stone material can also be used to fill the holes in order to increase the stiffness of the soil. The 'stop code', in particular the 'Final Set' parameter, provides indirect information about the soil improvement. A measurable correlation between the indirect

soil improvement information and the direct measurement of the improved soil usually takes place via a soil penetration test, such as the Dynamic Probing Heavy (DPH), which is carried out in the course of the so-called calibration field phase. More on this in Chapter 5.



Fig. 5. Resulting craters from the compaction process

The following soil parameters and characteristics can be improved with the Impulse Compaction method:

- compactness of the soil particle packing (bulk density)
- soil stiffness (soil modulus, modulus of subgrade reaction),
- bearing capacity (friction angle, cohesion),
- settlement behaviour
- uniformity of the soil parameters
- weak zones identified
- shear wave modulus (thus mitigating the liquefaction risk)

3.1 Components and Equipment of an Impulse Compactor

In Europe, the nine tonne drop weight and the 1.5 m diameter foot, as shown in Fig. 6, have proven to be the most economical combination. A heavier drop weight provides relatively little further depth effect, but it does speed up the compaction process because fewer blows are required per pass. Further equipment used in the Impulse Compaction process are shown in Fig. 7: the onboard monitor, the data logger and the rover of the GPS system are all installed in the excavator cabin, while the GPS reference station is placed in a secure location on site.

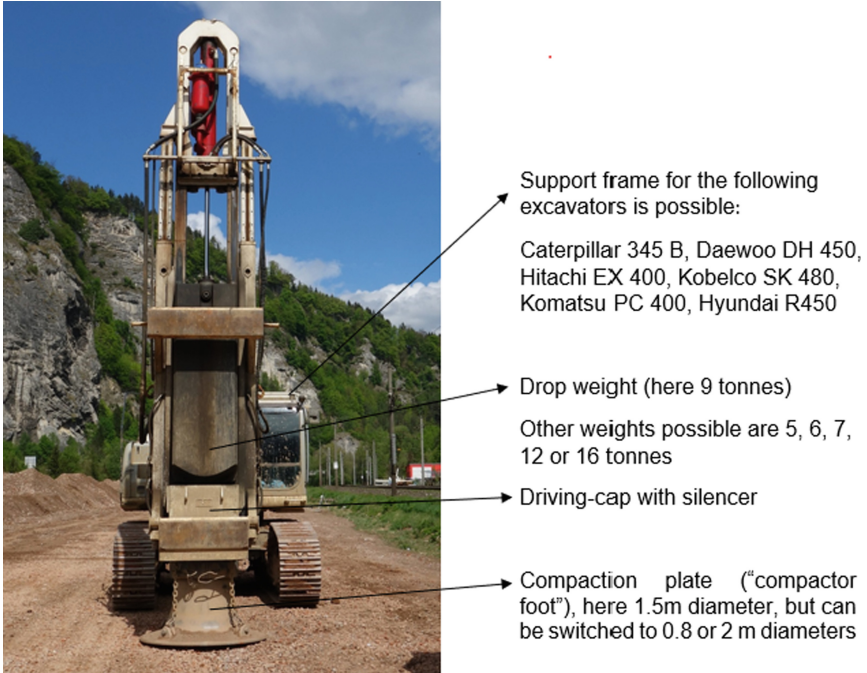


Fig. 6. Components of an impulse compactor (standard version in Europe)

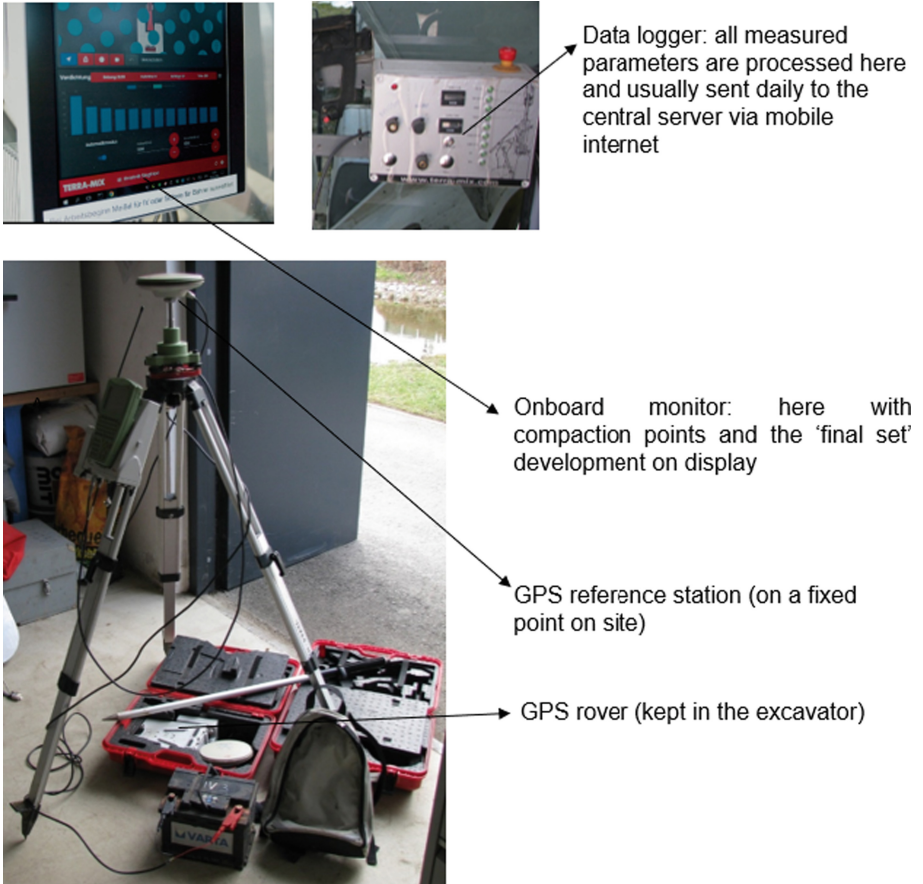


Fig. 7. Further equipment: onboard monitor, data logger and the GPS system

3.2 Additional Attachments for Impulse Compactor

To date, the following impulse compactor attachments have been successfully used: a special foot as an 'icebreaker' (Fig. 8), a noise mitigation attachment (Fig. 8) and a drilling attachment (Fig. 9).



Fig. 8. Ice breaker attachment (left), noise mitigation attachment (right)

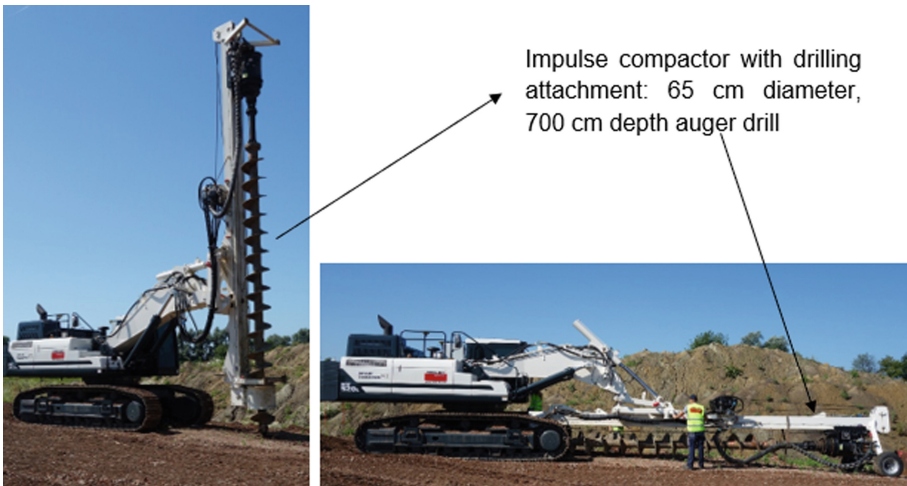


Fig. 9. Impulse compactor with drilling attachment

3.3 Other Applications and Combinations

The most common Impulse Compaction method in Europe is the combination of a medium-depth Impulse Compaction with a load-distributing layer, usually for improving the ground under a foundation slab. A single or multi-layer soil stabilization with lime or cement is usually used as the load-distributing layer (Fig. 10). Alternatively, geogrids or thick stone layers can also be used to distribute the load over the resulting cones of compacted ground.

Impulse Compaction can also be combined with other ground improvement methods in order to achieve an economical ground improvement. For example, when combined with subsequently produced concrete piles, Impulse Compaction increases the soil surface friction of the piles and thus saves required pile length. Another Impulse Compaction use is in combination with vertical drains in road embankments that results in special synergies: Impulse Compaction allows the vertical drains to be sunk much

deeper and therefore significantly reduces the required time for the pre-load filling to be in place. In extremely soft soils, considerations are currently underway to combine Impulse Compaction with stone pillars encased with geotextile in sections.

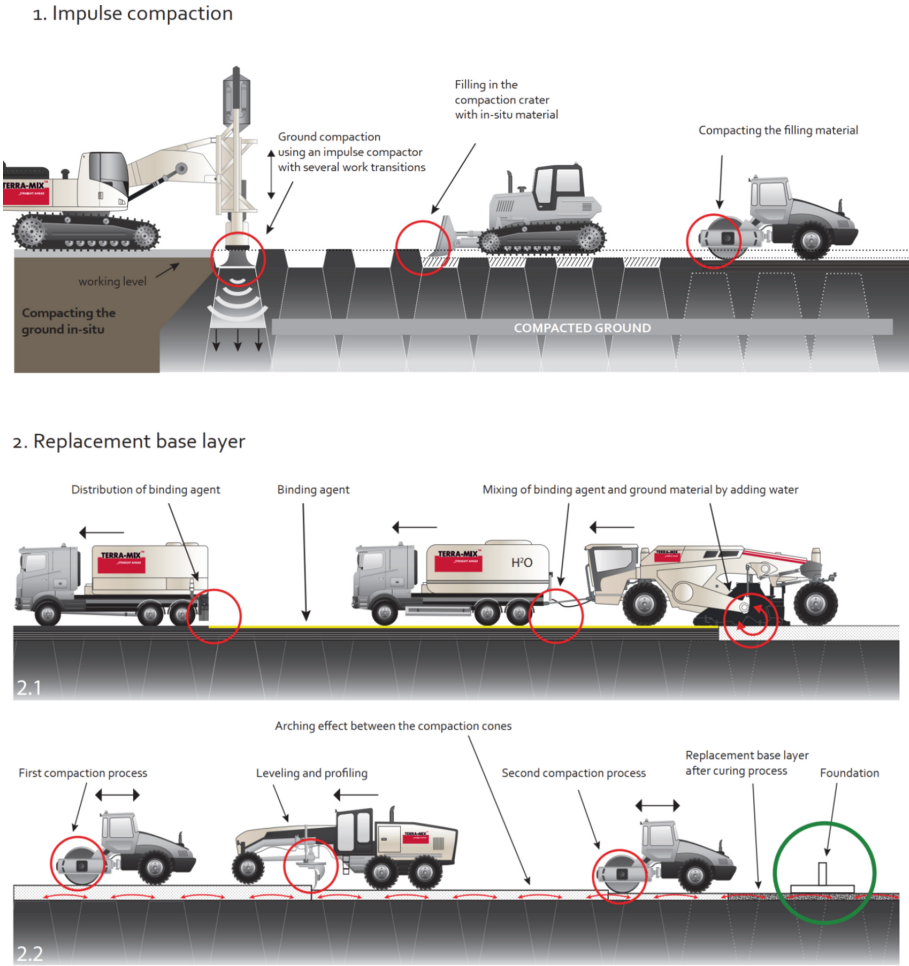


Fig. 10. Procedure of the terra-mix hybrid foundation system

3.4 Predrilled Stone Columns

The most important development in recent years has been the use of the Impulse Compaction method in combination with crushed or pre-drilled gravel columns. To make the best use of the excavator machine used in Impulse Compaction, a mast and drill can be attached to it to enable shallow holes to first be drilled with either continuous flight augering (CFA) or displacement type drills. Once filled with stone, these columns can be

subsequently treated by Impulse Compaction to produce a more effective load bearing foundation. Using this drilling attachment, stone columns can be produced up to a depth of approximately 6–7 m. Either very coarse gravel can be used as a filling material in order to create a drainage effect or fine-grained material can be used for the opposite effect, to minimize waterways. The stone columns are usually struck with a 80 cm diameter foot. Then the last 1–2 passes are usually made with a larger diameter foot in order for the soil to better absorb the stress concentrations near the surface (Fig. 11). This enables a very economical grid spacing of the holes. More details of this method will be covered in the case studies.

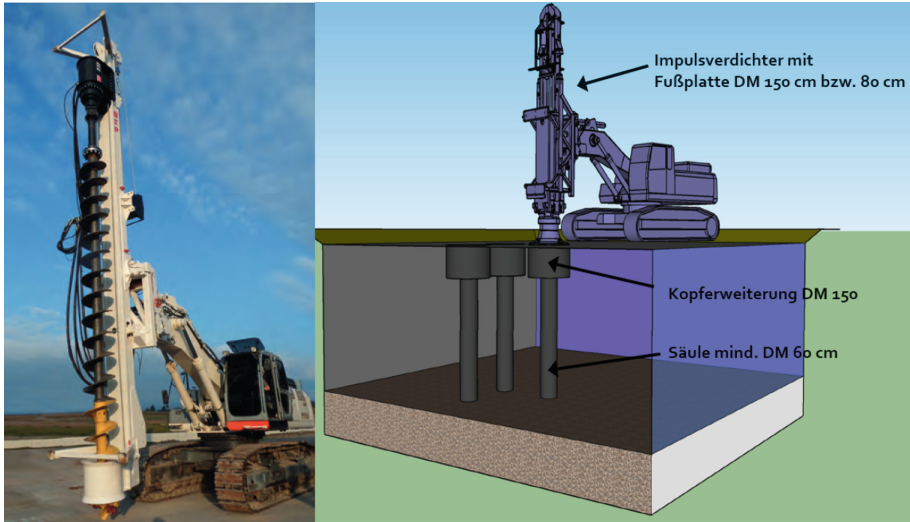


Fig. 11. Impulse compactor with drilling attachment (left); Impulse Compaction with 80 cm and 150 cm diameter feet after column infilling

4 Limits of Standard Impulse Compaction

Originally, Impulse Compaction was only intended for sandy and gravelly or mixed-grained soils, in which there can be a deep compaction effect of up to 7 m. In certain sandy soils in Northern Germany or in coastal areas in Southeast Asia, compaction depth effects of up to 9 m have been documented, using the common drop weight of 9 tonnes and the 1.5 m foot. A heavier drop weight and a larger foot diameter allow for a significantly higher compaction speed, but the soil improvement effect at depth is rather small. In certain fine-grained soils, the compaction effect at depth decreases to 4.0–4.5 m. Table 1 can be used as a guideline for the use of Impulse Compaction technology in various soil types. The following values describe general limits of Impulse Compaction application in soft soils:

- coefficient of water permeability (K_f -value): max 10^{-6} m/s
- silt (grain size < 0,063 mm) content: max 15%

As the soil becomes more fine grained (the yellow cells in Table 1), it generally becomes required to undertake a more thorough soil investigation in order to ascertain the suitability of Impulse Compaction for those soils. In clayey and organic soils, consideration of Impulse Compaction without any additional measures should be rejected from the outset.

Table 1. Guideline for application of Impulse Compaction in various soil types

Main group	General group	Abbreviation Group symbol	Replacement base layer System	Impulse Compaction Effective depth	Hybrid foundation System	RIC Stone columns without pre-drilling	RIC Stone columns with pre-drilling
Coarse-grained soil	Coarse gravel	cGr		max. 6-8 m			
Coarse-grained soil	Medium gravel	mGr		max. 6-8 m			
Coarse-grained soil	Fine gravel	fGr		max. 6-8 m			
Coarse-grained soil	Coarse sand	cSa		max. 7-9 m			
Coarse-grained soil	Medium sand	mSa		max. 7-9 m			
Coarse-grained soil	Fine sand	fSa		max. 7-9 m			
Mixed-grained soil	Silty gravel	siGr		max. 5-7 m		approx. 3m	approx. 5m
Mixed-grained soil	Gravelly silt	grSi		max. 4-7 m		approx. 3m	approx. 5m
Mixed-grained soil	Clayey gravel	clGr		max. 4-7 m		approx. 3m	approx. 5m
Mixed-grained soil	Silty sand	siSa		max. 4-7 m		approx. 3m	approx. 5m
Mixed-grained soil	Sandy silt	saSi		max. 3-6 m		approx. 3m	approx. 5m
Mixed-grained soil	Clayey sand	clSa		max. 4-5 m		approx. 3m	approx. 5m
Fine-grained soil	Silt	CSi		max. 3-5 m		approx. 3m	approx. 5m
Fine-grained soil	Silt	MSi, FSi				approx. 3m	approx. 5m
Fine-grained soil	Clay	Cl				approx. 3m	approx. 5m

technically possible
 technically eventually possible
 technically NOT possible

N.B.: The data apply for a 9t drop weight with

Ground water levels must also be taken into account with regard to Impulse Compaction suitability. In homogeneous coarse-grained soils, the ground water level has hardly any consequence for Impulse Compaction. For practical reasons, however, the ground water level should be at least 50 cm below the site working level; this enables, for example, the subsequent compaction of the surface with rollers. It should also be noted that during ram probe control tests of the compaction, results in non-cohesive soil below the ground water level can show as up to 50% lower than when dry due to the lower frictional resistance, and must therefore be corrected to be comparable to results above the ground water level. In silty soils, on the other hand, Impulse Compaction cannot be used if the ground water level is shallower than 5 m.

5 Documentation and Quality Control

For an Impulse Compaction soil improvement program to be considered successful, an increase in soil stiffness and the homogenization of the soil under individual foundations are required. In Europe, the soil stiffnesses are thus far mostly measured indirectly

with Dynamic Probing Heavy (DPH) (Fig. 12), but Cone Penetration Test (CPT) or Standard Penetration Test (SPT) can also be used. Sometimes, the soil improvement measurements are also carried out by means of geophysics, for example, Continuous Surface Wave (CSW) analysis or similar. DPH soundings, taken before and after Impulse Compaction, show the resulting increase in soil stiffness (Fig. 13). In [4], Yanulova presents an overview of over 27 projects and the effect of the impulse compaction in different soils.



Fig. 12. Performing DPH soundings in the Impulse Compaction field

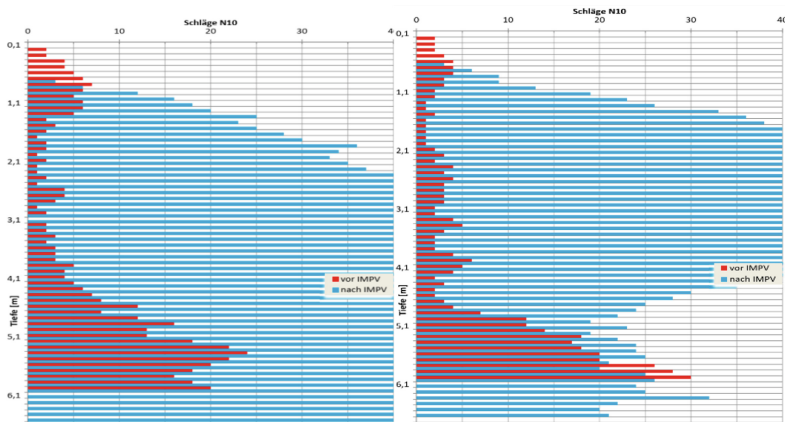


Fig. 13. Examples of DPH soundings before (red) and after (blue) Impulse Compaction (Color figure online)

While the heavy ramming probe (DPH) is the method mostly used for Impulse Compaction inspection and calibration in Europe, this method can sometimes lead to misinterpretations. This is why pressure probing (CPT) is becoming increasingly important

for this purpose, especially for larger projects, as it provides more reliable data. Another argument for the use of CPT in measuring soil stiffness is that it also records horizontal stress, and Massarsch has been pointing out for years that the increase in horizontal stress must be taken into account in this type of work [14]. This can lead to significantly more realistic and more favorable results in the settlement calculation.

In order to be able to prove a successful soil improvement program, an exact documentation of the effects on the soil is required. During soil compaction, the following data of each point can be recorded continuously and stored daily on the central server:

- local or transferred GPS coordinates (X, Y, Z) (with an assigned point ID)
- date and time
- number of compaction blows
- number of passes (if within certain criteria (depth, time, number of strokes) the desired target is not reached, the hole must be filled again and a new pass from the working plane must be started)
- the penetration depth into the ground per blow
- the total (summed) penetration depth per pass and per point (“Deep Total”)
- possibly also vibration and noise measurements

With the recording of these parameters, one of the most important tasks of Impulse Compaction can be verified directly: the homogenization of the subsoil. In practice, this means that every single point is worked on until the same “answer” from the ground can be documented in the form of the ‘Final Set’. Furthermore, the choice of the grid of compaction points, or the distance between points under individual or strip foundations, as well as the compaction plate diameter play a big role in the resulting quality of the Impulse Compaction program. These are usually determined beforehand in the geotechnical design according to empirical values and geotechnical calculations and later re-evaluated so that the soil mechanical properties such as stiffness and packing density are improved to the desired levels.

For quality control, the impulse compactor must be “calibrated” to each soil before starting work. This is done in a so-called “calibration field”, where a field of at least 3×3 points is defined on the construction site, and in which geotechnical investigations are first carried out. After the initial testing, the calibration field is compacted with the impulse compactor according to the preliminary geotechnical plan. Then the same geotechnical soil investigations are carried out again to determine soil improvement and to check that the required improvement has been reached. Depending on the results, the machine parameters are then confirmed or adjusted if necessary. These become the “stop codes”, as the on-board computer automatically stops the compaction work at that point once these parameters are reached.

After the calibration process, compaction can be rolled out over the entire construction site. Figures 14 and 15 show a resulting compaction plan and document sheet, respectively. Compaction quality control continues with regular checks using the investigation methods used in the calibration phase. The continuous recording and documentation of the machine parameters usually means a significant reduction in control testing.

While Impulse Compaction is in progress, simultaneous recording of vibrations on any neighbouring objects of concern can guarantee that the vibrations do not exceed

predefined values as the machine operator is alerted by mobile radio or similar when a threshold value is reached. In most cases when a threshold is reached, compaction can still continue by reducing the drop height or implementing other measures (see [6]).

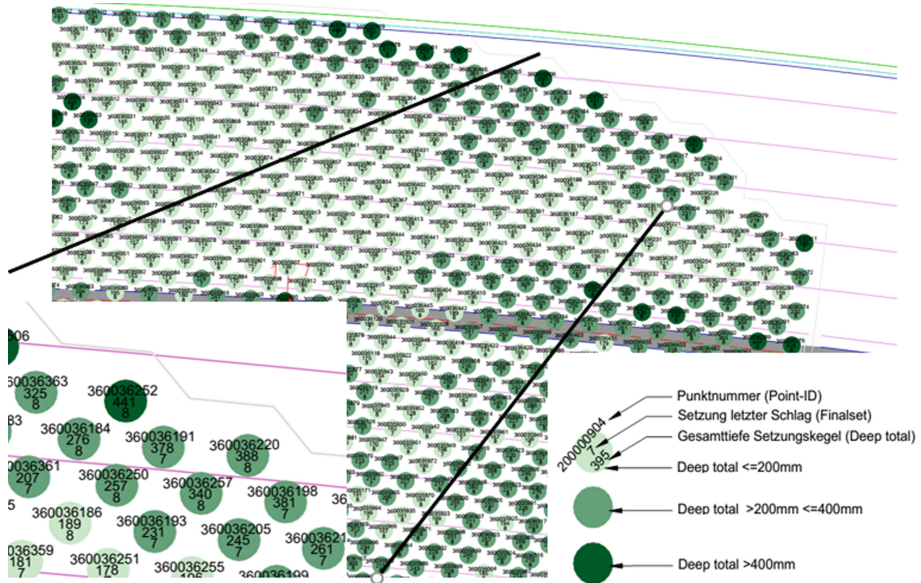


Fig. 14. Extract from a compaction plan after work

POINT-ID	POINT-DESCRIPT.	X	Y	DATE	BLO-WS	FIN.-SET	DEEP	DEEP-TOTAL	ENERGY	ST-CO	PASS	LAYER
360034430		-6915,44	32129,48	15.04.2014	31	8	385	385	269	S	1	IV_Flae
360034431		-6900,69	32128,44	16.04.2014	25	8	301	301	222	S	1	IV_Finis
360034432		-6917,4	32131,76	14.04.2014	26	7	314	314	225	S	1	IV_Flae
360034433		-6921,32	32136,3	12.04.2014	34	8	412	412	303	S	1	IV_Flae
360034434		-6919,36	32134,03	14.04.2014	24	8	298	298	200	S	1	IV_Flae
360034435		-6904,91	32128,74	16.04.2014	21	7	242	242	184	S	1	IV_Finis
360034436		-6906,86	32131,02	15.04.2014	28	7	294	294	240	S	1	IV_Finis
360034437		-6902,95	32126,47	16.04.2014	21	7	223	223	178	S	1	IV_Finis
360034438		-6902,64	32130,71	16.04.2014	20	8	238	238	177	S	1	IV_Finis
360034439		-6904,6	32132,99	15.04.2014	29	8	335	335	254	S	1	IV_Finis
360034440		-6913,2	32131,48	15.04.2014	29	9	356	356	246	S	1	IV_Flae

Fig. 15. Extract from a document sheet after work

6 Case Studies (from Construction Reports)

6.1 Breuninger Storage Hall in Sachsenheim, Germany

Project description:

For the erection of a new storage depot, a ground improvement was necessary. The ground consisted of a surface artificial filling, a layer of decalcified loess with insufficient bearing capacity and below a suitable load bearing layer of residual soil. For the foundation slab of the high bay warehouse, a maximum admissible angular displacement of 1:2000 had to be guaranteed.

Solution:

The layers of decalcified loess were bridged by pre-drilling gravel columns down to the layer of load bearing residual soil, both below the foot and the strip foundations (Fig. 16). Below the foundation slab of the high bay warehouse, a hybrid foundation system was implemented, where the Impulse Compaction craters were filled with graded material with grain sizes from 0 to 90 mm, and followed by three layers (each one 45 cm thick) of binding agent stabilized material.

Results:

The high stresses (from the high bay warehouse) on the foundations were successfully diverted into the subsoil using the systems described above.



Fig. 16. Impulse compactor with drilling attachment in Sachsenheim (left), and resulting gravel columns (right).

6.2 Jaguar Europe Center in Nitra, Slovakia

Project description:

In Nitra, for the Jaguar Land Rover's manufacturing plant, soil improvement measures were required in order to reduce the expected settlements and settlement differences of the foundation slabs considering the expected surface loads of up to 60 kN/m^2 .

The encountered soils below the topsoil (thickness between 0.20 m and 0.40 m) and down to a depth of between approximately 2.10 m to 5.30 m below the natural ground level were composed of deposits of sandy, clayey silts and silty, sandy clays with moderate to extremely high plasticity, stiff to very stiff consistency and light brown

to brown gray colors. These cohesive soils presented a relatively low bearing capacity and were followed by deposits of poorly graded gravels; sandy gravels; silty and clayey sands with medium dense state and brown gray color with a higher bearing capacity. These non-cohesive soils reached depth of 6.2 m and 11.3 m below the natural ground level and were followed by deposits of silty clays and sandy, clayey silts, with moderate to high plasticity, stiff to very stiff consistency and gray to brown gray colors followed by clayey, silty sands with medium dense state, with gray color.

Within predefined trial areas, 3 different soil improvement methods were tested. One of these measures was the Impulse Compaction in combination with gravel columns.

Trial testing of the Impulse Compaction in combination with gravel columns:

In elevation, the working level for the trial area was prepared with a 25 cm thick layer of crushed stone 0/125 mm. The soil improvement works within the trial area were carried out with Impulse Compaction in combination with gravel columns. The gravel columns were executed from the working level by drill holes, with a diameter of approximately 60 cm, prior to the Impulse Compaction. The material used for the columns was crushed stone 0/110 mm with a low quantity of fine grains (max. 5 M-% grains < 0.063 mm).

The trial area was divided into 4 equal sections, on which the following grids were executed:

1. Triangular grid with $3.22 \text{ m} \times 3.22 \text{ m} \times 3.22 \text{ m}$, with 72 compaction points (1 column for each 8.98 m^2);
2. Rectangular grid with $3.67 \text{ m} \times 3.67 \text{ m}$ and a finish point, with 85 compaction points, of which 49 primary and 36 finish compaction points (1 column for each 6.73 m^2);
3. Triangular grid with $2.686 \text{ m} \times 2.686 \text{ m} \times 2.686 \text{ m}$, with 104 compaction points (1 column for each 6.25 m^2);
4. Triangular grid with $3.67 \text{ m} \times 3.67 \text{ m} \times 3.67 \text{ m}$, with 52 compaction points (1 column for each 12.24 m^2).

The drill holes for each gravel column were carried out to a depth of approx. 4.30 m (the top edge of the non-cohesive soil layer, based on the observations made by TERRA-MIX Bodenstabilisierung GmbH on the first few drilling points). After the drilling for the column of a compaction point was completed, the borehole was filled with crushed stone 0/110 mm. The gravel columns were afterwards compacted with the impulse compactor (hammer with a diameter of 1.5 m). At least 2 passes were performed for each point. After each of the passes, the compaction craters were filled with crushed stone 0/110 mm once more and the next pass was carried out. This continued until the material filled after the last pass was compacted by means of a heavy roller.

To assure the quality of the performed works, the following termination criteria (stop codes) were defined during the execution works of the Impulse Compaction, and they had to be achieved in order to finalize one compaction point:

- Final settlement $\leq 10 \text{ mm}$;
- Total settlement $\geq 800 \text{ mm}$;
- Total number of blows ≥ 50 .

Thus, at least 2 passes were needed for each compaction point, resulting in the following statistics:

- Grid 1: 10 out of 72 compaction points needed 3 passes (86% of the compaction points with 2 changeovers and 14% of the compaction points with 3 passes).
- Grid 2: 15 out of 85 compaction points needed 3 passes (82% of the compaction points with 2 changeovers and 18% of the compaction points with 3 passes).
- Grid 3: 18 out of 104 compaction points needed 3 passes (83% of the compaction points with 2 passes and 17% of the compaction points with 3 passes).
- Grid 4: 3 out of 52 compaction points needed 3 passes (94% of the compaction points with 2 changeovers and 6% of the compaction points with 3 passes).

In total, 46 out of 313 compaction points needed 3 passes. Thus, 85% of the total compaction points were executed with 2 passes and 15% of the total compaction points were executed with 3 passes.

To analyze the effectiveness of the carried-out soil improvement works within the trial area, 8 cone penetration tests (CPT) were executed before carrying out the soil improvement measures, and 16 cone penetration tests with pore water pressure measurements were executed after carrying out the soil improvement measures.

Additionally, 8 dynamic probe heavy (DPH) were carried out within the gravel columns. The DPH results showed that the material within the gravel columns had a medium dense compactness (10 days after the execution of the gravel columns).

The CPT results were analyzed over their entire depth (approximately 7 m below the working level) and particularly within the length spanning the cohesive soil layer, which was the layer that had to be improved. The CPT results taken after the soil improvement measures were compared with the CPT results taken before the soil improvement measures, and the increases in soil stiffness were averaged into resulting improved stiffness moduli for the cohesive soil layer as well as resulting mean improvement factors for all CPT. Considering the position of the CPT relative to the columns, weighted mean improvement factors for the grid area for each soil improvement grid, as well as their mean improved stiffness moduli for the cohesive soil layer, were calculated. The following Table 2 contains the results of the analysis of the CPT results for the trial area.

Notations:

- E_{oed} ...initial stiffness modulus of the cohesive soil layer [MN/m²];
- q_{cB} ...cone tip resistance for the CPT-Before, mean value for the cohesive soil layer [MN/m²];
- q_{cA} ...cone tip resistance for the CPT-After, mean value for the cohesive soil layer [MN/m²];
- iE_{oed} ...improved stiffness modulus of the cohesive soil layer [MN/m²];
- f_i ...improvement factor [-].

Table 2. Analysis of the CPT results for the trial area

Position of the CPT relative to the gravel columns within the grid	Before		Improvement		
	q_{cB} [MN/m ²]	E_{oed} [MN/m ²]	q_{cA}/q_{cB} [-]	q_{cA} [MN/m ²]	iE_{oed} [MN/m ²]
Grid 1: Triangular 3.22 m × 3.22 m × 3.22 m (8.98 m ²)					
In the middle of the grid	1.37	7	1.21	1.65	8
Near the column	1.37	7	2.98	4.08	20
Mean improved stiffness modulus iE_{oed} [MN/m ²]:					11
Mean improvement factor f_i [-]:					1.57
Grid 2: Rectangular 3.67 m × 3.67 m + Finish (6.73 m ²)					
In the middle of the grid	1.28	6	1.04	1.33	7
Near the column	1.28	6	2.26	2.88	14
Mean improved stiffness modulus iE_{oed} [MN/m ²]:					11
Mean improvement factor f_i [-]:					1.66
Grid 3: Triangular 2.686 m × 2.686 m × 2.686 m (6.25 m ²)					
In the middle of the grid	1.10	5	1.30	1.43	7
Near the column	1.10	5	2.71	2.96	15
Mean improved stiffness modulus iE_{oed} [MN/m ²]:					9
Mean improvement factor f_i [-]:					1.72
Grid 4: Triangular 3.76 m × 3.76 m × 3.76 m (12.24 m ²)					
In the middle of the grid	1.19	6	1.21	1.45	7
Near the column	1.19	6	2.87	3.43	17
Mean improved stiffness modulus iE_{oed} [MN/m ²]:					9
Mean improvement factor f_i [-]:					1.52

The assessment of the improvement factors, as these resulted from the trial area tests, was done by relating the improvement factors to the grid areas. Additionally, these values were corrected by means of the resulted relation between the improvement factors and the grid areas (area allocated for one column – improvement point). The relation for the corrected improvement factor $corf_i$ is valid only for the grids of up to 20 m². Figure 17 presents the graphic representation of the mean corrected improvement factors and the measured improvement factors.

Solution and results:

Based on the trial area results, and depending on the expected surface loads on the different future foundation slabs, the soil improvement by means of Impulse Compaction in combination with gravel columns was carried out in different grids (Table 3).

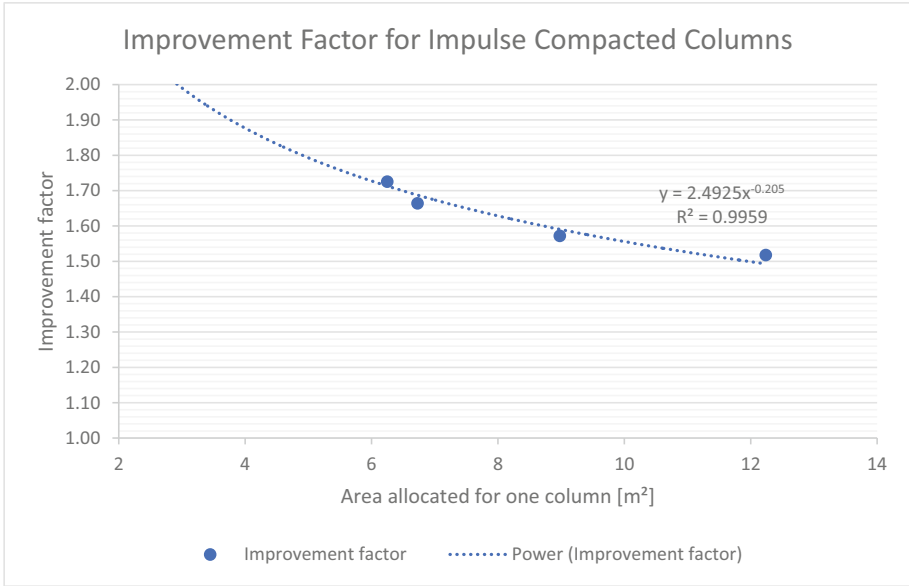


Fig. 17. Graphic representation of the mean corrected improvement factors and the measured improvement factors for the trial area.

Table 3. Carried-out soil improvement grids

Uniform load on the slab [kN/m ²]	Impulse compacted gravel columns (Ø ≥ 60 cm, down to the non-cohesive layer)	
	Rectangular grids [m × m]	Triangular grids [m × m × m]
20	3.8 × 3.8	4.08 × 4.08 × 4.08
30	3.25 × 3.25	3.49 × 3.49 × 3.49
50	2.6 × 2.6	2.79 × 2.79 × 2.79

A total of 38,544 impulse compacted gravel columns were carried out (Fig. 18). The success of the executed soil improvement works was confirmed by numerous cone penetration tests (CPT): 2 CPT (1 near the gravel column and 1 in the middle of the grid) for each 4,500 m².



Fig. 18. Four impulse compactors ready for use in Nitra, Slovakia

6.3 R76 Express Road in Hungary

Project description:

In late 2017, the European construction group STRABAG SE received the road construction contract for the R76 expressway from Zalaegerszeg to the Hollád junction on the M7 motorway. Swamp and bog areas along the planned route, which consist of soft silt and clay layers, were particularly challenging in this project and TERRA-MIX was brought in to improve the ground conditions.

Solution:

The solution for the extremely unfavourable conditions (groundwater just below the surface and very soft soils) was relatively simple: approximately 50 cm of coarse ballast, with particle sizes from 0 to 300 mm, was placed overtop and hammered into the ground by Impulse Compaction. The compaction points were in a $3\text{ m} \times 3\text{ m}$ grid using a 1.5 m diameter compactor foot. For the more than 1300 compaction points, an average of 2.6 passes per point was required. In the summer of 2019, TERRA-MIX was again commissioned to work on another section of the expressway. The aim was to improve the ground footprint for a planned bridge ramp approximately 140 m long and 40 m wide with similarly difficult ground conditions (Fig. 19). The following combination was used to accelerate the consolidation of the soil: vertical drains and gravel columns. Vertical drains with a depth of 10 m were placed in a grid of $3\text{ m} \times 3\text{ m}$. Pre-drilled impulse compactor gravel pillars were then constructed at the diagonal points. The diameter of the holes was 60 cm. These were filled with very coarse-grained material (particle size of 200 mm) and then compacted with the impulse compactor in several passes, using a 1.5 m diameter foot.



Fig. 19. Impulse Compaction ground improvement plan for a bridge ramp (left) and augering for gravel pillars (right)

6.4 Yogyakarta Airport

Project description (see as well [5, 15]):

The newly planned Yogyakarta Airport in Kulan Progo, Indonesia is only about 400 m away from the Indian Ocean and needed to be designed in such a way that it could withstand an 8.8 magnitude earthquake and 12 m high waves from a tsunami. The preliminary soil investigations revealed a loose to dense, very thin sand layer up to eight meters below ground level, as seen in Table 4, in a relevant area under the runway. This layer would need to be improved to meet the design requirements.

Solution:

The design of the Impulse Compaction work resulted in a triangular grid with compaction point spacing of 3.5 m for the primary pass and for the secondary pass, a grid which, due to geometry, contained twice the number of compaction points.

Results:

During the works, it turned out that in a few areas, at depths of 3 m to 5 m, the required SPT values according Table 5 were not quite met (after compaction) or, that after the secondary pass points were hit, there was a deterioration in the soil compaction between the compaction points. It was determined that the compaction points were situated too closely together. After the affected areas were remediated, the required values were met. Impulse Compaction work started on June 25th, 2018 and was able to be completed successfully and on time by August 31st, 2018, which means that an average daily output of nearly 2000 m² of improved soil area was achieved.

Table 4. Geological long section along main runway

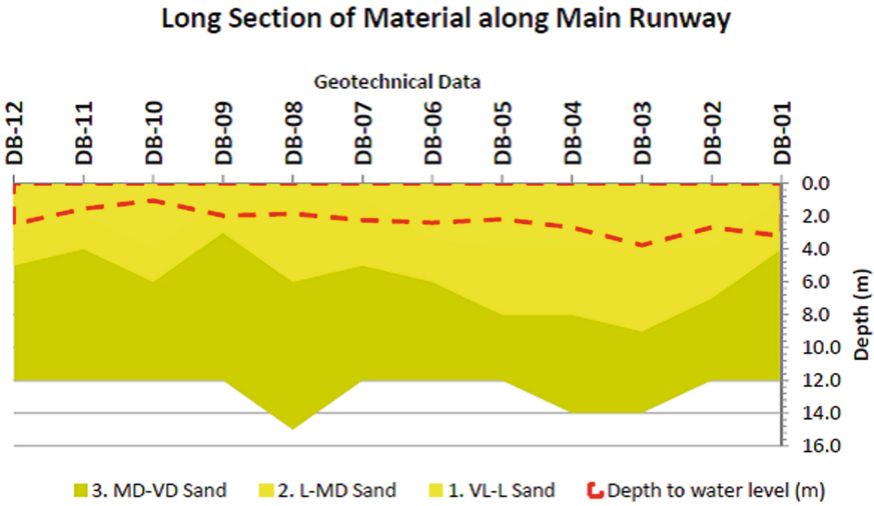


Table 5. Acceptance criteria for soil compaction:

Depth (m)	N-SPT	CPT – qc (MPa)	Dr (%)
2	16	7	> 70
4	22	9	> 70
6	26	13	> 70
8	30	15	> 70

Source: PT.PP

6.5 Runway Repair at Palu Airport After an Earthquake

Project description (see as well [5, 16]):

In autumn 2018, a terrible earthquake shook the island of Sulawesi, Indonesia, causing over 2000 people to lose their lives and causing enormous damage, not least in the provincial capital Palu, which was also hit by a tsunami up to six meters high. The runway at Palu Airport required immediate repairs. The high work speed of the Impulse Compaction method was a decisive factor in choosing it for the repair works. Flights continued operating during the soil compaction works. The affected runway was dug up in stages, and once the soil had been improved, the overlaying runway layers were immediately applied for that stage (Fig. 20).

After initially only working during the night for safety reasons, a work permit was issued after a few days to also work during the day, with the condition that the mast of the impulse compactor was folded down during plane take-offs and landings so as to not

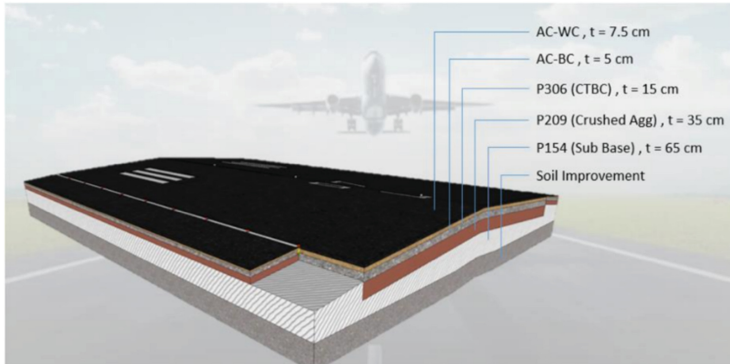


Fig. 20. Repair scheme for the suburban airport runway in Palu, Indonesia

irritate the pilot (Fig. 21). Only a month later, the construction site with about 35,000 m² of compacted subsoil was successfully handed over at the beginning of February 2019.



Fig. 21. RIC rig with mast folded down while a plane lands on the Palu airport runway

6.6 Flood Protection Dam

By means of the Impulse Compaction, a high water protection dam in Austria could be completely renovated and had the porosity and permeability of its embankment material reduced to those the in-situ layer of gravel below (Fig. 22). At the same time, the dam experienced an increase in its load carrying capacity and stability, leading to a further reduction of the danger of erosion. However, this process also meant a reduction in material volume so the client supplemented the dam with additional material and also had it widened.



Fig. 22. Impulse Compaction embankment improvements for a high water protection dam in Austria

7 Discussion/Conclusions

Impulse Compaction or RIC is now considered “state of the art” when it comes to economical solutions for soil improvement and homogenisation of non-cohesive soils. In its most basic application, the idea is to improve the ground, primarily the soil stiffness, such that it can support the structural loads with a shallow foundation only. This would help to avoid needing more expensive deep foundation solutions. Therefore, the geotechnical conception and calculation for Impulse Compaction are relatively simple, as improving soil stiffness is the main desired outcome. However, thorough preparatory work (including subsoil investigation) is still essential in order to undertake a successful Impulse Compaction program. An example of a common preparatory workflow is shown in Fig. 23.

This paper has shown that Impulse Compaction works very well in granular soils to reduce pore spaces and create a stiffer ground. In softer, more cohesive soils, it is also possible to work with this technology, but this requires more detailed preliminary investigations, a greater geotechnical understanding and the selection of an appropriate Impulse Compaction application or combination, such as the variant that combines Impulse Compaction with predrilled stone columns. The calculation and verification

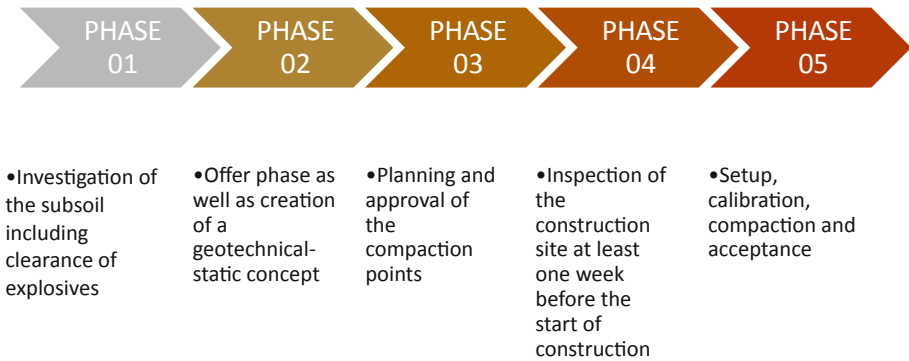


Fig. 23. The work flow before the job on the site

of the Impulse Compaction method can be carried out analogously to the recognized method of Priebe [13], which is often used for the dimensioning of vibro compaction.

An interesting aspect of Impulse Compaction is that the soil is usually reduced in volume as a result of the compaction. This can lead to additional savings in the cost of excavating a construction pit, especially if the material is contaminated but compactable.

Finally, the noise and vibration of the Impulse Compaction method do not necessarily exclude it from ground improvement choices in sensitive areas. It is important to know the country-specific regulations and to take the correct precautionary measures. A problem-solving mindset may also find solutions before a problem comes up. For example, in the construction of a building with a planned future expansion, an extra 10–20 m wide strip can be pre-compacted in the direction of the planned expansion so that future compaction work does not have to be undertaken close to the existing building.

In conclusion, Impulse Compaction has already established itself as a particularly economical method for improving medium-deep soils. Looking forward, current ongoing research into noise and vibration reductions, into a more direct determination of the improved soil stiffness, and into a reduction of the system's weight will likely find innovations to make Impulse Compaction even more attractive as a soil improvement method.

References

1. Adam, D., Herrmann, R.A.: Vortragsband Baugrundverbesserung in der Geotechnik. In: Symposium TU Siegen, s.111–176. Eigenverlag (2010)
2. Adam, D., Paulmichl, I.: Rapid impact compactor – an innovative dynamic compaction device for soil improvement. Improvement of Soil Properties, Bratislava, 4–5 June 2007 (2007)
3. Bißmann, M.: Die Impulsverdichtung- eine wirtschaftliche und ökologische Alternative in der Bodenverbesserung. In: Baugrundverbesserung Méthodes de confortation en géotechnique 170 MITTEILUNGEN DER GEOTECHNIK SCHWEIZ, s. 77–88. Frühjahrstagung vom 7 Mai 2015 Luzern (2015)
4. Yanulova, D.: Master Thesis Auswertung und Interpretation von Messdaten zur Erfassung des Verdichtungserfolgs (2015)

5. Bißmann, M.: DIE IMPULSVERDICHTUNG IM EINSATZ IN ERDBEBENREGIONEN IN INDONESIA. In: D-A-CH Tagung Erdbebeningenieurwesen & Baudynamik (D-A-CH 2019) am 26. und 27. September 2019 Universität Innsbruck (2019)
6. Przemysaw Dobrzycki et al.: J. Phys.: Conf. Ser. 1425 012202 (2019)
7. Herbut, A.: The efficiency of an active generator in the case of a deep foundation location. Stud. Geotech. Mech. **39**(1), 3–12 (2017)
8. Kristiansen, H., Davies, M.: Ground improvement using rapid impact compaction. In: 13th World Conference on Earthquake Engineering, Vancouver, BC, 1–6 August (2004)
9. Becker, P.J.: Assessment of rapid impact compaction for transportation infrastructure applications. Graduate Theses and Dissertations. 10261 (2011). <https://lib.dr.iastate.edu/etd/10261>
10. Faun Trackway (2020). Rapid Runway Repair. Faun MV Ltd. <https://fauntrackway.co.uk/defence/aviation/rapid-runway-repair>. Accessed Okt. 2020
11. Serridge, C.J., Synac, O.: Application of the rapid impact compaction (RIC) technique for risk mitigation in problematic soils. In: Proceedings of IAEG2006, London, Paper No. 294 (2006)
12. Braithwaite, E.J., du Preez, R.W.: Rapid impact compaction in Southern Africa. In: Proceedings of the Conference on Geology for Engineering, Urban Planning and the Environment. South African Institute of Engineering Geologists, 13–14 November 1997 (1997)
13. Priebe, H.: Die Bemessung von Rüttelstopfverdichtungen. Die Bautechnik **72**(3), 183–191 (1995)
14. Massarsch, K.R., Fellenius, B.H.: Deep compaction of sand causing horizontal stress change. In: Geotechnical Engineering Journal of the SEAGS and AGSSEA, June 2020, vol. 51, no. 2, pp. 9–21 (2020). (ISSN 0046–58289)
15. <http://www.vantage-commerce.com/portfolio-item/ric-nyia>. Accessed December 2020
16. <http://www.vantage-commerce.com/portfolio-item/ric-palu>. Accessed December 2020



A Preliminary Laboratory Study of Fatigue Performance of Geogrid-Reinforced Asphalt Beam

Tom Darzins, Hangyu Qiu, and Jianfeng Xue^(✉)

School of Engineering and IT, University of New South Wales, Canberra, ACT, Australia
jianfeng.xue@adfa.edu.au

Abstract. Geogrid has been used widely as reinforcement in asphalt layer to reduce reflective crack. However, the effectiveness of glass-fiber geogrid reinforcement on the fatigue life of asphalt layer has not been fully understood. This paper presents an initial experimental study to investigate the loading behavior of unreinforced asphalt beam and the geogrid benefits on asphalt beam for comparison, which could contribute to the quantification of the benefits of using geogrids within asphalt layers. A number of four-point cyclic loading tests were performed on geogrid-reinforced asphalt beams to investigate their fatigue performances. Results demonstrated a detrimental impact of overloading that could significantly affect the fatigue life of pavement system and a beneficial effect of geogrid reinforcement on asphalt beam. These results will be used to further explore the quantification of the geogrid benefits within asphalt layers and the reinforcement mechanism.

Keywords: Glass-fiber geogrid · Asphalt beam · Fatigue performance · Four-point bending test

1 Introduction

Since early 1980s, researches of geogrid-reinforced asphalt layers have commenced (Brown et al. 1985; Brown et al. 2001). The main purpose of installing geogrids in asphalt layer is to increase resilience of pavement, which could lead to the extension of its life of service or reduction of pavement thickness. (Zofka and Maliszewski 2019). Specifically, geogrid can provide the following two excellent features to improve the performance of flexible pavements (Al-Qadi et al. 2008; Al-Qadi et al. 2009; de Bondt 2000). Firstly, geogrid can provide reinforcement, which means the improvement in the shear and tensile strength of asphalt layers for the reduction in permanent deformations (rutting) and differential settlement. Secondly, stress relief and strain absorption are also significant features of it in order to mitigate reflective cracking and fatigue cracking.

Considerable amount of research has been conducted on the practical use of geogrid reinforcement in flexible pavements. For example, geogrid can be used for reinforcing the subgrade and subbase or used at the soil-asphalt interface (Arsenie et al. 2017), and

it can also extend the design life of asphalt pavements on airport runways, taxiways and aprons as an asphalt interlayer (Penman and Hook 2008). However, it should be noted that while considering geogrid reinforcement in a pavement structure, one has to differentiate between products installed within asphalt layer or within unbound layer. Both locations are within pavement structure but require different properties, and geogrids would serve different purposes (Zofka et al. 2017). This paper is focusing on geogrid installed within asphalt layer.

It is should be emphasized that many research outcomes of geogrid used within asphalt layer are generally displayed qualitatively as “good” or “improved”. Wathugala et al. (1996) has investigated and measured the geogrid performance using FEM (finite element method) analysis by ABAQUS, the outcomes of which indicate that placing geosynthetic reinforcement at the soil-asphalt interface can lead to the highest reduction of the tensile fatigue strain by 46–48%. However, this does not necessarily directly translate to the same improvement when used as an asphalt interlayer. In addition, the geogrid reinforcement cannot be directly simulated in pavement design with current engineering software.

Therefore, it is necessary to characterize and quantify the benefits of using geogrids within asphalt layers. This article presents as a preliminary study to achieve the above goal. A number of four-point cyclic loading tests were performed on asphalt beams reinforced with glass-fiber geogrids of different tensile strengths. The objective of this initial experimental study is to investigate the loading behavior of unreinforced asphalt beam and the effects of geogrid reinforcement on the fatigue life of asphalt beam used in local road services in Australia.

2 Methodology

2.1 Materials

The square-meshed geogrids with woven composites used in the present study are provided by Nantong Dingfeng New Materials Co., Ltd. All glass-fiber geogrids were cut into rectangles in accordance with the relevant standard AS3706.1 (Austroads 2012), with dimensions at least 10mm larger in each dimension than the asphalt beams to which the geogrid was to be attached to and ensuring that each rectangle had three longitudinal strips of reinforcement weave. Ormonoid Bitumen Paint was used as the adhesive to bond the geogrid to the asphalt and as an analogue to industrial tack coat used in road construction. As indicated by Zofka et al. (2017), geogrids should be installed in the tension zone below the neutral axis, all geogrid sheets in this study were placed at the depth of 50 mm (tension zone) in the asphalt samples as interlayers. A photo of adopted geogrid models can be seen in Fig. 1. The detailed parameters of the adopted geogrid models (GG40, GG60 and GG80) are shown in Table 1.

The asphalt mix used in this study is prepared at the Downer Group laboratory in Hume, ACT. The particle size distribution of the aggregates used in the asphalt mix is presented in Fig. 2. Bitumen binder content is about 5.4%. To prepare asphalt beam samples, wood moulds were used with the dimension of $390 \times 571.5 \times 50 \text{ mm}^3$. Hot asphalt was poured into the moulds and then immediately compacted with a Crommelins CC60R compactor in accordance with the standard AST05 and AS 1012.8.2 (Austroads

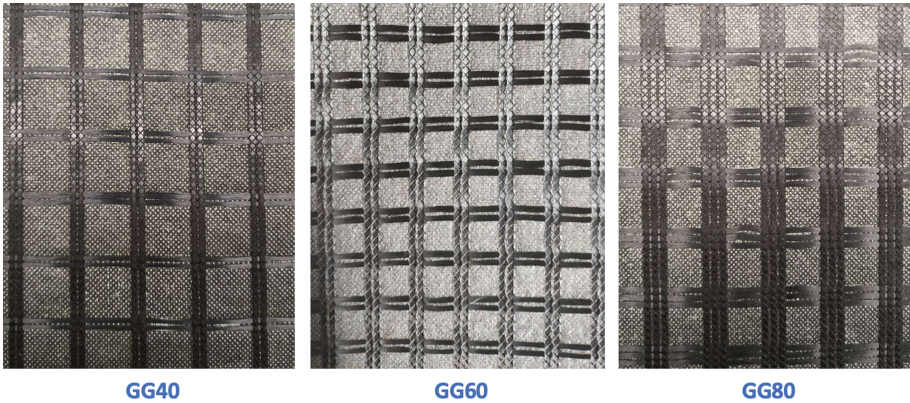


Fig. 1. Photo of geogrid models used in the present study.

Table 1. The characteristics of glass-fiber geogrids used in the tests.

Model	Breaking strength (kN/m)		Elongation at break (%)	
	Longitudinal	Transverse	Longitudinal	Transverse
GG40	40	40	4	4
GG60	60	60	4	4
GG80	80	80	4	4

2012). Subsequently, the asphalt slabs were left to rest for 24 h and removed from the moulds. The slabs were cut into $390 \times 63.5 \times 50 \text{ mm}^3$ beams using a masonry saw. As the beams were cut from the slabs created using the same materials and technique. The densities of the beams had good consistency and reasonably low standard deviations among the beam samples. To further ensure the consistency of the samples, the difference in air-void contents of the slabs need to be mitigated, it can be achieved by adjusting the modulus of elasticity according to the research of Steiner, Hofko, and Blab (2016). Thus, the homogeneity of all slab samples can be guaranteed.

The bitumen paint was then applied with a paint brush on the surface of the asphalt beams and the geogrid was installed on the top. Weights were placed on the geogrid to maintain pressure on the surface to help promote the cooperation with adjacent asphalt beams. Weights were removed after 24 h and then the beams were allowed a further 48 h of air dry.

2.2 Test Methods

The four-point cyclic loading tests were performed using an Instron 8033 fatigue testing system as depicted in Fig. 3. Loading is applied as a sine wave with a frequency of 2 Hz, the controlled maximum load can be set to the desired loading level, and the loading cycles have a minimum value of 10N in all tests to prevent the machine from losing

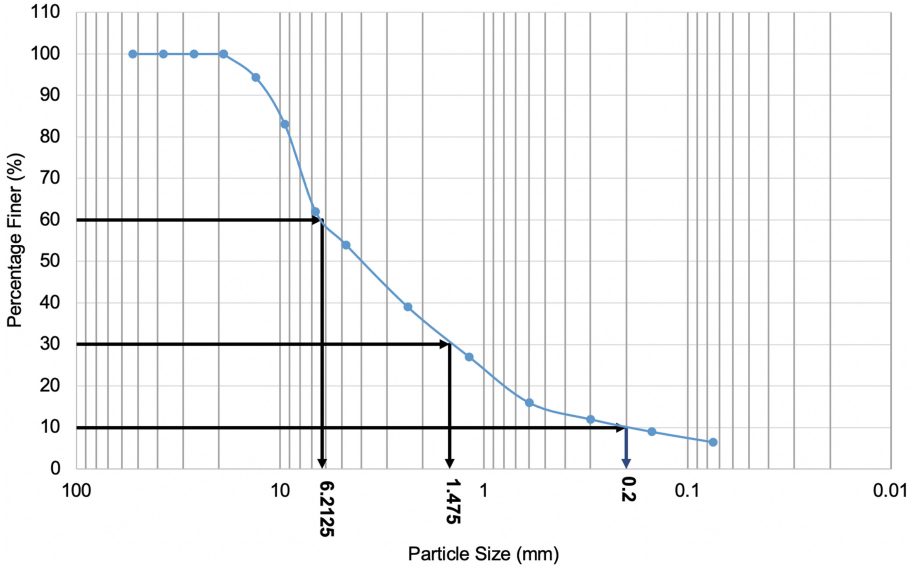


Fig. 2. Particle size distribution of the aggregate used in the asphalt mix.

contact with the sample and moving the beam during the test. Prior to beginning cyclic loading, the load is linearly ramped from zero to half of the maximum load level. All experimental tests were conducted indoors at 23 °C.

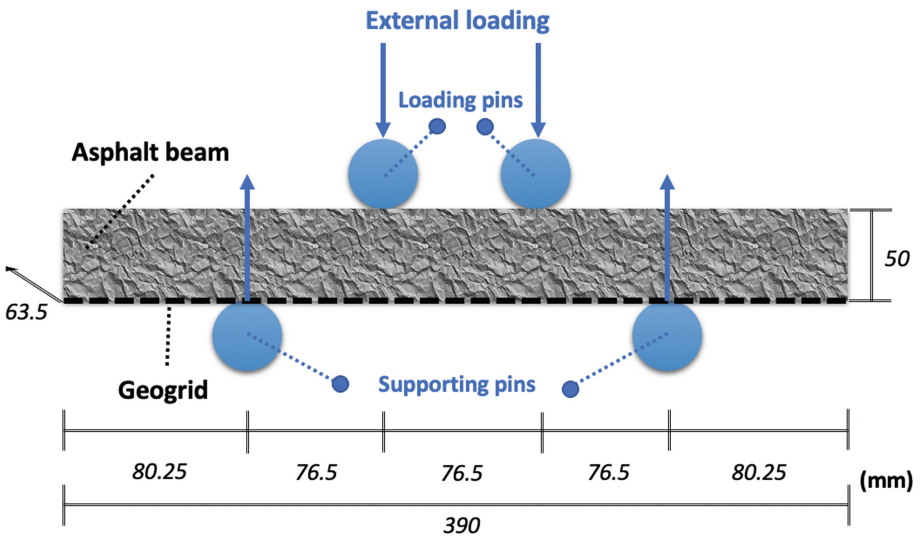


Fig. 3. Schematic of an asphalt beam sample placed in a four-point bending machine.

An initial test with static loadings was conducted to find the static failure load of the unreinforced asphalt beams, the result of which is 450N. Accordingly, three cyclic loading levels with the maximum load of 270N, 450N and 540N respectively, were determined to be used in further tests to study the effects of load level on the fatigue life of the samples. The corresponding stress ratios (maximum cyclic load/static failure load) calculated for different groups of tests are 60%, 100% and 120%. The testing IDs for all test cases in this study can then be determined in accordance with stress ratios and types of geogrids, as presented in Table 2.

Table 2. Testing cases used in the experiments, value of 0 in geogrid tensile strength indicates no geogrid is attached on the corresponding asphalt specimen.

Testing ID	Applied load (N)	Stress ratio	Geogrid tensile strength (kN/m)
Static load test	450	N/A	0
60-g0	270	60%	0
60-g40	270	60%	40
60-g60	270	60%	60
60-g80	270	60%	80
100-g0	450	100%	0
100-g40	450	100%	40
100-g60	450	100%	60
100-g80	450	100%	80
120-g0	540	120%	0

The deflections of the asphalt beam samples under loadings were measured with a custom brace and two LVDTs. The LVDTs were attached to the beam and measured the movement of the brace as it moved with the deflecting beam. The adopted LVDTs here are Micro-Epsilon DTA-10G-1.5-CA models. The average value of the LVDT readings was used to represent the middle-span deflection of the asphalt beam.

3 Results and Discussions

3.1 Loading Behavior of Unreinforced Asphalt Beams

Figure 4 shows the increment of the deflection at the middle span of the beams with increasing loading cycles. The results point out that under the same loading cycles, the deflection of the beams increases dramatically with higher stress ratios. Virgili et al. (2009) pointed out that a fatigue process includes two phases, namely hardening and damage. It has been confirmed by many researchers that the failure point of a fatigue curve is the point where the evolution curve changes geometry, indicating a phase shift (Bognacki et al. 2007; Charmot et al. 2005; Roberts et al. 1991; Van Dijk 1975). To determine the fatigue life of a beam, the number of load cycles for the deflection and loading

cycle curve to reach a flex point is considered as the failure criterion. An example graph of the flex point can be seen in Fig. 5(a), and the second derivative of the deformation curve is shown in Fig. 5(b). The minimum point shown in Fig. 5(b) represents the flex point.

Using the method described, the number of loading cycles to fatigue failure and the deflection at fatigue failure can be determined for the asphalt beams with no geogrid installed and the results are summarized in Table 3. It shows that for the fatigue life of asphalt beams increases with the applied loading level. However, the deflections of the beams with the stress ratio of 60% and 100% are almost the same, which are both slightly less than 6mm. In comparison, when the stress ratio reaches to 1.2, the fatigue life of asphalt beam becomes much shorter and the deflection at failure is much less at about 3mm. This observation supports that overloading is a major factor that affects the fatigue life of pavement system. Also, as shown in Fig. 6, a linear correlation can be seen between the fatigue life of unreinforced asphalt beam and the stress ratio. A further investigation can be conducted to testify whether it can be a universal method for characterizing the fatigue behaviour of the reinforced asphalt beams.

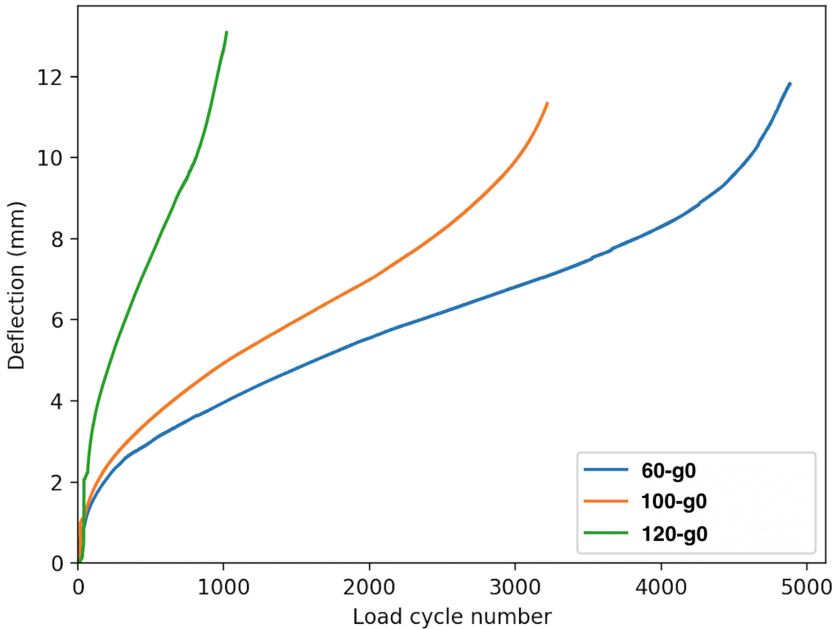


Fig. 4. Deflections of unreinforced beams with varying stress ratios.

3.2 Effect of Geogrid Strength on Fatigue Life

Changes in fatigue life of the asphalt beams reinforced with geogrids of different strengths are presented in Fig. 7. The figure demonstrates that the fatigue life of asphalt beams can be extended exponentially with stronger geogrid installed, regardless of applied loading level.

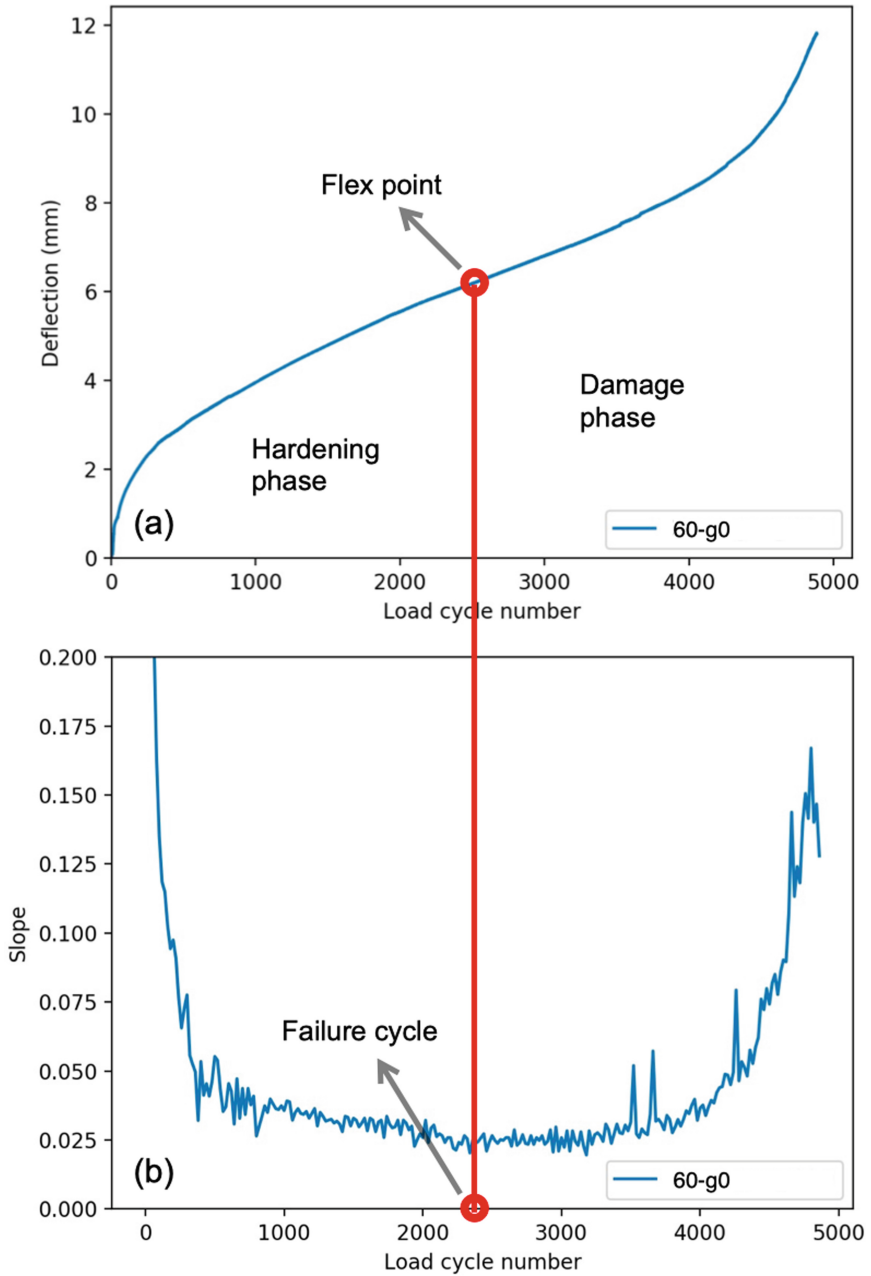


Fig. 5. Determination of flex point: (a) deflection of the unreinforced beam under the stress ratio of 60%; (b) second derivative of the deflection curve.

Table 3. Fatigue life and deflection at failure point of unreinforced asphalt beams.

Testing ID	Fatigue life	Deflection at failure (mm)
60-g0	2381	5.95
100-g0	1504	5.91
120-g0	537	2.99

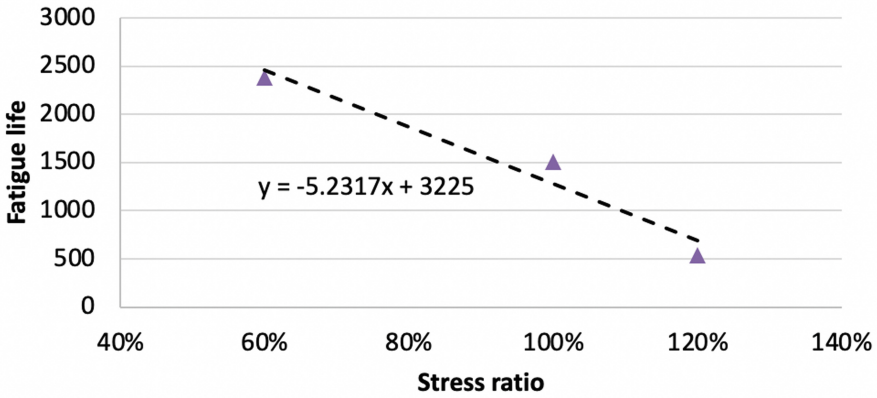


Fig. 6. Fatigue performance of unreinforced asphalt samples under varying loadings.

As displayed in Table 4, note that the life extension rate at a given stress ratio is calculated by the fatigue life of reinforced asphalt beam (g40, g60 or g80) divided by the corresponding fatigue life of unreinforced asphalt beam (g0). Under the stress ratio of 60%, it can be observed that the fatigue life of the beam reinforced with GG40 is about 4 times the beam sample with no geogrid reinforcement. When the strength of geogrid doubles (GG80), the fatigue life of the reinforced beam increases by more than 10 times. While under greater loading level (stress ratio of 100%), the inclusion of lower strength geogrid is not as effective as higher strength of geogrid. It can be observed that under the stress ratio of 100%, including GG40 only increases the fatigue life of the beams by about 50%, but including GG80 could increase the fatigue life of the beams by approximately 7 times. This suggests that when overloading is anticipated over the life span of a road, using geogrid of higher strength could be more efficient in improving the fatigue life of asphalt pavement.

This research presents some correlations based on the experimental data to help quantify the effects of geogrid. However, it is worth mentioning that other geogrid factors, such as mesh shape and size, will also affect the enhancement capability of geogrid on pavement fatigue life. Additional variables such as dependency on the type of asphalt mix the geogrid is bonded to and the depth of the overlaying asphalt layer are likely to affect the effectiveness of the geogrid. Although the suitability of geogrid for improving pavement life has been shown from the results of this study, further research

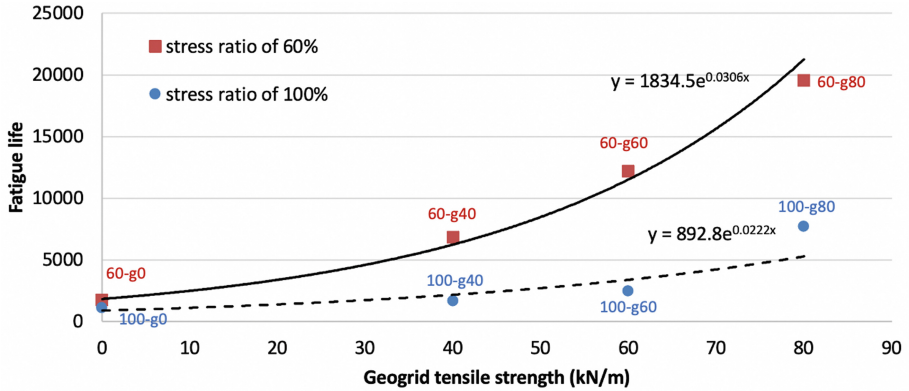


Fig. 7. The number of bearing load cycle until failure as a function of geogrid breaking strength with the loading of 270N and 450N.

Table 4. Extension of fatigue life for geogrid-reinforced asphalt beams.

Testing ID	Life extension rate	Testing ID	Life extension rate
60-g0	1	100-g0	1
60-g40	3.92	100-g40	1.51
60-g60	7.03	100-g60	2.20
60-g80	11.27	100-g80	6.97

into the confirmation of the correlation presented is expected to be conducted to include other factors that can affect pavement life.

4 Summary

This paper serves as a preliminary study of geogrid-reinforced asphalt beams with the overall goal of characterizing and quantifying the benefits of using geogrids within asphalt layers. A number of four-point cyclic loading tests were performed on the asphalt beams with and without geogrid reinforcement installed at the depth of 50mm for the purpose of comparison.

As the preliminary results, the following observations are presented in this paper:

- Overloading is a major factor that affects the fatigue life of pavement system without geogrid reinforcement.
- A linear correlation can be seen between the fatigue life of unreinforced asphalt beam and the stress ratio.
- The presence of geogrid does improve the fatigue life of asphalt beams, with the increasing tensile strength of geogrid, the beam fatigue life could increase exponentially.

- Applied loading level can impact the effectiveness of asphalt reinforcement, higher stress ratio can lead to the reduction in the fatigue life of asphalt beam with the same geogrid installed.
- Under greater loading level, lower strength geogrid may not be as effective as higher strength of geogrid, which indicates that using geogrid of higher strength could be more efficient in improving the fatigue life of asphalt pavement at the regions prone to overloading.

The results presented are limited to the glass-fiber geogrid used in the present study considering the shape and mesh size of geogrid would also affect fatigue life of asphalt beam. Therefore, the effects of these geogrid factors together with other parameters that can potentially affect the benefits of using geogrids within asphalt layers can be considered for the future testing in order to help build the quantification model of geogrid benefits.

Acknowledgement. The authors acknowledge the UNSW staff and Technical Support Group, in particular Mr James Baxter and Mr Umesh Kaini for preparing the samples and performing the tests. It is also appreciated for the help of Mr Ryan Burgin and Mr Sam Sarris staff from Downer Group, ACT in preparing the asphalt slabs. The project received funding from the ARC Industrial Transformation Research Hub Project Grant - IH180100010 (Project No. IH18.09.1) in collaboration with Fujian Yonking Geotechnical.

References

- Al-Qadi, I., Morian, D., Stoffels, S., Elseifi, M., Chehab, G., Stark, T.: Synthesis on use of geosynthetics in pavements and development of a roadmap to geosynthetically-modified pavements. Federal Highway Administration, McLean, VA, Report No. FHWAHRT, pp. 1–195 (2008)
- Al-Qadi, I.L., Buttlar, W., Baek, J., Kim, M.: Cost-effectiveness and performance of overlay systems in Illinois volume 1: effectiveness assessment of HMA overlay interlayer systems used to retard reflective cracking (2009)
- Arsenie, I.M., Chazallon, C., Duchez, J.-L., Mouhoubi, S.: Modelling of the fatigue damage of a geogrid-reinforced asphalt concrete. *Road Mater. Pavement Des.* **18**(1), 250–262 (2017)
- Austrroads: geotextiles - methods of test. In: Part 1: General requirements, sampling, conditioning, basic physical properties and statistical analysis: Standards Australia (2012)
- Bognacki, C.J., Frisvold, A., Bennert, T.: Investigation of asphalt pavement slippage failures on runway 4R-22L, Newark International Airport. Paper presented at the 2007 Worldwide Airport Technology Transfer Conference Federal Aviation Administration American Association of Airport Executives (2007)
- Brown, S., Brunton, J., Hughes, D., Brodrick, B.: POLYMER GRID REINFORCEMENT OF ASPHALT (WITH DISCUSSION). Paper presented at the Association of Asphalt Paving Technologists Proceedings (1985)
- Brown, S., Thom, N., Sanders, P.: A study of grid reinforced asphalt to combat reflection cracking (with discussion). *J. Assoc. Asphalt Paving Technol.* **70**, 543–571 (2001)
- Charmot, S., Romero, P., Dunning, M.: Forensic analysis of slippage cracking. In: Paper presented at the Proceeding of the 84th TRB annual meeting. Washington (2005)
- de Bondt, A.: Effect of reinforcement properties. In: Paper presented at the Proceedings of the 4th RILEM Conference on Reflective Cracking, Ottawa (2000)

- Penman, J., Hook, K.: The use of geogrids to retard reflective cracking on airport runways, taxiways and aprons (2008)
- Roberts, F.L., Kandhal, P.S., Brown, E.R., Lee, D.-Y., Kennedy, T.W.: Hot mix asphalt materials, mixture design and construction (1991)
- Steiner, D., Hofko, B., Blab, R.: Effect of Air void content and repeated testing on stiffness of asphalt Mix specimen. In: Paper presented at the Civil Engineering Conference in the Asian Region (2016)
- Van Dijk, W.: Practical fatigue characterization of bituminous mixes. *J. Assoc. Asphalt Paving Technol.* **44**, 38–72 (1975)
- Virgili, A., Canestrari, F., Grilli, A., Santagata, F.: Repeated load test on bituminous systems reinforced by geosynthetics. *Geotext. Geomembr.* **27**(3), 187–195 (2009)
- Wathugala, G.W., Huang, B., Pal, S.: Numerical simulation of geosynthetic-reinforced flexible pavements. *Transp. Res. Rec.* **1534**(1), 58–65 (1996)
- Zofka, A., Maliszewski, M.: Practical overlay design method for geogrid reinforcement of asphalt layers. *Road Mater. Pavement Des.* **20**(sup1), S163–S182 (2019)
- Zofka, A., Maliszewski, M., Maliszewska, D.: Glass and carbon geogrid reinforcement of asphalt mixtures. *Road Mater. Pavement Des.* **18**(sup1), 471–490 (2017)



Low Temperature Crack Resistance of Recycled Asphalt Mixture with Waste Frying Oil Based on Semi-circular Bending Test

Yingbiao Wu^{1,2}, Jinjin Shi^{1,2}(✉), Yu Zhang^{1,2}, and Jinyan Liu^{1,2}

¹ Cangzhou Municipal Engineering Company Limited, Cangzhou 061000, China

² Hebei Province Road Materials and Technology Engineering Technology Research Center, Cangzhou 061000, China

Abstract. Using AC-20 asphalt mixture (Nominal maximum size 19 mm), the semi-circular bending test of recycled asphalt mixture with different amounts of waste frying oils rejuvenators, were conducted and compared with the virgin asphalt mixture. The test results show that the fracture energy of recycled asphalt mixture increased significantly when a waste frying oil rejuvenator was added. When the RAP (reclaimed asphalt pavement) contents were between 30% and 40%, and the rejuvenator contents were between 10.5% and 12.5%, the fracture energy of recycled asphalt mixture can be restored to 62%–72% of that of the virgin asphalt mixture. Therefore, it demonstrated that the waste frying oil rejuvenator was able to effectively improve the low-temperature crack resistance of the recycled asphalt mixtures.

Keywords: Semi-circular bending test · Waste frying oil · Reclaimed asphalt mixture · Low-temperature crack resistance

1 Introduction

In recent years, China's asphalt pavement construction has entered a large-scale rehabilitation and maintenance stage, which produces a large amount of reclaimed asphalt mixture (RAP) annually. Among these, about 5% is aging asphalt and 95% are various grades of aggregates. When RAP is treated as garbage waste, it will occupy land and pollute the environment [1]. The key to recycled asphalt pavement technology is to ensure road performance, which is inseparable from the development and application of asphalt rejuvenator. Waste cooking oil is a general term for all kinds of inferior oils and fats, mainly including three types: first, oil made by simply refining and processing the greasy floats in sewage or the leftovers from hotels and restaurants, as well as leftovers (commonly known as slops); the second is the oil extracted and processed from animal offal and inferior meat; third, the oil used for frying food is reused or re-used after some new oil is added after it has been used more than the prescribed requirements [2–4]. The third waste cooking oil, namely waste frying oil, is mainly composed of triglycerides and contains a large number of fatty acids, which is similar to the oil in asphalt and

can adjust the components of asphalt to achieve the purpose of regeneration [5, 6]. It is feasible to be used as an asphalt rejuvenator.

To evaluate the effect of waste frying oil on the regeneration of aged asphalt, it is necessary to study their performances in the laboratory. Low-temperature crack resistance is one of the important road performances of asphalt mixtures. With cracking, moisture will enter the asphalt mixture and deteriorate the roadway pavement structure. The repetitive traffic loading will accelerate the destruction of the roadway pavement structure that leads to a decrease in pavement service life. The main objective of this paper is to study the low-temperature crack resistance of waste frying oil reclaimed asphalt mixture. Different amounts of waste frying oils were added as a rejuvenator to the RAP and remixed with new mineral materials and base asphalt to prepare recycled asphalt mixture. Through Semi-Circular bending (SCB) tests, this paper explores the low-temperature crack resistance of waste reclaimed asphalt mixture rejuvenated by waste frying oil.

2 Test Raw Materials

2.1 Waste Frying Oil Rejuvenator

The waste frying oil used in the study was treated by a company and its technical indicators such as density, viscosity, moisture, and volatile matter are shown in Table 1. It can be seen from the test results that the waste frying oil has a high flash point, low viscosity, low moisture, and volatile content. Those properties meet the technical index requirements of “Highway Asphalt Pavement Recycling Technical Specification” (JTG/T 5521-2019) [7] and can be used as an asphalt rejuvenator.

Table 1. Performance test results of waste frying oil rejuvenator

Project	Test results	Experiment method [8, 9]
Appearance and state	Yellowish-brown liquid, uniform surface, no delamination	Observed
Density at 15 °C (g/cm ³)	0.909	JTG E20 T0603
Brookfield viscosity at 20 °C (Pa·s)	0.058	JTG E20 T0625
Flash point (°C)	242	JTG E20 T0611
Moisture and volatile matter (%)	0.06	GB 5009.236
Quality changes before and after the film oven test (%)	0.43	JTG E20 T0609
Viscosity ratio before and after film oven test	2.72	

2.2 Rap

The RAPs used in the study were recovered from the upper layer of a road project. The milling depth was about 2–3 cm. The upper layer construction of the project was completed in September 2007 with AC-13 asphalt mixture, and asphalt binder using Binzhou No. 70 road asphalt. RAPs were sampled in quarters, using an asphalt analyzer and a rotary evaporator, and recovering pure old asphalt through extraction, centrifugal separation, and distillation. The asphalt content was found to be 4.6%. The material properties of the recovered old asphalt are shown in Table 2. The comparison of the RAP material before and after passing through the asphalt analyzer is shown in Fig. 1.



Fig. 1. Comparison of RAP material before and after asphalt analyzer

Table 2. Material properties of recycled asphalt and virgin asphalt

Pilot projects	Recycling old asphalt	Virgin asphalt	Technical requirements for No. 70 asphalt [10]
Penetration at 25 °C (0.1 mm)	21.8	70.7	60–80
Softening point (°C)	57.5	49	≥ 46
Ductility at 15 °C (cm)	5.45	> 137.6	≥ 100
135 °C viscosity (Pa·s)	1.95	0.455	/

After centrifugal extraction, the old ore materials were screened. The screening results are shown in Table 3. The water content of the RAP is 1.9% and it meets the technical requirements of 3% or less per Technical Specification for Highway Asphalt Pavement Regeneration (JTG/T 5521-2019) [7].

Table 3. Gradation composition of mineral materials in the upper layer RAP of a road project

Screen size (mm)	Percentage of mass passing the following sieve (%)									
	16	13.2	9.5	4.75	2.36	1.18	0.6	0.3	0.15	0.075
Mineral material in RAP	100.0	97.2	89.2	66.0	47.7	36.6	26.4	20.5	17.9	15.9

2.3 Virgin Asphalt and Virgin Aggregate

The virgin asphalt used for mixing the reclaimed asphalt mixture was the A-level No. 70 road petroleum asphalt produced in Shandong, China. The material properties are shown in Table 2.

The coarse aggregates are made of 10–20 mm, 5–10 mm, and 0–3 mm crushed stones. The fine aggregates consist of 0–5 mm limestone machine-made sands. The slags are made of limestone ore powders. The technical indicators of the above raw materials met the technical requirements of “Highway Asphalt Pavement Construction Technical Specifications” (JTG F40-2004) (JTG F40-2004) [10].

3 Effects of Waste Frying Oil on Physical Properties of Recycled Asphalt

To study the rejuvenation effects of waste frying oil on the recovery of aged asphalt, waste frying oil with different blending amounts (mass ratio of waste frying oil to asphalt) were mixed into the aged asphalt to prepare lab specimens for physical material properties testing. The preparation method of waste frying oil reclaimed asphalt is as follows:

- (1) The waste frying oil was decontaminated and dehydrated;
- (2) The corresponding quality of waste frying oil was weighed according to the blending amount;
- (3) The RAP was heated to 150 °C; and
- (4) The mixtures contained RAP and waste frying oil were stirred with high-speed shear emulsifier until the waste frying oil was evenly dispersed. The stirring rate was 5000 ± 200 r/min, the stirring time was 30 ± 2 min, and the stirring temperature was controlled at 145 ± 5 °C.

The penetration, softening point, ductility, and viscosity of RAP with waste frying oil were tested. The test results are shown in Table 4.

It can be seen from the test results that with increasing waste frying oil, the penetration and ductility of asphalt gradually increased, while the softening point and viscosity gradually decreased. Waste frying oil has a certain regeneration effect on the recovery of old asphalt. When the amount of waste frying oil gets to 8%–10%, the penetration and softening point of recycled asphalt could be restored to the level of No. 70 virgin (new) asphalt. However, the ductility could not be restored to the level of No.70 virgin (new) asphalt. Note that the material requirements for No. 70 virgin (new) asphalt are 25 °C

Table 4. Physical properties of waste frying oil recycled asphalt

Sample	The amount of waste frying oil (%)	Penetration at 25 °C (0.1 mm)	Softening point (°C)	Ductility at 15 °C (cm)	135 °C viscosity (Pa·s)
Waste frying oil recycled asphalt	4	39.4	53.5	10.4	1.19
	6	54.2	52.5	20.2	0.948
	8	67.9	52	34.2	0.868
	10	77.3	49	65.2	0.745
	12	102.8	47	86	0.595

penetration ($60 \leq P \leq 80$) and softening point ($46 \leq T \leq 52$). Efforts were made to compute the optimal amount of waste frying oil. It was calculated the reasonable content of waste frying with the regression equation ($P = 0.2509x^2 + 3.5243x + 22.018$, $R^2 = 0.9907$; $T = 0.0119x^2 - 0.6893x + 57.226$, $R^2 = 0.9717$), the optimal content of waste frying oil was 10.5%, considering the recovery of asphalt duration.

4 Design of Mixture Ratio of Waste Frying Oil Recycled Asphalt Mixture

The RAP contents in the recycled asphalt mixture are 20%, 30%, and 40%. AC-20 was used in the testing. The amount of waste frying oil rejuvenator should be increased because of the loss of waste frying oil during the mixing, molding, and dispersion process with the asphalt mixture. Combined with the physical performance test results of recycled asphalt from waste frying oil, the mixing amounts of waste frying oil rejuvenator in the recycled asphalt mixture were 0%, 8.5%, 10.5%, and 12.5% (Percentage of waste frying oil and old asphalt in RAP). Also, a set of virgin (new) materials without RAP and waste frying oil rejuvenator were prepared and tested for comparison purposes. Thus, a total of 13 asphalt mixtures were evaluated.

The experiment adjusted the mineral aggregate synthetic gradation of the mixture. Thus, the mineral aggregate synthetic gradation of AC-20 recycled asphalt mixture with different RAP content was the same as that of the virgin (new) material. The final target mixture is shown in Table 5. The grading curve of the mineral material is shown in Fig. 2. The Marshall test [8] was used to determine the best oil-stone ratio for AC-20 virgin material and it was found to be 4.3%. The waste frying oil reclaimed asphalt mixture used the same oil-rock ratio as the virgin new material. The asphalt mixtures composed of three parts: (1) virgin asphalt; (2) aged asphalt in RAP; and (3) waste frying oil rejuvenator.

Table 5. Target mix ratio of AC-20 virgin material and different RAP regenerated mixtures

Mineral material name	RAP	10–20 mm gravel	5–10 mm gravel	3–5 mm gravel	Machine-made sand	Mineral powder
Virgin material	0%	34%	18%	16%	30%	2%
20% RAP recycled mixture	20%	33%	12%	17%	17%	1%
30% RAP recycled mixture	30%	32%	10%	16%	12%	/
40% RAP recycled mixture	40%	31%	6%	22%	1%	/

Note: With 30% and 40% RAP content, the quality passing rate of 0.075 mm sieve hole of the mixture synthesized according to the mixing ratio in the table is close to the upper limit required by the standard [10], so no mineral powder is added.

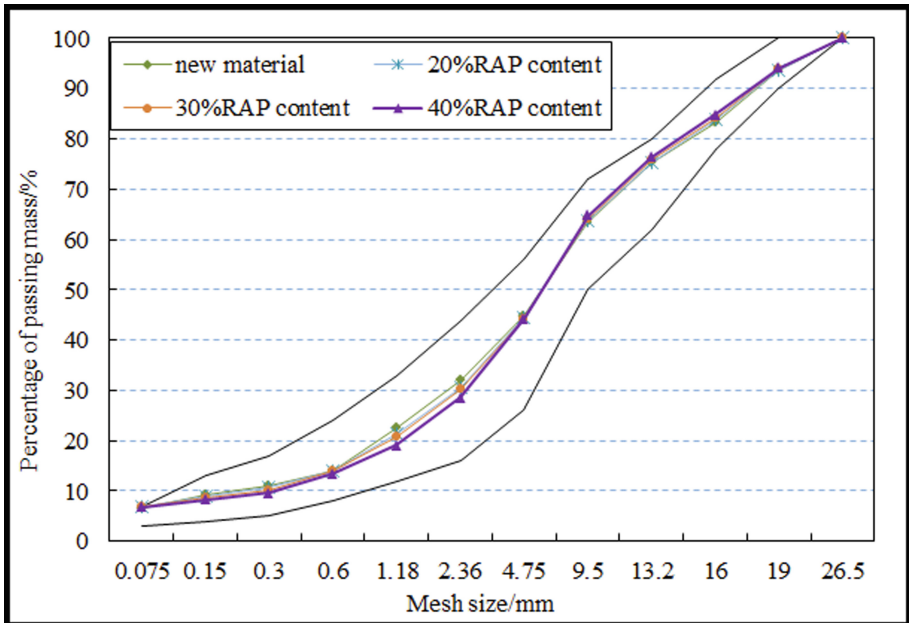


Fig. 2. Gradation curve of virgin (new) material and waste frying oil recycled asphalt mixture

The preparation method of waste frying oil recycled asphalt mixture is given as follows:

- (1) Preheat RAP to 90–110 °C and pour it into the mixing pot;
- (2) According to the mixing ratio of the waste frying oil, evenly add the waste frying oil rejuvenator into the mixing pot, and mix for 30 s;
- (3) Add new aggregate preheated to 175–195 °C and mix for the 60 s;
- (4) Add new asphalt preheated to 155–165 °C and continue mixing for the 60 s;
- (5) Finally, add filler mineral powder and mix for the 60 s;
- (6) Pour the mixture out of the mixing pot and prepare the test pieces required for the test.

5 Semicircular Bending Test of Recycled Asphalt Mixture from Waste Frying Oil

5.1 Semi-circular Bending Test Method

The ability of asphalt pavement to resist low-temperature shrinkage, deformation, and cracking is called low-temperature crack resistance, which is an important index for asphalt pavement performance. SCB test [11] has been used to evaluate the low-temperature cracking behavior and fatigue cracking characteristics of asphalt mixtures, as shown in Fig. 3. Its main working principle is to use a three-point loading method to vertically load a half-cylinder asphalt mixture specimen with prefabricated cuts to test the crack propagation of the asphalt mixture to evaluate the crack resistance of the asphalt mixture. At the bottom of the semicircular specimen, there are two round bars as fulcrums. The distance between the fulcrums is determined by the requirements of the test. At the top of the semicircle, a round bar is used for loading purposes. Based on testing purposes, static load or cyclic load can be applied in the SCB test [8]. In this study, the SCB test with static load was used to evaluate the low-temperature crack resistance of asphalt mixture at -10°C .



Fig. 3. SCB test principle diagram and the SCB specimen after cutting

The SCB tests were used to evaluate the low-temperature crack resistance of waste frying oil recycled asphalt mixture at -10°C . The SGC specimen was prepared at a

diameter of 150 mm with a thickness of 62.5 mm. Then, the specimen was cut into a semicircle along the diameter. Finally, a hand-held cutting machine was used to cut a small groove of about 3 mm in the middle of the bottom of the specimen. The void ratio of the SCB specimen was controlled at $7 \pm 1\%$. A universal testing machine (UTM) was used for the semicircular bending test. The SCB test specimen was placed in a UTM environment box and kept it at -10°C for at least 5 h to ensure that the internal temperature of the test specimen met the test requirements. Then, the specimen was put on the support of the testing machine with a center distance of 120 mm between the fulcrums. The loading rate was controlled at 0.5 mm/min. The applied load and corresponding displacements were recorded every 0.02 s. Each mixture was tested in parallel with 3 specimens, and the average values were taken as the final results. Figure 4 and Fig. 5 show the SCB specimen in the UTM, and SCB specimen after fracture, respectively.



Fig. 4. SCB specimen in UTM



Fig. 5. Fractured SCB specimen

The typical load-displacement curves are presented. The fracture energy or fracture toughness can be obtained by calculating the area under the load-displacement curve.

Fracture energy is the energy required for crack propagation per unit area. The larger the value, the greater the energy required during the fracture process of the asphalt mixture specimen, and the better the crack resistance. The calculation method of fracture energy G_f is given in Eq. 1 and 2 [11]:

$$G_f = \frac{W_f}{A_{lig}} \quad (1)$$

$$W_f = \int P du \quad (2)$$

G_f —Fracture energy, J/m^2 ;

W_f —Work of fracture, J;

P —Test load, N;

U —Displacement, m;

A_{lig} —Fracture surface area, m^2 ; $A_{lig} = (r - a) \times t$

r —Specimen radius, m;

a —Cut length, m;

t —Specimen thickness, m.

SCB test is based on fracture mechanics, and the crack tip stress intensity factor K_I (Unit: $\text{MPa} \times \text{m}^{0.5}$) is used to express the state of the crack tip [12]. When the stress intensity factor of the plastic zone at the front end of the crack of the SCB specimen reaches the cracking toughness of the asphalt mixture, the crack begins to develop upward and the specimen fractures. Fracture toughness K_{IC} is the stress intensity factor under critical load P , which reflects the ability of the material to resist brittle fracture. The critical load is assumed to be the maximum load recorded during the test. The specific calculation formulas are given as follows [11, 12]:

$$K_I = Y_I \sigma_0 \sqrt{\pi a} \quad (3)$$

$$K_{IC} = Y_I \sigma_{max} \sqrt{\pi a} \quad (4)$$

$$\sigma_0 = \frac{P}{2rt} \quad (5)$$

K_I —Stress intensity factor, $\text{MPa} \times \text{m}^{0.5}$;

K_{IC} —Fracture toughness, $\text{MPa} \times \text{m}^{0.5}$;

σ_0 —Stress at the crack, MPa;

P —Test load, MN;

r —Specimen radius, m;

a —Cut length, m;

t —Specimen thickness, m;

Y_I —The standardized stress intensity factor (dimensionless), Y_I of SCB specimen size used in this test method is calculated as follows:

$$Y_I = 4.782 + 1.219 \left(\frac{a}{r} \right) + 0.063 \exp(7.045 \left(\frac{a}{r} \right)) \quad (6)$$

5.2 Analyses

SCB tests were carried out on 13 groups of asphalt mixtures, and the results are shown in Fig. 6 and 7. According to the test results the observations are given as follows:

- (1) The fracture energy of the recycled asphalt mixture is less than that of virgin asphalt mixture. In the case of the same rejuvenator content, when RAP content increased, the fracture energy of the mixture decreased. It means the RAP content reduces the low-temperature crack resistance of the renewable asphalt mixture. This is because RAP contains more aged and brittle asphalt. Comparing to virgin (new) asphalt, it can withstand the greater load, but its low-temperature deformation ability is worse, and it is more likely to be damaged during the accumulation of load. This makes the recycled asphalt mixture more prone to cracking under the action of low temperature in winter and vehicle load. This affects the performance of the asphalt pavement.

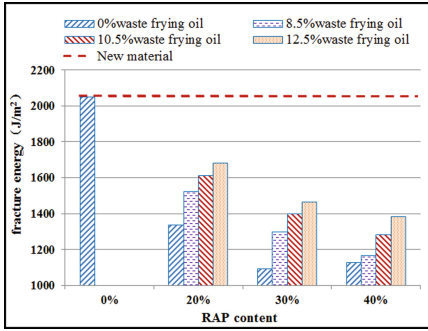


Fig. 6. The fracture energy of mixture changes with RAP and waste oil content

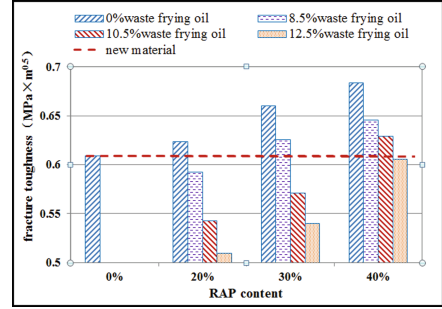


Fig. 7. The fracture toughness of mixture changes with RAP and waste oil content

- (2) Under the same RAP content, the fracture energy of the mixture increased with the increasing rejuvenator content. When the RAP contents were between 20%–40%, the fracture energy of the recycled asphalt mixture under the 12.5% rejuvenator content increased by more than 160 J/m^2 as compared to 8.5% rejuvenator content. When the RAP contents were between 30% and 40%, and the rejuvenator contents were between 10.5% and 12.5%, the fracture energy of the recycled mixture can be restored to 62%–72% of that of the virgin material. Thus, the regeneration effects are obvious. The results show that the low temperature ductility of asphalt can be effectively improved by waste frying oil, thus improving the low temperature crack resistance of the mixture.
- (3) The fracture toughness of recycled asphalt mixture (without regenerating agent) increases after RAP is added. This shows that the blending of RAP can increase the strength of the mixture. With the increasing amount of waste frying oil rejuvenator, the fracture toughness of the recycled asphalt mixture gradually decreases. This shows that the addition of a waste frying oil rejuvenator made the aged asphalt in the RAP material soft, and the strength of the recycled asphalt mixture decreased.

6 Conclusions

The enormous quantity of waste products from by-products of frying activity could cause negative impacts if not properly managed and recycled. The observations and conclusions from this study are given as follows:

- (1) The semi-circular bending test can well evaluate the anti-cracking performance of waste frying oil recycled asphalt mixture at low temperature.
- (2) The addition of waste frying oil can effectively regenerate the aged asphalt in RAP and improve the crack resistance of the asphalt mixture. When the RAP contents were between 30% and 40%, and the rejuvenator contents were between 10.5% and 12.5%, the fracture energy of the recycled mixture can be restored to 62%–72% of that of the virgin material.

- (3) Although the anti-cracking performance of the recycled asphalt mixture has been restored to a certain level after adding the waste frying oil rejuvenator, there is still a certain gap compared with that of the virgin (new) asphalt mixture. If the RAP content of the recycled asphalt mixture is higher than 30%, it is suggested that the recycled asphalt mixture should be used as the middle and lower layers of asphalt pavement.
- (4) The recycled asphalt mixture can comprehensively utilize the waste frying oil and RAP, which can not only find a reasonable way to recycle the waste frying oil and avoid its return to the table, but also effectively save the natural stone and asphalt, so as to realize the double resource utilization of kitchen waste and road surface recycling materials.

References

1. Qi, M.: Performance Evaluation of the Recycling Asphalt mixture Regenerated with Vegetable Oil. Beijing University of Civil Engineering and Architecture (2016)
2. Binbin, L.: Influence of Waste Edible Vegetable Oil on Physical, Chemistry, and Rheological Properties of Aged Asphalt Binders. Wuhan University of Technology (2014)
3. Chen, L., Hongxing, Z., Jun, S., Xiangyang, L.: Characteristics and harm of waste oil. *Agric. Prod. Process.* **06**, 69–70 (2010)
4. Di Su, X., Shijie, L.X., Wei, L., Xiang, J.: Technical progress of waste oil resource utilization. *Agric. Mach.* **35**, 34–36 (2013)
5. Binbin, L., Meizhu, C., Shaopeng, W.: Analysis on the application prospect of waste edible oil in asphalt regeneration. *Petrol. asphalt* **27**(05), 49–53 (2013)
6. Zhuorui, L., Jinjin, S., Yingbiao, W., et al.: Research on Road Performance of Waste Edible Oil Recycled Asphalt Mixture. *China Water Transp. (the latter half of the month)* **20**(05), 223–225 (2020)
7. JTG/T 5521-2019: Technical specification for highway asphalt pavement regeneration. Beijing People's Communications Publishing House (2019)
8. JTG E20-2011: Highway engineering asphalt, and mixture test regulations. Beijing People's Communications Publishing House (2011)
9. GB 5009.236-2016: National Food Safety Standard Determination of Moisture and Volatile Matter of Animal and Vegetable Oils. China Quality Inspection Press (2016)
10. JTG F40-2004: Technical specification for highway asphalt pavement construction. Beijing People's Communications Publishing House (2005)
11. Standard Method of Test for Determining the Fracture Energy of Asphalt Mixtures Using the Semi-Circular Bend Geometry. AASHTO TP 105-13 (2013)
12. Xiaoying, W., Geng Litao, X., Qian, L.K.: Stress intensity factor analysis of asphalt mixture semicircular bending test. *J. Shandong Jianzhu Univ.* **30**(04), 351–355 (2015)



Viability Assessment of the Use of Ground Tire Rubber (GTR) as a Modifier in Asphalt Binders

Zahid Hossain¹(✉), Biswajit Bairgi², Musharraf Zaman³, and Edgar O'Rear⁴

¹ Civil Engineering, Arkansas State University, State University, PO Box 1740, LSW#239, Jonesboro, AR 72467, USA
mhossain@astate.edu

² Arkansas State University, State University, PO Box 1740, LSW#239, Jonesboro, AR 72467, USA
biswajit.bairgi@smail.astate.edu, bkumar@unm.edu

³ David Ross Boyd Professor and Aaron Alexander Professor of Civil Engineering and Alumni Chair Professor of Petroleum and Geological Engineering, The University of Oklahoma, 202 West Boyd Street, #334, Norman, OK 73069, USA
zaman@ou.edu

⁴ Francis W. Winn Professor for Chemical, Biological and Materials Engineering, The University of Oklahoma, 100 E. Boyd Street SEC T301, Norman, OK 73019-1004, USA
eorear@ou.edu

Abstract. The total number of generated scrap automobile tires in the U.S. exceeds 300 million per year, which is roughly one scrap tire per person. Improper disposal of these scrap tires is a major concern to environmental protection agencies as they become a nuisance for public health and the environment. The objective of the present study is to assess the viability of the use of scrap tires in the form of ground tire rubber (GTR) in preparing new asphalt mixes. To this end, this study evaluated a commonly used performance graded (PG) asphalt binder (PG 64-22 marketed as PG 67-22) modified with different amounts (0%, 10%, 15%, and 20% by the weight of the binder) of two different graded GTR samples (Mesh #30 and Mesh #40). The blended GTR-modified binder or asphalt rubber (AR) samples were then investigated through a series of laboratory tests that included Fourier Transform Infrared (FTIR), Atomic Force Microscopy (AFM) imaging, Standard Penetration, Rotational Viscometer (RV), Dynamic Shear Rheometer (DSR), and a moisture susceptibility test via the Sessile Drop (SD) method. The FTIR analysis revealed the presence of alkanes, alkyl halides, carboxylic acids, etc. in the PG 64-22 binder, whereas the GTR-modified binders exhibited various amines and nitro compounds. The AFM image analysis showed that there were 'bee-like' structures in the PG 64-22 binder, and GTR-modification densified the 'bee-like' structures, indicating an additional concentration of Styrene-Butadiene-Styrene (SBS) and/or Styrene-Butadiene-Rubber (SBR) in the GTR-modified binder. Penetration, RV, and DSR test results showed that GTR addition increased stiffness and rutting resistance of the base binder. Moisture susceptibility analysis showed that the addition of GTR increased the surface free energy, cohesive energy, and aggregate compatibility, which are desired for improved moisture resistance. Based on the findings of this study, GTR is found to be a viable modifier for asphalt binders.

Keywords: Asphalt binder · Ground tire rubber (GTR) · Moisture damage · Surface free energy · Compatibility

1 Introduction

About one scrap tire per person is being generated every year in the U.S., and thus the total number of generated scrap tires is about 300 million (about 5.4 million tons) per year (Bureau of Waste Prevention 2006; Recycling Research Institute 2015). Improper disposal of these scrap tires in stockpiles, landfills, or illegal dumping is a major concern to the environmental protection agencies (EPA) of the U.S. (EPA 2015). These scrap tires provide ideal breeding sites for mosquitoes, rodents, and some other disease-carrying insects (EPA 2020). Due to the disposal of scrap tires, the landfills and stockpiles deplete available spaces for solid waste (EPA 2020). Additionally, fire in stockpiles can cause disastrous environmental impacts. To find a possible solution to these scrap tire-related disposal problems, some research projects have been conducted by various transportation agencies. These studies demonstrated that scrap tires have high potentials to be used in the form of ground tire rubber (GTR) for the modification of asphalt binders. The GTR-modified asphalt binder is often referred to as asphalt rubber (AR). The AR production process was initially introduced by Charles H. McDonald in the mid-1960s in Phoenix, AZ (Caltrans 2006). Primarily, AR was developed as a maintenance seal coat material for crack repairing of old pavement until a resurfacing is accomplished (Way et al. 2011). Over the years, AR was found to possess good resilience, strong bonding properties, and absorbance. Thus, AR is reported to provide longer-lasting pavements, reduced maintenance cost, lower noise level, higher skid resistance, and reduced pavement distress (Way et al. 2011). Way et al. (2011) illustrated that the usage of AR provides lower design thickness of pavement compared to a conventional asphalt binder considering the same level of service. Since the work of McDonald, tire composition and performance has changed a great deal. High surface area fillers like silica and alumina as well as improved dispersion methods have increased durability. Expected wear life for automotive tires has risen from 20,000–30,000 miles to as much as 50,000–80,000 miles. Such changes in composition offer potential benefits with the use of GTR-modified binders.

Besides some improved structural properties, AR also provides a series of environmentally sustainable behavior while using surface course materials in pavements. Since AR mixes result in thin pavement layers, they reduce the amount of raw materials (aggregates and binders), and mining and transportation cost (EPA 2020). Thus, asphalt pavement containing AR conserve energy and reduce CO₂ emissions compared to conventional hot mix asphalt (HMA) pavements. The usage of AR as a surface course material lowers the pavement noise level by 5.7 dB or even more, where human hearing can distinguish the noise level difference of 3.0 dB (ATRC 1996). It also reduces the degree of heat island effect as illustrated by Kaloush et al. (2008). Nowadays, asphalt binders are typically modified with polymer modifiers, which increase the cost of an HMA by about 30% compared to that containing an unmodified binder. Thus, the replacement of polymer modified binders by AR is expected to reduce the construction cost and conserve the commonly used polymer modified binders (Caltras 2015). However, only

4.3% of the total produced scrap tires are being recycled into GTR for modification of asphalt binders (EPA 2015). Some departments of transportation (DOTs) such as California, Arizona, Florida, New Mexico, Georgia, and Texas have been front-runners in using GTR in asphalt modification, whereas other states (e.g., Arkansas, Oklahoma, Mississippi, and Missouri) are not yet convinced to embrace this innovative practice.

2 Objectives

The main objective of this study is to assess the viability of the use of GTR in modifying asphalt binders through a series of laboratory experiments. Toward characterizing the GTR-modified asphalt binders, specific objectives of this study are given below:

- Perform chemical analysis through Fourier Transformation Infrared (FTIR) spectra,
- Examine micro-structure of the tested binder samples by using an Atomic Force Microscope (AFM),
- Obtain stiffness properties of binder samples by conducting Penetration, Rotational Viscometer (RV), and Dynamic Shear Rheometer (DSR) tests.
- Analyze moisture damage resistance of GTR-modified binders by a surface science approach, namely the Sessile Drop (SD) method.

3 Materials Selection and Mixing Protocol

3.1 Materials Selection

A widely used performance graded (PG) asphalt binder (PG 64-22; marketed as PG 67-22) and two different graded GTR samples (Mesh #30 and Mesh #40) have been collected from Ergon Asphalt and Emulsions Inc. in Memphis, TN, and Liberty Tire Recycling Inc. in Pittsburgh, PA, respectively. The certification data of the unmodified PG 64-22 binder is presented in Table 1. Regarding the gradations of the GTR samples, sieve analyses have been performed using the U.S. standard sieves. For Mesh #30 GTR samples, about 96% particles passed through Sieve #30 (0.60 mm) and 7% particles retained in Sieve #100 (0.12 mm). For Mesh #40 GTR samples, 94% particles passed through Sieve #40 (0.42 mm) and 5% materials retained in Sieve #100 (0.12 mm). The gradations of GTR samples were found to be well-graded and consistent with multiple state DOTs' (Texas, Arizona, and Florida) GTR specifications (Caltrans 2005).

3.2 GTR-Modified Asphalt Binder Preparation

There are some different technologies of GTR incorporation in asphalt binders such as the wet process, the dry process, the terminal blend, devulcanized rubber, liquid rubber (Caltran 2006; Way et al. 2011). Literature shows that the wet process and the dry process, are widely followed by various agencies to incorporate GTR into AR pavements (Way et al. 2011). In the wet process, the GTR sample is directly added to hot asphalt binder at ambient temperature before mixing with aggregates (Caltrans 2006; Way 2011; Ergon 2014; Hicks 2002). The wet process is used to produce different types of AR

Table 1. Certification data of PG 64-22 asphalt binder (Ergon 2014)

Test name	Test designation	Test temp. (°C)	AASHTO limits	Test results
<i>Original/unaged binder</i>				
Flash point test	AASHTO T 48	n/a	Flash point: 230 °C Min.	310 °C
Specific gravity test	AASHTO T 228	15.56	Specific gravity: 1.039 at 15.6 °C	1.0320 @ 15.6 °C
Rotational viscosity test	AASHTO T 316	135	Rotational viscosity: 3000 mPa.s max. at 135 °C	870 mPa.s
		150		417 mPa.
		165		127 mPa.s
		180		56 mPa.s
Dynamic shear rheometer	AASHTO T 315	64	G*/sinδ: 1.00 kPa min	1.19 kPa
			Phase angle (°): N/A	86.2°
<i>Rolling thin film oven residue</i>				
Rotational thin film oven test	AASHTO T240	163	Volatile mass loss: 1% Max	0.06%
Dynamic shear rheometer	AASHTO T 315	70	G*/sinδ: 2.20 kPa min	3.89 kPa
			Phase angle (°), δ: (N/A)	81°
<i>Pressure aging vessel residue</i>				
Dynamic shear rheometer	AASHTO T 315	25	G*/sinδ: 5000 kPa min	3110 kPa
			Phase angle, δ: N/A	44.6°
Bending beam rheometer	AASHTO T 313	-12	Stiffness, S (Max. 300 MPa)	123 MPa
			Slope, m-value (Min. 0.300)	0.325

Note: N/A = Not available, G* = Complex Shear Modulus

based on their physical properties such as viscosity, softening point, and shear modulus. The rotational viscosity is the most distinctive property to classify different types of AR (Cantrans 2006). To meet the desired viscosity, the GTR content and the blending protocol are adjusted. For instance, CalTrans blends a 15% GTR with a PG 64-22 binder at high agitation to maintain their threshold viscosity of 1,500 mPa.s at 190 °C (Cantrans 2006). On the other hand, in the dry process, GTR is used as a substitute for 1% to 3% of total aggregates in the asphalt mix (Cantrans 2006). Since, GTR acts as a portion

of aggregates in asphalt mixes, relatively coarse graded GTR (6.5 mm to Mesh #8 or 2.36 mm) can be used in this process (Cantrans 2006). There is limited interaction between the asphalt binder and GTR during mixing and blending processes in an asphalt mix plant. Thus, the asphalt binder is not considered to be modified by GTR in the dry process.

Following a previously established blending protocol (Hossain et al. 2013), the present study followed the wet process to blend three different percentages of GTR (10%, 15%, and 20% by weight of base binder) of two selected graded GTR (Mesh #30 and Mesh #40) with a base binder, namely, PG 64-22. Firstly, about 150 gm of asphalt binder was heated in an oven at 160 °C for 2 h and different percentages of GTR were added to the hot binder. The mixture was stirred with a hand stirrer for 1 min and put into the oven at 160 °C for 10 min. The interior surfaces of the sample container were scrapped after every stirring to prevent the sticking of rubber. The heating and stirring cycle was continued for an hour and the resulted blend was allowed to keep in the oven at 160 °C for an additional 45 min to ensure all possible chemical reactions are completed.

4 Test Results

4.1 Chemical Analysis

A single beam Thermo Nicolet 8700 FTIR system with a deuterated triglycine sulfate (DTGS) detector and a potassium bromide (KBr) beam splitter has been utilized for the FTIR spectra analysis. FTIR tests have been performed employing a disposable crystal IR card coated with asphalt binder over 50 scans at 4 cm^{-1} resolution for 30 s and a spectrum range from 350 cm^{-1} to 7400 cm^{-1} under dry air condition (relative humidity < 5%) (Hossain et al. 2015; ICL 2020). Functional group analysis has been conducted by using the FTIR absorption assignment chart found in Scribd (Scibd 2015). The detected functional groups as shown in Table 2, analyzed from the FTIR spectra (Fig. 1), reveal the presence of alkyl halides, various classes of alkanes, alkenes, and carboxylic acids in the PG 64-22 binder, which are consistent with Jia et al. (2013). The GTR is made of 70% rubber (carbon black, synthetic rubber, natural rubber, and inorganic fillers), in which various amines group and nitro compounds are governing functional groups (Way 2011; Mika 2007). These amine groups and nitro compounds act as antioxidants and lubricating agents in the binder and eventually may reduce the aging effect and improve moisture resistance. This analysis bridges some research gaps between physical and chemical analysis of the GTR modified binder. The functional groups of asphalt binders are also reported to be correlated well with the mechanistic properties of binders (Way 2011).

4.2 Micro-structure Analysis

A Bruker Dimension Icon® AFM system has been employed in this study to evaluate the morphology of the binder through the Tapping™ mode in air. The AFM test samples have been prepared on a glass slide by following recommendations of a previous study (Tarefder and Arifuzzaman 2011). All samples have been imaged with a 10 μm \times 10 μm

Table 2. Functional group detection of unmodified and GTR-modified binders

Peak wavenumber range	Absorbance	Recommended functional group	Recommended frequency range (cm ⁻¹)	Bond
<i>For unmodified PG 64-22 asphalt binder</i>				
810–816	1.1	Alkyl halides	850–550	C-Cl rock
		Alkenes	350–1000	
1020–1040	0.8	Aliphatic amines	1020–1250	C-N stretch
1360–1380	1.4	Alkanes rock	1350–1370	C-H rock
1440–1470	1.4	Alkanes bend	1450–1470	C-H Bend
2870–2980	1.4	Alkanes stretch	2800–3000	C-H stretch
		Carboxylic acids	2500–3300	O-H stretch
<i>For 15% GTR (#30) modified asphalt binder</i>				
964–976	1.5	Alkenes bend	650–1000	
~1030	1.7	Aliphatic amines	1020–1250	C-N stretch
1316–1320	2.1	Aromatic amines	1250–1335	C-N stretch
~1380	3.1	Alkanes rock	1350–1370	C-N stretch
~1460	4.4	Alkanes bend	1450–1470	C-H Bend
1600–1610	1.9	1-degree amine	1580–1650	N-H bend
2870–2930	6.0	Alkanes stretch	2850–3000	C-H stretch
		Carboxylic acids	2500–3300	O-H stretch

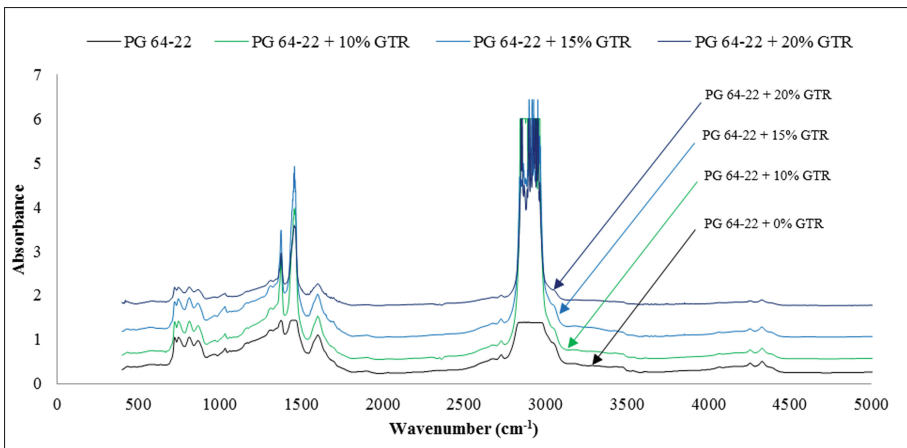


Fig. 1. FTIR spectra of unmodified and GTR-modified (Mesh #30) asphalt binders.

area. As shown in Figs. 2a and 2b, an asphalt binder has a complex microstructure, which is composed of several maxima and minima of “disc-like” substances concentrated in an elliptical fashion with a short span. This structure is referred to as ‘bee-like’ structures. Similar “bee-like” structures have been observed in some previous studies (Loeber et al. 1996; Durado et al. 2011; McCarron et al. 2012). Loeber et al. (1996) reported that these “bee-like” structures represent the wax crystal composed of Styrene-Butadiene-Styrene (SBS) and Styrene-Butadiene-Rubber (SBR) in a chain format. As shown in Figs. 2c and 2d, the “bee-like” structures are densified with the addition of GTR, which represent higher concentrations of SBS and SBR in GTR-modified asphalt binders. Further, Moraes et al. (2010) reported the disappearance of the “bee-like” structures at high temperatures (above 57 °C) and their reformation while cooling down. It is well established that asphalt binder is a temperature and time-dependent or viscoelastic material, in which the elastic component dominates at low temperatures (stiff), and the viscous component dominates at higher temperatures (soft). Thus, the disappearance of “bee-like” structures at high temperatures and their reappearance at low temperatures reveal that they are also related to the stiffness of asphalt binder. Since the GTR-modified binder is found to have a densified “bee-like” structures, it is an implication of increased stiffness of GTR-modified binder based on this microstructure analysis. The GTR image (Fig. 2d) also displays some smaller particles not evident in the PG 62–22 binder sample. These particles are attributed to carbon black and mineral oxide fillers used in tire manufacture.

4.3 Mechanistic Performance Analysis

For the mechanistic evaluation of GTR-modified binders, the American Association of State Highway and Transportation Officials (AASHTO) recommended test methods have been followed in the present study. These AASHTO test methods include Penetration (AASHTO T 49), Rotational Viscometer (RV) (AASHTO T 316), Dynamic Shear Rheometer (DSR) (AASHTO T 315), and Multiple Stress Creep and Recovery (MSCR) (AASHTO P 70). The RV tests have been conducted at four temperatures: 135 °C, 150 °C, 165 °C, and 180 °C. The DSR test has been conducted at three different temperatures 64 °C, 67 °C, and 70 °C at a constant frequency of 10 rad/sec. It is noted that the DSR test at 10 rad/s angular frequency simulates shearing action corresponding to moving traffic at 55 mph speed. These AASHTO test results are shown in Fig. 3.

Penetration test results (Fig. 3a) reveals that average penetration depth decreases with an addition of the GTR content. For instance, a 20% GTR (Mesh #30) addition results in a decrease of penetration depth from 29 d-mm (unmodified binder) to 15.5 d-mm. Way et al. (2011) reported that an AR of PG 64-16 modified with a 15% GTR exhibited a penetration value between 22 d-mm and 26 d-mm, which is in agreement with the findings of the current study. The plot of RV test results (Fig. 3b) shows that viscosity increases significantly with the addition of GTR. For instance, at 135 °C, 20% GTR (Mesh #30) increases the viscosity of the unmodified binder from 517 mPa.s to 5,200 mPa.s, which is about 10 times of the unmodified binder. Such an increasing trend of viscosity is also reported by Way et al. (2011). These trends of decreasing penetration depth and increasing viscosity indicate an increased stiffness of the GTR-modified binder, which implies an improved performance of GTR-modified binders against rutting and moisture

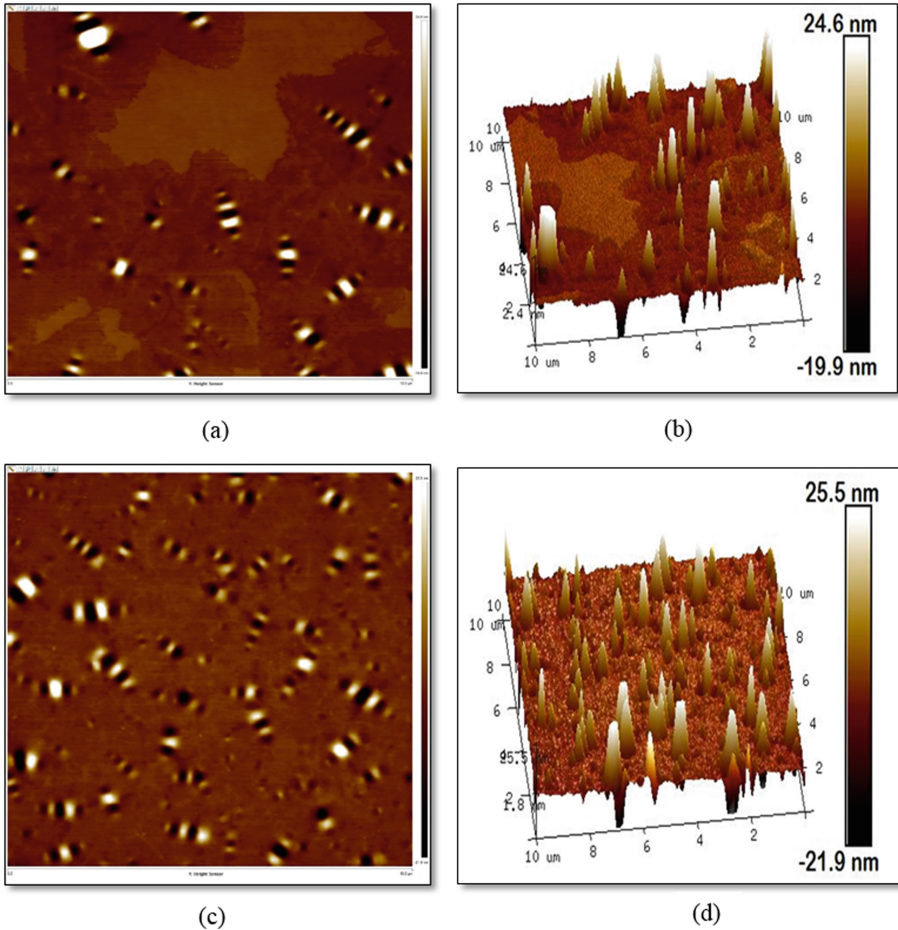


Fig. 2. (a) Topographic image of PG 62-22 binder, (b) 3-D image of PG 64-22 binder, (c) Topographic image of Mesh #30 GTR-modified asphalt binder, and (d) 3-D Image of 15% Mesh #30 GTR-modified asphalt binder.

damages of pavement (Xiao and Amir Khanian 2009). The complex shear modulus (G^*) and phase angle (δ), and the Superpave rutting factor ($G^*/\sin \delta$) obtained from the DSR tests are shown in Figs. 3c and 3d, respectively. As expected, the G^* value increases and δ value decreases with the addition of GTR in asphalt binders (Fig. 3c). As seen in Fig. 3d, the rutting factors of all tested unaged binders are greater than 1.00 kPa, which satisfies the Superpave specification. It is also seen that the addition of GTR increases the rutting factor. Besides, an increased $G^*/\sin \delta$ value at a higher GTR content indicates an increase in the performance grade of the binder.

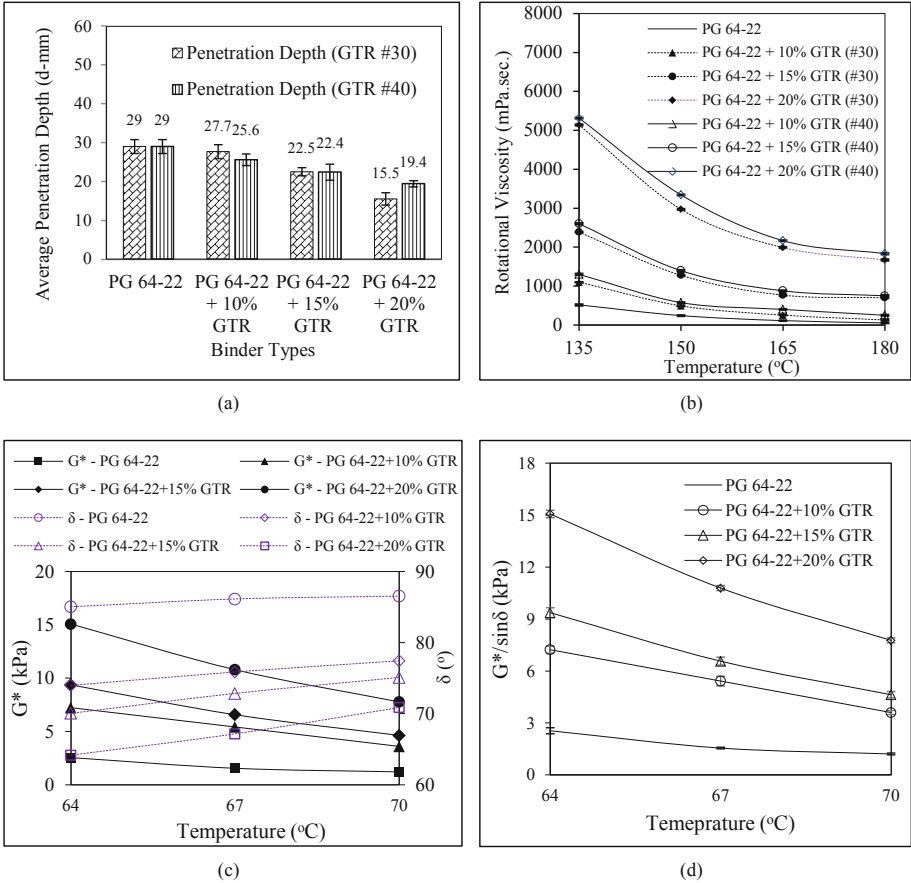


Fig. 3. Plot of the (a) penetration depth, (b) rotational viscosity, (c) complex modulus (G^*) and phase angle (δ), and (d) superpave rutting factor.

4.4 Moisture Susceptibility Analysis

Moisture damage to the pavement is a progressive deterioration of asphalt mixes through the loss of strength and stiffness due to the presence of water in asphalt pavement (Huang et al. 2009). It is a complex phenomenon encompassed by a series of factors such as materials properties, mix composition, drainage condition, and environmental characteristics (Lu and Harvey 2005). No pavement is impermeable to moisture due to the existing air voids in asphalt mixes, which provides major access for moisture ingress (Tarrel and Al-Swailmi 1994; Huang and Qian 2011). Though a 4% air voids is designed in laboratories, it varies from 6% to 12% in field conditions (Tarrel and Al-Swailmi 1994). In such conditions, moisture can enter into asphalt mixes but cannot escape freely, thereby getting trapped into the asphalt mixes. The inhibited moisture causes several adverse effects such as loss of cohesion of binder, loss of adhesion between binder and aggregates, development of pore pressure, and hydraulic scouring (Lu and

Harvey 2005; Wasiuddin et al. 2010). As a result of these drawbacks, various types of pavement damages such as stripping and bleeding occur in asphalt pavements.

4.4.1 Moisture Susceptibility Theories

A molecule of a liquid, inside the liquid body, never subjects to any force as it is well balanced by equal attraction force from all directions. However, the molecule, located on the surface of the liquid, subjects to an inward attraction force due to the absence of neighbor molecules in the direction of air (Bahriamian 2002). This phenomenon, which also occurs at the surface of solids, yields unbalanced energy called free energy or surface free energy (SFE) (Fini et al. 2011). The *SFE* of a material has three components: mono-polar acidic component (Γ^+), a mono-polar basic component (Γ^-), and an apolar or Lifshitz-van der Waals (Γ^{LW}) component (Van Oss et al. 1998; Cheng et al. 2001). A majority of the *SFE* equations used in this study are presented in Table 3. While expressing the total SFE (Γ^{total}) (Eq. 1), Γ^+ and Γ^- are combined into a single term called the acid-base component (Γ^{AB}), and total *SFE* is the summation of Γ^{AB} and Γ^{LW} (Eq. 2). The Γ^{total} is also related to the work of cohesion or cohesive energy (W_C) of a material as shown in Eq. 3. Thus, the work of adhesion (ΔG_{ad}) between a liquid (*L*) and a solid (*S*) is the summation of its Lifshitz-van der Waals (ΔG_{ad}^{LW}) and acid-base (ΔG_{ad}^{AB}) components (Eq. 4). The expressions ΔG_{ad}^{LW} and ΔG_{ad}^{AB} are shown in Eqs. 5

Table 3. Major SFE equations (Buddhala et al. 2012; Bhasin et al. 2006)

Equation no.	Equation
1	$\Gamma^{AB} = 2\sqrt{\Gamma^+\Gamma^-}$
2	$\Gamma^{total} = \Gamma^{LW} + \Gamma^{AB}$
3	$W_C = 2 * \Gamma^{total}$
4	$\Delta G_{ad} = \Delta G_{ad}^{LW} + \Delta G_{ad}^{AB}$
5	$\Delta G_{ad}^{AB} = -2\left(\sqrt{\Gamma_L^+\Gamma_S^-} + \sqrt{\Gamma_L^-\Gamma_S^+}\right)$
6	$\Delta G_{ad}^{LW} = -2\sqrt{\Gamma_L^{LW}\Gamma_S^{LW}}$
7	$G_{dry}^{ad} = \Gamma_L^{total}(1 + \cos\theta) - 2\left(\sqrt{\Gamma_L^{LW}\Gamma_S^{LW}} + \sqrt{\Gamma_L^+\Gamma_S^-} + \sqrt{\Gamma_L^-\Gamma_S^+}\right)$
8	$\Delta G_{wet}^{ad} = \left\{2\Gamma_W^{LW} + 2\sqrt{\Gamma_B^{LW}\Gamma_A^{LW}} - 2\sqrt{\Gamma_B^{LW}\Gamma_W^{LW}} - 2\sqrt{\Gamma_A^{LW}\Gamma_W^{LW}} + 4\sqrt{\Gamma_W^+\Gamma_W^-} + 2\sqrt{\Gamma_B^+\Gamma_A^-} - 2\sqrt{\Gamma_B^-\Gamma_A^+} + 2\sqrt{\Gamma_B^+\Gamma_W^-} - 2\sqrt{\Gamma_B^-\Gamma_W^+} - 2\sqrt{\Gamma_A^-\Gamma_W^+}\right\}$
9	$Compatibilty\ Ratio\ (CR) = \frac{\Delta G_{dry}^{ad}}{\Delta G_{wet}^{ad}}$

and 6, respectively. Again, the ΔG_{ad} between a liquid and a solid is related to Γ^{total} of the liquid and the contact angle (θ) of the liquid over the solid surface (Eq. 7). The ΔG_{ad} can also be termed as adhesive energy in the absence of water or under the dry condition termed as ΔG_{dry}^{ad} . The adhesive energy in the presence of water or under the wet condition (ΔG_{wet}^{ad}) can be expressed as shown in Eq. 8. The ratio of ΔG_{dry}^{ad} and ΔG_{wet}^{ad} is referred to as the compatibility ratio (CR), as shown in Eq. 9, which quantifies the moisture resistance of an asphalt-aggregate system (Bhasin et al. 2006; Little and Bhasin 2006). In Eq. 9, parameters A, B, and W denote aggregates, binders, and water, respectively.

4.4.2 The SD Method

Regarding SFE measurements of asphalt binders, the Wilhelmy Plate (WP), the Sessile Drop (SD), the Atomic Force Microscopy (AFM), and the Inverse Gas Chromatography (IGC) methods are recommended in surface science research (Little and Bhasin 2006). The present study utilized the SD method considering its advantages and limitations of the other methods. In the SD method, an optical contact angle analyzer (OCA) device is utilized for contact angle measurements of various probe liquids on a binder substrate. A drop of probe liquid is dispensed on the sample and video images of the drop are recorded, and the video images are then analyzed with a controlling software (SCA 20) for determining the contact angles. Considering the criteria of probe liquid selection found in Little and Bhasin (2006), this study selected water, ethylene glycol, and formamide for contact angle measurements. The OCA samples (Fig. 4) were prepared by coating glass slides with hot liquid binders as adopted in a previous study by Tarefder and Arifuzzaman (2011).

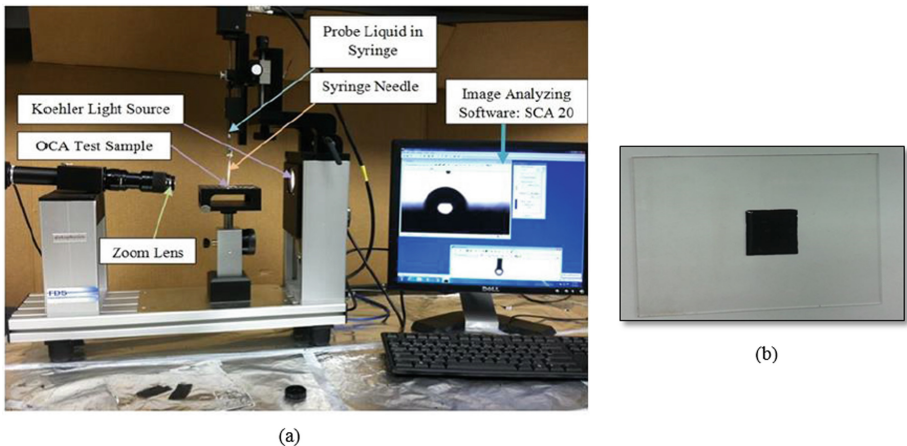


Fig. 4. (a) The OCA device, and (b) An OCA test sample.

Surface roughness influences the contact angle data (Kittu et al. 2014). The smoothness of the SD specimens was ascertained by measuring the thickness at multiple points

using a Vernier caliper. Other thickness measuring devices such as ultrasonic thickness gauge could be a better choice in this regard. However, the contact angle measurements did not vary much over time. The reported angle was the average of hundreds of raw contact angles on both sides (left and right) of the drop. These measurements were taken within two minutes after the drop of probe liquid was placed on top of the test specimen. There were some variations of contact angles over time as well as locations (left and right). That is why the average value was taken for the SFE calculations.

4.4.3 SFE and Compatibility Analysis

Table 3 presents the measured contact angles of various binder samples. A contact angle provides the relative wetting ability of a liquid. A contact angle of greater than 90° indicates poor wetting, and the wetting ability increases when a contact angle decreases from a higher value to a lower value (Budhala et al. 2012). As shown in Table 4, contact angles of probe liquids with asphalt binder coated glass slides reduced with an increase of the GTR content. It indicates that the addition of GTR increases the wetting ability of the binder by the probe liquids.

Table 4. Static contact angles of various probe liquids on binder substrates

Binder types	Water		Ethylene Glycol		Formamide	
	Mean	SD	Mean	SD	Mean	SD
PG 64-22	98	0.16	91	0.11	88	0.11
PG 64-22 + 10% GTR (#30)	91	0.19	84	0.14	83	0.24
PG 64-22 + 10% GTR (#40)	91	0.20	77	0.30	75	0.38
PG 64-22 + 15% GTR (#30)	88	1.60	81	1.44	76	1.39
PG 64-22 + 15% GTR (#40)	88	1.40	73	1.37	71	1.36
PG 64-22 + 20% GTR (#30)	83	2.27	76	1.39	73	1.83
PG 64-22 + 20% GTR (#40)	79	0.56	68	2.10	67	1.65

Note: SD = Standard Deviation

The SFE components of the three probe liquids were used in determining the SFE components of the binder samples through a solution of Eq. 7. Table 4 shows the SFE components, total SFE , and W_C of unmodified and GTR-modified binders along with those of the probe liquids and aggregates used in this study.

As shown in Table 5, the I^{LW} values are significantly higher than either I^+ or I^- for all tested binder samples. Thus, the I^{LW} is found to be the most significant contributor to the total SFE , which is consistent with the findings of the corresponding study of Little and Bhasin (2006). It is also seen that the SFE components, total SFE , and W_C increase with an addition of GTR into the base binder. As the W_C is twice the total SFE , both the W_C and total SFE followed a similar increasing trend with an addition of GTR. Lu and Harvey (2005) showed that the loss of cohesion of binder is one of the major causes of moisture damage. Thus, an increasing trend of W_C provides a preliminary indication of improved resistance to moisture damage of the GTR-modified binders. To get a better understanding of the moisture resistance of GTR-modified binders, other estimated energy parameters such as ΔG_{dry}^{ad} and ΔG_{wet}^{ad} are discussed next.

Figure 5 shows ΔG_{dry}^{ad} and ΔG_{wet}^{ad} of tested binder samples. It is seen that ΔG_{dry}^{ad} increases with an increase of the GTR content in the binder-aggregate systems, indicating improved compatibility strength. Among all aggregates, gravel showed the highest ΔG_{dry}^{ad} for all binder-aggregate systems, and it was followed by sandstone, limestone, granite, and basalt. On the other hand, ΔG_{wet}^{ad} decreased with an increase of the GTR content in cases of all binder-aggregate systems. The ΔG_{wet}^{ad} is essentially the de-bonding energy (negative value) at the binder-aggregate interface due to the presence of water, indicating a higher compatibility strength with a lower value of ΔG_{wet}^{ad} . Thus, a decreasing trend of ΔG_{wet}^{ad} with an increase of the GTR content also indicates improved compatibility strength of the GTR-modified binder. Among the five aggregates, basalt showed the lowest value of ΔG_{wet}^{ad} , thereby providing the highest compatibility strength and it was followed by granite, limestone, sandstone, and gravel. To assess the best performing binder-aggregate system, a CR analysis has been conducted and results are explained next.

The CR, the ratio of ΔG_{dry}^{ad} and ΔG_{wet}^{ad} , is another indicator of moisture resistance of a binder-aggregate system. Table 6 shows the quantitative values of CR and qualitative compatibility grades of all binder-aggregate systems of the present study. It is seen that the addition of GTR results in a significant increase in the CR value. According to Bhasin et al. (2006), a CR value of greater than 1.5 provides the desired compatibility (Grade A), and a decrease of the CR value indicates a decrease of compatibility strength of the binder-aggregate system. It is seen that for a 20% GTR content, all aggregate-binder systems exhibit the desired compatibility ($CR > 1.5$ or Grade A). Among five aggregates, basalt exhibited the highest CR value, thereby providing the highest compatibility strength, and it was followed by granite, limestone, sandstone, and gravel.

4.5 Effects of GTR Size

The size of GTR particles has little effect on mechanistic performance and moisture resistance of the GTR-modified binders, and no particular trend was observed. As presented earlier (Fig. 3a), with 10% and 15% GTR contents, Mesh #40 (0.42 mm) showed

Table 5. SFE components, total SFE, and cohesive energy of binders, aggregates, and probe liquids

(a) Unmodified PG 64-22 and GTR-modified asphalt binders					
Binder types	Γ^+ (mJ/m ²)	Γ^- (mJ/m ²)	Γ^{LW} (mJ/m ²)	$\Gamma^{(total)}$ (mJ/m ²)	W_c (mJ/m ²)
PG 64-22+ 0% GTR	2.58	2.65	10.33	15.56	31.12
PG 64-22 + 10% GTR (Mesh #30)	5.31	5.28	10.88	21.48	42.96
PG 64-22 + 10% GTR (Mesh #40)	3.60	3.56	10.30	17.46	34.92
PG 64-22 + 15% GTR (Mesh #30)	6.17	6.15	11.42	23.74	47.48
PG 64-22 + 15% GTR (Mesh #40)	5.91	5.88	11.28	23.07	46.14
PG 64-22 + 20% GTR (Mesh #30)	7.79	7.77	12.51	28.07	56.14
PG 64-22 + 20% GTR (Mesh #40)	6.80	6.78	11.85	25.43	50.86
(b) Various aggregates					
Sandstone ^a	28.20	555.20	43.50	168.63	337.26
Gravel ^b	23.00	972.00	57.50	207.10	414.20
Granite ^c	24.10	96.00	133.20	181.30	362.60
Basalt ^c	0.60	164.00	52.30	67.22	134.44
Limestone ^a	13.00	540.70	51.90	135.74	271.48
(c) Various probe liquids (28)					
Water	25.50	25.50	21.80	72.80	145.60
Ethylene Glycol	1.92	47.00	29.00	48.00	96.00
Formamide	2.28	39.60	39.00	58.00	116.00

Note: Γ^+ = Acid Component, Γ^- = Basic Component, Γ^{LW} = Lifshitz van der Waals Component, $\Gamma^{(total)}$ = Total Surface Free Energy, W_c = Cohesive Energy

^a: Source Wasiuddin *et al.*(33), ^b: Source Little and Bhasin (32), ^c: Source Cheng *et al.* (29),

a slightly lower penetration value than Mesh #30. However, with a 20% GTR content, Mesh #30 (0.60 mm) provided slight lower penetration value than Mesh #40 (0.42 mm). Viscosity data of binders modified with Mesh #30 and Mesh #40 exhibit a similar trend. As shown in Fig. 3b, binders modified GTR Mesh #40 (0.42 mm) exhibited slightly higher viscosity than GTR Mesh #30. The *SFE* and compatibility analyses reveal that Mesh #40 (0.42 mm) graded GTR showed relatively higher *SFE*, W_c , compatibility ratio. Thus, GTR Mesh #40 (0.42 mm) exhibited relatively higher stiffness, *SFE*, and compatibility strength compared to GTR Mesh #30. For statistical evaluation of GTR

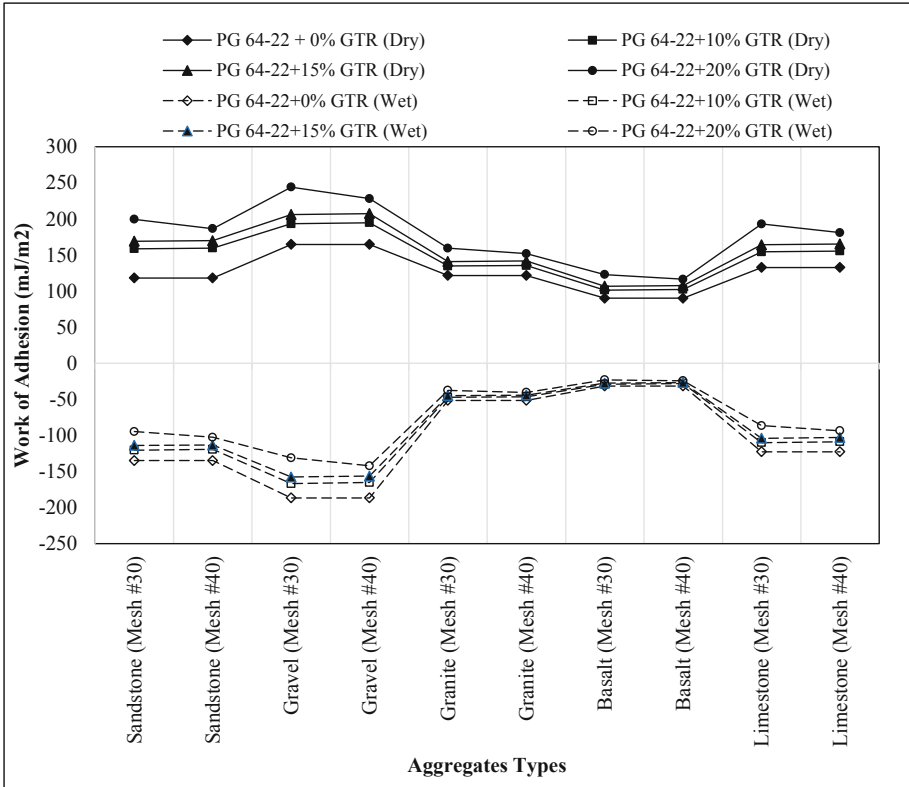


Fig. 5. Work of adhesion (dry and wet) of binder-aggregates combinations (Note: Solid Line for Dry and Dash Lines for Wet Condition).

size effects, an Analysis of Variance (ANOVA) of three replicate specimens of each test has been conducted at a 95% confidence interval (CI). This analysis used GTR-modified binder properties such as viscosity, $G^*/\sin\delta$, SFE , W_C , ΔG_{dry}^{ad} , ΔG_{wet}^{ad} , and CR as response variables and two different GTR sizes as factors. The statistical p -value has been determined for each test. It is known that the p -value indicates the probability of accepting or rejecting a null or alternative hypothesis. When the p -value is smaller than 0.05 (for 95% CI), the null hypothesis, which infers no significant differences among different tested factors, is rejected and the alternative hypothesis is accepted. The statistical p -values for all properties are found to be higher than 0.05. This indicates the properties of GTR-modified binders produced from two different GTR sizes (Mesh#30 and Mesh#40) are not statistically different but equivalent. The similarity may mean GTR essentially breaks down into its component on heating and mixing with the binder.

4.6 GTR-Modified Binders Versus Polymer Modified Binders

For comparison purposes, selective rheological and SFE test data of two polymer-modified binders (PG 70-22 and PG 76-22) from the same source and GTR-modified

Table 6. Compatibility ratio and corresponding qualitative compatibility description

Quantitative values of compatibility ratio					
Binder type	Sandstone	Gravel	Granite	Basalt	Limestone
PG 64-22	0.88	0.88	2.36	2.85	1.08
PG 64-22 + 10% GTR (#30)	1.34	1.18	2.91	3.63	1.43
PG 64-22 + 10% GTR (#40)	1.34	1.16	3.63	3.47	1.40
PG 64-22 + 15% GTR (#30)	1.50	1.33	3.20	4.01	1.60
PG 64-22 + 15% GTR (#40)	1.48	1.31	4.01	3.85	1.58
PG 64-22 + 20% GTR (#30)	1.82	1.60	3.76	4.77	1.93
PG 64-22 + 20% GTR (#40)	2.11	1.86	4.77	5.34	2.23
<i>Qualitative description of compatibility</i>					
PG 64-22	B	B	A	A	B
PG 64-22 + 10% GTR (#30)	B	B	A	A	B
PG 64-22 + 10% GTR (#40)	B	B	A	A	B
PG 64-22 + 15% GTR (#30)	A	B	A	A	A
PG 64-22 + 15% GTR (#40)	B	B	A	A	A
PG 64-22 + 20% GTR (#30)	A	A	A	A	A
PG 64-22 + 20% GTR (#40)	A	A	A	A	A

Note: CR > 1.5 means Very Good (A), CR 0.75 to 1.5 means Good (B), CR 0.5 to 0.75 means Poor (C) and CR < 0.5 means Very Poor (D).

binders have been analyzed and presented in Table 7. As seen from Table 7, viscosities of GTR-modified binders are significantly higher than the polymer-modified binders. The increase in viscosity seems to be higher when the GTR content is increased. Thus, the mixing and compaction temperature of GTR-modified mixes are expected to be higher compared to polymer-modified mixes. As seen from DSR test data, the rutting resistance of GTR-modified mixes is expected to increase significantly compared to the polymer-modified mixes. However, the low-temperature resistance is expected to decrease when GTR-modified mixes are used. The true PGs of tested GTR- and polymer modified binders, presented in Table 7 reflect the aforementioned observations. Thus, from the low-temperature performance, workability, and compactability perspectives, 15% GTR (Mesh #40) is found to be the most effective GTR content.

When SFE of GTR-modified binders are compared with polymer-modified PG 70-22 binder, for GTR Mesh #40, the cohesive energies of 15% and 20% GTR-modified binders are about 82% and 120%, respectively, higher than the tested PG 70-22 binder. The higher cohesive energy in the GTR-modified binder indicates increased bonds among binder molecules against breakage or separation, thus an increased resistance against moisture damage in GTR-modified binders.

Table 7 also shows MSCR test results that include non-recoverable creep compliance (J_{nr}), MSCR % Recovery, and MSCR grades for four traffic loading conditions (Standard,

Table 7. Performance properties of GTR-modified versus polymer-modified binders

Binder type	Superpave tests			SFE analysis			MSCR test results at 64 °C			
	Viscosity at 135 °C (Pa.s)	Viscosity at 165 °C (Pa.s)	True high PG based on DSR tests (°C)	True low PG based on BBR tests (°C)	Cohesive energy (mj/m ²)	MSCR-based J _{nr} .1.0 (kPa ⁻¹)	MSCR-based J _{nr} .3.2 (kPa ⁻¹)	MSCR-based recovery (%)	MSCR grade	
15% GTR-modified binder (#30)	2.39	0.77	78	-18	42.29	0.21	0.28	44.05	PG 64E-16	
15% GTR-modified binder (#40)	2.14	0.62	79	-20	46.38	0.09	0.12	72.25	PG 64E-16	
20% GTR-modified binder (#30)	5.14	1.09	86	-16	50.86	0.07	0.10	66.39	PG 64E-16	
20% GTR-modified binder (#40)	4.95	1.07	88	-17	56.14	0.03	0.04	84.71	PG 64E-16	
Polymer modified PG 70-22	1.27	0.31	73	-24	25.49	0.52	0.64	29.51	PG 64V-22	
Polymer modified PG 76-22	1.93	0.45	78	-23	28.22	0.27	0.32	30.63	PG 64E-22	

Heavy, Very Heavy, and Extreme). According to AASHTO M 332, if the load is standard traffic and less than 10 million Equivalent Single Axle Loads (ESALs), it is designated as Standard (S). If the load is between 10 and 30 million ESALs or slow-moving traffic loading, then it is called Heavy (H) traffic. On the other hand, if the load is standing or greater than 30 million ESALs, then the traffic designation is Very Heavy (V). Lastly, if the loading is greater than 30 million ESALs and standing traffic, the corresponding traffic designation is Extreme (E). The MSCR test results suggest that the compliance values at different stress levels are significantly lower compared to the polymer-modified binders. The MSCR % Recovery values are significantly higher compared to the tested polymer modified binders. The MSCR grade of 15% and 20% GTR modified binders is PG 64E-16, which is the same as that of polymer-modified PG 76-22 binder. On the other hand, the MSCR grade of the other tested polymer-modified PG 70-22 binder is PG 64V-22.

As illustrated earlier, there are some issues (e.g., workability and thermal cracking resistance) associated with the use of GTR-modified binders even though there are apparent beneficial effects in terms of rutting and moisture resistance. As the incorporation of GTR results in a significant increment of binder viscosity, GTR-asphalt mixtures would have inadequate workability and higher mixing and compaction temperatures. Besides, it can be assumed that the GTR-modified binder would not be suitable in relatively cold climatic regions (i.e., Wisconsin, Minnesota, and North Dakota). To overcome the aforementioned issues, the authors recommend to include some warm-mix additives in GTR-modified asphalt technology, which is expected to provide better workability, improved fatigue life, and balanced thermal properties. It is also recommended to conduct similar investigations for different binders in terms of source, and grades and compare results with additional polymer modified binders. It is envisioned that the properties of binders from a different source or different grade are expected to be different as their chemical constituents are different. However, based on the findings of this study, it is apparent that GTR is a viable asphalt modifier and can be successfully implemented especially in hot climatic regions.

This study is limited to laboratory evaluations of two different sizes (#30 and #40) of GTR samples, five types of aggregates, and one selected PG binder from one source. Additional sizes of GTR and PG binders will have to be evaluated to get a better understanding. The high service temperature and moisture resistance properties have been the primary focus of this study. Fatigue and low-temperature properties are recommended to study. Further, asphalt mix samples will be tested to understand the interaction of GTR-modified binders with different aggregates.

5 Concluding Remarks

In the present study, GTR-modified asphalt binders have been characterized through laboratory tests to assess the viability of the use of GTR in paving materials. A base performance grade (PG) binder (PG 64-22 marketed as PG 67-22) and different dosages (10%, 15%, and 20%) of two selected sizes (Mesh #30 and Mesh #40) of GTR samples were evaluated in this study. Besides a chemical analysis via the Fourier Transform Infrared (FTIR) spectroscopy technique and microstructure evaluation through an atomic force

microscope (AFM) system, selective rheological properties of GTR-modified binders were evaluated in the laboratory. Rheological tests of binders were conducted by conducting penetration (AASHTO T 49), rotational viscosity (RV) (AASHTO T 316), and dynamic shear rheometer (DSR) (AASHTO T 315) tests. Further, the moisture resistance of the GTR-modified binders was evaluated by following the sessile drop (SD) method. Based on the laboratory test results and discussions, the following conclusions are drawn:

- The base asphalt binder contains various types of alkanes, carboxylic acids, alkyl halides, etc., and the GTR-modification adds various amines and nitro compounds in the binder, and they act as antioxidants and lubricating agents, which reduce aging and improve moisture resistance.
- The base asphalt binder has complex micro-structures containing numerous ‘bee-like’ structures, representing long chains of wax crystals (SBS and/or SBR), and these “bee-like” structures are densified due to the addition of GTR. GTR also adds carbon black and inorganic filler particles.
- An addition of GTR improves the stiffness and rutting resistance of the base asphalt binder.
- GTR modification increases the total surface free energy (SFE), and cohesive energy of the base binder. It also increases adhesion energy in binder-aggregate interfaces and compatibility strength, indicating improved moisture resistance.
- A 15% (by the weight of the base binder) GTR is found to be the optimum dosage in this study. There is no significant difference in performance properties between Mesh #30 and Mesh #40 graded GTR-modified binder samples. However, the finer GTR (Mesh #40) is found to exhibit more favorable performance properties.
- Among the five aggregates examined in the current study, basalt shows the highest compatibility strength with GTR-modified binders, and it is followed by granite, limestone, sandstone, and gravel.

References

- ATRC. Asphalt-rubber Friction Course Reduces Traffic Noise. Arizona Transportation Research Center, ADOT, Phoenix, Arizona (1996)
- Bahriamian, A.: Evaluating Surface Energy Components of Asphalt Binders Using Wilhelmy Plate and Sessile Drop Techniques. Degree Project in Highway and Railway Engineering, Stockholm, Sweden (2002)
- Bhasin, A., Masad, E., Little, D., Lytton, R.: Limits on adhesive bond energy for improved resistance of hot-mix asphalt to moisture damage. *Transp. Res. Rec. J. Transp. Res. Board* **1970**(3), 3–13 (2006)
- Buddhala, A., Hossain, Z., Wasiuddin, N.M., Zaman, M., O’Rear, E.A.: Effects of an amine anti-stripping agent on moisture susceptibility of sasobit and asphamin mixes by surface free energy analysis. *J. Test. Eval.* **40**(1), 1–8 (2012)
- Bureau of Waste Prevention. Best Management Practices for Automotive Recyclers Waste Tires. Massachusetts Department of Environmental Protection, Boston, MA 02108-4746 (2006)
- CalTrans. Use of Scrap Tire Rubber - State of Technology and Best Practices. State of California Department of Transportation, Sacramento, California (2005)

- CalTrans. Asphalt Rubber Usage Guide. State of California Department of Transportation, Materials Engineering and Testing Service, Office of Flexible Pavement materials, 5900 Folsom Blvd, Sacramento, California 95819 (2006)
- CalTrans. Selection of Asphalt Binder Grade (2011). <http://www.dot.ca.gov/hq/construc/CPDatives/CPD06-11attach2.pdf>. Accessed 18 June 2015
- Cheng, D.X., Little, D.N., Lytton, R.L., Holste, J.C.: Surface free energy measurement of asphalt and its application to predicting fatigue and healing in asphalt mixtures. *J. Transp. Res. Board* **1810**, 44–53 (2001)
- Dourado, E.R., Simao, R.A., Leite, L.F.M.: Mechanical properties of asphalt binders evaluated by atomic force microscopy. *J. Microsc.* **245**, 119–128 (2011)
- EPA. Common Wastes and Materials – Scrap Tires” Environmental Protection Agency (2015). <http://www.epa.gov/osw/conserves/materials/tires/basic.htm>. Accessed 7 July 2015
- EPA. Wastes - Resource Conservation - Common Wastes & Materials - Scrap Tires (2020). <https://archive.epa.gov/epawaste/conserves/materials/tires/web/html/basic.html>. Accessed Nov 2020
- Ergon. Certificate of Analysis of Performance Graded Asphalt Binder PG 64-22. Ergon Asphalt & Emulsion, Certification No. EM 3441, Certification Date: December 4, 2014, Memphis TN 38113 (2014)
- Fini, E.H., Al-qadi, I.L., Abulebdeh, T., Masson, J.F.: Use of surface energy to evaluate the adhesion of bituminous crack sealants to aggregates. *Am. J. Eng. Appl. Sci.* **4**(2), 244–251 (2011)
- Hicks, R.G.: Asphalt Rubber Design and Construction Guidelines. Volume 1-Design Guidelines, Northern California Rubberized Asphalt Concrete Technology Center, Sacramento, California (2002)
- Hossain, Z., Lewis, S., Zaman, M., Buddhala, A., O’Rear, E.: Evaluation for warm mix additive-modified asphalt binders using spectroscopy techniques. *J. Mater. Civ. Eng.* **25**(2), 149–159 (2013)
- Hossain, Z., Braham, A., Baumgardner, G.: Performance of asphalts modified with polyphosphoric acid, TRC 1501. Final report, Arkansas Department of Transportation, Little Rock, AR (2015)
- Huang, J.F., Wu, S.P.L., Ma, X., Liu, Z.F.: Material selection and design for moisture damage of HMA pavement. *Mater. Sci. Forum* **614**, 269–274 (2009)
- Huang, W., Qian, Z.D.: Theory and Methodology of Advanced Asphalt Pavement Design. Science Publishing House, Beijing (2001)
- ICL. Disposable IR Sample Cards (2020). <https://www.internationalcrystal.net/ir-sample-cards/>. International Crystal Laboratories (ICL). Accessed Nov 2020
- Jia, X., Huang, B., Bowers, B.F., Zhao, S.: Infrared spectra and rheological properties of asphalt cement containing waste engine oil residue. *J. Constr. Build. Mater.* **50**, 683–691 (2013)
- Kaloush, K., et al.: Asphalt rubber asphalt concrete friction course overlay as a pavement preservation strategy. In: Proceedings of the 4th International Conference on Roads, Qatar, pp. 559–569 (2008). ISBN: 978-0-415-48979-9
- Kittu, A.T., Bulut, R., Puckette, J.: Effects of surface roughness on contact angle measurements on a limestone aggregate. *Recent Developments in Evaluation of Pavements and Paving Materials*, GSP 249 © ASCE 2014
- Little, D.N., Bhasin, A.: Using surface energy measurements to select materials for asphalt pavement. Texas Transportation Institute, Draft Final Report, Project 9-37, National Cooperative Highway Research Program, Washington, D.C. (2006)
- Loeber, L., Sciton, O., Morel, J., Valleton, J.M., Muller, G.: New direct observation of asphalts and asphalt binders by scanning electron microscopy and atomic force microscopy. *J. Microsc.* **182**(1), 32–39 (1996)
- Lu, Q., Harvey, J.T.: Investigation of conditions for moisture damage in asphalt concrete and appropriate laboratory test methods. California Department of Transportation, Division of Research and Innovation, Research Report: UC-RR-2005-15, Sacramento, CA (2005)

- McCarron, B., Yu, X., Tao, M., Burnham, N.: The investigation of 'bee-structures' in asphalt binder. Final report of Major Qualifying Project 2011–2012, Department of Physics, Worcester Polytechnic Institute, Worcester, MA (2012)
- Mika, T.F.: The use of epoxy resins in synthetic rubber compositions. *J. Appl. Chem.* **6**(9), 365–375 (2007)
- Moraes, M.B.D., Pereira, R.B., Leite, L.F.M.: High temperature AFM study of CAP 30/45 pen grade bitumen. *J. Microsc.* **239**, 46–53 (2010)
- Recycling Research Institute. The Source for Information About Scrap Tires and Rubber Recycling. *Scrap Tire News* (2015). <http://www.scraptirenews.com/tdf.php#prettyPhoto>. Accessed 7 July 2015
- Scribd. Table of Characteristic IR Absorption (2015). <http://www.scribd.com/doc/129244226/Table-of-Characteristic-IR-Absorptions#scribd>. Accessed 12 June 2015
- Tarefder, R., Arifuzzaman, M.A.: Study of moisture damage in plastomeric polymer modified asphalt binder using functionalized AFM tips. *Syst. Cybern. Inform.* **9**(6), 23–24 (2011)
- Terrel, R.L., Al-Swailmi, S.H.: Water Sensitivity of Asphalt-Aggregate Mixes: Test Selection. SHRP A-403, Strategic Highway Research Program, National Research Council, Washington, D.C. (1994)
- Van Oss, C.J., Chaudhury, M.K., Good, R.J.: Interfacial Lifshitz-van der Waals and polar interactions in macroscopic systems. *Chem. Rev.* **88**(6), 941–972 (1998)
- Wasiuddin, N.M., Zaman, M., O'Rear, E.A.: Polymeric aggregate treatment using styrene-butadiene rubber (SBR) for moisture-induced damage potential. *Int. J. Pavement Res. Technol.* **3**(1), 3–6 (2010)
- Way, G.B., Kaloush, K.U., Biligiri, K.P.: Asphalt-rubber practice guide. Final report, Rubber Pavement Association, Tempe, Arizona (2011)
- Xiao, F., Amirhanian, S.: Laboratory investigation of moisture damage in rubberized asphalt mixtures containing reclaimed asphalt pavement. *Int. J. Pavement Eng.* **10**(5), 319–328 (2009)



Role of Graphene Oxide Nanosheet on Mixing and Compacting Temperature of Bitumen

Hillol Chakravarty^(✉), Sanjeev Sinha, Pramanand Kumar, and Subrata Das

National Institute of Technology Patna, Patna, Bihar, India
hillol1140870@nitp.ac.in

Abstract. Durability of flexible pavements is a major concern. The durability is greatly influenced by construction practice wherein properly compacted mixes have longer life. The mixing and compaction temperature which ultimately depends upon viscosity of bitumen affects durability. In order to achieve proper bitumen-aggregate mixing, the bitumen should attain a viscosity range beyond which the bitumen would be sufficiently thick to properly coat the aggregates and below which the bitumen flows. On construction site, laying and proper compacting is achieved only when the bitumen remains within certain viscosity range. Below this range, the rolling process leads to lateral movement of the mix and above which the mix becomes too stiff for proper compaction to achieve requisite density. Viscosity is determined using the equiviscous temperature method wherein kinematic viscosities are obtained at varying temperatures using rotational viscometer (RV) and a viscosity-temperature graph is plotted. Temperature range corresponding to 0.17 ± 0.02 Pa.s is chosen as mixing temperature and 0.28 ± 0.03 Pa.s is chosen as compacting temperature respectively. Achievement of significant improvements in the rheological properties by the use of nano sized particles has motivated for identification and usage of new nano materials in the field. Recent usage and encouraging result using Graphene Oxide (GO) nanosheet had served as the motivation for its usage in the present study. GO was synthesized using modified Hummers' method and Fourier Transformation infrared (FTIR), UV-Vis and X-ray diffraction was done to characterize the synthesized GO. High speed stirrer was used to produce the GO modified binder at 0.2%, 0.5% and 1% GO by weight of binder and compared with virgin binder. RV was thereafter used to obtain viscosity-temperature graphs varying the temperature and mixing and compacting temperature was obtained using the equiviscous temperature method. It was observed that viscosity kept on decreasing with increase in GO concentration. This reduction of viscosity can be attributed to sheet structure of GO which internally mobilizes the binder. This result in significant reduction in mixing and compacting temperature renders environmental benefits. However, several other tests and evaluations are needed to justify the cost associated with the synthesis and use of this nanomaterial in flexible pavements.

1 Introduction

Pavements comprise of different materials and are used to cater vehicular load. Flexible pavements are those where load transfer happen by using grain to grain transfer

mechanism. The flexible pavements are widely preferred over their counterparts; rigid pavements due to various advantages such as rapid construction pace, easier supervision practices during construction etc. [1]. However, the primary concern for flexible pavement is the durability issues. The upper layers in these pavements are composed of bituminous mixes comprising of bitumen and aggregates along with filler material; where bitumen acts as the binder material. Bitumen being a temperature dependent viscoelastic material, proper control of temperature becomes important for managing the workability during the construction thereby enhancing the durability. For proper workability during mixing, the binder should attain a certain viscosity range above which the binder would be sufficiently thick to properly coat the aggregates; and below which the binder gets too fluid to stay bonded with the aggregates. The bituminous mixes are prepared at plant and thereby are brought for laying and compacting at site. While undertaking the compaction operation, the accepted density can be achieved when the binder remain at certain viscosity range. Below the range, the rolling process leads to lateral movement of the mix resulting in non-uniform thickness of layers; above which the mix becomes too stiff thereby failing to achieve requisite density upon rolling. The process of improper mixing and compaction potentially lead to early failure of pavements. The importance of maintaining proper viscosity while working with bitumen can thus be assessed.

The importance being understood, researches were carried to find the optimal viscosity which would serve the purpose and in turn the correct corresponding temperatures could be obtained. Various techniques to study the viscosity and criteria were developed to identify the mixing and compacting temperatures viz Equiviscous temperatures, High Shear Rate Viscosity, Steady Shear Flow, Zero (low) shear viscosity, Mixture Workability, Compaction test [2]. Most widely used viscosity determination is done using the Equiviscous Temperatures wherein rotational (kinematic) viscosities are obtained at varying temperatures and a viscosity-temperature graph is plotted. Temperature range corresponding to 0.17 ± 0.02 Pa.s is chosen as mixing temperature and temperature range corresponding to 0.28 ± 0.03 Pa.s is chosen as compacting temperature.

Modification of bitumen is one of the preferred options chosen by a various researchers to achieve better pavement performance. Modified binders are generally recommended [3, 4] for pavements carrying high traffic volumes and subjected to high pavement temperatures. Apart from polymer and crumb rubber modified bitumen, certain types of fillers have shown improvement in the performance of bituminous mixes in resisting different types of distresses. The use of nano-modifiers to enhance pavement materials have gained significant pace in recent years [1, 5–9]. Nanomaterials show special surface effects, elevated functional density, large surface area, high strain resistance, catalytic effects and high sensitivity thereby promoting usage for better functionality and improved performance. Graphene oxide (GO) is one of such nano-modifiers which have been used to modify construction materials since its emergence. Upon usage of GO, reinforcement of polymers and composites and improvement in functional properties as well as increase in tensile strength and durability of cement concrete have been demonstrated [10, 11]. Graphite is a prerequisite material for GO synthesis and its usage in bituminous mixes revealed that the unaged sample did show any significant influence in mechanical properties. However, the results improved with aging [12]. The

thermal conductivity of materials was enhanced by GO modifiers [13]. Low temperature rheological properties showed improvement for GO modified binders. However, at intermediate and high serviceable temperatures, no significant influence of GO was observed [14–16]. A small amount of GO was sufficient to induce viscosity changes. Cross linkage degree increased suggesting proper interaction. Reinforcement by GO was found not to significantly influence low temperature behavior. However, SBS modified binders required comparatively more GO dosage as compared to unmodified binder for improvement in properties [16]. Whereas no chemical interaction was observed between GO and unmodified binder and the synthesized CO_2 was attributed to decomposition of GO with temperature which leads to stripping and scattering of laminar layer into a single layer. That leads to improvement of rheological and mechanical properties of bituminous binders using GO [17, 18]. It is also predicted that GO had lubricating effect on construction materials which could improve the workability [14]. Research on GO as modifier is however still limited due to its recent introduction for modification of bituminous binder [19]. Hence, this research was undertaken to ascertain the influence of GO on functionality of bituminous material.

2 Objectives

The first objective of the research was to synthesize GO. Secondly, the GO nano-sheets were characterized to obtain the properties of the synthesized material. Thereafter, the binder was modified using GO using high speed stirrer. Final objective was to perform equiviscous test to determine the mixing and compacting temperatures and check the effect on viscosity and in turn the mixing and compacting temperatures in case of GO modified bitumen.

3 Methodology

Initially, the GO was synthesized using modified Hummer's method. Thereafter, FTIR spectroscopic analysis, UV Vis spectrometry and XRD analysis was done to characterize the synthesized material. High speed stirrer at 2000 rpm was used for 30 min. at 150 °C to obtain GO modified binders. The modification was done at 0.2%, 0.5% and 1% GO, and the samples were thereafter considered for viscosity analysis. The binder that was used was VG-30. Rotational Viscosity (RV) test as per ASTM 4402 was conducted on each of the samples to determine the kinematic viscosity for applying the equiviscous method to determine the mixing and compacting temperatures.

4 Synthesis

The GO was synthesized using modified Hummer's method. In this method, the natural graphite flake was mixed with H_2SO_4 , H_3PO_4 and KMnO_4 was added into mixture and thereafter, the resulting mixture was cooled. Then the mixture was heated up to 35 °C for 30 min and 95 °C for 3 h and stirred for the whole process. H_2O_2 was added along with H_2O to terminate the reaction. The resulting mixture was cooled, filtered and

washed with dilute HCl so that final product become sulphate free and finally washed with ethanol. Thereafter sample was dried in to the vacuum oven at 60 °C till complete dry.

5 Results and Discussion

Fourier-transform infrared (FTIR).

Fourier-transform infrared (FTIR) spectroscopy was used to record the spectra of the samples in ATR mode using Shimadzu, IR-Affinity-1S in the range of 4000–400 cm^{-1} to characterize the synthesized GO. The GO has the spectral band at 3205 cm^{-1} ascribed as the presence of the OH group. The peaks for C = O, C-O-C, and C = C were observed at 1716 cm^{-1} , 1037 cm^{-1} , and 1618 cm^{-1} respectively [20].

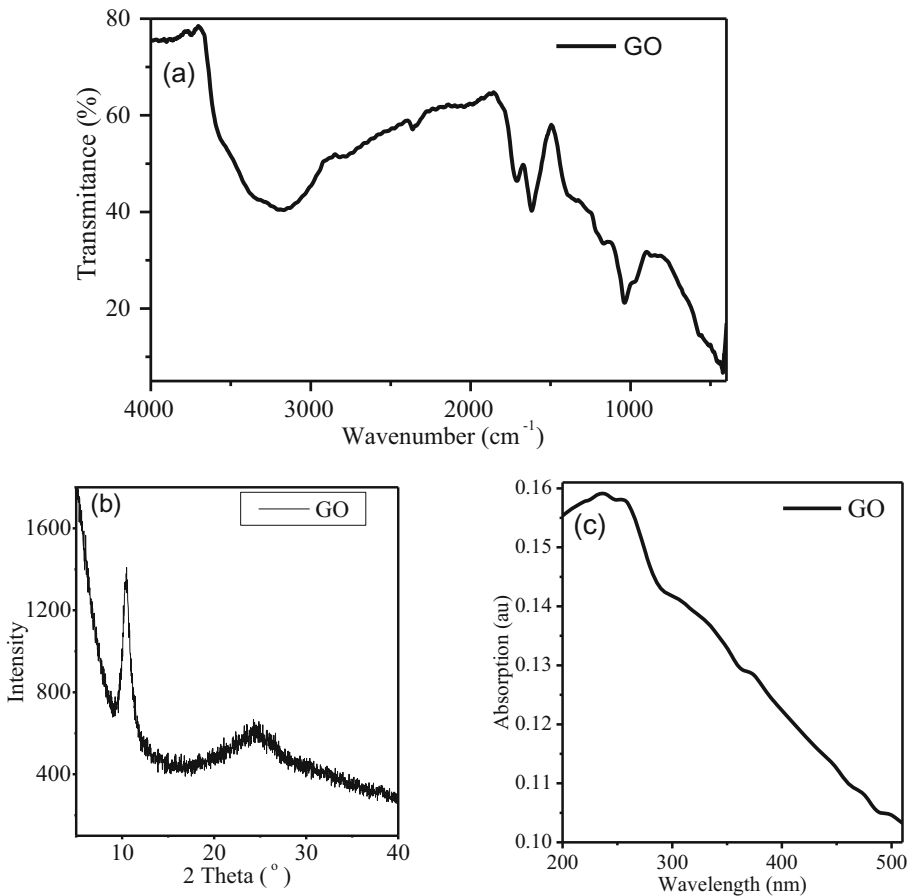


Fig. 1. The Characterization of Graphene Oxide (a) FTIR spectra, (b) XRD spectra, (c) Uv-Vis Spectra.

Uv-Vis Spectroscopy

The Uv-Vis spectroscopic analysis confirmed the proper synthesis of GO as the observed absorption band at λ_{max} 236 nm and about 300 nm due to π - π^* and n - π^* transition, respectively corresponded to GO [20, 21].

X-ray Diffraction (XRD)

The characteristic diffraction peak of GO was observed at a 2θ value of 10.42° in the XRD spectra. The broad peak at around 23° may be due to the incomplete oxidation of graphite (Fig. 1).

Thus, bitumen of grade VG 30 was used and various physical characterization tests on base bitumen were conducted to obtain the penetration value and softening point (Table 1).

Table 1. Physical characterization of base bitumen

Test	Result	Specification limit
Penetration	52	50–70
Softening point	64	Above 47

Modification of base binder was done by using high speed shear stirrer at 2000 rpm and for duration of 30 min. at 150°C . The modified binders were prepared at a concentration of 0.2%, 0.5% and 1% by weight of bitumen.

After the preparation of samples, Bohlin's viscometer was used to find the kinematic viscosity in Pa.s at varying temperatures. Thereafter, a graph is plotted between temperature and viscosity with the varying concentrations of GO. Accordingly, by using Equiviscous temperature criteria, the temperature range required to obtain a viscosity of 0.17 ± 0.02 Pa.s is chosen as mixing temperature and temperature range corresponding to 0.28 ± 0.03 Pa.s is chosen as compacting temperature.

Figure 2 was used thereafter to determine the mixing and compacting temperatures. These are summarized and are given in Table 2 below.

It can be observed from the findings that the mixing and compacting temperature decreased marginally with increment of additive percentage signifying lesser energy expenditure during the initial construction phase of the pavements. However, for 0.2% GO modification, a slight change in the pattern was observed. At higher temperature however, the influence of GO however ceases to exist. Introduction of more characterization tools is pivotal to characterize the interaction, although literature provides some evidence of the interaction mechanism of GO and asphalt binders.

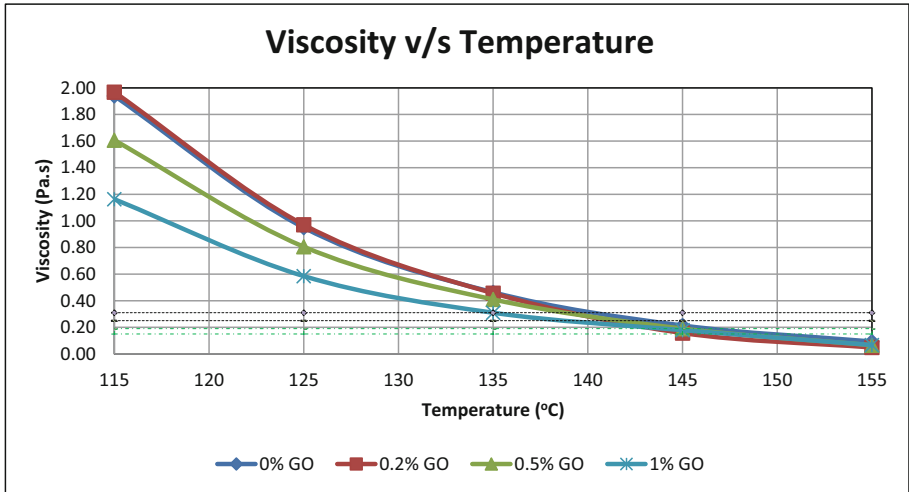


Fig. 2. Temperature v/s Viscosity plot with variation in concentration of GO.

Table 2. Maximum and minimum values for mixing and compaction temperatures

Binder type	Mixing temperatures (°C)		Compaction temperatures (°C)	
	Max	Min	Max	Min
Unmodified Binder	152	146.43	143.04	140
0.2% GO modified	145.7	144.4	141.25	139
0.5% GO modified	147.68	145	141.61	138.88
1% GO modified	145.54	143.57	138.93	135

6 Conclusions

Literature shows that GO nano-sheets holds potential to address many problems of Civil engineering. However, its usage for pavement engineering purpose was found to be limited. As such, the material was considered for the research to address the influence of the nano material on mixing and compacting temperature of bituminous binder. Based on the above results for this research of bitumen modification using GO, following conclusions can be drawn.

1. Modified Hummer's method was found to be an effective technique for developing GO nano-sheets using limited resources. However, considering the time required for the synthesis and the quantity of material being synthesized will prove as an obstruction for synthesizing it for pavement purpose.
2. Spectroscopic characterization of GO nano-sheets revealed that the material was synthesized accordingly. However, XRD analysis revealed incomplete oxidation might have occurred in some sites.

3. The viscosity showed in general a decreasing trend with GO modification. This reduction of viscosity might be due to sheet structure of GO which internally mobilizes the binder. However, with low modification (0.2% GO), a slight diversion from the trend was observed. This behavior led to marginal decrease in mixing and compacting temperature during construction phase, which could decrease the energy consumption during that phase rendering environmental benefits.
4. Wide scale study using various types of binders and various other tests needs to be performed to provide rationalization for its usage, since the time and efficiency of the synthesis process is yet to be modified for bulk scale usage. However, test results nullified a significant influence of GO on mixing and compaction temperature of binder.

References

1. Chakravarty, H., Sinha, S.: Moisture damage of bituminous pavements and application of nanotechnology in its prevention. *J. Mater. Civil Eng.* **32**(8), 03120003 (2020). [https://doi.org/10.1061/\(ASCE\)MT.1943-5533.0003293](https://doi.org/10.1061/(ASCE)MT.1943-5533.0003293)
2. West, R.C., Watson, D.E., Turner, P.A., Casola, J.: *Mixing and Compacting Temperatures of Asphalt Binders in Hot Mix Asphalt*, NCHRP Report 648, Transportation Research Board (TRB), Washington D.C. (2010)
3. *Guidelines on Use of Polymer and Rubber Modified Bitumen in Road Construction*. 2nd revision, IRC: SP: 53, Indian Road Congress, New Delhi, India (2010)
4. *Polymer and Rubber Modified Bitumen Specification*, IS: 15462, Bureau of Indian Standards, New Delhi (2010)
5. Yang, J., Tighe, S.: A review of advances of nanotechnology in asphalt mixtures. *Procedia-Soc. Behav. Sci.* 1269–1276 (2013)
6. Abdelrahman, M., Katti, D., Ghavibazoo, A., Upadhyay, H., Katti, K.: Engineering physical properties of asphalt binders through nanoclay-asphalt interactions. *J. Mater. Civil Eng.* **26**(12) (2014)
7. Jahromi, S., Ghaffarpour, K.A.: Effects of nanoclay on rheological properties of bitumen binder. *Constr. Build. Mater.* **23**, 2894–2904 (2009). <https://doi.org/10.1016/j.conbuildmat.2009.02.027>
8. Yao, H., et al.: Rheological properties and chemical bonding of asphalt modified with nanosilica. *J. Mater. Civil Eng.* **25**(11), 1619–1630 (2013). [https://doi.org/10.1061/\(ASCE\)MT.1943-5533.0000690](https://doi.org/10.1061/(ASCE)MT.1943-5533.0000690)
9. Arabani, M., Faramarzi, M.: Characterization of CNTs-modified HMA's mechanical properties. *Constr. Build. Mater.* **83**, 207–215 (2015). <https://doi.org/10.1016/j.conbuildmat.2015.03.035>
10. Young, R.J., Kinloch, I.A., Gong, L., Novoselov, K.S.: The mechanics of graphene nanocomposites: a review. *Compos. Sci. Technol.* **72**, 1459–1476 (2012). <https://doi.org/10.1016/j.compscitech.2012.05.005>
11. Du, H., Pang, S.D.: Mechanical response and strain sensing of cement composites added with graphene nanoplatelet under tension. In: Sobolev, K., Shah, S.P. (eds.) *Nanotechnology in Construction*, pp. 377–382. Springer, Cham (2015). https://doi.org/10.1007/978-3-319-17088-6_49
12. Kok, B.V., Yilmaz, M., Erkus, Y.: Effects of graphite on mechanical properties of stone mastic asphalt pavement. *J. Civ. Eng. Manage.* **23**(8), 1013–1020 (2017)

13. Sedaghat, A., Ram, M.K., Zayed, A., Kamal, R., Shanahan, N.: Investigation of physical properties of graphene-cement composite for structural applications, *Open. J. Compos. Mater.* **4**, 12–21 (2014). <https://doi.org/10.4236/ojcm.2014.41002>
14. Marasteanu, M., Le, J.-L., Turos, M.: Graphene nano-platelet (GNP) reinforced asphalt binders and mixtures. In: 6th Eurasphalt & Eurobitume Congress, Prague Czech Republic (2016). <https://doi.org/10.14311/EE.2016.104>.
15. Habib, N.Z., Aun, N.C., Zoorob, S.E., Ing, L.P.: Use of graphene oxide as a bitumen modifier: an innovative process optimization study. *Adv. Mater. Res.* **1105**, 365–369 (2015)
16. Liu, K., Zhang, K., Shi, X.: Performance evaluation and modification mechanism mechanism analysis of asphalt binders modified by graphene oxide. *Constr. Build. Mater.* **163**(28), 880–889 (2018)
17. Li, Y., Wu, S., Airkhanian, S.: Investigation of the graphene oxide and asphalt interaction and its affect on asphalt pavement performance. *Constr. Build. Mater.* **165**, 572–584 (2018)
18. Li, Y., Wu, S., Airkhanian, S.: Effects of Graphene Oxide on Asphalt Binders. *Nanotechnology in Eco-efficient Construction (Second Edition)*. Elsevier (2019)
19. Moreno-Navarro, F., Sol-Sanchez, M., Gamiz, F., Rubio-Gamez, M.C.: Mechanical and thermal properties of graphene modified asphalt binders. *Constr. Build. Mater.* **180**(2018), 265–274 (2018)
20. Kumar, P., Bora, C., Kumar, B., Sukula, P.K., Das, S.: Synthesis and characterization of 5-nitroso-6-amino-uracil functionalized reduced graphene oxide for the detection of chromium ion in aqueous medium. *Synthetic Metals* **264**, 116381 (2020)
21. Zhang, Y., et al.: Facile synthesis of well-dispersed graphene by γ -ray induced reduction of graphene oxide. *J. Mater. Chem.* **22**, 13064–13069 (2012)



Performance Evaluation of Fiber-Reinforced Expansive Subgrade Soil Stabilized with Alkali Activated Binder, Lime, and Cement: A Comparative Study

Mazhar Syed¹, Anasua GuhaRay¹(✉), and Ankit Garg²

¹ Civil Engineering Department, BITS-Pilani Hyderabad Campus, Secunderabad 500078, India
{p20170007, guharay}@hyderabad.bits-pilani.ac.in

² Civil, and Environmental Engineering Department, Shantou University, Shantou, China
ankit@stu.edu.cn

Theme: Transportation Geotechnical Engineering

Subtheme: Innovative and Sustainable Geomaterials and Geosystems

Abstract. Expansive subgrade soil exhibits a high degree of volumetric instability upon periodic moisture fluctuation, resulting in low bearing strength and loss of pavement serviceability. However, the use of conventional binders has a significant impact on the atmosphere by releasing greenhouse gases. In the present study, an attempt is made to enhance the strength characteristics of the expansive subgrade soil by stabilizing with an eco-friendly alkali activated binder (AAB) reinforced by two distinct types of fibers, polypropylene (PF) and chemically treated hemp fiber (CHF). The research also compares PF and THF reinforcement's effectiveness in AAB with the conventional lime and cement binders. AAB is synthesized by adding an aluminosilicate precursor (slag and low calcium fly ash) to the alkali activator solution for sodium hydroxide and sodium silicates. In the alkaline binder, a minimum water to solids ratio (w/s) of 0.4 is maintained. The effects of varying PF and CHF content in lime, cement, and slag-fly ash-based AAB soil mixture is evaluated through a series of tests, including swelling potential, compressive shear, strength, and penetration resistance tests. California bearing ratio (CBR) is chosen as a subgrade performance indicator for both PF and CHF reinforced soil. Reliability analysis using Monte Carlo Simulation (MCS) is further conducted to determine indices for CBR and strength tests that help to analyze the impact of uncertainties associated with the design of the fiber-reinforced AAB treated subgrade layer. Microstructural and morphological studies are carried out for lime, cemented, and AAB treated soil reinforced with PF and CHF. It is observed that PF reinforced soil has achieved a higher interfacial bonding with strong interlocking density under low tensile and shrinkage cracking compared to other fibers. The study also shows that the subgrade strength improvement under higher fiber dosages is prominent when AAB is used as an additive compared to lime and

cement. The reliability analysis results show that the optimum dosages of fiber and slag-fly ash ratio in AAB-soil mixture are essential factors for strengthening the subgrade parameters.

Keywords: Expansive subgrade soil · Alkali activated binder · Polypropylene fiber · Hemp fiber · Reliability analysis

1 Introduction

Expansive subgrade soils undergo large volumetric changes (heave/shrink) due to moisture imbalance and exhibit cracking upon desiccation, alters the long-term sealing effect. This periodic volumetric stability fluctuation is majorly attributed to the existence of montmorillonite and smectite group. The annual cost of repairing and restoring damaged structure due to expansive soil instability is projected at \$9 billion in the US, \$1 billion in China, and \$0.5 billion in the UK. Between 1970 and 2000, the total annual loss increased by around 140%, with just \$4 billion for paving and lightweight structures (Saride and Dutta 2016). The use of conventional cemented binders effectively reinforced the subgrade bearing ratio and regulated the swelling potential. However, the production of these binders contributes to 7–8% annual greenhouse gases, and by 2050 the growth in binders demand will reach up to 200% worldwide (Bell 1996). A new approach to efficiently reinforce the weak soil is the combined use of industrial by-products (such as cement kiln dust, fly ash, ashes, blast furnace slag, and bagasse ash) with low-carbon binders as a complete or partial replacement of portland cement or lime binder (Amadi 2014; Miao et al. 2017; Yong and Ouhadi 2007).

Usage of low carbon binders like Alkali Activated Binder (AAB) is another useful approach for improving the weak subgrades soil. AAB is a polymeric long-chain compound of aluminosilicate sodium matrix synthesized from pozzolanic precursors (Davidovits 1994). Enviro-safe AAB offers two benefits as it limits the conventional binder's demand and saves the landfill related costs of dumping fly ash-slag. It also has superior workability, higher mechanical performance, and excellent durability with a low carbon footprint (80% less CO₂) than cement binder (Provis and van Deventer 2014; Syed et al. 2020a; 2020b). Rios et al. (2016) compared the soil structural performances treated with alkali activated and cement binder. They observed that the alkaline soil specimen attained higher mechanical resistance with long-lasting strength. Miao et al. (2017) proposed an optimal alkaline mixture of 10% volcanic ash with 7% KOH on geopolymerised expansive soil, where UCS increased by 62% and swelling reduced by 43%. Jiang et al. (2018) highlighted that the subgrade strength parameters and durability of lightweight alkali activated slag mixed clayey soil sand was higher than the lightweight Portland cement binder.

Although the compressive resistance of alkaline soil improved effectively, it contributed to weak tensile and flexural strength. Shrinkage cracking is a crucial issue in the summer season, as it is expected that this form of soil will shrink (Pourakbar et al. 2016; Tang et al. 2016). The issue of soil tensile cracking can be overcome by reinforcing the discrete fibers. The random inclusion of fiber reinforcement does not prevent the propagation of soil crack but indirectly regulates the number and width of shrinkage

cracking behavior (Moghal et al. 2018b). In recent years, many researchers have proved the effectiveness of fibers reinforcement with cementitious materials in different soils and considered the excellent earth reinforcement material for soil strengthening (Sudhakaran et al. 2018; Tang et al. 2016; Wei et al. 2018). Moghal et al. (2018a) compared the CBR behavior of 6% lime blended polypropylene fiber cast and fiber mesh as soil reinforcement and concluded that the lime-fiber CBR is a good performance subgrade strength indicator. While the geopolymerization process is recently used in geoen지니어ing applications, there is still limited study on the combination of fiber reinforcement with fly ash-slag dependent AAB in expansive soil.

In this study, an attempt has been made to strengthen the subgrade strength parameters of slag-fly ash AAB-soil reinforced with different fibers. This research's primary focus is to evaluate the geotechnical behavior of AAB treated expansive soil reinforced with randomly mixed polypropylene (PF) and chemically treated hemp (CHF) at various slag/fly ash ratios in the alkaline solution. The study also aims to compare the effectiveness of geomechanical characteristics among AAB, lime, and cement-treated fiber-reinforced soil. An effort has been made to improve the durability of the fiber and soil-fiber interaction by chemically processing the hemp fiber with 10 M of NaOH. A series of microstructural analyses were also carried out to examine the mineralogical and molecular bonding behavior. Moreover, the uncertainties in AAB-fiber-soil mixtures' subgrade strength behavior are predicted through reliability analysis for failure against the California bearing ratio (CBR) strength test by Monte Carlo Simulation (MCS) method.

2 Materials Used

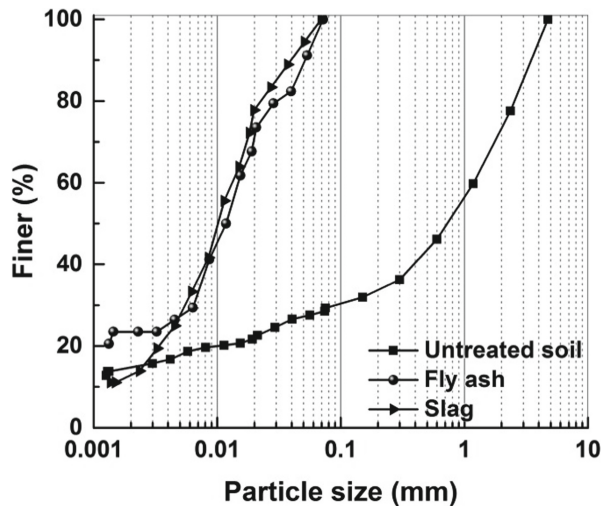
2.1 Raw Materials

The expansive soil from the Nalgonda region of Telangana was obtained in the present analysis. Disturbed samples were obtained from 30 cm below the soil surfaces. The in-situ moisture content, as determined in the field, was approximately 1.46%. In the laboratory, this soil was pulverized and then oven-dried before use. The soil was listed as Highly Compressible clay (CH) as per the Unified Soil Classification System (USCS). Class F fly ash and slag from the Ramagundam thermal power plant and JSW cement India limited, Andhra Pradesh, were collected, respectively. Ordinary Portland cement (53 grades) and hydrated lime were procured from Finechem, Hyderabad. Table 1 presented the basic physical-mechanical properties of soil, polypropylene, and hemp fibers, as calculated in the ASTM test method. The grading curves of particle sizes of fly ash, slag, untreated, and AAB treated soil were shown in Fig. 1.

The elemental compositions of expansive soil, fly ash, slag, polypropylene, untreated, and chemically treated hemp fiber were summarized in Table 2. Slag and Class F fly ash (low calcium as per ASTM C618-17a) was procured from JSW Cement Ltd., Andhra Pradesh, and National thermal power corporation (NTPC) Ramagundam, respectively. The chemical compound present in raw materials was obtained from X-ray fluorescence (XRF) analysis using the PANalytical Epsilon-1 spectrometer. When interacting with high-energy X-radiations under 7kV excitation voltage, atoms' activity was examined by the significant elements in soil, fibers, and other raw materials by maintaining constant

Table 1. Soil and fiber material properties

Properties	Soil	Properties	PF	HF
pH	8.2	Density (kg/m^3)	910	820
Specific gravity	2.58	Diameter (mm)	0.033	0.035
Sp. Surface area (m^2/g)	49	Tensile strength (MPa)	330	110
Free swell index (%)	89	Elastic modulus (MPa)	3500	3400
Liquid limit (%)	63	Burning Point ($^{\circ}\text{C}$)	588	—
Plasticity index (%)	38	Hemicellulose (%)	—	11
Dry density (g/cc)	1.6	Cellulose (%)	—	65
Moisture content (%)	24	Lignin (%)	—	6
Tensile strength (kPa)	6.6			
Compression strength (kPa)	186			
Soaked CBR (%)	1.93			

**Fig. 1.** Particles size distribution curves of fly ash, soil, and slag

temperature and air pressure. The main components of fly ash comprise 47.1% silicon dioxide (SiO_2), 20.1% aluminum oxide (Al_2O_3), 15.3% magnesium oxide (MgO), and 7.1% ferric oxide (Fe_2O_3). In addition, slag was rich in calcium oxide (CaO) of around 40.6%, with (>52%) of Al_2O_3 , MgO , and SiO_2 content. The presence of high calcium content in the slag can result in Calcium Silicate Hydrate (C-S-H) formation, which coexisted in the alkaline soil mixture with pozzolanic products. The leaching of heavy metals from the fly ash and slag combination was very negligible. The fly ash and slag composition of heavy metals such as chromium (Cr), arsenic trioxide (As_2O_3), lead

oxide (PbO), and zinc oxide (ZnO) were not found. Chemical compounds in fly ash and slag (such as Cao, MgO) can also easily monitor pH and soil leachate.

India produces almost 95–110 million tons of fly ash and slag from power and steel plants every year (IRC-SP-20–2002). In developing countries like India, the disposal of industrial waste by-products (such as slag and fly ash) is a big concern. The utilization of these wastes by combining with cementitious material in the soil enhances the subgrade properties, thereby preventing the need for disposal. These techniques save the associated costs of dumping into landfills and eliminate the demand for traditional binders. As most of these plants donate fly ash and slags, the cost of producing AAB is also lesser than that of Portland cement. AAB is found to act as an auxiliary cementing binder with a higher grade of serviceability performances with low ecological harm. India is the second-largest producer of fiber in the world. These fibers (synthetic and chemically treated natural fibers) are not affected by salts in soils, have low biological and ultraviolet degradation and survive in high-temperature conditions. Practically, the fiber-AAB-soil mixtures have been thoroughly mixed using a rotavator and layer compacted using a roller compactor. Practically, the fiber-AAB-soil mixtures have been thoroughly mixed using a rotavator and layer compacted using a roller compactor. Most of the construction of subgrade layers under Pradhan Mantri Gram Sadak Yojna (PMJSY) of unpaved roads (low-volume roads) and rural roads are stabilized with chemical binders using rotavator and compactor. Combining fly ash, slag, and fibers in the alkaline soil can offer a sustainable and economical solution for improving the poor subgrade properties.

Table 2. Chemical composition of raw materials

Elements (%)	Expansive soil	Fly ash	Slag	PF	HF	CHF
Magnesium Oxide	17.93	15.30	18.38	90.3	0.02	0.2
Aluminum oxide	12.46	20.17	12.09	0.00	2.90	2.9
Silicon dioxide	43.49	47.13	22.66	00.0	3.70	4.11
Phosphorus oxide	01.27	01.24	00.00	1.30	14.1	13.2
Sulfur trioxide	00.43	00.57	01.74	1.40	0.20	10.2
Chlorine	00.78	03.65	00.55	2.3	24.7	28.9
Potassium oxide	03.76	02.55	00.60	0.6	8.71	5.1
Calcium oxide	08.97	03.11	40.65	2.4	33.4	25.3
Titanium dioxide	01.34	02.00	01.23	0.1	1.5	0.95
Ferric oxide	09.34	07.12	01.11	0.8	10.6	7.4

2.2 Fiber Reinforcement

Two types of fibers, polypropylene and hemp fiber, used as reinforcement material in this study, were obtained from Go-green industries, Tamil Nadu. Based on soil-fiber contact, interlocking density (greater contact area with higher gripping around the fiber and pozzolanic compounds), interfacial bonding, and friction, a constant length of 12 mm and

25 mm were chosen for polypropylene and hemp fiber (Bordoloi et al. 2017; Moghal et al. 2017). Hemp fiber was chemically treated with 10M sodium hydroxide (NaOH) for 28 days to improve its quality and service life in the soil before being used as a soil reinforcement (Sudhakaran et al. 2018). The primary reasons for using polypropylene and hemp fiber in the AAB-soil are their negligible effects on the environment, sustainability, local accessibility, cost-effectiveness, and the ability to monitor the soil dispersivity, swell-shrink potential in the expansive soil (Syed and Guharay 2020; Mazhoud et al. 2017; Tang et al. 2007). Several studies have shown the research on the effectiveness of fiber reinforcement (type, length, and amount) with conventional cementitious binders on untreated soil. However, in past findings, the microstructural and geomechanical activity between polypropylene chemically modified hemp fibers in expansive soil has not been compared. This paper contributes to this where the influence of the effect of two fibers (PF and CHF) on AAB mixed soil was studied and compared with different cementitious binders. Figure 2 displayed polypropylene's surface images, untreated, and chemically treated hemp fibers using a stereomicroscope. Alkali activated binder (AAB) was generated by mixing alkaline solution consisting of sodium hydroxide and sodium silicate (mass ratio 10.57:29.43) in precursors of aluminosilicate (such as slag and fly ash class F). Within the alkaline binder, the fly ash and slag ratios are varied to get the optimal blend.

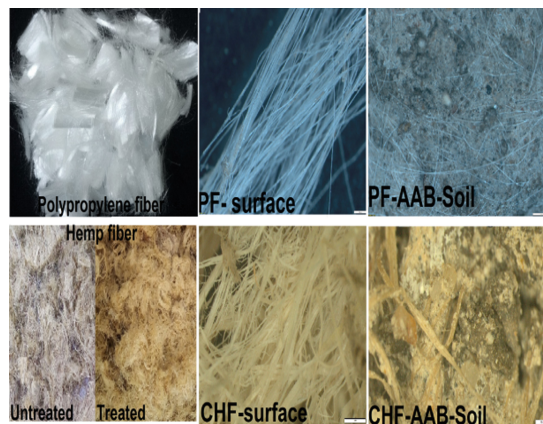


Fig. 2. Stereomicroscopic images of PF and CHF reinforced AAB soil

2.3 Sample Preparation

The expansive soil was mixed separately with 5% dry cement, 5% lime, and 5% AAB paste (by dry mass of soil) at different slag/fly ash ratios (0/100, 20/80, 40/60 proportions) in the AAB. 5% binder content in the soil was selected as optimum based on pH, alkaline reactivity, binding efficiency with low greenhouse gas emissions, and cost-effective compared to other dosages (Yong and Ouhadi 2007). Binder mixed soils were manually compacted in separate containers into three layers with a steel compactor rammer.

Moreover, compacted soil samples were covered with a moist jute bag for 28 days at room temperature for continuous curing. Before random mixing of polypropylene and chemically treated hemp fiber (0.2, 0.4, 0.6, and 0.8% dry weight of soil) in AAB, Lime, and cemented soil mixtures, the soil was oven-dried at 110 °C for 24 h. The terminology used for fiber-reinforced AAB, lime, and cemented soils was defined in Table 3.

Table 3. Sample definition of mixture proportion of fiber-reinforced soils

Sample designation	Sample definition
E.A5(Sm/Fn).Px E.A5(Sm/Fn).Hy m + n = 100 E.C5 E.L5 E.A5 (S ₀ / F ₁₀₀)P _{0.8} E.A5 (S ₂₀ / F ₈₀)P _{0.8} E.A5 (S ₄₀ / F ₆₀)P _{0.8} E.A5 (S ₀ / F ₁₀₀)H _{0.8} E.A5 (S ₂₀ / F ₈₀)H _{0.8} Similarly for other samples	E = Expansive soil; A ₅ = Mixing of 5% Alkali Activated Binder in the soil; C ₅ = Mixing of 5% Cement in the soil; L ₅ = Mixing of 5% Lime in the soil; S = slag; F = Fly ash; S _m /F _n = slag-fly ash ratio in the AAB mixture (0/100, 20/80 and 40/60); P = Polypropylene fiber; H = Chemically treated hemp fiber; m = Slag content in the AAB mixture (0, 10, 20, 30, and 40); n = Percentages of fly ash in the AAB mixture (100, 90, 80, 70, and 60); x = Percentages of polypropylene fiber mixed in soil (0%, 0.2%, 0.4%, 0.6% and 0.8%); y = Percentages of chemically treated hemp fiber mixed in the soil (0%, 0.2%, 0.4%, 0.6% and 0.8%)

3 Methodology

3.1 Microstructural Characterisation

A series of microstructural experiments were conducted with Fourier-transform infrared (FTIR), X-ray powder diffraction (XRD), Surface micrographs, and Energy-dispersive X-ray spectroscopy (EDS) on untreated, lime, AAB, and cemented fiber-reinforced soils. Such studies helped to examine the changes in soil structure's mineralogy, bonding activity with fibers matrix, and their reaction products. The JASCO FTIR 4200 setup was used to perform the FTIR absorbance spectroscopy through K.Br. Pellet arrangement. The spectral absorbance range for both untreated and chemically treated soils was 4000–500 cm⁻¹ was selected. XRD was carried out using the RIGAKU Ultima-IV diffractometer with an operating step of 0.02° for 2θ values. At 40 mA and 40 kV, CuKα rays were passed from 0° to 80° of 2θ at 2 s per step. Using Thermo Science Apreo SEM given by FEI at various spot regions and magnifications, soil surfaces and elemental composition were analyzed. The EDS spectra are calculated using Aztec's Oxford Instruments analyzer method. For a mass sample of 20 mg up to 800 °C under a nitrogen-rich atmosphere, TGA on both untreated and chemically treated hemp fiber was analyzed using Shimadzu/DTG-60 with a 10 °C/min heating rate.

Before and after applying cementitious binders in the soil, these tests help examine mineralogy and molecular bonding behavior variation. Moreover, it also ascertains the alterations in soil structure morphology, with fibers matrix, and their reaction products. FTIR and XRD provide qualitative information about the chemical composition of

the materials. Stereomicroscopy also offers qualitative information about the materials' physical characteristics. SEM, in conjunction with EDS analysis, is carried out in order to gain quantitative information.

3.2 Geotechnical Characterisation

A series of undrained shear (according to ASTM D2166–00), consolidation (following ASTM D2435–04), California bearing ratio (ASTM D1883–16), and flexural strength (ASTM D-1635) tests were performed for lime, cement, and AAB treated soil and reinforced with different fiber dosages. Both proportions of soil samples treated with slag/fly ash-based ratios of AAB mixture, cement, and lime were prepared at the respective MDD and OMC values.

The soil swell-consolidation tests were performed using the 2 cm height and 6 cm diameter one-dimensional Oedometer following the ASTM D2435–04 standard. Swell potential and e-log (p) curves were determined against a seating pressure of 6.25 kPa with different cementitious binder mixed soil specimens by ensuring their dry density. Swell potential (S%) was recorded as the soil thickness (H) increase ratio to the specimen's original thickness (H). In standard UCS split molds, both fibers reinforced soils were compacted in a mold of diameter 3.8 cm and height 7.6 cm. An automatic, strain-controlled compression system with a maximum 20 KN capacity at a fixed strain rate of 0.125 cm/min was used for the UCS test. Soaked CBR tests on lime, cement, and AAB with varying fly ash-slag composition were conducted as per ASTM D-2435. Specific soil specimen binders and fiber dosages were compacted at their MDD-OMC values in a standard CBR mold of 15 cm diameter and 17.5 cm height. Compacted soil-fibers specimens were soaked in water for four days with a 5 kg surcharge before testing at a fixed strain rate of 0.125 cm/min through a 50 mm diameter plunger.

In the Marshall Stability Machine, soil-fiber tensile tests are carried out by adding a loading strip of 12.5 mm to the load frame by preparing the 100 mm cylindrical sample of height 80 mm with a steady strain rate of 50.5 mm/minute during the tests. Similarly, the flexural strength was carried out by molding a 280 mm long flexure beam, 70 mm wide, and 70 mm thick in a three-point bending flexure machine. The flexure beam was compacted into five layers using a 3 kg steel rammer with a free fall of 310 mm. The beam specimens were removed after 48 h and mounted on two supports having a span length of 130 mm under a fixed loading strain rate of 0.1 mm/min. The following equation gives the ITS (S_t), modulus of rupture (R_m), and elastic modulus in mPa.

$$S_t = \frac{2 P_{max}}{\pi t d} \quad (1)$$

P_{max} = maximum load at which failure of soil sample occurred (N),
 t = thickness of soil specimen (mm), d = diameter of the soil specimen (mm).

$$R_m = \frac{3p_{ult} * l}{2bh^2} \quad (2)$$

$$E = \frac{p_{ult} * l^3}{4\Delta bh^3} \quad (3)$$

P_{ult} = ultimate breaking load at which sample failure occurred (N),
 l = length of beam specimen (mm), b = width of the beam specimen (mm),
 h = depth of the beam specimen (mm), Δ = deflection of beam (mm).

3.3 Reliability Analysis

The stability of structures is always impaired if they do not incorporate geotechnical variables' randomness into their design. The principle of reliability analysis is a proven mathematical method that considers these uncertainties of field variables (GuhaRay and Baidya 2015). The nonlinear form of equation used for regression analysis for both fibers reinforced AAB-soil is as follow below:

$$y = p (D_{Fiber}) + q(D_{SFR}) + r (D_{Fiber})^2 + s(D_{Fiber} * D_{SFR}) + t(D_{SFR})^2 + K_0 \quad (4)$$

Where p , q , r , s , and t = regression coefficient; K_0 = constant; D_{SFR} = dosage of slag/fly ash ratio in the alkaline solution; D_{Fiber} = dosage of polypropylene and chemically treated hemp fiber in AAB-soil respectively.

$$CBR_{PF} = 6.7198 \times (D_{PF}) + 8.9886 \times (D_{SFR}) - 1.4179 \times (D_{PF})^2 + 6.1394 \times (D_{PF} \times D_{SFR}) - 7.4595 \times (D_{SFR})^2 + 4.7295 \quad \text{with } R^2 = 0.993 \quad (5)$$

$$CBR_{CHF} = 3.7237 \times (D_{PF}) + 8.8624 \times (D_{SFR}) + 1.8611 \times (D_{PF})^2 + 3.9371 \times (D_{PF} \times D_{SFR}) - 7.2152 \times (D_{SFR})^2 + 4.7545 \quad \text{with } R^2 = 0.996 \quad (6)$$

Table 4. Statistics of input random variables

Random variables	Statistics		
	Mean (μ)	COV (%)	Distribution
D_{PF} & D_{CHF}	0.2, 0.4, 0.6, & 0.8%	5%	Normal
D_{SFR}	0.0, 0.25, & 0.66	5%	Normal
CBR_{min}	7 (%)	10–40%	Log-normal

For predicting the uncertainties in alkaline subgrade fiber-reinforced soil performance, a minimum specified soaked CBR (CBR_{min}) value is assigned from experimental observations. Table 4 describes the independent random variables, such as fiber dosages (D_{PF} & D_{CHF}) and the slag-fly ash ratio (D_{SFR}), defined by their mean and standard variation coefficient. The coefficient of variation (COV) of D_{PF} , D_{CHF} , and D_{SFR} was considered as 5% based on variations in loading conditions and testing environment. The COV for CBR_{min} was considered in the range of values proposed in the literature as 10–40% (Moghal et al. 2017). The present analysis presumed that the soaked CBR_{min} for both fiber-AAB-soils was approximately equal to 7% against the subgrade failure.

Monte Carlo simulation (MCS) was used to calculate the probability of failure (P_f) for different fiber content and slag-fly ash ratio in the AAB subgrade soil by simulating 30,000 variables in commercially available MATLAB software. It was consistent with Zevgolis and Bourdeau (2010) that the value converged for approximately 30,000 realizations. The P_f for CBR was defined as follows:

$$P_f = P(CBR - CBR_{min} < 0) = P\left(\frac{CBR}{CBR_{min}} < 1\right) \tag{7}$$

The reliability index (β) is defined as follows.

$$\beta = \log \text{inv} (P_f) \tag{8}$$

4 Results and Analysis

4.1 Microstructural Studies

4.1.1 Fourier Transfer Infrared Spectroscopy (FTIR)

In order to support the new functional group of soil crystallinity, the untreated, AAB, and cement treated soils were analyzed through FTIR spectroscopy. The relative transmittance spectra curve of untreated soil, shown in Fig. 3, was generally characterized by montmorillonite at 3660 cm^{-1} , followed by 3460 cm^{-1} for O-H stretching bound groups and water. A slight reduction of montmorillonite peak intensity was observed in cemented soil at around 3650 cm^{-1} . This decrement might be due to chemical weathering action on clay surfaces (Miao et al. 2017). Furthermore, the broadband was observed at 1650 cm^{-1} and 1440 cm^{-1} corresponded to C = C alkene and C-O-H's stretching vibration in both untreated soil and AAB-cemented soil. Due to the active presence of Na in the soil matrix, this carbonation reaction can be inducted. The band attributed a range of $1004\text{--}1029 \text{ cm}^{-1}$ to the asymmetric stretching vibration of the Si-O and Al-O group. Some quartz was also present at 798 cm^{-1} with a lower frequency of Si(Al)-O stretching vibrations. The Si-Al in-plane bending vibration was located in the wavenumber of approximately 560 cm^{-1} . Related bonds with a chemical change of around 20 cm^{-1} from untreated soil, AAB, and cement treated soil were seen in the spectrum peaks.

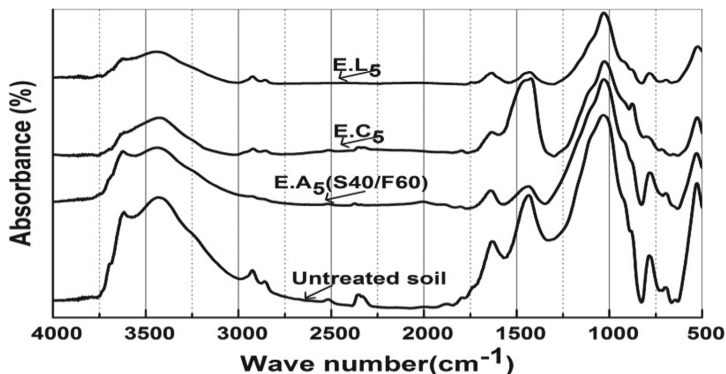


Fig. 3. FRIR spectroscopy of untreated soil, AAB, cement, and lime treated soil

4.1.2 X-ray Diffraction (XRD)

XRD is a fundamental investigative technique providing a broad range of comprehensible data on crystalline compounds found in clay minerals. Figure 4 showed the powdered XRD profile for untreated soil, AAB, cement, and lime treated soil. Untreated soil exhibited the crystalline peaks of quartz (Q), calcite (C), muscovite (Ms), and montmorillonite (M) (Sivapullaiah et al. 2010). The diffraction pattern of montmorillonite (M) and muscovite (Ms) decreased for AAB and cemented soil. XRD showed additional mullite (Mu) peak in AAB treated soil, indicating the active dissolution of sodium aluminosilicate compounds in soil by geopolymerisation (Miao et al. 2018). In addition, the cementitious compounds such as calcium silicate hydrate (CSH) and calcium aluminum hydrate (CAH) along with kaolinite (K) occurred in lime and cemented soil (Al-Mukhtar et al. 2012). The formation of these minerals might be because of the rapid hydration and pozzolanic reactions in the soil. For both untreated and cementitious binder treated soils, flatter portions of XRD indicated the amorphous phases.

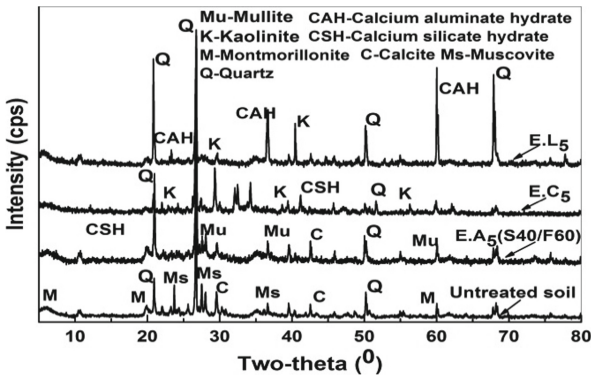


Fig. 4. XRD crystalline peaks of untreated soil, AAB, cement, and lime treated soil

4.1.3 Scanning Electron Microscope (SEM)/EDS Analysis

The surface micrographs of untreated soil, lime, cement, and fiber-reinforced AAB treated soils at different magnifications were presented in Fig. 5 (a-g). The untreated soil exhibited dispersed undulating microstructure in Fig. 5a, which was typically found in the clay matrix's montmorillonite-smectite group and imparted high volumetric instability and low shear strength upon moisture variations (Sivapullaiah et al. 2010). The soil-lime mixtures at 28 days (Fig. 5b) showed a series of floppy-like aggregated crystalline microstructure exhibited due to rapid exothermic cation exchange around the clay particles. In Fig. 5c, the cemented soil morphology developed into bladed crystals (needle shape) with long slender prism texture (Al-Mukhtar et al. 2012). Besides, the soil matrix showed the filling of voids with rods like ettringite needles along with cementitious compounds and aggregated particles. AAB soil based on fly ash-slag changed the clay composition by shaping the flocculated structure with a combination of hollow spherical particles (unreacted fly ash) and thin, smooth pitted gel layers (reacted fly ash)

in Fig. 5d. Figures 5e and f demonstrated the discrete reinforcement of polypropylene and hemp fibers in AAB soil as a spatial thread groove network. Hence, the fiber inclusions restricted the relative changes in crack widths' movement by actively retaining the clay particles through their interfacial friction. A detailed elemental composition of the quantitative graph is provided in Fig. 5g in order to support the above micrographs.

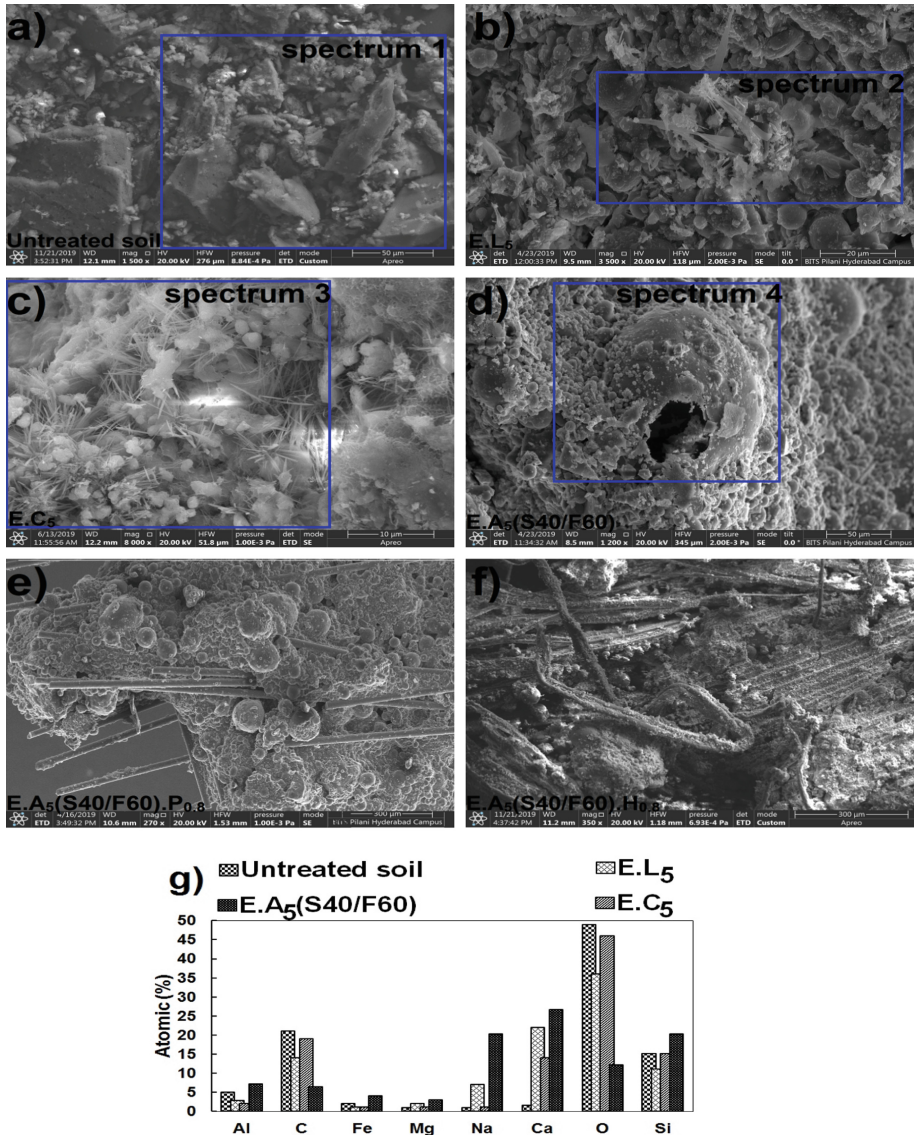


Fig. 5. SEM/EDS images of a) Untreated soil b) Lime-soil, c) Cemented-soil, d) AAB-soil, e) PF-AAB soil, f) CHF-AAB soil, g) Elemental compositions of soils.

4.1.4 Thermogravimetric Analysis (TGA)

Figure 6 shows the TGA curve for hemp fibers before and after chemical treatment in the form of mass loss upon temperature. The first significant loss happens in both fiber samples at around 110 °C and 300 °C. This reduction is due to the removal of free moisture and evaporation of volatile matters. The second mass loss is associated with biomass ranged at 350–390 °C, and this can happen due to the decomposition of hemicellulose and cellulose (Syed et al. 2020a). Comparing the results with parent fibers, the bands' position for treating fibers has changed and shifted towards the right side. The changes in the positions of peaks in treated fibers confirm the alteration of fiber surface structure and the formation of new chemical compounds after NaOH's addition. Further, it is also pointed out that the percentage of initial mass loss for coir fiber (6–8%) is relatively higher than hemp (4–5%). The low mass loss in treated fiber maybe because of encapsulation with NaOH around the fiber surfaces. TGA curves beyond 600 °C show minimal losses and mostly follow asymptotic behavior.

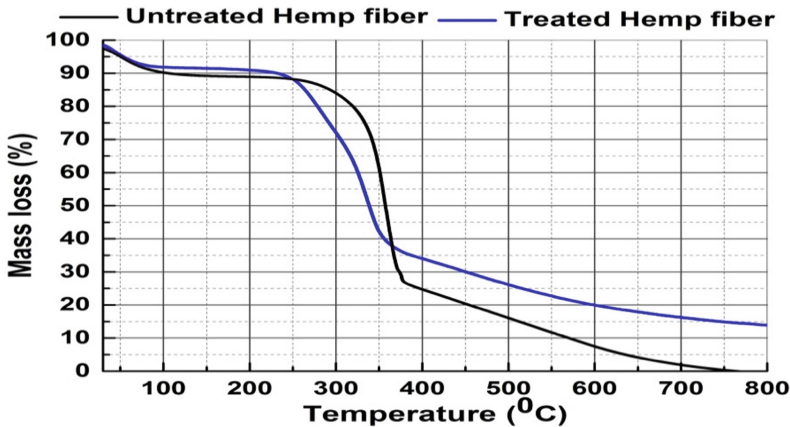


Fig. 6. TGA curve of untreated and chemically treated hemp fiber

4.2 Geotechnical Characterisation

A set of geomechanical tests on cemented, lime, and AAB treated soil were conducted at different slag/fly ash ratios as per ASTM norms. For comparison, the basic geoenvironmental properties are summarized in Table 5.

4.2.1 Consolidation

Figure 7(a-b) exhibited typical consolidation and swelling potential curves of soil amended with lime, cement, and AAB mixture at varying slag-fly ash ratios. Figures 7a and b revealed that the untreated soil attained the highest swelling potential and equilibrium void ratio with steeper slope relative to chemical binder reinforced soils. The volumetric expansion activity of lime and AAB stabilized soils was reduced marginally.

Table 5. Basic geotechnical tests for lime, cement, and AAB treated soils

Properties	E.L5	E.C5	E.A ₅ (S0/F100)	E.A ₅ (S20/F80)	E.A ₅ (S40/F60)	Test method
MDD (kN/m ²)	16.98	17.82	17.65	18.01	18.20	ASTM-D654
OMC (%)	20.18	18.66	19.21	18.46	18.32	ASTM-D654
PI (%)	24.11	21.26	22.69	20.75	19.9	ASTM-D4318
K (m/sec) (10 ⁻⁹)	0.896	0.846	0.82	0.864	0.0840	ASTM-D5084
Ls (%)	6.56	6.24	6.39	6.22	6.08	AS1289-C177
CC	0.16	0.14	0.16	0.15	0.14	ASTM-D2435
FSI (%)	41.26	36.42	38.16	33.8	31.9	IS 2720-40

When replacing fly ash with slag content in the AAB soil increased, the void ratio and swelling percentages further decreased. Minimizing the soil compressibility behavior upon addition of lime and the pozzolanic precursor is aided to activate the cationic exchange process, resulting in the formation of more soil flocculated matrix. The surface area and moisture retention potential of soil samples decreased due to the transition to a flocculated structure. Furthermore, in the existence of alkali solution, the rupture of sodium aluminosilicate precursors with a subsequent combination of cations might arise under geopolymerization, which capsulated the clay particle surfaces, resulting in less moisture absorbance and heaving (Miao et al. 2017; Rios et al. 2016). Besides, cemented soil effectively reduced the void ratio from 1.06 to 0.84 and the swell potential from 13.6 to 6.4%, respectively. In the presence of soil moisture, cemented soil actively generated the calcium-based alumina-silicate hydrated gel from its available calcium and silica, which indirectly influenced to limit the soil volume changes. Thus the consistent formation of new mineralogy in cementitious binder regulated the soil compressibility activity efficiently.

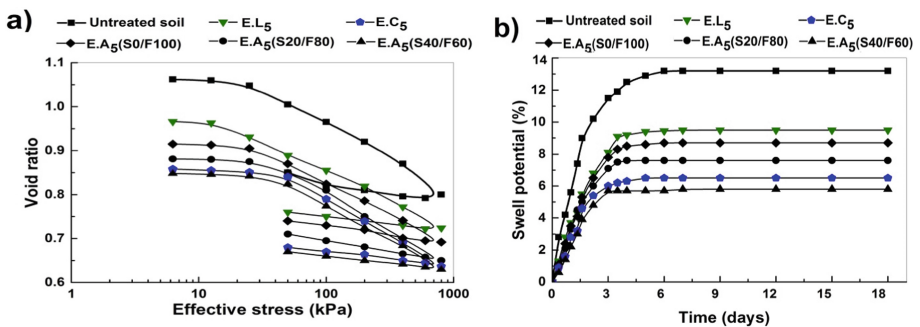


Fig. 7. Consolidation curve of lime, cement, and AAB treated soils a) void ratio versus effective stress b) Variation of swelling potential

4.2.2 Unconfined Compression Strength (UCS)

Figure 8 showed the variation of UCS values treated with three different chemical binders (lime, cement, and AAB) reinforced with polypropylene (represented in solid lines) and hemp fiber (dotted lines) at various percentages. It was evident from the results that the combined addition of cemented binders with fiber reinforcement shows a significant improvement in the shear resistance capacity. The UCS trend of mixed lime, cement, and AAB soils increased with increasing fiber dosages. The shear strength increment was more consistent with the alkaline binder through a higher ratio of slag-fly ash in both fibers reinforcement. Combining fly ash with slag volume in the AAB soil matrix was advantageous as it increased the level of geopolymerisation process and altered the mineral composition by formulating the active cementitious compounds across the fiber clay surfaces (Miao et al. 2017; Pourakbar et al. 2016; Zhang et al. 2013). On the other hand, the percentage gain in compressive shear strength was increased by around 32% for lime-fiber and 44% fiber-cemented soil mixtures. The substantial variations might be due to hydrated cementitious silicate gel formation in cemented soil upon the activation of hydration reaction. Moreover, the improvement was much greater in PF-soil than CHF-soil reinforcement in all chemically binder mixed soils. This enhancement might be attributed to their higher interfacial friction mobilization friction and bonding produced around the fiber surfaces during loading (Moghal et al. 2017; Tang et al. 2016; Wei et al. 2018). Also, polypropylene fibers were easily distributed in the soil matrix and bear the pulling stress with a higher linkage effect than the hemp fiber. It was also noteworthy that in the AAB soil, the 40/60 slag/fly ash ratio increased 35% compressive shear resistance than 0/100 (pure fly ash). Hence the increase in fiber dosages with slag replacement (up to 40%) in the AAB soil mixtures aids in improving the compression shear resistance capacity by restricting the relative moment of fiber in the soil.

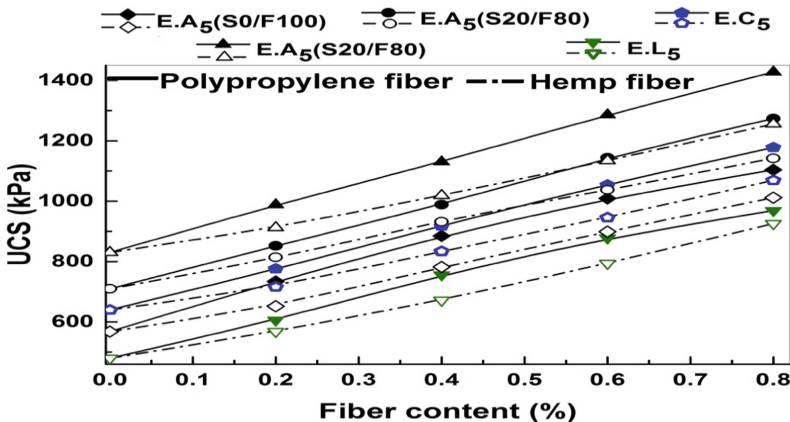


Fig. 8. UCS results of lime, cement, and AAB soil reinforced with PF and CHF at varying slag-fly ash ratio

4.2.3 California Bearing Ratio (CBR)

The effect of discrete fibers in lime, cement, and AAB treated soil mixtures on improving subgrade strength bearing ratio was calculated in terms of soaked CBR, which indirectly estimated the material’s durability and its efficiencies. Figure 9 showed the soaked CBR for PF and CHF reinforced soil treated with three cementitious binders at different fiber dosages. Observations were made between the loads applied against penetration of the plunger at 2.5 mm. The CBR (both soaked and unsoaked) value of untreated soil was 1.96% and 5.5%, respectively, implying low strength bearing resistance. The efficiency of CBR penetration resistance for all chemical binders of mixed soils increased as fiber dosages increased. From the graphs, it was noticed that AAB-fiber soil specimens, dependent on slag-fly ash, had the highest CBR values than specimens of lime-admixed fiber soil. Combining fly ash with slag material in the alkaline soil mix potentially activated the cementation compounds due to the early deposition of pozzolanic substances in the presence of reactive alumina and silica soil substances (Murmu et al. 2018). Also, PF-soil had attained 8–12% higher penetration resistance in comparison to CHF-soil mixture in all cemented treated soils mixtures. The occurrence of this substantial variation in the CBR strength of PF-soil might be due to its higher interfacial confinement bonding, good surface roughness, contact area, and more significant mobilization of friction during loading (Moghal et al. 2018b; Sudhakaran et al. 2018). In addition, PF might effectively distribute specimens in the soil and offer more excellent resistance to plunger penetration. By effectively gel-forming aluminosilicate ions during soaking, the composite application of fiber and slag-fly ash in the AAB soil mix helped to form the soil-fiber spatial thread-bridge networks.

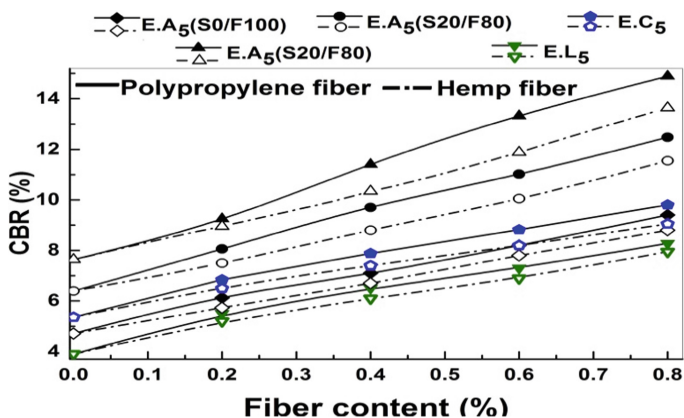


Fig. 9. Soaked CBR results of lime, cement, and AAB soil reinforced with PF and CHF at varying slag-fly ash ratio

4.2.4 Indirect Tensile Strength (ITS)

The results of ITS provide evidence to examine the effectiveness of soil fiber reinforcement by transferring shear stress to the fiber matrix that indirectly regulates soil cracking.

Figure 10 Exhibits variance of ITS values for soil treated with lime, cement, and AAB reinforced with two different fibers (polypropylene and hemp). It also reveals that the fiber type, dosage, and slag ratios play a significant role in strengthening the soil tensile property. The outcome of the ITS result follows a parallel trend with that of UCS for both fiber-reinforced treated soils. Upon comparison, slag based AAB-soil-fiber mixture attained the highest potential for tensile resistance than other cementitious binder mixed soil fiber. The marginal percentage gain in ITS performance was observed in lime and pure fly ash based alkaline soil-fiber samples. It also found that the effects of ITS on cemented and AAB soils have greatly improved between 0.2–0.6% of fiber dosages of more than 20% slag in the alkaline solution. The drastic enhancement in tensile force maybe because of bridge effect formation through interfacial friction and particles bonding around the fiber (Cristelo et al. 2015; Tang et al. 2007). Moreover, the combined addition of PF-AAB exhibits more stretching and sliding resistance over CHF-AAB-BCS soil. As a result, frictional bonding and surface roughness produce higher interlocking density and soil stiffness, indirectly overcoming the soil’s brittleness (Correia et al. 2015; Elkhebu et al. 2020). Thus, the increase in fiber dosages in lime cemented and AAB soil mixtures aid to upgrade the tensile bearing efficiency by restricting the relative moment of fiber in the soil.

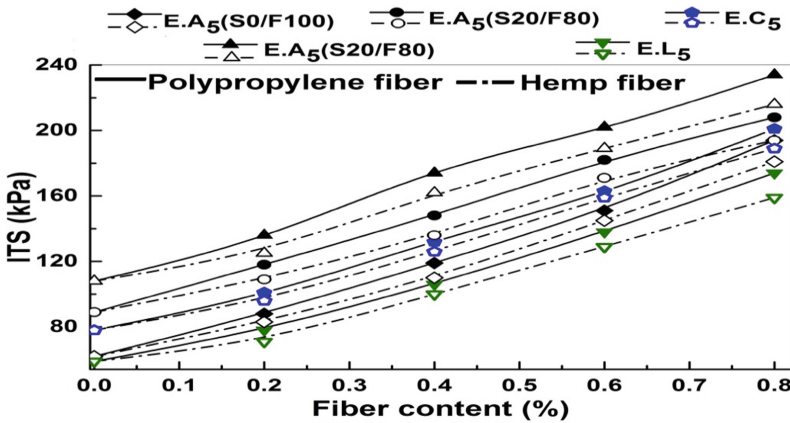


Fig. 10. Variation of ITS values for PF and CHF reinforced soil treated with lime, cement, and AAB mixtures at varying slag-fly ash ratio

4.2.5 Modulus of Rupture and Elasticity

Figure 11 (a-b) shows the flexural strength (modulus of rupture) and elastic modulus of lime, cement, and AAB treated fiber soils that are analyzed through the load-deflection curve. Figure 11a shows the results of flexural strength in the soil mixture on different combinations of cemented binders and fibers. It showed that the form of fiber and its proportions in the chemically treated soils played a leading role in strengthening flexural behavior. The flexural strength trend also follows a similar pattern, such as tensile strength on binder and fiber addition in soil. The AAB’s 0.66 slag fly ash ratio was attained 16%

and 28% higher than the cement and lime fiber soil mixture. Besides, the percentage growth in flexural strength in lime and cemented soil for PF and CHF reinforced soil was marginal above 0.6% of fiber dosage. Fiber and slag dosages in the AAB-soil mixture impart the stiffness and compression shear, transforming the brittle to ductile behavior by interfacial mechanism interaction (Anggraini et al. 2016; Elkhebu et al. 2020; Pourakbar and Huat 2017). Figure 11b exhibits the variation of fiber-reinforced soil elastic modulus. In order to avoid the cluster of data, only an optimal fiber dosage (0.8%) mixed in lime, cement, and 40/60 slag fly ash ratio in AAB soils were shown for comparison. The increase in elasticity is proportional to the increase in flexural and compressive shear resistance (Figs. 11a and 9). In the lime, cement AAB soil mixture, PF-soil elastic moduli are also found higher than CHF-soil. The relatively higher gain in compression shear strength in PF may be due to the higher mobilization of interfacial friction produced around the fiber (Chandra et al. 2007; Kutanaei and Choobbasti 2017; Yetimoglu et al. 2005).

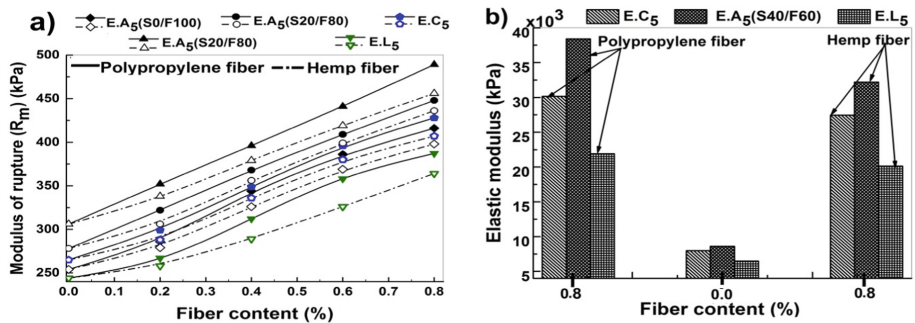


Fig. 11. Variations of a) Modulus of rupture b) Elastic modulus of PF and CHF reinforced soil treated with lime, cement, and AAB mixtures

4.3 Effect of Reliability Indices on CBR Strength

A comparison of the reliability indices for both PF and CHF AAB-soils against CBR failures is shown in Fig. 12 (a-d). In the alkaline soil mixture, the combined effect of slag-fly ash ratio and fiber reinforcement played a vital role in the magnitude of β_{CBR-PF} and $\beta_{CBR-CHF}$ failure. For both fiber-reinforced AAB soil, the reliability results presented in these figures are obtained for a typical value of $CBR_{min} = 7%$ at 10–40% of the variation in COV. The minimum specified CBR value ensures the safety level of reliability of subgrade strength bearing capacity at different COVs for predicting the soil-fiber behavior in terms of the stability of the subgrade material. Figure 12a and 12b indicate the CBR reliability index (β_{CBR}) maintaining CBR_{min} COV = 10 to 20% for different fiber dosages (0.2–0.8%). The reliability index’s magnitude can be observed to increase with an increase in the slag/fly ash ratio (0, 0.11, 0.25, 0.42, and 0.66) of AAB soil. In addition, PF-AAB soil achieves higher reliability indices for all CBR_{min} COV relative to CHF-AAB-soil mixture. This change may be attributed to the fact that

PF induces higher interfacial friction mobilization (rough surfaces) in soil compared to the CHF-soil matrix. The reliability index for both PF and CHF AAB soils against CBR failure (β_{CBR}) values shows the linear pattern of increase with an increase in fiber content and decrease with an increase in COV, and this pattern is in agreement with those of Moghal et al. (2017, 2018a). It is also interesting to emphasize in Fig. 12c that there is high variability in COV of CBR_{min} ($\geq 30\%$) for both $\beta_{\text{CBR-PF}}$ and $\beta_{\text{CBR-CHF}}$; the maximum reliability index reaches up to 3, which can be an acceptable performance of soil subgrade strength. Figure 12d represents that the reliability index's magnitude reduces due to higher COV of $\text{CBR}_{\text{min}} = 40\%$ under the same proportions of slag-fly ash and fibers.

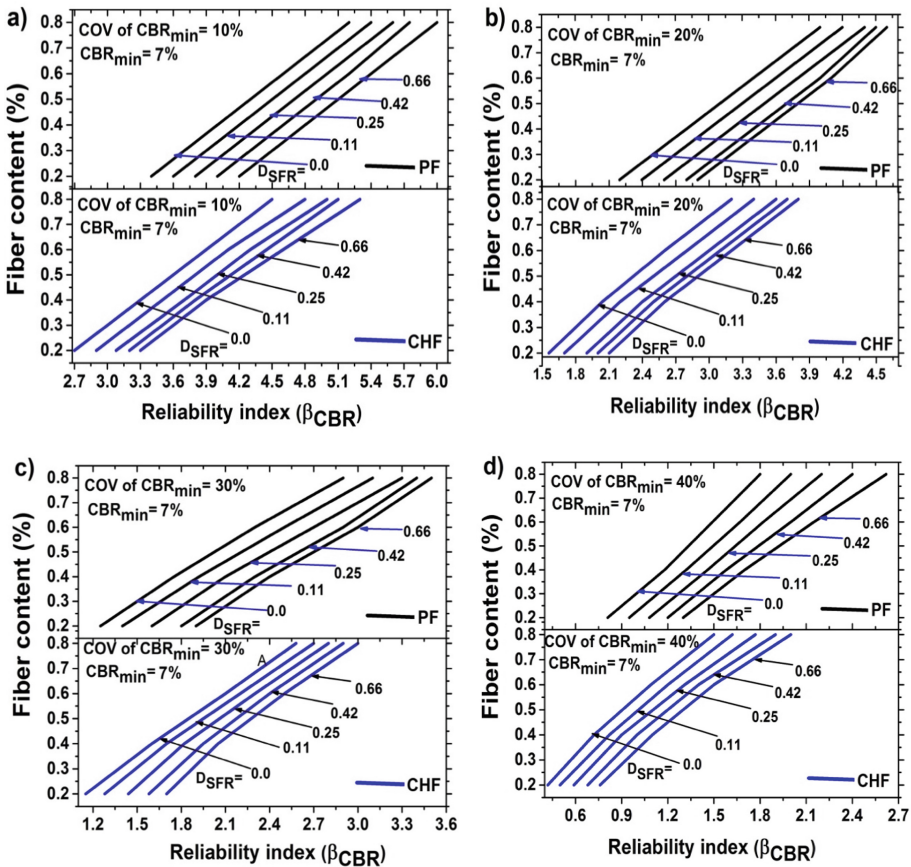


Fig. 12. Variation of reliability index against CBR failure (β_{CBR}) for both PF, CHF-AAB soils with varying slag-fly ash ratio at different COV a) 10%; b) 20%; c) 30%; d) 40%.

It may be noted that the use of high dosages of alkaline binders in the soil does not produce any volatile compounds. Besides, the heavy metals leaching from the mixture of fly ash and slag is very negligible. The heavy metals such as chromium (Cr), arsenic

trioxide (As_2O_3), lead oxide (PbO), and zinc oxide (ZnO) are not present in fly ash and slag. The chemical compound of fly ash and slag (such as Cao, MgO) can easily monitor the pH and leachate, which does not impact the surrounding flora and fauna significantly. However, the manufacturing process of AAB manufacturing does not generate any CO_2 emissions as it utilizes already available industrial wastes as raw materials compared to Portland cement (PC), which emits almost to 750–850 kg CO_2e/ton for 1 ton of Portland cement production. Polypropylene and hemp fibers consume less natural resources to be produced. They are biodegradable and widely recyclable. Burning of PF and CHF does not generate toxic gases like chlorine. Hence a combination of AAB and CHF or PF is an eco-friendly solution.

5 Conclusions

The following conclusion are drawn from the geotechnical and microstructural studies:

- Substantial mobilization of friction and interfacial bonding made PF-soil offer higher penetration resistance than CHF-soil, regardless of the lime, cement, and slag/fly ash ratio in the AAB mixture.
- At 28 days of curing, geotechnical studies showed that the fiber-AAB-soil mixtures had achieved 32% and 58% higher compressive shear strength, 47%, and 79% higher subgrade strength bearing ratio (in terms of CBR strength) relative to fiber-cemented and lime-fiber reinforced soils.
- With the increasing replacement of fly ash with slag content (0 to 40%) in the AAB mix, soil compressibility (in terms of void ratio and swelling potential) decreases. The volumetric stability of both AAB and cemented soil has been greatly improved through the development of active pozzolanic cementitious products.
- Microstructural studies have identified new molecular bonds and crystalline phases around the cemented lime and alkaline clay matrix. Moreover, the PF and CHF-AAB-soil micrographs formed the spatial thread bridge network surface, regulating the tensile cracks around the subgrade layers
- Elastic modulus and modulus of rupture of soil increase with fiber and slag content; this improvement is proportional to the increase in ITS and UCS values, which substantially regulate the flexural and tensile crack propagation.
- The reliability index for both β_{CBR-PF} and $\beta_{CBR-CHF}$ AAB-soils against the subgrade strength failures decreases with an increase in COV of CBR_{min} . Based on the findings, it is recommended that adding up to 0.8% of fiber (both PF and CHF) and 40% slag in alkaline soil mixture help to improve the subgrade stability significantly to a large extent.

Acknowledgments. The authors would like to express their sincere gratitude to the Central Analytical Laboratory Facilities at BITS-Pilani, Hyderabad Campus, for providing the setup for the FTIR, SEM/EDS, and XRD analyses.

References

- Al-Mukhtar, M., Khattab, S., Alcover, J.-F.: Microstructure and geotechnical properties of lime-treated expansive clayey soil. *Eng. Geol.* **139–140**, 17–27 (2012). <https://doi.org/10.1016/j.enggeo.2012.04.004>
- Amadi, A.A.: Enhancing durability of quarry fines modified black cotton soil subgrade with cement kiln dust stabilization. *Transp. Geotech.* **1**(1), 55–61 (2014)
- Angraini, V., Asadi, A., Farzadnia, N., Jahangirian, H., Huat, B.B.K.: Reinforcement benefits of nanomodified coir fiber in lime-treated marine clay. *J. Mater. Civ. Eng.* **28**(6), 1–8 (2016)
- Bell, F.G.: Lime stabilization of clay minerals and soils. *Eng. Geol.* **42**(4), 223–237 (1996)
- Bordoloi, S., Garg, A., Sekharan, S.: A Review of physio-biochemical properties of natural fibers and their application in soil reinforcement. *Adv. Civil Eng. Mater.* **6**(1), 20160076 (2017)
- Chandra, S., Viladkar, M.N., Nagrale, P.P.: Mechanistic approach for fiber-reinforced flexible pavements. *J. Transp. Eng.* **134**(1), 15–23 (2007)
- Correia, A.A.S., Venda Oliveira, P.J., Custódio, D.G.: Effect of polypropylene fibres on the compressive and tensile strength of a soft soil, artificially stabilised with binders. *Geotext. Geomembr.* **43**(2), 97–106 (2015)
- Cristelo, N., Cunha, V.M.C.F., Dias, M., Gomes, A.T., Miranda, T., Araújo, N.: Influence of discrete fibre reinforcement on the uniaxial compression response and seismic wave velocity of a cement-stabilised sandy-clay. *Geotext. Geomembr.* **43**(1), 1–13 (2015)
- Davidovits, J.: Properties of geopolymer cements. *Alkaline Cements and Concretes*, Kiev, Ukraine, pp. 1–19 (1994)
- Elkhebu, A., et al.: Effect of incorporating multifilament polypropylene fibers into alkaline activated fly ash soil mixtures. *Soils Found. Jpa. Geotech. Soc.* **59**(6), 2144–2154 (2020)
- GuhaRay, A., Baidya, D.K.: Reliability-based analysis of cantilever sheet pile walls backfilled with different soil types using the finite-element approach. *Int. J. Geomech.* **15**(6), 1–11 (2015)
- Jiang, N.J., Du, Y.J., Liu, K.: Durability of lightweight alkali-activated ground granulated blast furnace slag (GGBS) stabilized clayey soils subjected to sulfate attack. *Appl. Clay Sci.* **161**(April), 70–75 (2018)
- Kutanaei, S.S., Choobasti, A.J.: Effects of nanosilica particles and randomly distributed fibers on the ultrasonic pulse velocity and mechanical properties of cemented sand. *J. Mater. Civ. Eng.* **29**(3), 1–9 (2017)
- Mazhoud, B., Collet, F., Pretot, S., Lanos, C.: Mechanical properties of hemp-clay and hemp stabilized clay composites. *Constr. Build. Mater.* **155**, 1126–1137 (2017)
- Miao, S., et al.: Mineral abundances quantification to reveal the swelling property of the black cotton soil in Kenya. *Appl. Clay Sci.* **161**, 524–532 (2018). <https://doi.org/10.1016/j.clay.2018.02.003>
- Miao, S., Wei, C., Huang, X., Shen, Z., Wang, X., Luo, F.: Stabilization of highly expansive black cotton soils by means of geopolymerization. *J. Mater. Civ. Eng.* **29**(10), 04017170 (2017)
- Moghal, A.A.B., Chittoori, B.C.S., Basha, B.M.: Effect of fibre reinforcement on CBR behaviour of lime-blended expansive soils: reliability approach. *Road Mater. Pav. Des.* **19**(3), 690–709 (2018a)
- Moghal, A.A.B., Chittoori, B.C.S., Basha, B.M., Al-Mahbashi, A.M.: Effect of polypropylene fibre reinforcement on the consolidation, swell and shrinkage behaviour of lime-blended expansive soil. *Int. J. Geotech. Eng.* **12**(5), 462–471 (2018b)
- Moghal, A.A.B., Chittoori, B.C.S., Basha, B.M., Al-Shamrani, M.A.: Target reliability approach to study the effect of fiber reinforcement on UCS behavior of lime treated semiarid soil. *J. Mater. Civ. Eng.* **29**(6), 04017014 (2017)
- Murmu, A.L., Dhole, N., Patel, A.: Stabilisation of black cotton soil for subgrade application using fly ash geopolymer. *Road Mater. Pav. Des.* **0**(0), 1–19 (2018)

- Pourakbar.: Application of alkali-activated agro-waste reinforced with wollastonite fibers in soil stabilization. *J. Mater. Civ. Eng.* **29**(2), 04016206 (2016)
- Pourakbar, S., Huat, B.B.K.: Laboratory-scale model of reinforced alkali-activated agro-waste for clayey soil stabilization. *Adv. Civil Eng. Mater.* **6**(1), 20160023 (2017)
- Provis, J.L., Deventer, J.S.J. (eds.): Alkali activated materials. RSR, vol. 13. Springer, Dordrecht (2014). <https://doi.org/10.1007/978-94-007-7672-2>
- Rios, S., Cristelo, N., Viana, A., da Fonseca, C.F.: Structural performance of alkali-activated soil ash versus soil cement. *J. Mater. Civil Eng.* **28**(2), 04015125 (2016). [https://doi.org/10.1061/\(ASCE\)MT.1943-5533.0001398](https://doi.org/10.1061/(ASCE)MT.1943-5533.0001398)
- Saride, S., Dutta, T.: Effect of fly-ash stabilization on stiffness modulus degradation of expansive clays. *J. Mater. Civil Eng.* **28**(12), 04016166 (2016). [https://doi.org/10.1061/\(ASCE\)MT.1943-5533.0001678](https://doi.org/10.1061/(ASCE)MT.1943-5533.0001678)
- Sivapullaiah, P.V., Sankara, G., Allam, M.M.: Mineralogical changes and geotechnical properties of an expansive soil interacted with caustic solution. *Environ. Earth Sci.* **60**(6), 1189–1199 (2010)
- Sudhakaran, S.P., Sharma, A.K., Kolathayar, S.: Soil stabilization using bottom ash and areca fiber: experimental investigations and reliability analysis. *J. Mater. Civ. Eng.* **30**(8), 1–10 (2018)
- Syed, M., Guharay, A.: Effect of fiber reinforcement on mechanical behavior of alkali-activated binder-treated expansive soil: reliability-based approach. *Int. J. Geomech. ASCE* **20**(12), 1–14 (2020)
- Syed, M., GuhaRay, A., Goel, D., Asati, K., Peng, L.: Effect of freeze–thaw cycles on black cotton soil reinforced with coir and hemp fibres in alkali-activated binder. *Int. J. Geosynt. Ground Eng.* **6**(2), (2020a). <https://doi.org/10.1007/s40891-020-00200-7>
- Syed, M., GuhaRay, A., Kar, A.: Stabilization of expansive clayey soil with alkali activated binders. *Geotech. Geol. Eng.* **38**(6), 6657–6677 (2020b). <https://doi.org/10.1007/s10706-020-01461-9>
- Tang, C.-S., Shi, B., Li, J., Wang, D.-Y., Cui, Y.-J.: Tensile strength of fiber-reinforced soil. *J. Mater. Civ. Eng.* **28**(7), 04016031 (2016)
- Tang, C., Shi, B., Gao, W., Chen, F., Cai, Y.: Strength and mechanical behavior of short polypropylene fiber reinforced and cement stabilized clayey soil. *Geotext. Geomembr.* **25**(3), 194–202 (2007)
- Wei, L., Chai, S., Zhang, H., Shi, Q.: Mechanical properties of soil reinforced with both lime and four kinds of fiber. *Constr. Build. Mater.* **172**, 300–308 (2018). <https://doi.org/10.1016/j.conbuildmat.2018.03.248>
- Yetimoglu, T., Inanir, M., Inanir, O.E.: A study on bearing capacity of randomly distributed fiber-reinforced sand fills overlying soft clay. *Geotext. Geomembr.* **23**(2), 174–183 (2005)
- Yong, R.N., Ouhadi, V.R.: Experimental study on instability of bases on natural and lime/cement-stabilized clayey soils. *Appl. Clay Sci.* **35**(3–4), 238–249 (2007)
- Zevgolis, I.E., Bourdeau, P.L.: Probabilistic analysis of retaining walls _ Elsevier Enhanced Reader.pdf. *Comput. Geotech.* (2010)
- Zhang, M., Guo, H., El-Korchi, T., Zhang, G., Tao, M.: Experimental feasibility study of geopolymer as the next-generation soil stabilizer. *Constr. Build. Mater.* **47**, 1468–1478 (2013)



Assessing a Sand Clay Liner Material for Protecting Highways and Road Shoulders

Muawia Dafalla¹(✉), Abdullah Shaker¹, and Abdul Naser Abdul Ghani²

¹ Bughshan Research Chair in Expansive Soils, Civil Engineering, King Saud University, Riyadh 11421, Saudi Arabia

{mdafalla, ashaker}@ksu.edu.sa

² School of Housing Building and Planning, Universiti Sains Malaysia, 11800 Penang, Malaysia
anaser@usm.my

Abstract. The damage and distress caused to highways and roads within areas of high swell potential are of great concern in the design of infrastructure projects. The Subgrade is a significant part of the road structural systems. Variation in moisture content due to seasonal weather fluctuation and flooding could result in harming the road foundation support. This is because the capacity and consistency of the support provided by the subgrade are dependent on the soil type, density, and moisture contents. Different rainfall pattern and intensity from one place to another makes the subgrade response more complicated. The common approach to the water or moisture influence on road structures is to prevent moisture or water from entering the systems. However, in the case of severe flooding, it will not be easy to divert all the flood water away from the road structures. Therefore, efficient protection is required. This study is aimed at assessing clay sand liners of variable mix designs to be constructed as a dressing layer along the shoulder or within the body of the shoulder and extending beyond the foot of the slope. Materials of highly expansive clay from Saudi Arabia were mixed with fine to medium sand at variable proportions to introduce the required protection liners. Characterization tests and hydraulic conductivity tests were performed. Relationship between hydraulic conductivity and clay content was obtained and compared to other studies. Compressibility was obtained from the void ratio and vertical stress relationship. Designs were proposed for specific section geometries and shoulder slopes.

1 Introduction

Arid and semi-arid areas involving near-surface expansive soils suffered severe damage and distress to buildings and infrastructure projects due to the behavior of ground in different seasons. Damage examples are shown in Fig. 1, Fig. 2, and Fig. 3. Many researchers highlighted a high cost of maintenance and repairs which is estimated into multi-billions of dollars globally (Jone and Jones 1987). Most of the damage estimates were made for buildings and light structures. The damage to roads and highways is not observed due to the nature of flexible asphalt roads which can tolerate some of the movement for one or two seasons. Repeated upward and downward displacement



Fig. 1. Tayma-Tabuk abandoned road (Saudi Arabia); severe distress.

can ultimately result in cracks and serious damage if not maintained regularly. Rigid pavements are as bad as other light concrete structures and distress can be observed as early as the first wetting season following construction. Zumrawi (2015) stated that structural problems and premature failures of roads built on expansive soils originate mainly due to inadequate or insufficient site investigation in addition to poor drainage design and lack of regular maintenance. Settlement or heave due to expansive soils causes serious distress in asphalt pavements leading to substantial discomfort, safety hazard, and vehicle damage (Ahmed et al. 2019). Schemes studying frequency and count of cracks using imaging proved to be quicker and less time consuming than conventional and manual approaches. Works of (Xiao et al. 2006) is an example of the current techniques in this regard. Dafalla and Al-Shamrani (2008, 2011) listed the parameters influencing damage to asphalt pavement as subgrade soil type and mineralogy, road geometry, road drainage, and adjacent topography.

Subgrade Soil Type and Mineralogy

The soil formation immediately below the pavement is referred to as subgrade. This can be natural or imported material. In areas known for expansive soils, the assessment of its characteristics is essential. Index properties can provide a quick guide. Swell tests and detailed mineralogy are necessary to predict the level of risk.

Road Geometry

The thickness of the embankment and the pavement are related to the stresses applied to the subgrade. Figure 4 shows King Abdul-Aziz access road to Al-Ghatt town with mounds and depressions due to variable road thicknesses on soils with the same expansion properties. The heave was found to be a function of the overburden soil pressure and poor drainage. Small differences of 50 cm can result in different heave. This road geometry also includes shoulders and their slopes towards drainage ditches.

Road Drainage

Asphalted roads are generally drained towards two directions with a crest at the center except for conditions of turns and super elevated sides where a single direction is used to

drain the water. The main concern for roads within expansive soil is not to allow water to access the underneath of the asphalt pavement. This is likely to result in immediate distress. Poor drainage is reported for many roads subjected to damage in Saudi Arabia. The shoulders shall be less permeable and steep or impermeable directing the flow towards drains. Cut off walls with or without slope dressing can be useful.



Fig. 2. Close-up view of localized distress (Tayma-Tabuk Road, Saudi Arabia)



Fig. 3. A road under frequent maintenance due to expansive soil, Al-Rowda district, Tabuk, Saudi Arabia

Adjacent Topography

The adjacent topography may affect the performance of the pavement if surface or subsurface water is directed towards the pavement (Dafalla and Al-Shamrani 2011). High ranges of hills close to roads can increase the hydraulic head of subsurface water and cause wetting to subgrade formation. The adjacent topography and general hydrology of the area are of prime consideration when designing for road drainage.

Impact of Floods and Repeated Floods

Subgrade capacity to support pavement will be affected due to flooding and repeated

flooding. Initially-dry subgrade formation will expand and exerts upheaval forces on the pavement when subjected to flooding while initially-wet subgrade formation will deteriorate and reduce in the supporting capacity. Works of Ismail et al. (2020) surveyed the influence of flooding on the subgrade soils supporting pavements. They were able to simulate the impact of flood duration and water height on subgrade for unrepeated and repeated conditions. These works were carried out for non-expansive soils in Malaysia where expansive soils are not an issue but the study highlighted the negative influence of initially wet subgrade exposed to water under a hydraulic gradient. For heavy rainfall or flooding in expansive soil zones standing water will flow towards the subgrade at the shoulders and edges of asphalt pavement. Hydrological analysis needs to be conducted to evaluate the run-off along with the site topography and water standing time. Hydraulic conductivity is increased by the height of water and water passways within the subgrade.



Fig. 4. King Abdul-Aziz Access Road- Al Ghatt

Forms and Types of Cracks

The cracks and damage taking place in asphalt pavements were surveyed by many researchers. The most commonly known types were classified based on the directions, magnitude, and cause of cracks.

The longitudinal and transverse cracks occur when the subsurface water flow takes longitudinal or transverse directions and this is reflected when the subgrade of the road is of a significant swelling potential and the heave is beyond the tolerance of the designed asphalt mix. The position of cracks is either on the top of the mount or the bottom of the depression. Block cracks are combinations of longitudinal and traverse cracks. (Dafalla and Al-Shamrani 2011) introduced three new types of cracks that can be classified based on the cause of the distress these are; yield cracks, spot cracks, and green zones cracks.

2 Materials and Test Methods

The clay material used in forming liners for this work is brought from the eastern province of Saudi Arabia. Al-Qatif clay is known for its high plasticity and linear shrinkage (Azam

2003). Table 1 presents the index properties for Alqatif clay used in the present study. The sand used in this study is fine to medium poorly graded dune sand. The uniformity and curvature coefficients for this sand are $C_u = 1.737$ and $C_c = 1.078$, respectively. The specific gravity of sand is 2.66.

The soil moisture and dry density relationship were investigated for different clay contents. The compaction tests were carried out following the standard Proctor compaction method (ASTM D698-02, method A). For sand-Alqatif clay mixtures, the range of clay content investigated included 0, 5, 10, 15, 20, 25, 30, 40, and 60% by dry weight of sand. The maximum dry density was obtained in the range of 16.6 to 17.5 kN/m³ at an optimum moisture content of 15 to 16.5%.

Table 1. Geotechnical characteristics of Al-Qatif clay

Property	Value
Specific gravity, G_s	2.75
Liquid limit, LL (%)	140
Plastic limit, PL (%)	45
Plasticity index, PI (%)	95
Unified soil classification system	CH
Swelling pressure (kN/m ²)	550–600
Swelling potential (%)	16–18

The hydraulic conductivity tests were carried out using the ASTM test method designated as ASTM D5084: Standard Test Methods for Measurement of Hydraulic Conductivity of Saturated Porous Materials Using a Flexible Wall Permeameter. The compressibility tests were carried out for different sand clay content following ASTM D-2435: Standard Test Methods for One-Dimensional Consolidation Properties of Soils.

Suggested Geometry

This study suggests two geometrical designs for shoulder protection as indicated in Fig. 8 and Fig. 9.

3 Analysis of Test Results

The test results obtained for the hydraulic conductivity and the compressibility of the clay-sand mixtures tests are presented in a graphical format as presented in Figs. 5, 6, and 7. Some previous studies investigated the relationship between the hydraulic conductivity and the clay content of clay-sand mixtures. These studies included the works of Komine 2004, Ameta 2005, Chalermyanont, and Arrykul 2005, and Shigeyoshi et al. 2009. Figure 5 shows the profile of Al Qatif clay-sand mixtures compared to mixtures used in other studies. From Fig. 5 we can observe that the sand material used by the selected researchers is not identical and of different hydraulic conductivity at 0% clay addition.

The variation in hydraulic conductivity for 0 to 5% sand content is understood and can be attributed to the porosity and other sand properties. Beyond 10% clay content we can see that the gradient of the hydraulic conductivity versus the clay content is nearly equal. The type and nature of sand as well as the clay mineralogy controls the magnitude of the hydraulic conductivity. The steep gradient of the curve at low clay content shown in the previous studies is mainly due to the coarse nature of the sand used. Al-Qatif clay indicates that there is no further significant improvement in the hydraulic conductivity beyond 25% clay content. Clay sand mixtures with more than 30% clay behave similarly to pure clays concerning compressibility and shear strength. The hydraulic conductivity of clay-rich mixtures (>30%) is not very much different from that of pure clay. The sand grains remain as inert inclusions. They can obstruct the channels transporting fluids but with little influence on the overall hydraulic conductivity of the clay. The compressibility of sand-clay liners is influenced by the sand content and grain to grain contact. Low compression is expected when the sand grains are in contact or closer to each other. The compressibility index measured for the sand alone decreases by adding a small amount of clay until the clay occupies all the voids within the sand. The compressibility index then increases with the increase of clay content. Stress partitioning between the clay and sand is dependent on the sand porosity and the clay content. A liner with high clay content may introduce some settlement if subjected to high stress. This settlement is not likely to be significant if the liner is thin or consisting of a single layer located at the bottom of the pavement. In this case, the stresses exerted by the tires vanish when reaching the proposed liner level. The settlement of the liner layer can be computed when the compressibility index is known. The compression rebound factor C_r is parallel to the compressibility index except for the zone close to pure sand or zones of mixtures with high clay content. The tests carried out can provide an estimation tool for

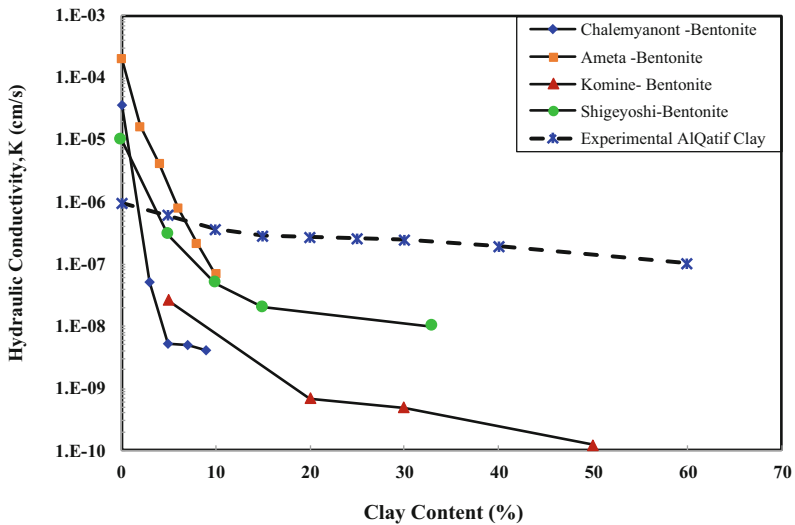


Fig. 5. Relationship between hydraulic conductivity and clay content compared to other studies.

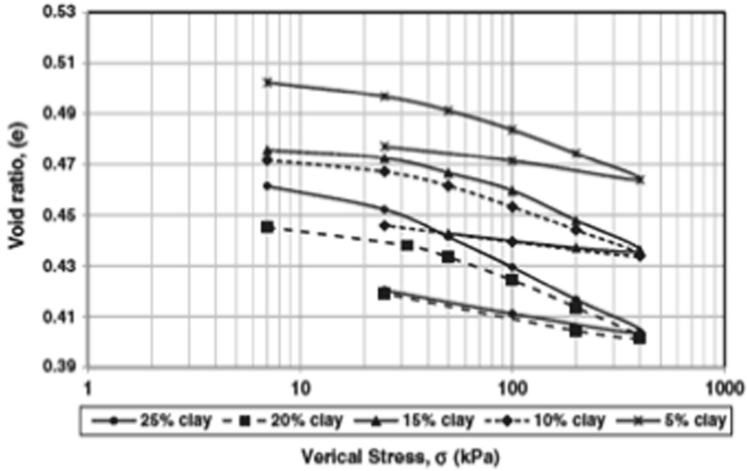


Fig. 6. Relationship between void ratio and vertical stress for Al-Qatif clay-sand mixture.

practicing engineers to predict the displacement due to loads applied on the pavement or the shoulders.

The proposed geometry and the suggested protection is a key factor in this study along with the hydrological data of the site. Also, the time, duration, and height of standing water are important parameters to be considered in the design of this protection system. The height of the water can influence and increase the hydraulic conductivity. The effective stress within the clay-sand mixture plays a role in reducing permeability (Dafalla et al. 2015).

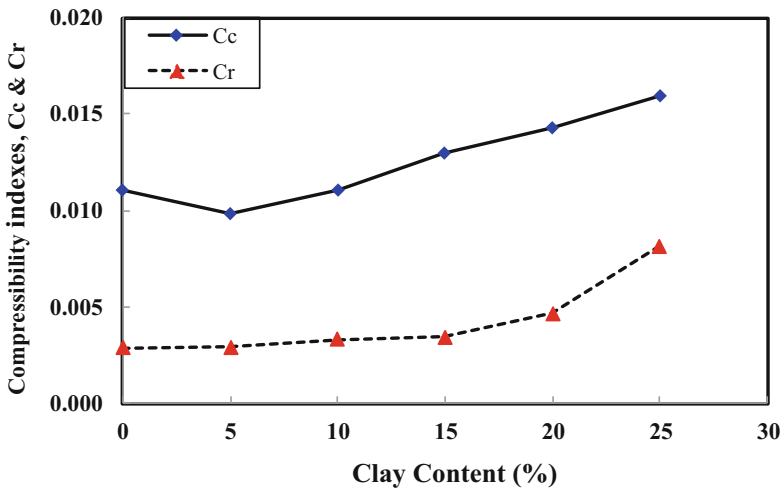


Fig. 7. Variation of compressibility index with clay content.

The construction of the liner along the top of the shoulders will be an easy practice and can be similar to the shoulder dressing layers. Top layer liners need to be richer in clay content to allow for possible erosion down the slope of the shoulder and the toe. Slope erosion is not covered in the present study and will be addressed as further research on this subject. The practicing engineers can select a liner layer depth and slope based on the guidance presented in Fig. 8. Slopes of 3%, 5%, and 10% can be confidently used with little and insignificant erosion (Dafalla and Obaid 2013).

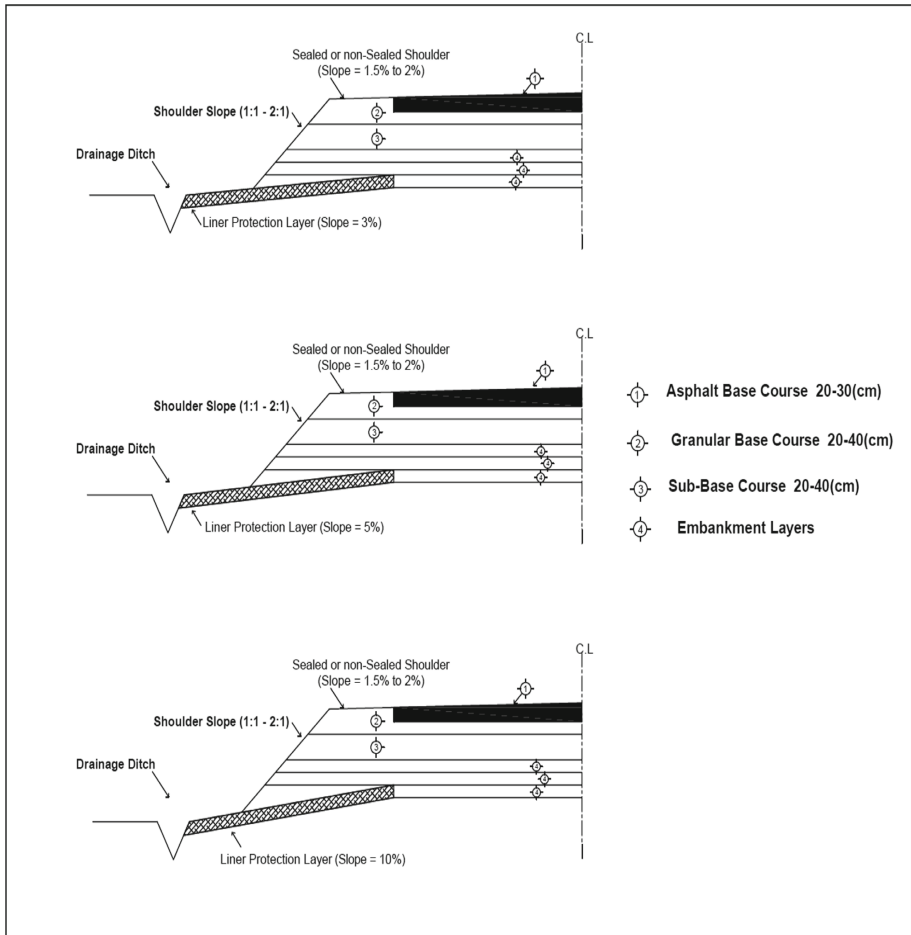


Fig. 8. Proposed liners towards the bottom of the shoulder.

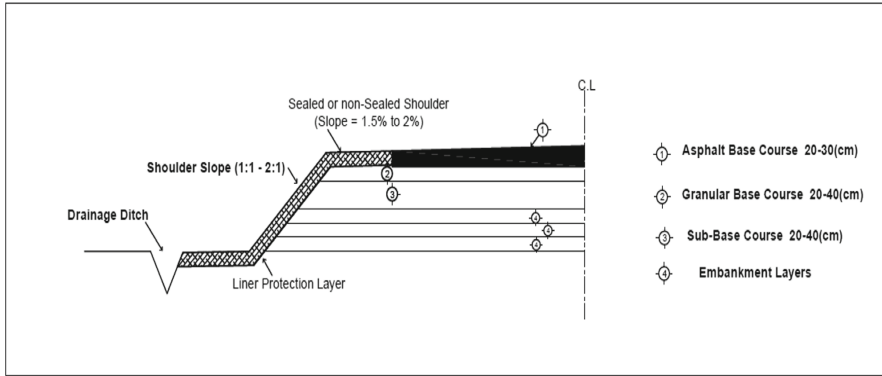


Fig. 9. Proposed liners following the profile of the shoulder.

4 Conclusion

The clay sand liners can be efficiently used to protect asphalt pavements in areas where expansive soils pose a significant hazard. The main control parameters include the hydraulic conductivity and compressibility of the mixture used in the design. Two configurations were suggested as a possible design. The first configuration is to follow the profile of the top and side levels of the shoulder and the second configuration is to adopt a bottom layer with a slope to direct water towards a drainage canal. The thickness and level of the bottom protection layer are dependent on the hydraulic conductivity and the compressibility of the liner. This considers the minimum clay content to provide a satisfactory hydraulic conductivity and provides compressibility within the design limits.

Acknowledgements. The authors extend their appreciation to the Deanship of Scientific Research, King Saud University for funding this study through Vice Deanship of Scientific Research Chairs.

References

- Ahmed, A., Hossain, M.D., Pandey, P., Sapkota, A., Thian, B.: Deformation modeling of flexible pavement in expansive subgrade in texas. *Geosciences* **9**(10), 446 (2019)
- Ameta, N.K., Abhay, S.W.: Effect of bentonite on permeability of dune sand. *EJGE.Vol13, Bund. A* (2008)
- ASTM D2435 Standard Test Methods for One-Dimensional Consolidation Properties of Soils Using Incremental Loading, ASTM International, West Conshohocken, PA (2020). www.astm.org
- ASTM D698 - 02 B Standard Test Methods for Laboratory Compaction Characteristics of Soil Using Standard Effort (12 400 ft-lbs/ft³ (600 kN m/m³), vol. 15.09, Annual book of ASTM Standards, West Conshohocken, PA
- ASTM D5084-03. standard Test Methods for Measurement of Hydraulic Conductivity of Saturated Porous Materials Using a Flexible Wall Permeameter. American Society for Testing and Materials, West Conshohocken, PA

- Azam, S.: Influence of mineralogy on swelling and consolidation of soils in eastern Saudi Arabia. *Can Geotech. J.* **40**(5), 964–975 (2003)
- Chalermyanont, T., Arrykul, S.: Compacted sand-bentonite mixtures for hydraulic containment liners. *Songklanakarinn J. Sci. Technol.* **27**(2) (2005)
- Dafalla, M.A., Al-Shamrani, M.A.: Performance-based solutions for foundations on expansive soils-Al-Ghatt region, Saudi Arabia. In: *International Conference on Geotechnical Engineering, Chiangmai*, pp. 10–12 (2008)
- Dafalla, M.A., Al-Shamrani, M.A.: Road damage due to expansive soils: Survey of the phenomenon and measures for improvement. In: *Design, Construction, Rehabilitation, and Maintenance of Bridges*, pp. 73–80 (2011)
- Dafalla, M., Shaker, A.A., Elkady, T., Al-Shamrani, M., Dhowian, A.: Effects of confining pressure and effective stress on hydraulic conductivity of sand-clay mixtures. *Arab. J. Geosci.* **8**(11), 9993–10001 (2015). <https://doi.org/10.1007/s12517-015-1925-1>
- Dafalla, M., Obaid, A.: The role of polypropylene fibers and polypropylene geotextile in erosion control. In: *IACGE 2013: Challenges and Recent Advances in Geotechnical and Seismic Research and Practices*, pp. 669–676 (2013)
- Ismail, M.S.N., Ghani, A.N.A., Ghazaly, Z.M., Dafalla, M.D.: A study on the effect of flooding depths and duration on soil subgrade performance and stability. *Int. J. Geomate* **19**(71), 182–187 (2020)
- Jone, D.E., Jones, K.A.: Treating Expansive Soils. *Civ. Eng. ASCE* **43**, 11 (1987)
- Komine, H.: Simplified evaluation on hydraulic conductivities of sand–bentonite mixture backfill. *Appl. Clay Sci.* **26**, 13–19 (2004)
- Shigeyoshi, I.M.W., Naoki, T., Yoichi, D.: Estimation of critical ratio of bentonite addition to tuff sand. *J. Mater. Cycles Waste Manag.* **11**, 299–304 (2009)
- Xiao, W., Yan, X., Zhang, X.: Pavement distress image automatic classification based on density-based neural network. In: *International Conference on Rough Sets and Knowledge Technology*, pp. 685–692. Springer, Heidelberg, July 2006
- Zumrawi, M.M.: Geotechnical aspects for roads on expansive soils. *Int. J. Sci. Res.* **4**, 896–902 (2015)



The Thermo-mechanical Behaviour of Clay in Different Stress and Temperature Paths

Kuanjun Wang^{1,2}, Zhigang Shan^{1,2}, Kanmin Shen¹(✉), Mingyuan Wang^{1,2},
Wenbo Du^{1,2}, and Boyu Mao²

¹ Key Laboratory of Far-Shore Wind Power Technology of Zhejiang Province, POWERCHINA
Huadong Engineering Corporation Limited, Hangzhou, China

² Zhejiang Huadong Construction Engineering Corporation Limited, Hangzhou, China

Abstract. During the service period of oil-gas pipelines, marine cables and energy pile, the surrounding soil will be strongly influenced by the high temperature, which changes the mechanical properties (strength and stiffness) of the surrounding soil and causes additional deformation, and ultimately leads to instability of the structure. As the submarine oil-gas pipeline are always shallow buried, where the seabed soil at the top of the surface is generally overconsolidated. Therefore, the undrained shear behaviour of overconsolidated clay is of great important in submarine pipeline design considering the global buckling. In this study, the undrained shearing behaviour of kaolin under different overconsolidation ratios ($OCR = 1, 2, 4$) and different heating paths are carried out based on the temperature-controlled triaxial system. For normally consolidated kaolin, the test results show that under drained heating, the undrained shear strength is increased approximately 20% with the increasing temperature from 20 °C to 55 °C; after a heating-cooling cycle (20 °C–55 °C–20 °C), the undrained shear strength is still 10% higher than the strength in room temperature 20 °C, which indicates that the soil strength is influenced by the temperature history. For overconsolidated kaolin, the undrained shear strength is weakly influenced by the temperature. The temperature has a weak effect on the final pore pressure in undrained shearing process, both for normally consolidated and overconsolidated kaolin. The slope M of the critical state line will be affected by the temperature, which increases from about $M(20\text{ °C}) = 1.00\text{--}1.05$ to $M(55\text{ °C}) = 1.11\text{--}1.18$. More interestingly, the M value for kaolin after heating-cooling cycle (20 °C–55 °C–20 °C) is consistent with the value in high temperature (55 °C), which means the slope M of the critical state line is dependent on the temperature history.

Keywords: Thermo-mechanical behaviour · Drained heating · Kaolin · Overconsolidated · Heating-cooling cycle

1 Introduction

With the development of offshore oil and gas, underground heat supply pipelines, the soil around these underground geothermal structures are affected by the temperature during the service period (Yu et al. 2017). During the operation and shutdown of the pipelines, the

surrounding clay, which is always overconsolidated on the seabed surface, is subjected to heating-cooling cycle. The thermo-mechanical behaviour of overconsolidated clay during heating-cooling cycle has become a focus of geotechnical engineering (Moel et al. 2010), which has not been sufficiently studied.

A series of studies have been carried out on the undrained shear strength of clay under drained heating. Towhata et al. (1993) and Kuntiwattanakul et al. (1995) found that for MC clay under drained heating, the undrained shear strength of normally consolidated clay increased with temperature increase, the influence of temperature on undrained shear strength of clay was weakened with OCR increasing. Abuel-Naga et al. (2007) carried out a series tests on Bangkok clay, the variation of undrained shear strength for normally consolidated clay was same as the results of previous researchers. However, for overconsolidated clay, the undrained shear strength was also increased with temperature increase, which was inconsistent with the tests results of MC clay.

The thermo-mechanical behaviour of clay under the heating-cooling cycle is still unclear. Kuntiwattanakul et al. (1995) conducted temperature-controlled triaxial tests on reconsolidated MC clay (normally consolidated), and the results indicated that the undrained shear strength of high temperature sample was the highest, followed by the heating-cooling cycle sample and the room temperature (20 °C) sample. However, for Todi clay (Burghignoli et al. 2000), the heating-cooling sample had the highest undrained shear strength, no evidence was found that the undrained shear strength of room temperature sample would be the lowest, which might be higher than the undrained shear strength of the high temperature sample. And the pore water pressure responses during the undrained shearing process of the room temperature, high temperature and heating-cooling Todi clay samples were observed to be the same. However, the excess pore pressure response of Bangkok clay (Abuel-Naga et al. 2007) was different from Todi clay, high temperature Bangkok clay sample would have less excess pore pressure than room temperature and heating-cooling cycle samples, the OCR would change the pore water pressure response during the undrained shearing process, which had not been fully known.

The influence of temperature on the slope M of the critical state line (CSL) had also been conflicted concluded by previous researchers (Hueckel and Pellegrini 1991,1992; Hueckel 1997; Marques et al. 2004; Abuel-Naga et al. 2009; Hueckel et al. 2009; Qi et al. 2015; Wang et al. 2020). Hueckel and Pellegrini (1992) found that the M value of Pontida clay was almost unchanged at different temperatures. Hueckel (1997) conducted a series of experiments on Boom clay, and found that the M value increased with temperature. Marques et al. (1997) discovered that the M value of St-Roch-de-l'Achigan clay in Quebec was slightly affected by temperature. Abuel-Naga et al. (2009) presented the test results of Bangkok clay, which were independent of temperature. (Hueckel et al. 2009) summarized all the results in previous studies, and concluded that the temperature effect on M value might be related to the type of clay. For Boom clay, the M value might be increased by about 20% when temperature was increased by 70 °C, but for kaolin, the M value increased by about 12.5% when temperature was increased by 68 °C. The correlation between the slope M of critical state line and temperature of soft clay needs further research.

In conclusion, all the researchers have same understanding of the change of the undrained shear strength of the normally consolidated clay after drained heating and heating-cooling cycle. However, the undrained shear behaviour of overconsolidated clay after heating and heating-cooling cycle are still controversial. In this article, series tests of kaolin at different OCR and temperatures (20 °C, 55 °C, 20 °C–55 °C–20 °C) have been presented to analyse the undrained shear behaviour of clay under different stress and temperature path. The tests results have been preliminary verified by the thermo-elastic-plastic constitutive model (Wang et al. 2016), which presents good prediction for the thermo-mechanical behaviour of clay.

2 Theoretical Basis

The thermo-elastic-plastic constitutive model proposed by Wang et al. (2016) have been adopted to simulate the results of kaolin under different OCR and temperature. This section will give a brief introduction of the constitutive model.

The thermo-mechanical constitutive model (Wang et al. 2016) was established based on the framework of Modified Cam-Clay (MCC) model, i.e., elastic-plastic constitutive model. Inclined ellipse yield surfaces (Fig. 1a) of current and reference (Wheeler et al. 2003) and associated flow rule (Graham et al. 2001) had been adopted. The equations of current and reference yield surfaces are shown as following:

$$f = \frac{(M^2 - \alpha^2) + (q/p' - \alpha)^2}{M^2 - \alpha^2} p' - p'_c = 0 \quad (1)$$

$$\bar{f} = \frac{(M^2 - \alpha^2) + (\bar{q}/\bar{p}' - \alpha)^2}{M^2 - \alpha^2} \bar{p}' - \bar{p}'_c = 0 \quad (2)$$

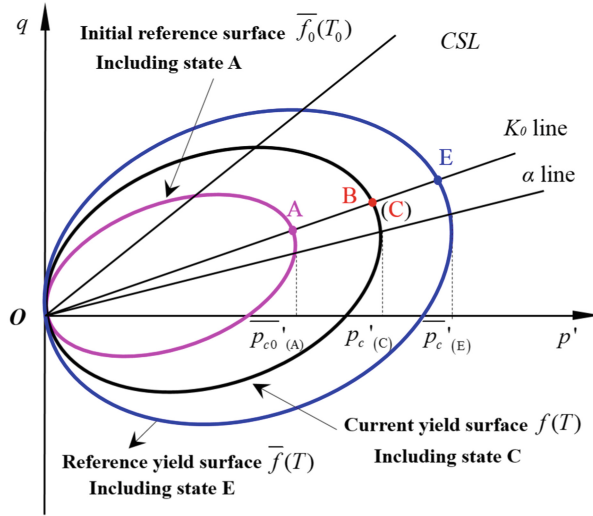
where M is the slope of the critical state line, parameter α is defined as the inclination of the elliptical yield surfaces (i.e., f and \bar{f}), which represents the stress-induced anisotropy. p' and q are the current mean effective stress and deviator stress, while \bar{p}' and \bar{q} are referred to the reference mean effective stress and deviator stress, respectively. The intersections between the α line and the current and the reference yield surfaces (i.e., f and \bar{f}) are corresponding to the current and the reference preconsolidation pressures, i.e., p'_c and \bar{p}'_c .

The hardening rule is consistent with MCC, where the size of the yield surface is mainly dependent on the plastic volumetric strain:

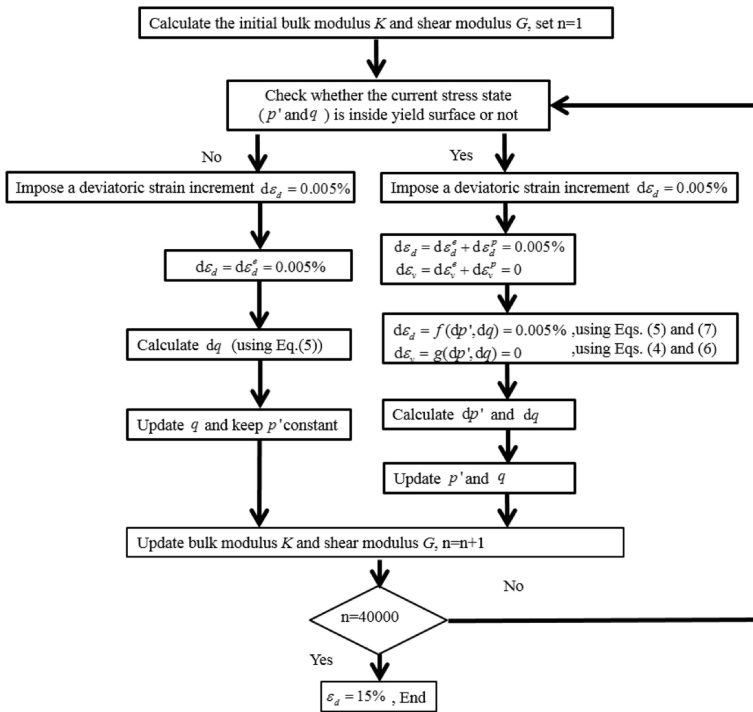
$$\bar{p}'_c = \bar{p}'_{c0} \cdot \exp\left(\frac{\varepsilon_v^p}{(\lambda - \kappa)/v_i}\right) \quad (3)$$

where \bar{p}'_c is the corresponding preconsolidation pressure of the intersection between the α line and initial reference yield surface $\bar{f}_0(T)$, ε_v^p is the plastic volumetric strain (including the mechanical and thermo-induced plastic volumetric strain).

In this thermal-mechanical model, strains are induced due to both mechanical loading and thermal loading. The elastic strain is assumed to be isotropic for simplicity, with



(a) the reference and current inclined ellipse yield surface



(b) calculation flow chart

Fig. 1. Theoretical framework for the thermo-elastic-plastic constitutive model

elastic increments of volumetric ($d\varepsilon_v^e$) and deviatoric strain ($d\varepsilon_d^e$) defined in the same manner as the Modified Cam-Clay model:

$$d\varepsilon_v^e = \frac{\kappa dp'}{v_i p'} \quad (4)$$

$$d\varepsilon_d^e = \frac{\kappa}{3G} dq \quad (5)$$

where v_i is initial specific volume, λ and κ are the compression and recompression index, respectively. G is the elastic shear modulus, which is a function of bulk modulus K and Poisson's ratio ν' , following the relationship $G = 3(1 - 2\nu')K/[2(1 + \nu')]$, K is equal to $v'p'/\kappa$.

Only one temperature-related parameter had been introduced to represent the temperature effect of clay. The derived increment of plastic volumetric strain and plastic deviator strain (Wang et al. 2016) are as following:

$$d\varepsilon_v^p = \frac{(\lambda - \kappa)}{v_i p'} \left(\frac{M^2 - \eta^2}{(M^2 - \alpha^2) + (\eta - \alpha)^2} \right) dp' + \frac{(\lambda - \kappa)}{v_i p'} \left(\frac{2(\eta - \alpha)}{(M^2 - \alpha^2) + (\eta - \alpha)^2} \right) dq + \frac{\theta(\lambda - \kappa)}{v_i T} dT \quad (6)$$

$$d\varepsilon_d^p = \frac{(\lambda - \kappa)}{v_i p'} \left(\frac{2(\eta - \alpha)}{(M^2 - \alpha^2) + (\eta - \alpha)^2} \right) dp' + \frac{(\lambda - \kappa)}{v_i p'} \left(\frac{4(\eta - \alpha)^2 / (M^2 - \eta^2)}{(M^2 - \alpha^2) + (\eta - \alpha)^2} \right) dq + \frac{2\theta(\lambda - \kappa) \cdot (\eta - \alpha)}{v_i T (M^2 - \eta^2)} dT \quad (7)$$

where η is the stress ratio q/p' . The flow chart for calculating the stress and strain response under undrained shearing is shown in Fig. 1b.

3 Temperature-Controlled Triaxial Test

3.1 Temperature- and Rate-Controlled Triaxial Apparatus

The temperature- and rate-controlled triaxial testing system are consisted of GDS triaxial testing apparatus and JULABO refrigerated & heating circulator with a working temperature range between -28°C and 100°C (for temperature control), which is shown in Fig. 2. The water in the circulator is continuously circulated through a spiral metal tube in the triaxial cell. The temperature of the soil can be measured by a Type T thermocouple, which is about one centimeter away from the specimen.

3.2 Experimental Material

Malaysia Kaolin is adopted as the testing material. The Physical and mechanical properties of kaolin are listed in Table 1.

The kaolin powder was mixed with water in proportion of 1: 1.7 w_L , which is widely used in slurry mixing, and then saturated for 6 h after no gas bubbles are existed in the saturation apparatus. After that, poured the slurry into the consolidation apparatus, which is 80 cm in height and 20 cm in diameter, and consolidated under 70 kPa surcharge in multistage, until the settlement rate is less than 1mm/d, the consolidation of soil sample can be regarded as finished, which lasted for nearly 10 days. Then the consolidated kaolin could be cut into cylindrical sample of 50 cm in diameter and 100 cm in height as the triaxial specimen.

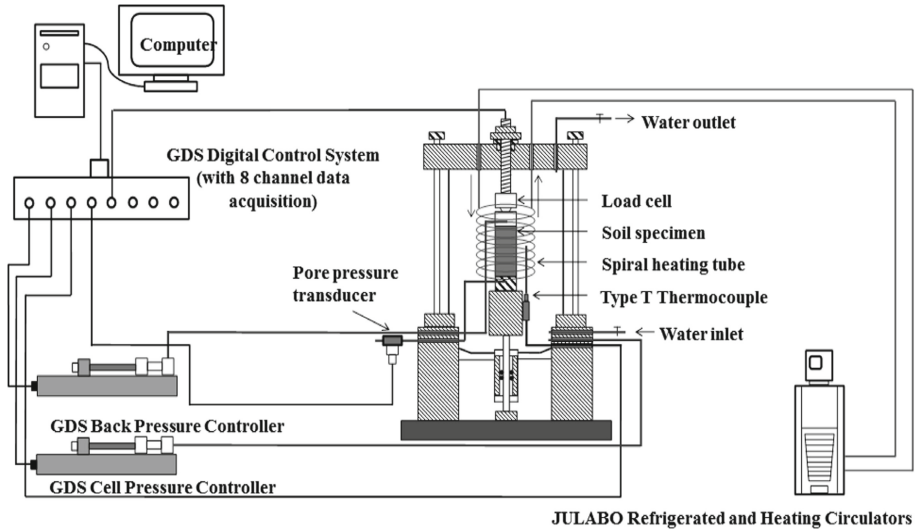


Fig. 2. Temperature- and rate-controlled triaxial testing system

Table 1. Physical and mechanical properties of Malaysia Kaolin

Physical properties	Value	Grain size distribution	Value
Liquid limit w_L (%)	65	Sand (%)	0
Plasticity index I_p	27	Silt (%)	35.1
Water content w (%)	59–61	Clay (%)	64.9
Specific gravity G_s	2.73		
Void ratio e	1.65–1.78		
Unit weight γ (kN/m ³)	16.7		
Compression properties			
Slope of the normal compression line in e - $\ln p$ space: λ			0.17
Slope of the unloading line in e - $\ln p$ space: κ			0.026
Intersect of normal compression line in e - $\ln p$ space: N			2.02

3.3 Test Procedures

In order to reveal the undrained shear behaviour of kaolin, series tests were conducted with different OCR (1, 2 and 4) under drained heating (55 °C) and heating-cooling cycle (20 °C–55 °C–20 °C). The OCR values 1, 2, and 4 are representative for normally consolidated clay (OCR = 1), lightly consolidated clay (OCR = 1–2, wet side in cam-clay model) and heavily consolidated clay (OCR > 2, dry side in cam-clay model), which can be referred from Wood (1990).

Table 2. Testing conditions for all the specimens

Test no.	Temperature	Consolidation pressure	Confined pressure before shearing	OCR
DT1	20 °C	300 kPa	300 kPa	1
DT2	20 °C	300 kPa	150 kPa	2
DT3	20 °C	300 kPa	75 kPa	4
HT1	55 °C	300 kPa	300 kPa	1
HT2	55 °C	300 kPa	150 kPa	2
HT3	55 °C	300 kPa	75 kPa	4
HC1	20–55–20 °C	300 kPa	300 kPa	1
HC2	20–55–20 °C	300 kPa	150 kPa	2
HC3	20–55–20 °C	300 kPa	75 kPa	4

All the specimens were saturated under back pressure in multistage until the B value was greater than 0.97. All the specimens were first consolidated under effective pressure of 300 kPa in 20 °C, then unloaded to different confined pressure (different OCR), finally heated to 55 °C or cooled back to 20 °C. The test conditions are shown in Table 2.

4 Test Results

4.1 Effect of Different Temperature Path on Undrained Shear Strength

Figure 3 presents the measured deviator stress-shear strain curve for kaolin under different OCR (1, 2 and 4) and different temperature path (20 °C, 20 °C–55 °C, 20 °C–55 °C–20 °C). From Fig. 3(a), the peak deviator stresses of the three normally consolidated kaolin specimens are different, the DT1 specimen under room temperature (20 °C) presents the lowest maximum deviator stress of 193 kPa. The HT1 specimen of 55 °C (drained heating) shows the highest maximum deviator stress of 228 kPa. The HC1 specimen, which has experienced heating-cooling cycle, presents an intermediate maximum deviator stress of 208 kPa. The results show that drained heating has effect on the normally consolidated soil, with a temperature rise of each 10 °C, the strength increases approximately 5%. Despite the current temperature of the soil, the temperature path would also affect the undrained shear strength of the normally consolidated soil, which means that the heating-cooling cycle induces unrecoverable volumetric strain (drained condition). Moreover, the initial shear stiffness has been influenced by heating-cooling cycle, the initial shear stiffness of HC1 specimen is larger than the other two specimens, which indicates that the heating-cooling cycle would strengthen the stiffness of the soil.

For the lightly consolidated kaolin (OCR = 2), the maximum deviator stresses of these three specimens are nearly the same (Fig. 3b), where $q_{\max}(\text{DT2}) \approx 167$ kPa, $q_{\max}(\text{HT2}) \approx 160$ kPa, $q_{\max}(\text{HC2}) \approx 165$ kPa, with a difference less than 4%. The results show that the temperature has slight effect on the undrained shear strength of

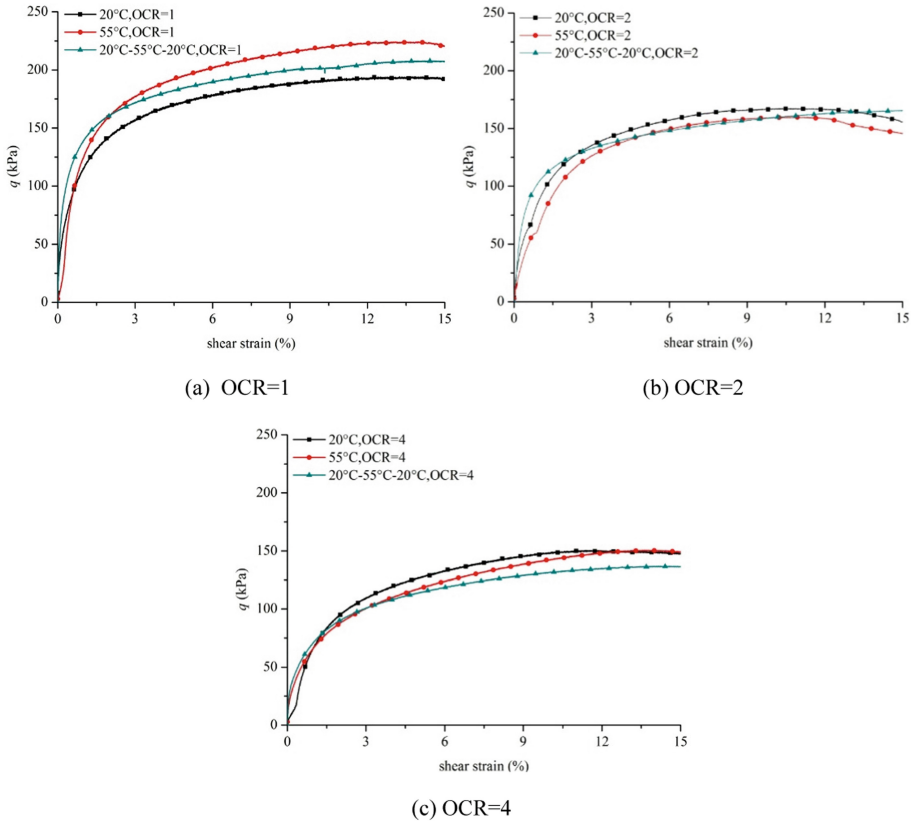


Fig. 3. Measured stress–strain relationship of Kaolin during undrained shearing under different temperature path

lightly consolidated kaolin. It should be noted that the initial shear stiffness of the HC2 specimen is increased by the heating-cooling cycle comparing to the other two specimens.

For the heavily consolidated kaolin (OCR = 4), the maximum deviator stresses of DT3 and HT3 are equal to 150 kPa, which means that the heating effect of heavily consolidated kaolin would be neglected. However, the HC3 specimen of heating-cooling cycle still has the largest initial shear stiffness.

In conclusion, for the normally consolidated clay, the drained heating would increase the undrained shear strength of the clay, and the drained heating-cooling cycle influences the strength with less effect. For the overconsolidated clay, the temperature effect on the strength is very weak, if the experimental deviations are taken into consideration. The heating-cooling cycle would enhance the initial shear stiffness, no matter the clay specimen is normally consolidated or overconsolidated.

4.2 Effect of Different Temperature Path on Pore Pressure Respond During Shearing

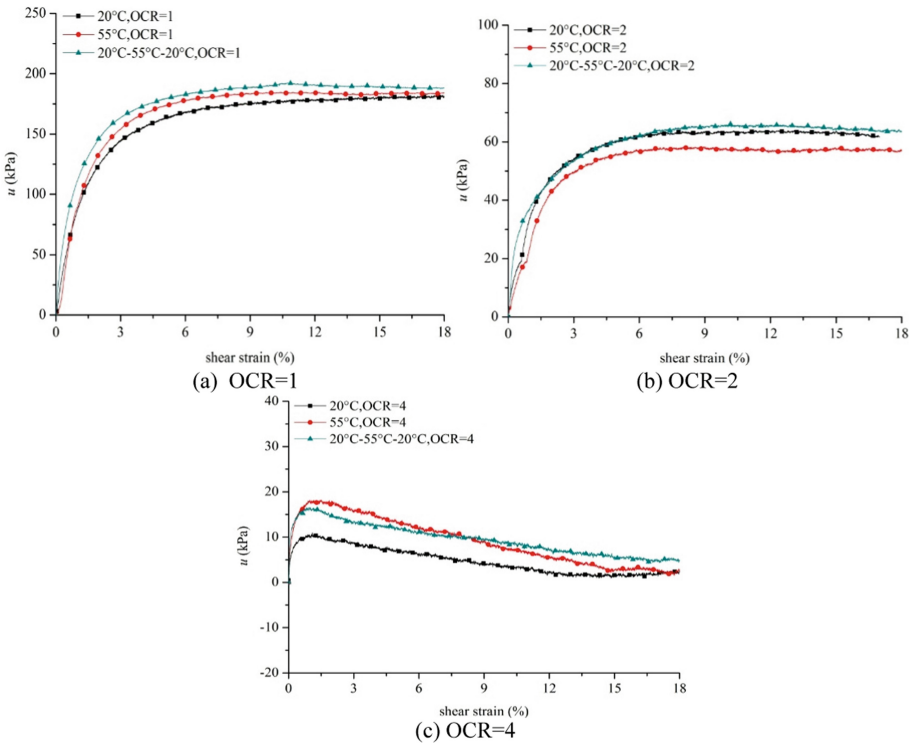


Fig. 4. Measured pore pressure–strain relationship of Kaolin during undrained shearing under different temperature path

The measured excess pore pressures for all the specimens during undrained shearing are plotted in Fig. 4. For normally consolidated kaolin, the final excess pore pressures are respectively 182 kPa, 184 kPa and 188 kPa for room temperature specimen, heating specimen and heating-cooling cycle specimen, with a maximum difference less than 6 kPa.

For $OCR = 2$, the final pore pressure of HC2 is the largest of 64 kPa. The room temperature DT2 specimen has the intermediate final pore pressure of 62 kPa, where the final pore pressure of HT2 specimen is the lowest of 57 kPa.

For the heavily consolidated clay, the clay exhibits shear shrinkage with increasing excess pore pressure, then changes to shear dilatancy with pore pressure decreasing. The maximum excess pore pressures of DT3, HT3 and HC3 are 11 kPa, 18 kPa and 16 kPa respectively. The final excess pressures of the three specimens are respectively 2 kPa, 2 kPa and 5 kPa, with small difference.

The excess pore pressure results during undrained shearing present that temperature has less effect on the kaolin, despite of the overconsolidation ratio. The results are

consistent with the results of Todi clay (Burghignoli et al. 2000), but the results of Bangkok clay carried out by Abuel-Naga et al. (2007) show different behaviour, where the excess pore pressure response is weakened after drained heating. The temperature effect on the excess pore pressure response during the undrained shear process might be dependent on the soil type.

4.3 Temperature Effect on the Slope M of Critical State Line

The slope M is the stress ratio at critical state. Schofield and Wroth (1968) proposed that the pore pressure gradient would be equal to zero, i.e. the pore pressure coefficient A equals to zero (Skempton 1954), when the soil was at critical state.

$$A = \frac{\Delta u}{\Delta q} \quad (6)$$

where Δu and Δq are the excess pore pressure variation and deviator stress variation, respectively. The M values of all the tests are plotted in the following figure.

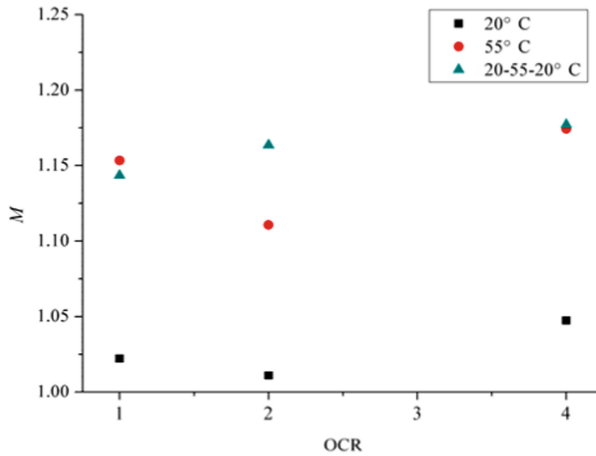


Fig. 5. M value under different stress and temperature paths

Figure 5 exhibits that the M values for the DT soil specimens at room temperature vary from 1.00 to 1.05. After drained heating, the M values are increased with an increment of approximately 0.12, from 1.11 to 1.17. It is worth nothing that although the temperature of the HC specimens at shearing are 20 °C, the HC specimens still have higher M values from 1.14 to 1.18. The results reflect that not only the temperature but also the temperature history will influence the M values.

5 Theoretical Verification

5.1 Constitutive Model Parameters of Kaolin

The compression parameters used in theoretical calculations are based on one-dimensional consolidation test. The M values were referred from the triaxial test result

by the method mentioned in Sect. 4.3. The Poisson's ratio ν of clay varies from 0.3 to 0.42, in this paper, $\nu = 0.38$ was used. Considering that the kaolin specimens were reconsolidated under isotropic condition of 300 kPa, the initial anisotropy could be ignored, then the Initial anisotropic parameter α_0 can be zero. The temperature related parameter θ is calculated by the experience equation between θ and plasticity index I_p proposed by Wang et al. (2016):

$$\theta = 0.1120 + 0.0012I_p \quad (7)$$

Table 3. Constitutive model parameters of kaolin

Slope of the normal compression line in e - $\ln p$ space: λ	0.17
Slope of the unloading line in e - $\ln p$ space: κ	0.026
Intersect of normal compression line in e - $\ln p$ space: N	2.02
Stress ratio at critical state for 20 °C: M_{20}	1.026
Stress ratio at critical state for 55 °C: M_{55}	1.154
Poisson's ratio ν	0.38
Initial anisotropic parameter α_0	0
Temperature related parameter θ	0.1456

5.2 Analysis of DT Specimens

Figure 6a shows the measured and predicted results of deviator stress and shear strain in the undrained shear process of room temperature DT specimens. The predicted results show a good agreement with the measured results under different OCR, which also means that the tests results are reliable.

Figure 6b present the experimental and predicted results of pore pressure during undrained shearing of DT specimens. For normally consolidated kaolin (DT1), the predicted results are agreed with the measured results. The calculated results for DT2 (OCR = 2) meet well with the measured results at the beginning, when the shear strain increases, the calculated results decrease to 42 kPa after reaching the peak value of 56 kPa. However, the measured results have kept growing until the failure of the soil specimen, with a final pore pressure of 63 kPa. For the heavily consolidated kaolin (OCR = 4), the measured results show a very short growing in the section of 0% to 1% strain, with a maximum pore pressure of 11 kPa and final pore pressure of -2 kPa. But for predicted results, the pore pressure increases to 42 kPa within the shear strain of 3%, then the pore pressure reduces to -22 kPa, with a difference of 20 kPa comparing to the measured results.

The overestimate of the pore pressure for OCR = 4 in Fig. 6b might be due to the shortcoming of the constitutive model, which is an elastic-plastic model based on the framework of modified cam-clay model. The elastic-plastic model ideally divided the

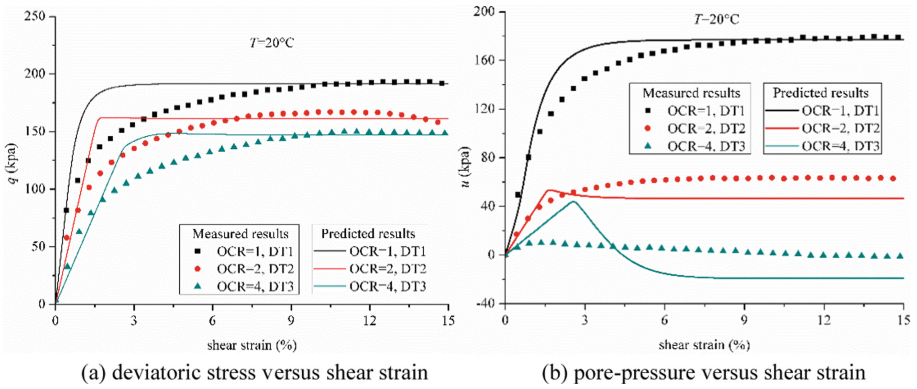


Fig. 6. Comparison between measured and predicted results of Kaolin under room temperature

shearing into elastic section (purely elastic strain) and plastic section. However, there are no obvious boundary between the elastic and plastic sections, small plastic strain is generated in the early stage of shearing. In the elastic section, the effective stress path is vertically upward to the yield surface in the p' - q plane, which means no changes are presented in the effective mean stress p' , and so as the stiffness. This is the shortcomings for the MCC model (elastic-plastic model), which is more serious in overconsolidated clay, because a very long elastic section is assumed for overconsolidated clay comparing to the lightly overconsolidated and normally consolidated clay. That is the reason for the overestimate of the pore pressure for heavily overconsolidated clay.

In summary, the constitutive model has a good quality in prediction for the undrained shear strength of clay. The prediction of excess pore pressure for normally consolidated clay is well, but the model lacks in predicting the pore pressure response for overconsolidated clay.

5.3 Analysis of HT Specimens

The predicted and measured results for HT specimens are presented and compared in Fig. 7.

At the initial segment of the deviator stress and shear strain curve, shown in Fig. 7a, the simulation results of OCR = 1 and OCR = 2 specimens meet well with the measured results. Since the model doesn't consider the softening of the shear stiffness, the predicted results are overestimated when the shear strain increases. However, when the deviator stress reaches its peak, the predicted results become the same to the measured results. Figure 7b exhibits the pore pressure response during the undrained shearing for heating specimens (55°C), the prediction of normally consolidated kaolin shows good agreement with the measured results, with a final pore pressure of 184 kPa. In the prediction of HT2 specimen, the final pore pressure has small difference of 4 kPa higher than the measured results. For heavily overconsolidated kaolin (OCR = 4), the model overestimates the positive pore pressure of nearly 46 kPa, where the measured positive pore pressure is only about 18 kPa. But the final pore pressure of the prediction results has only a small difference of 3 kPa comparing to the measured results.

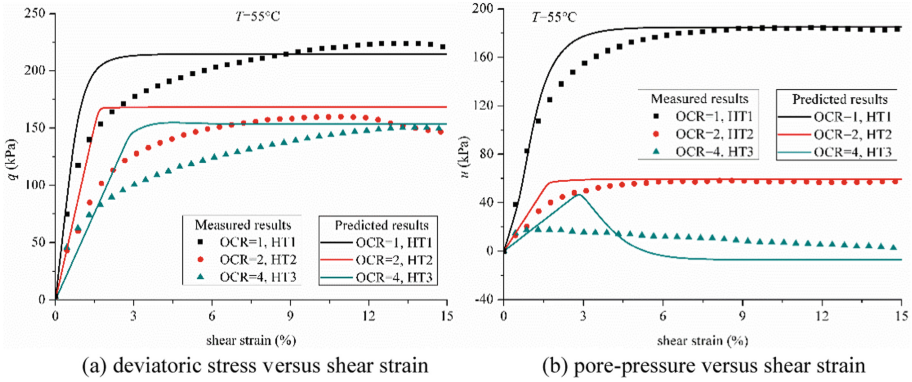


Fig. 7. Comparison between measured and predicted results of Kaolin under high temperature

5.4 Analysis of HC Specimens

The drained heating-cooling process is more complicated than drained heating process. Temperature would affect the size of the yield surface, when temperature increases, the yield surface would shrink, and vice versa (Graham et al. 2001).

For the normally consolidated clay (initial confined pressure of 300 kPa), during the drained heating process, the yield surface would first shrink, the apparent pre-consolidation pressure would be reduced, and thermal-induced excess pore pressure would be generated. Then the current vertical stress will consolidate the clay to the initial confined pressure of 300 kPa, after dissipation of the excess pore pressure, namely thermal consolidation, the strength of clay will be increased due to the hardening of the volumetric strain.

For the heavily consolidated clay ($\text{OCR} = 4$, the current mean effective stress is 75 kPa), the temperature arise from 20°C to 55°C will lead to the shrinkage of the yield surface, but the preconsolidation pressure after heating will be around 250 kPa (According to the equation proposed by Moritz 1995), which is larger than the current effective stress 75 kPa. For the overconsolidated clay, the drained heating and cooling process will not produce plastic volumetric strain, only elastic volumetric strain will be generated in ideal condition, as a result, temperature would have extremely weak effect on overconsolidated clay. The mechanical behaviour of overconsolidated clay after heating process and cooling process should be similar to the clay at room temperature.

The calculation results of 20°C (using M_{20}) and 55°C (using M_{55}) are both plotted for comparison with the measured results of heating-cooling cycle HC specimens, which are shown in Fig. 8. Figure 8a shows the curve of deviator stress and shear strain, the measured result of HC1 ($\text{OCR} = 1$) is closer to the simulation results of 55°C , which indicates that the temperature history will possibly affect the mechanical behaviour of clay. The measured results of HC2 ($\text{OCR} = 2$) and HC3 ($\text{OCR} = 4$) are closer to the simulation results of 20°C , which means that the temperature has less effect on the strength of the overconsolidated clay, the plastic volumetric strain induced by temperature is the main factor in strength variation.

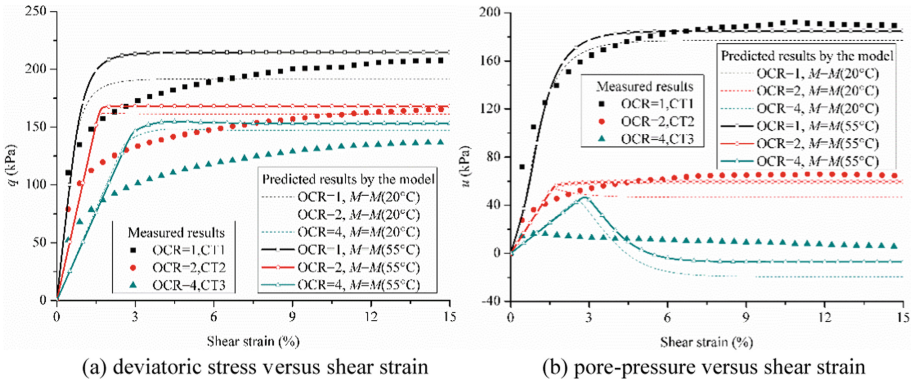


Fig. 8. Comparison between measured and predicted results of Kaolin under cyclic temperature

Figure 8b presents the calculation and measured results of excess pore pressure for OCR = 1, 2 and 4. All the experimental results are more consistent with the calculated results of 55 °C. For OCR = 1 and OCR = 2, the deviation between the calculated and measured results of the final pore pressure is less than 6 kPa. The deviation of the final pore pressure for the heavily overconsolidated specimen (OCR = 4) is approximately 12 kPa, indicating that the model should be improved in the future for overconsolidated clay.

6 Conclusion

Based on the temperature control triaxial system, the undrained shear behaviour of kaolin of different overconsolidation ratio under room temperature, high temperature and heating-cooling cycle has been studied. At the same time, a thermo-elastic-plastic constitutive model has been adopted to analyse and verify the measured results. The predicted results by the theoretical model and the measured results are in good agreement. The major findings are presented as follows:

(1) For normally consolidated kaolin (OCR = 1) after drained heating or drained heating-cooling cycle, the undrained shear strength are higher than the strength of specimen at room temperature, and the undrained shear strength of heating specimen HT1 is higher than the strength of heating-cooling specimen HC1, which is consistent with the results of Kuntiwattanakul et al. (1995). For the overconsolidated kaolin (OCR = 2, OCR = 4), the undrained shear strength of the room temperature, high temperature and heating-cooling specimens are very close each other, means that the temperature has less effect on the undrained shear strength on overconsolidated clay. In all the tests of different OCRs, heating-cooling cycle specimens have larger the initial shear stiffness, which might be influenced by the hardening effect of volumetric strain. To sum up, the unrecoverable (plastic) thermal-induced volumetric strain will increase the strength of clay, and recoverable (elastic) thermal-induced volumetric strain won't have great influence on the strength.

(2) The slope M of critical state line of kaolin is greatly affected by temperature. When the temperature rises from 20 °C to 55 °C, the M values of kaolin increase from

about 1.00–1.05 to 1.11–1.18, with a variation of 0.12 approximately. An interesting discover is that the heating-cooling specimens still have higher M values of 1.14 to 1.18, indicates that the temperature history would affect the mechanical properties of clay.

(3) The prediction results obtained by using the thermo-elastic-plastic constitutive model proposed by Wang et al. (2016) are well matched with the measured results. The prediction for normally consolidated clay ($OCR = 1$) and slightly overconsolidated clay ($OCR = 2$) show relative high accuracy. For heavily overconsolidated clay (OCR), the deviation is higher than the normally consolidated and slightly overconsolidated clay, the prediction is not so accurate, but relatively acceptable.

(4) The excess pore pressure responses during undrained shearing of kaolin of different overconsolidation ratio under room temperature, high temperature, heating-cooling cycle exhibit similar behaviours, which are similar to the results of Todi clay (Burghignoli et al. 2000). However, the results of Bangkok clay (Abuel-Naga et al. 2007) present that the excess pore pressure during undrained shearing would be weakened after heating. The contradiction illustrates that the temperature effect on the excess pore pressure response during undrained shearing may be associated with types of soil, which needs further research.

It should be reminded that the work is based on kaolin, the temperature effect on other clay might be different from kaolin, such as the M values and pore pressure response during undrained shearing under different temperatures. The paper is aimed at providing referable results for researchers to analyse the temperature effect of clay in the future, and it should be carefully used in engineering projects.

Acknowledgement. The authors gratefully acknowledge the supports of the National Natural Science Foundation of China (Grant No. 51779220), Zhejiang Provincial Natural Science Foundation of China (Grant No. LQ20E090001 and LQ19E090002), Key Science and Technology Plan of POWERCHINA Huadong Engineering Corporation (Grant No. KY2018-ZD-01) and Science and Technology project of POWERCHINA Huadong Engineering Corporation (Grant No. KY2020-KC-01).

References

- Abuel-Naga, H.M., Bergado, D.T., Lim, B.F.: Effect of temperature on shear strength and yielding behaviour of soft Bangkok clay. *Soils Found.* **47**(3), 423–436 (2007)
- Abuel-Naga, H.M., Bergado, D.T., Bouazza, A., Pender, M.J.: Thermomechanical model for saturated clays. *Géotechnique* **59**(3), 273–278 (2009)
- Burghignoli, A., Desideri, A., Miliziano, S.: A laboratory study on the thermomechanical behaviour of clayey soils. *Can. Geotech. J.* **37**(4), 764–780 (2000)
- Graham, J., Tanaka, N., Crilly, T., Alfaro, M.C.: Modified Cam-Clay modelling of temperature effects in clays. *Can. Geotech. J.* **38**(3), 608–621 (2001)
- Hueckel, T., Francois, B., Laloui, L.: Explaining thermal failure in saturated clays. *Géotechnique* **59**(3), 197–212 (2009)
- Hueckel, T., Pellegrini, R.: Thermo-plastic modeling of undrained failure of saturated clay due to heating. *Soils Found.* **31**(3), 1–16 (1991)
- Hueckel, T., Pellegrini, R.: Effective stress and water pressure in saturated clays during heating-cooling cycles. *Can. Geotech. J.* **29**(6), 1095–1102 (1992)

- Hueckel, T.: Chemo-plasticity of clays subjected to stress and flow of a single contaminant. *Int. J. Numer. Anal. Meth. Geomech.* **21**(1), 43–72 (1997)
- Kuntiwattanukul, P., Towhata, I., Ohishi, K., Seko, I.: Temperature effects on undrained shear characteristics of clay. *Soils Found.* **35**(1), 147–162 (1995)
- Marques, M.E., Leroueil, S., Almeida, M.S.: Viscous behaviour of St-Roch-de-l’Achigan clay, Quebec. *Can. Geotech. J.* **41**(1), 25–38 (2004)
- Moel, M.D., Bach, P.M., Bouazza, A., Singh, R.M., Sun, J.L.O.: Technological advances and applications of geothermal energy pile foundations and their feasibility in Australia. *Renew. Sustain. Energy Rev.* **14**(9), 2683–2696 (2010)
- Moritz, L.: Geotechnical properties of clay at elevated temperatures. Report: 47, Swedish Geotechnical Institute, Linköping (1995)
- Qi, L., Zheng, Y.R., Tao, H.B., Liu, G.B.: A study of the critical state parameter of the Ningbo soft clay considering the effect of temperature. *Hydrogeol. Eng. Geol.* **42**(5), 79–83 (2015). (in Chinese)
- Schofield, A.N., Wroth, P.: *Critical State Soil Mechanics*. McGraw-Hill, London (1968)
- Skempton, A.W.: The pore-pressure coefficients A and B. *Géotechnique* **4**(4), 143–147 (1954)
- Towhata, I., Kuntiwattanaku, P., Seko, I., Ohishi, K.: Volume change of clays induced by heating as observed in consolidation tests. *Soils Found.* **33**(4), 170–183 (1993)
- Wang, K., Wang, L., Hong, Y.: Modelling thermo-elastic–viscoplastic behaviour of marine clay. *Acta Geotech.* **15**(9), 2415–2431 (2020). <https://doi.org/10.1007/s11440-020-00917-9>
- Wang, L.Z., Wang, K.J., Hong, Y.: Modeling temperature-dependent behavior of soft clay. *J. Eng. Mech.* **142**(8), 04016054 (2016). [https://doi.org/10.1061/\(ASCE\)EM.1943-7889.0001108](https://doi.org/10.1061/(ASCE)EM.1943-7889.0001108)
- Wheeler, S.J., Naatanen, A., Karstunen, M., Lojander, M.: An anisotropic elastoplastic model for soft clays. *Can. Geotech. J.* **40**(2), 403–418 (2003)
- Wood, D.M.: *Soil Behaviour and Critical State Soil Mechanics*. Cambridge University Press, Cambridge, UK (1990)
- Yu, G.J., Yu, B., Liang, Y.T., Wang, M., Joshi, Y., Sun, D.L.: Further study on the thermal characteristic of a buried waxy crude oil pipeline during its cooling process after a shutdown. *Numer. Heat Transf. Part A Appl.* **71**(2), 137–152 (2017)



Assessment of the Pavement Subgrade Using Different In-situ Testing Methods

Kasun Wimalasena^{1(✉)}, Chaminda Gallage¹, Jianfeng Xue², and Jeffrey Lee³

¹ School of Civil and Environmental Engineering, Queensland University of Technology, Brisbane, Australia

kdilhara@cee.ruh.ac.lk

² School of Engineering and IT, University of New South Wales, Canberra, Australia

³ Australian Road Research Board, Brisbane, Australia

Abstract. Pavement Subgrade provides the basic support to the structural layers of a pavement system and hence, it is important to perform a reliable assessment of the condition of the subgrade prior to designing and constructing the road. Because, the failures in the subgrade level, during the design life of the pavement, will have the consequence of occurring pavement distresses before the end of expected pavement life. The condition of the subgrade can be assessed in a laboratory environment by collecting samples from the selected site. However, it is a time-consuming process and would be difficult to perform in more frequent intervals on a selected pavement section. Accordingly, in-situ subgrade assessment methods have gained the popularity owing to the expedite results and the ability to conduct at more frequent intervals in less time. This paper reports a comparison of subgrade assessment conducted on a selected experimental road stretch. In that road stretch, test sections were constructed to assess the field performance of geogrid reinforced roads. The bearing capacity of the subgrade (CBR value) was assessed by conducting borehole tests prior construction stage and Dynamic Cone Penetration Test (DCP), Variable Dynamic Cone Penetration Test (PANDA®), Light Weight Deflectometer Test (LWD) and Falling Weight Deflectometer (FWD) test were performed during and at the end of construction. The comparison of the subgrade CBR from different test methods reveals that DCP provides closer assessment to laboratory investigated CBR value while other test methods show an overestimation.

1 Introduction

The increasing population and the economic development of a country increase the demand for new roads in order to facilitate the growing transportation requirements. Both existing and new roads require substantial investments for construction and maintenance. Therefore, it is extremely important to construct well design pavements that would act resilient to pavement deterioration along with the design life (Marecos et al. 2017). In the process of designing a road pavement, accurate assessment of the subgrade condition is vitally important since it provides support for the entire pavement layers (Wimalasena and Jayalath 2020). In other words, the performance of the pavement through the design

life strongly depends on the condition of the subgrade. Over assessment of the subgrade condition would lead to the design of pavements that could not withstand the design traffic load and in contrast, under assessment would lead costly design alternatives.

The condition of the subgrade can be assessed based on the bearing capacity or the elastic modulus (Mittal and Shukla 2019). In Australian pavement design guidelines, the California Bearing Ratio (CBR) is used to assess the subgrade condition, and this value is directly used in the empirical design method while tenfold of the CBR value is considered as the subgrade modulus of the Australian mechanistic-empirical pavement design method (Austroads 2018). The CBR value is assessed by collecting the subgrade material from sites and perform the standard CBR test method in a laboratory environment under standard loading conditions. As a result, it is challenging to conduct CBR tests on a selected road stretch in frequent intervals due to the time and cost constrains.

Alternatively, in-situ tests have been developed and are preferred over the time-consuming traditional type of CBR test (Marecos et al. 2017). These tests can easily be conducted on one location at a site in a reasonably shorter time and therefore, possible to repeat on multiple locations that will provide results to assess the integrity of the subgrade. Moreover, some of these methods can provide on-site results and hence, could expedite the decision making. The Dynamic Cone Penetration Test (DCP), Instrumented Variable Energy Dynamic Cone Penetrometer (trademarked as PANDA®), Light Weight Falling Weight Deflectometer Test (LWD) and Falling Weight Deflectometer (FWD) are current in-situ tests being used in subgrade assessment (McHenry and Rose 2012). DCP test was first developed by Scala (1956) in Australia and originally, was developed as an alternative to measuring the strength and stiffness of subgrade soil aiming to replace the time-consuming core sampling and laboratory testing. This test is performed by releasing a dropping hammer from a certain falling height and recording the depth of penetration for each drop until reaching a decided penetration depth. Many researchers have investigated the relationship of DCP and CBR of subgrade and have developed equations that can be used to calculate subgrade CBR from DCP results (Salgado and Yoon 2003). In the state of Queensland, Australia, in-situ DCP test is being performed according to the Queensland Department of Transport and Main Roads (TMR) standard of Q114B.

The Variable Energy Dynamic Cone Penetrometer, trademarked as PANDA, is another in-situ test that can be performed to measure the subgrade and monitor layer compaction (Lee et al. 2019). This is an instrumented and lightweight DCP test performed by applying blows of hammers on the head of the tool. The microprocessor in the PANDA® instrument records the impact of the hammer and the depth of penetration and perform a real-time calculation of the dynamic cone resistance and current depth. Hence, the CBR value of the subgrade can be estimated by substituting the aforementioned parameters in developed relationships. In comparison to traditional DCP test, PANDA® is convenient to perform because of its lightweight and simple operation procedure. In addition, this test can be done anywhere, including the challenging terrains and assist decision making owing to the generation of real time results (Langton 1999).

Light Weight Deflectometer (LWD) is another portable device use to assess the in-situ layer modulus of subgrade and subbase layers (Puppala 2008). In this test, a drop hammer is released multiple times from four different heights and the instrument records

the load and deflection for each blow which will be used to back-calculate the elastic modulus of the layer. Although this test provides an immediate assessment of the layer modulus, the measuring depth comparatively lower than FWD tests because of the use of lower loads. Hence, the elastic modulus from LWD is mainly the modulus of the surface layer, which the instrument is in direct contact (Marecos et al. 2017). However, this has gained popularity in the road construction industry in assessing the subgrade modulus and quality controlling the pavement layers. The Falling Weight Deflectometer (FWD) is the most popular test in assessing the conditions of pavements around the world (Gallage et al. 2015). This replicates the traffic load by applying an impulsive load on a standard plate and capture the deflection at different distances away from the center of the plate, using an array of geophones. Studies have developed correlations between measured deflection and the subgrade CBR values that can be applied to assess the subgrade condition. However, studies have also highlighted that the FWD test overestimates the subgrade condition (Chai et al. 2013).

This study is a part of the project of conducting a real scale field trial to assess the performance of geogrids in improving the subgrade condition. This paper reports the assessment of subgrade in the selected test section by performing different in-situ tests in order to ensure the integrity of the subgrade bearing capacity along the proposed test stretch. Prior to commencing constructions, the subgrade was first assessed by the details of a borehole drilled at one location on the test section. During the construction stage, the subgrade was assessed by DCP, PANDA®, LFWD tests and subsequently, FWD test was performed on the granular surface of the pavement after completion of the construction. The results compare the CBR value of the subgrade along the test section obtained from aforementioned in-situ tests.

2 Test Site

In order to execute the project, a section of a 225 m in length was selected on a proposed road to rehabilitate in the Logan city of Australia. This is a two-lane road with one traffic lane for each direction with a total kerb to kerb width of 11.5 m including a parking lane at one side. The road had failed due to poor subgrade condition and therefore, the City Council proposed a subgrade improvement and a resurfacing. Series of boreholes were drilled on several locations of the road aiming to assess the existing condition. For this research project, a 225 m length of the road, which was proposed to rehabilitate, was selected along one traffic lane and that include 3 boreholes which are BH6, BH7 and BH8 as shown in Fig. 1. The selected 225 m section was divided into 14 sections to improve with different geogrid arrangements as shown in Fig. 2. A 30 m length stretch between section 8 and section 9 had to be avoided and rehabilitate with the conventional method of rock blanketing as a result of challenging terrain condition. The boreholes BH6, BH7 and BH8 are located in the sections 12, 8 and 4 respectively. The subgrade CBR values and the subgrade properties obtained from borehole analysis are given in Table 1 and 2.



Fig. 1. Areal view of experimental area

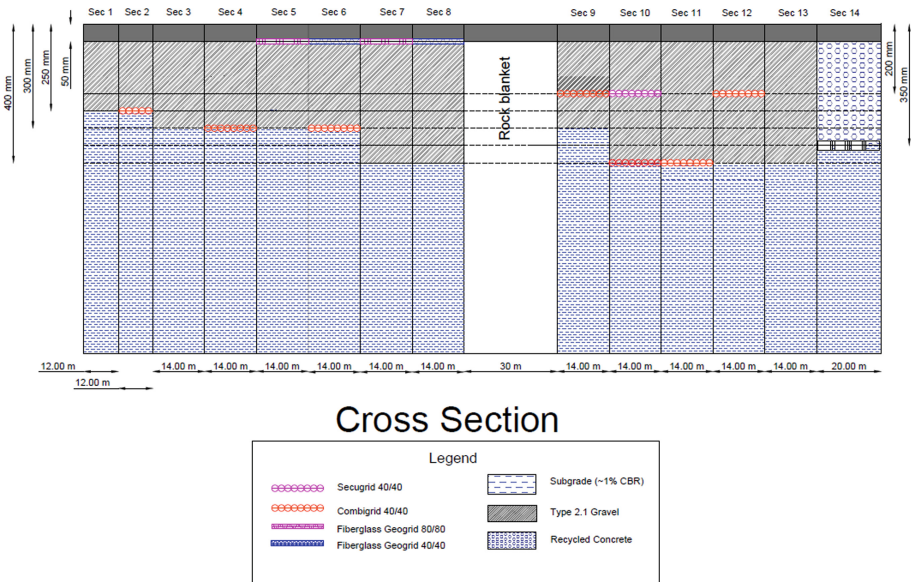


Fig. 2. Sections in experimental area

Table 1. Subgrade CBR in borehole locations

Location (Borehole)	CBR (%)
52- BH5 (Out of test area)	1.5
52 - BH6 (In Section 12)	2.0
52 - BH7 (In Section 8)	1.5
52 - BH8 (In Section 4)	2.5

Table 2. Subgrade material properties

Material description	Clay
% Sand & gravel	94
Moisture content (%)	21.3
Liquid limit (%)	88
Plastic index (%)	62
Linear shrinkage (%)	19

3 Subgrade Testing Methods

The constructions commenced by excavating the existing pavement up to the existing subgrade level (Fig. 3). Thereafter, DCP, PANDA® and LWD tests were performed on the exposed subgrade. For each section, two locations were marked i.e. selecting one location on the left-hand side from the centerline of the section, that divide the section to two equal lengths, and the other location on the opposite side. All three types of tests were conducted on the selected location as describes above in order to acquire data for comparison i.e. one test from each type at one location. Finally, FWD test was conducted on the granular surface after completion of construction.

DCP Test

The DCP test was performed at the selected location on the test section according to the Q114B standard testing procedure (Fig. 4). The ground penetration of the cone was recorded for every hammer drop until the required penetration depth is achieved. Thereafter, the average penetration rate was calculated and the CBR value of the subgrade layer was estimated from the equation given in Q114B (Eq. 1).

$$CBR = 10^{0.881+1.16\log_{10}\left(\frac{25}{r}\right)} \quad (1)$$

CBR = California Bearing Ratio

R = Average Penetration Rate (mm/blow)

PANDA® Test

The PANDA® test was performed at the same locations where the DCP test was conducted i.e. two tests were performed for each section of the test site (Fig. 5). This test was conducted by hammering the head of the tool to provide energy to penetrate the cone to the ground until the desired depth. The instrument records the speed of the impact on the machine from hammer blows and the penetration of the cone to the ground. The microprocessor of the unit uses these two parameters to calculate the dynamic cone resistance which can be substituted in the developed equation to estimate the CBR value of subgrade.

$$\text{Log}_{10}(CBR) = 0.352 - 1.057\text{Log}_{10}(q_d) \quad (2)$$



Fig. 3. Excavation of existing pavement in experimental area

CBR = California Bearing Ratio

q_d = Dynamic Cone Resistance (MPa)

LWD Test

The same locations of DCP and PANDA® tests were selected to conduct LWD tests. The LWD test was performed using PRIMA 100 instrument with a drop mass of 15 kg (Fig. 6). For each location, the test was performed using 100 mm, 200 mm and 300 mm diameter plates and 10 drops were released from four different heights. First, five drops were considered for plate seating, and the next five drops were used for the analysis. The vertical deformation of the plate was captured from the geophone fixed at the center of the plate and used in the calculation of dynamic elastic modulus. Hence, the CBR value was estimated by dividing the modulus from 10, which is the rule being used to estimate the subgrade modulus from CBR value in Australian Pavement Design (Austroads 2018).

FWD Test

The FWD test was performed after completion of the construction of the granular layer by selecting six locations for each section in the experimental area (Fig. 7). In this test, an impulsive load of 30 kN was applied on a loading plate of 300 mm diameter, and the deflection bowl was captured using a set of geophones located at 0 mm, 200 mm, 300 mm, 450 mm, 600 mm, 900 mm, 1200 mm and 1500 mm away from the center of the loading plate. The deflection recorded by the geophone, located at 900 mm away from the center of the loading plate (D_{900}), was used to calculate the subgrade CBR value using Eq. 2 developed by Queensland Department of Transportation and Main Roads, Australia (Transport and Roads 2020).

$$\text{CBR}_{\text{Subgrade}} = 0.5996(D_{900})^{-1.4543} \quad (3)$$

CBR = California Bearing Ratio

D_{900} = Deflection 900 mm away from the center of loading plate (mm)



Fig. 4. Dynamic cone penetration (DCP) test



Fig. 5. Variable dynamic cone penetration (PANDA) test



Fig. 6. Light weight deflectometer (LWD) test



Fig. 7. Falling weight deflectometer (FWD) test

4 Comparison of Subgrade Bearing Capacity from Different Tests

The subgrade CBR value of each section was estimated from DCP, PANDA, LWD and FWD tests. From each test, the CBR value of a section was calculated as the average CBR value of all tests conducted. Figure 8 compares the estimated CBR values from the different in-situ test methods conducted on each test section.

The DCP test indicates that the subgrade CBR along the experimental area is ranging between 2–4% except for Section 12, which has been estimated as 5%. On average, the DCP test shows that subgrade bearing capacity of the experimental section can be considered as CBR 3%. This agrees with the three borehole tests conducted in the experimental area before commencing the rehabilitation construction. As per Table 1, the borehole investigation shows that the subgrade CBR of the experimental area is approximately around 2.5%. The slight difference between the borehole investigated CBR and the DCP estimated CBR could be possible in comparing laboratory estimated value with a field estimated value. In addition, the ground condition of the experimental site is extremely weak and expansive clay was observed along the selected road section. Also, significant moisture variation of the subgrade, especially with adverse weather conditions, was observed from the moisture probes installed in subgrade for long term

monitoring. Therefore, the difference of moisture content during borehole investigation and DCP testing could be a possible reason for the slight difference between the CBR values.

The comparison of CBR values estimated from PANDA® and LWD tests shows higher estimation than the CBR values given by DCP test. However, both PANDA® and LWD results demonstrate the same trend of variation as DCP results along the test section. In PANDA® test, an empirically developed relationship is being used to estimate the CBR value from dynamic penetration resistance and therefore, it is possible that the used relationship does not show valid representation in a different soil condition. Although ten-fold of the CBR value is accepted as the subgrade modulus in Australian Pavement Design as a general rule, many researchers have raised the argument that the aforementioned rule does not valid for all subgrade conditions. Accordingly, direct use of the relationships developed under different conditions to subgrade CBR estimation of this experimental area could possibly overestimate or underestimate the real subgrade condition. Hence, the same in-situ tests could be still used in subgrade bearing capacity assessment through a calibration process with laboratory estimated CBR values.

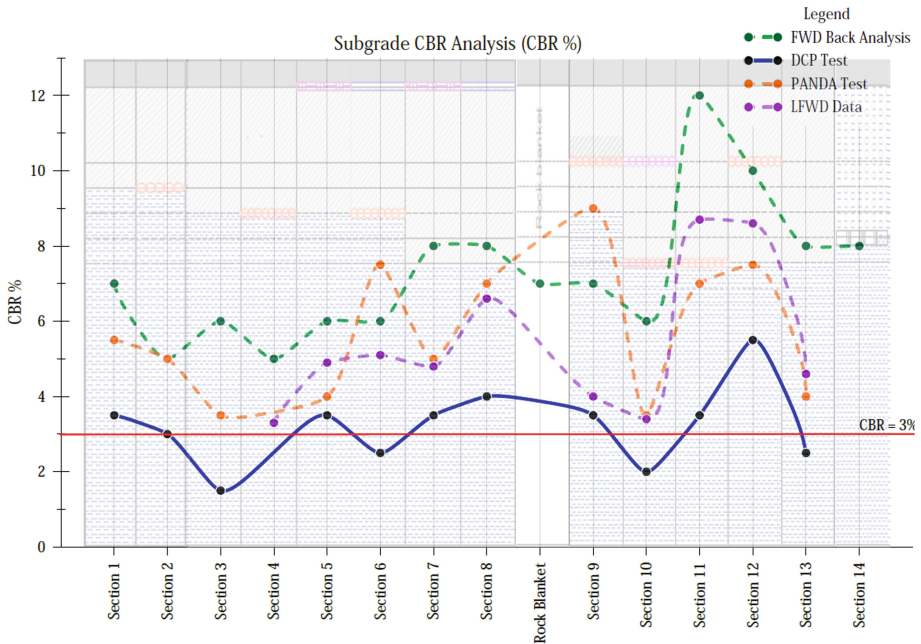


Fig. 8. Comparison of subgrade CBR from different in-situ tests

The subgrade CBR values estimated from D_{900} recorded in FWD test clearly shows that FWD overestimates the subgrade CBR. This result agrees with the study conducted by Chai et al. 2013, who has used the TMR model to estimate subgrade CBR from FWD tests and verified with DCP test results. The influence zone of the FWD impact load is around 1.5 times the diameter of the loading plate. Hence, the deflections at D_{200} ,

D_{300} and D_{450} show clear variation as D_0 increases. However, the similar behaviour is not observed in the deflections at D_{600} D_{900} D_{1200} and D_{1500} and usually, the recorded deflections are smaller in D_{900} . One possible reason for such phenomenon is the nonlinear behavior of subgrade. Hence, studies have suggested performing deflection corrections to D_{900} to account the nonlinearity of the subgrade to eliminate over prediction of CBR.

5 Conclusion

The subgrade is the base platform that provides the structural support for pavement layers constructed above to withstand the traffic loads during the design life. Failure of the subgrade will trigger pavement distresses. Therefore, accurate subgrade assessment is required during both the design and construction stage. This paper compared the bearing capacity of a selected pavement stretch obtained from different in-situ test methods. The findings of the comparison are summarized as follows:

- It is observed that Dynamic Cone Penetration Test (DCP) shows a closer estimation of subgrade CBR to the laboratory measured CBR.
- Both Variable Energy Dynamic Cone Penetrometer (PANDA®) and Light Weight Deflectometer (LWD) overestimated the subgrade CBR value. However, the trend along the experimental stretch is similar to the trend of the DCP test.
- Falling Weight Deflectometer (FWD) test overestimates the subgrade CBR due to its limitations, and this could be eliminated by correcting D_{900} to account subgrade nonlinearity

As all tests follow the same trend of variation along the experimental stretch, it would be possible to utilize all of the investigated in-situ tests for subgrade assessment by conducting laboratory CBR test for randomly selected locations in order to develop correlations and verification.

Acknowledgement. The authors would like to acknowledge the financial and technical support from Queensland Department of Transport and Main Roads and Australian Road Research Board. A special thank goes to the Logan City Council, Australia for providing an experimental section for the project and perform all civil engineering constructions to complete this real scale field trial successfully.

References

- Austrroads. Guide to Pavement Technology Part 2: Pavement Structural Design: Austrroads (2018)
- Chai, G.W., Argadiba, S., Stephenson, G., Condric, I., Oh, E.Y., Sittam, P.: Prediction of subgrade CBR using FWD for thin bituminous pavements. *Int. J. Pavement Res. Manoharan Technol.* **6**(4), 280 (2013)
- Gallage, C., Eom, T., Barker, D., Ramanujam, J.: Falling weight deflectometer (FWD) tests on granular pavement reinforced with geogrids—case study. In: *Proceedings of the International Conference on Geotechnical Engineering (ICGE—Colombo-2015): Geotechnics for Sustainable Development*, edited, pp. 597–600 (2015)

- Langton, D.D.: The Panda lightweight penetrometer for soil investigation and monitoring material compaction. *Ground Eng.* **32**, 33–37 (1999)
- Lee, J.S., Kim, S.Y., Hong, W.-T., Byun, Y.H.: Assessing subgrade strength using an instrumented dynamic cone penetrometer. *Soils Byun Found.* **59**(4), 930–941 (2019)
- Marecos, V., Solla, M., Fontul, S., Antunes, V.: Assessing the pavement subgrade by combining different non-destructive methods. *Constr. Build. Mater.* **135**, 76–85 (2017)
- McHenry, M.T., Rose, J.G.: *Railroad subgrade support and performance indicators: a review of available laboratory and in-situ testing methods* (2012)
- Mittal, A., Shukla, S.: Effect of geosynthetic reinforcement on strength behaviour of weak subgrade soil. *Mater. Sci. Forum.* **969**, 225–230. *Trans Tech Publ.* (2019)
- Puppala, A.J.: *Estimating stiffness of subgrade and unbound materials for pavement design*, vol. 382. *Transportation Research Board* (2008)
- Salgado, R., Yoon, S.: *Dynamic cone penetration test for subgrade assessment*. FHWA/IN/JTRP-/30, *Purdue Univ., West Lafayette, IN* (2003)
- Scala, A.J.: Simple methods of flexible pavement design using cone penetrometers. *J. N. Z. Eng.* **11**(2), 34 (1956)
- Transport, Department of and Main Roads. *Pavement rehabilitation manual: Technical Reference Centre, Engineering and Technology Division Brisbane* (2020)
- Wimalasena, K., Jayalath, C.P.G.: Effect of Geogrid Reinforcement in Weak Subgrades. *Int. J. Geomate* **18**(65), 140–146 (2020)



Investigation of the Effect of Compaction Density on the Deformation Characteristics of Type 2.3 Granular Material

C. P. G. Jayalath^(✉) and Chaminda Gallage

School of Civil and Environmental Engineering, Queensland University of Technology,
Brisbane, Australia

Abstract. Type 2.3 granular material is widely used as an unbound pavement material in Queensland, Australia. The mechanical properties such as the permanent and resilient response of this unbound granular material (UGM) under cyclic loading are required in pavement design. Thus, accurate evaluation of these properties through laboratory testing is a prime concern of pavement engineers. These properties are greatly affected by the relative compaction of the material. Therefore, this study was conducted to investigate the effect of relative compaction on the resilient and permanent deformation behaviour of Type 2.3 UGM. A series of Reported Load Triaxial (RLT) tests were performed on the selected UGM by varying the relative density while maintaining the moisture content and stresses constant for all tested specimens. The results of this study indicate that the maximum permanent strain is reduced when the relative density is increased. However, the resilient modulus is approximately constant up to 95% relative compaction but increases when the density is further increased.

1 Introduction

Properties of pavement materials perform a key role in pavement designs as the designed thicknesses of each layer largely depend on these parameters. Therefore, an in-depth understanding of the resilient and permanent deformation behaviour of base materials under different influential factors is vital to characterise the properties of this pavement material (Jayakody Arachchige 2014; Jayakody et al. 2019; Jayakody et al. 2013). It is well known that limiting the development of rut depth in the pavement structure is one of the main aspects of designing flexible road pavements. However, predicting the rut development is complex even though measuring the rut depth is generally considered an easy task (Lekarp et al. 2000a). In addition, while the characterisation of the pavement materials is challenging, assessing the impact of the environmental conditions and calculating the appropriate stress distribution during the entire service life of a pavement are also extremely difficult.

Any pavement design procedure based on the elastic-layer theory requires an evaluation of the elastic properties of all materials in the pavement section. The elastic properties of materials are traditionally defined by the theory of elasticity using the modulus of elasticity (E) and Poisson's ratio (ν). However, UGMs subjected to repeated loading are

described referring to their resilient modulus (M_R) to explain the stress-dependency of elastic (recoverable) behaviour of these materials (Araya 2011; Sadrossadat et al. 2016). The resilient modulus is defined as the ratio of the dynamic deviator stress to the resilient strain at a specific load cycle.

It is well known that UGMs are not exactly elastic. These materials exhibit the elastoplastic behaviour, hence some non-recoverable deformation is experienced after each load application. Under repeated loading conditions, these pavement materials undergo recoverable and non-recoverable components of the deformation (Brown 1996). Figure 1 illustrates the permanent and recoverable components of deformation for a single load cycle. The recoverable component is known as the resilient deformation, whereas the non-recoverable component is referred to as permanent deformation. Plastic strains were calculated with the measurements of plastic deformation while the resilient deformation was used to calculate the M_R of the materials, as shown in Eq. 1.

$$\text{Resilient modulus} = \frac{\text{Deviator stress}}{\text{Resilient strain}} \quad (\text{Eq. (1)})$$

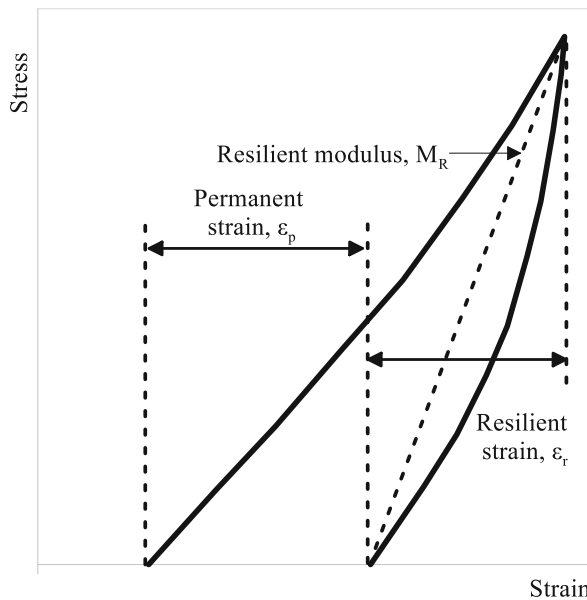


Fig. 1. Strains in pavement materials during one load cycle (Adapted from Brown (1996))

The repeated load triaxial (RLT) test is widely used to evaluate the M_R and permanent deformation of pavement materials. The RLT test can be used to measure the aforementioned characteristics under different vertical and confining stress conditions (Cong et al. 2019; Ghorbani et al. 2020; Jameson et al. 2010; Jayakody et al. 2019; Li et al. 2020). The outcomes of this test facilitate the calculation of the M_R and plastic strain of materials under repeated loading, simulating the tyre pressure.

It has been known for many years that granular materials become stiffer and stronger, significantly altering their response to static loading, as the compacted density increases. However, the findings of previous studies regarding the impact of density on the permanent and resilient response of granular materials are ambiguous to some extent. Mishra and Patel (2019) point out that the plastic strain is irreversibly proportional to the compacted density of UGMs. In addition, the outcomes of several studies prove that the increasing density causes an increased M_R (Hicks 1970; Kolisoja 1997; Rada and Witczak 1981; Robinson 1974). Increased density due to the additional compaction of the granular specimens is accountable for a great increment of the number of particle contacts per particle. Consequently, the average contact stress corresponding to a certain external load is decreased. Thus, the deformation in particle contacts decreases and the M_R increases (Kolisoja 1997). In contrast, Thom and Brown (1988) and Brown and Selig (1991) have highlighted that there is a relatively insignificant effect of the state of compaction on the resilient behaviour of tested granular materials. Hicks and Monismith (1971) stated that compared to fully crushed aggregates, partially crushed aggregates were greatly affected by the compacted density. The M_R has been reported to remain almost unchanged when the aggregate is fully crushed, whereas the M_R increases with the increasing DoC for the partially crushed aggregate. In addition, past studies suggest that the particle size distribution, or grading, of granular materials seems to have some influence on material stiffness, therefore on both permanent and resilient deformation characteristics. However, they are generally considered to be of minor significance for crushed rocks (Lekarp et al. 2000b). It is apparent that the magnitude of the influence of DoC on both resilient and permanent deformation behaviours greatly depend on the type of granular material that has been tested. Therefore, the in-depth knowledge on the variation of these behaviours with the deviation of the density of each type of base material is essential, especially to obtain the precise design parameters for numerical modelling and pavement design. Generally, the most widely used approach by pavement engineers and researchers to estimate the M_R of unbound granular materials is the correlation with California Bearing Ratio (CBR) (El-Ashwah et al. 2020). This is also the case in Australia as recommended by Austroads pavement design guide (Austroads 2019). However, CBR is technically an empirical strength property while M_R is a mechanistic measure (Alnedawi et al. 2019). There is also little known about the mechanical properties of the base and subbase layers particularly the local Type 2.3 granular material. This confirms it is more practical to characterise the granular materials under repeated loads based on their mechanical responses. Therefore, the RLT testing was performed in the present study to investigate the influence of the compacted dry density on the resilient and permanent deformation behaviour of Type 2.3 granular material.

2 Materials

The UGM used in this study has been classified as Type 2.3 granular materials based on 'Transport and Main Roads Specifications MRTS05-Unbound Pavements'. The particle size distribution of Type 2.3 UGM measured in the laboratory complied with the gradation requirement specified in the specification, as illustrated in Fig. 2(a). According to the standard Proctor compaction test, the Maximum Dry Density (MDD) and Optimum

Moisture Content (OMC) of granular material are 2.21 g/cm^3 and 7.5% respectively, as shown in Fig. 2(b). The specific gravity of this UGM is 2.69.

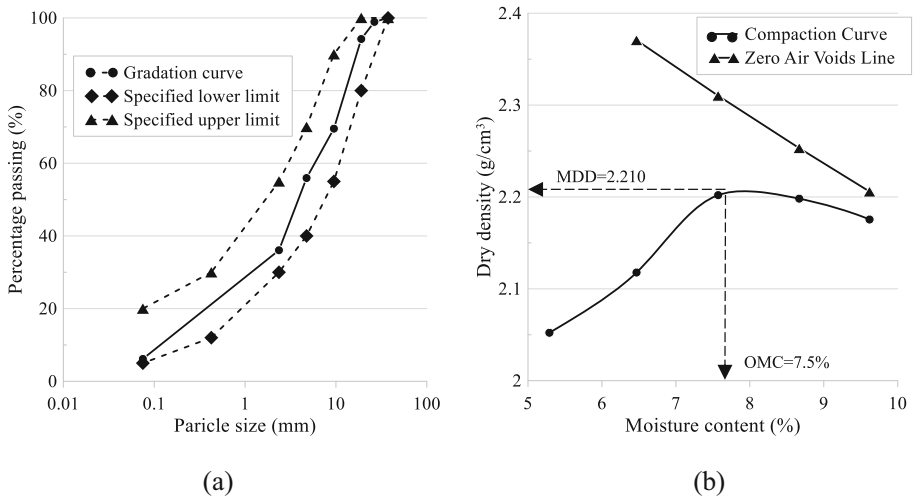


Fig. 2. Basic classification of base material (a) Particle size distribution (b) Compaction curve

3 Methodology

Firstly, UGMs were oven-dried at 60°C . Next, the dried materials were mixed with the moisture to obtain the required moisture content of $5.5\% \pm 0.5\%$ for each test condition and stored in air-tight plastic containers to cure for more than one day to equalise the moisture content. The test specimens with a 100 mm diameter and 200 mm height were prepared with four equal layers using the wet tamping method. The compacted dry density of material was varied to achieve three different Degree of Compaction (DoC) values, namely, 91%, 95%, 100% of MDD under the standard compaction. In the preparation of the test specimens, the required amount of wet materials to achieve the required dry density when compacted to the target thickness of 50 mm in each lift was measured and placed. After that, the material was manually compacted to the target thickness of 50mm using a standard rammer applying the blows evenly throughout the surface of the specimen. The testing was performed under deviator stress of 550 kPa to replicate the tyre contact pressure (equal to a single wheel load of 40 kN, which is half of an axle load of 80 kN). Confining stress of 125 kPa was selected as specified in the ‘Test Method Q137: Permanent Deformation and Resilient Modulus of Unbound Material’ of the Materials Testing Manual of the Department of Transport and Main Roads (TMR), Queensland, Australia. It is vital to mention that the moisture content and stress conditions were selected to replicate similar base conditions used in pavement model tests that have been conducted under the first author’s postgraduate studies. The compaction density values were chosen in order to provide the representative design parameters

required for the precise numerical modelling of the above-mentioned pavement models. Details of the UGM samples and the testing conditions used in the RLT testing are summarised in Table 1. The repeatability of the results for the test specimens was verified by conducting three identical tests for each test condition.

Table 1. Details of UGM samples used in the RLT testing

Sample number	Achieved moisture content (%)	Achieved dry density (g/cm^3)	Achieved DoC (%)
1	5.5	2.018	91
2	5.3	2.093	95
3	5.5	2.188	100

As recommended in the ‘Test Method Q137 of Materials Testing Manual of TMR, single-stage RLT tests were carried out using servo-controlled pneumatic equipment (See Fig. 3) with a 6 kN. The control data acquisition system captured the data, and the software saved the data to further process the test results. After the sample preparation was completed, the cylindrical specimen was mounted on the triaxial base and sealed at the top and the bottom by enclosing a latex membrane. Air was used to facilitate the confinement. The attached pressure transducer continuously measured the confining pressure in the cell. Repetitive passages of vehicle wheels over the materials were simulated by applying the repeated axial load on top of the compacted specimens. Trapezoidal-shaped load pulses (see Fig. 4) were exerted with a period of 3 s (i.e., frequency of 0.33 Hz), as specified in the TMR standard. A magnitude of 5% of deviator stress was applied as the contact stress at the end of each load cycle. Testing was carried out up to 10,000 loading cycles or 5% of permanent axial strain, whichever occurred first. For each loading pulse,

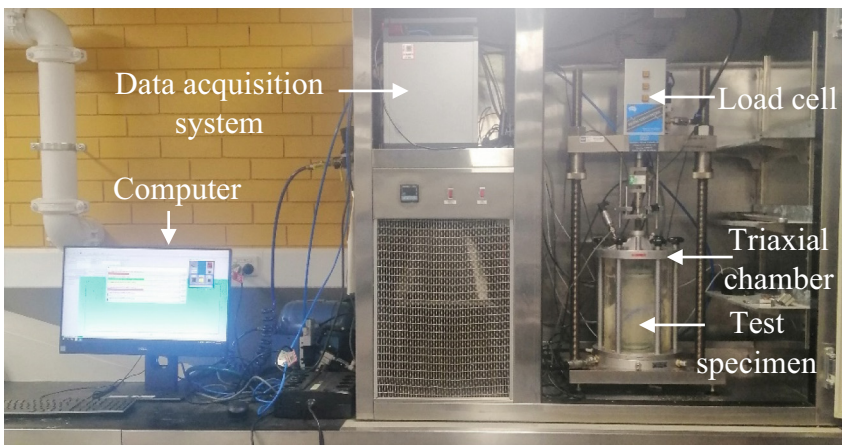


Fig. 3. RLT test apparatus

the resulting permanent strain and resilient strain were continuously read by two Linear variable differential transducers (LVDTs).

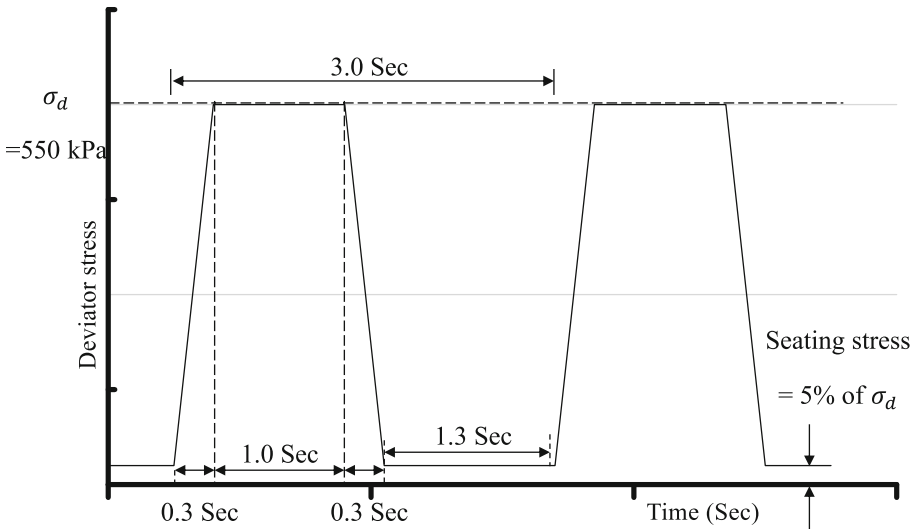


Fig. 4. Illustration of the repeated load waveform of RLT test

4 Results and Discussion

4.1 Resilient Behaviour of Base Material

Figure 5 compares the variation of M_R with the number of load cycles under three different DoC conditions of the base material with an approximate moisture content of 5.5%. The test specimen with 91% DoC reached the failure criteria of 5% plastic strain after being loaded for 2000 cycles. However, as the variation of M_R with load cycles for a selected test was negligible (i.e., M_R remains approximately equal), the M_R values up to 10,000 cycles were assumed/predicted to remain constant. Higher M_R values were obtained when the DoC was 100%, whereas lower values were recorded for DoC of 91%. As shown in Fig. 5, the M_R values of 262 MPa, 263 MPa and 293 MPa were calculated after 10,000 loading cycles for the DoC of 91%, 95% and 100% respectively. The test results shown in Fig. 6 suggest that there is no significant difference between the M_R values for the 91% and 95% of DoC. Thus, it can be concluded that the influence of DoC on the M_R is negligible for the DoC in between 91% and 95%. However, the M_R increases when the DoC of the test specimen increases beyond 95% of DoC. The general variation of the M_R versus the compacted density agrees with the M_R behaviours of typical quality crushed rocks that have been specified in Fig. 6 of the ‘Austroads Guide to Pavement Technology Part 2: Pavement Structural Design’, even though magnitudes of the obtained M_R values are slightly different to the specified values.

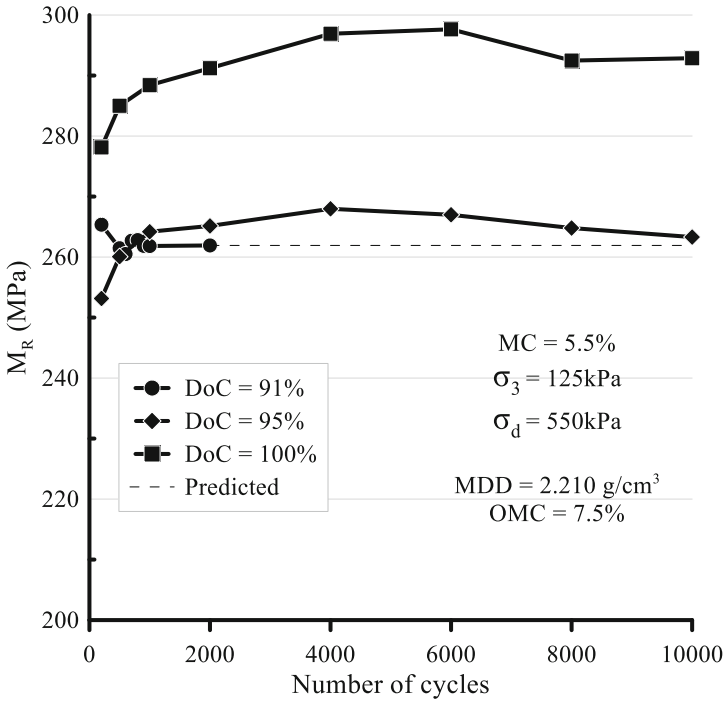


Fig. 5. Resilient behaviour of the base material at three different DoC values

4.2 Permanent Deformation Behaviour of Base Material

Figure 7 depicts the development of the accumulated plastic strain with the number of load cycles under three different DoC values. For the DoC of 91%, the plastic strain accumulated rapidly until it exceeded the 5% plastic strain just after reaching the 2000th cycle, recording higher permanent strains compared to the values obtained for the remaining two DoC conditions. The test results suggest that the accumulation of plastic strain reduces when the relative compaction of the base material is increased. The lowest plastic strain accumulation, which reached 1.18% after 10,000 cycles, was observed when the DoC of the test specimen was 100%. The plastic strain accumulated after 10,000 cycles for the 95% DoC is 3.19%, therefore 170% more permanent-vertical strain was observed when the base material was compacted to 95% instead of 100% of maximum compacted density.

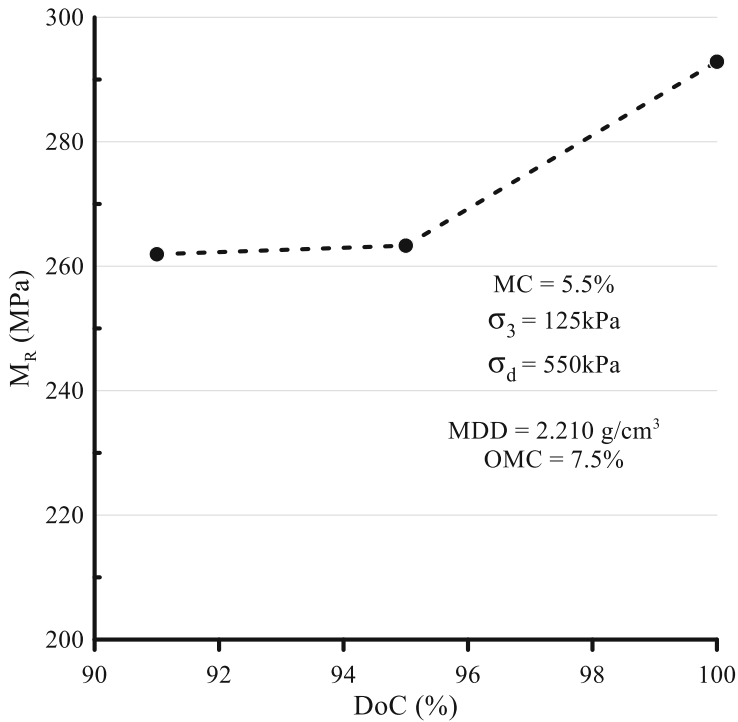


Fig. 6. Variation of M_R with the DoC after 10,000 cycles

Effects of compacted density on different UGMs has been considered in previous experimental studies. Barksdale (1972) stated that an average of 185% more plastic strain was observed when the relative compaction of granular materials was reduced from 100% to 95%. Allen (1973) also reported a 22% reduction in total plastic strain in gravel and an 80% reduction in a crushed limestone when the specimen density was increased from the standard Proctor to modified Proctor density. It can be concluded that the permanent deformation behaviour of granular base materials largely depends on the DoC of the material. However, the magnitude of reduction of plastic strain with the increasing DoC of material depends on the type of material, thus should be estimated separately for each type of material.

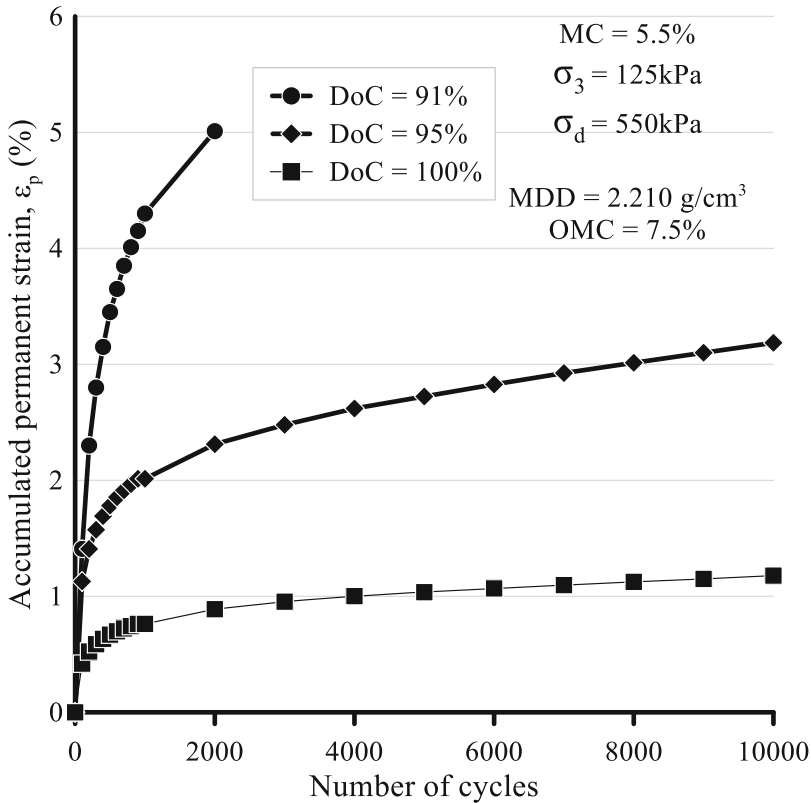


Fig. 7. Permanent deformation behaviour of the base material at three different DoC values

5 Conclusion

The effects of DoC on the permanent and resilient-deformation behaviour of base material were investigated through RLT testing by varying the relative density as 91%, 95% and 100%. The test results have revealed that the accumulation of plastic strain reduces when the DoC of the base material increases. A significant difference between the M_R values for the 91% and 95% of DoC could not be observed. Therefore, it can be concluded that the influence of DoC on the M_R is negligible when the achieved DoC value lies between 91% and 95%. However, beyond the 95% of DoC, the M_R increases with the increasing relative compaction.

References

Allen, J.J.: The effects of non-constant lateral pressure on the resilient response of granular materials. University of Illinois at Urbana-Champaign (1973)
 Alnedawi, A., Nepal, K.P., Al-Ameri, R.: New shakedown criterion and permanent deformation properties of unbound granular materials. *J. Mod. Transp.* **27**(2), 108–119 (2019). <https://doi.org/10.1007/s40534-019-0185-2>

- Araya, A.A.: Characterization of Unbound Granular Materials for Pavements (Ph.D. Thesis). University of Technology, Delft (2011)
- Austrroads: Austrroads Guide to Pavement Technology Part 2: Pavement Structural Design. Austrroads Inc., Sydney, Australia (2019)
- Barksdale, R.D.: Laboratory evaluation of rutting in base course materials. Presented at the 3rd International Conference on the Structural Design of Asphalt Pavements, Grosvenor House, Park Lane, London, England, 11–15 September 1972, vol. 1 (1972)
- Brown, S.: Soil mechanics in pavement engineering. *Geotechnique* **46**(3), 383–426 (1996)
- Brown, S., Selig, E.: The design of pavement and rail track foundations. In: *Cyclic Loading of Soils: from Theory to Design*, pp. 249–305 (1991)
- Cong, L., Wang, Q., Xiong, C.: Laboratory determination on stresses of resilient modulus of subgrade for flexible pavement within repeated loading triaxial test. In: *DEStech Transactions on Environment, Energy and Earth Sciences (EECE)* (2019)
- El-Ashwah, A.S., Mousa, E., El-Badawy, S.M., Abo-Hashema, M.A.: Advanced characterization of unbound granular materials for pavement structural design in Egypt. *Int. J. Pavement Eng.*, 1–13 (2020)
- Ghorbani, B., Arulrajah, A., Narsilio, G., Horpibulsuk, S., Bo, M.W.: Development of genetic-based models for predicting the resilient modulus of cohesive pavement subgrade soils. *Soils Found.* **60**(2), 398–412 (2020). <https://doi.org/10.1016/j.sandf.2020.02.010>
- Hicks, R.G.: Factors influencing the resilient response of granular materials (Ph.D. Thesis). University of California, Berkeley, California (1970)
- Hicks, R.G., Monismith, C.L.: Factors influencing the resilient response of granular materials. *Highway Res. Rec.* **345**, 15–31 (1971)
- Jameson, G., Vuong, B., Moffatt, M., Martin, A., Lourensz, S.: Assessment of rut-resistance of granular bases using the repeated load triaxial test (2010)
- Arachchige, J., Pradeep, S.: Investigation on characteristics and performance of recycled concrete aggregates as granular materials for unbound pavements (Ph.D.) (2014)
- Jayakody, S., Gallage, C., Ramanujam, J.: Performance characteristics of recycled concrete aggregate as an unbound pavement material. *Heliyon* **5**(9), e02494 (2019)
- Jayakody, S., Gallage, C., Ramanujam, J., Kumar, A.: Laboratory study on the performance of recycled concrete aggregates blended with reclaimed asphalt pavement as pavement granular material. In: *Proceedings of the 3rd International Conference-Geomate 2013 Geotechnique, Construction, Materials and Environment*, vol. 3, pp. 389–393. The Geomate International Society (2013)
- Kolisoja, P.: Resilient Deformation Characteristics of Granular Materials. Tampere University of Technology, Finland (1997)
- Lekarp, F., Isacsson, U., Dawson, A.: State of the Art. II: permanent strain response of unbound aggregates. *J. Transp. Eng.* **126**(1), 76–83 (2000a). [https://doi.org/10.1061/\(ASCE\)0733-947X\(2000\)126:1\(76\)](https://doi.org/10.1061/(ASCE)0733-947X(2000)126:1(76))
- Lekarp, F., Isacsson, U., Dawson, A.: State of the Art. I: resilient response of unbound aggregates. *J. Transp. Eng.* **126**(1), 66–75 (2000b). [https://doi.org/10.1061/\(ASCE\)0733-947X\(2000\)126:1\(66\)](https://doi.org/10.1061/(ASCE)0733-947X(2000)126:1(66))
- Li, N., Ma, B., Wang, H., Sun, W.: Development of elasto-plastic constitutive model for unbound granular materials under repeated loads. *Transp. Geotech.* **23**, 100347 (2020). <https://doi.org/10.1016/j.trgeo.2020.100347>
- Mishra, A., Patel, D.: Analysis of structural deformation in flexible pavement using KENLAYER programme. *Int. Res. J. Eng. Technol.* **6**, 1168–1173 (2019)
- Q137: Permanent Deformation and Resilient Modulus of Unbound Material. Department of Transport and Main Roads, Queensland (2020)
- Rada, G., Witczak, M.W.: Comprehensive evaluation of laboratory resilient moduli results for granular material (1981)

- Robinson, R.: Measurement of the elastic properties of granular materials using a resonance method (1974)
- Sadrossadat, E., Heidaripناه, A., Osouli, S.: Prediction of the resilient modulus of flexible pavement subgrade soils using adaptive neuro-fuzzy inference systems. *Constr. Build. Mater.* **123**, 235–247 (2016). <https://doi.org/10.1016/j.conbuildmat.2016.07.008>
- Thom, N., Brown, S.: The effect of grading and density on the mechanical properties of a crushed dolomitic limestone. In: 1988 14th Conference on Australian Road Research Board (ARRB), Canberra, vol. 14 (1988)
- Transport and Main Roads Technical Specification-MRTS05 Unbound Pavements. Transport and Main Roads (2020)



Investigation on the Performance of Railway Ballast Track Stabilized by Cement Asphalt Mortar

Tri Ho Minh Le¹, Seong-Hyeok Lee², Dae-Wook Park¹ (✉), and Jung-Woo Seo¹

¹ Department of Civil and Environmental Engineering, Kunsan National University, Gunsan, Korea

dpark@kunsan.ac.kr

² Korea Railway Research Institute, Gyeonggi-do, Korea

Abstract. Under tremendous transportation services, the exhausted track irregularities and ballast deterioration lead to the vast increment in railway track-bed maintenance costs annually. This research aims to develop new material to reinforce the performance of high-speed railway track-bed. The unique characteristic of this cement asphalt mortar (CAM) mixture is to incorporate the flexibility of bitumen and the strong resilient modulus of cement hydration products. From different cement (C) and asphalt emulsion (AE) ratios, the dynamic modulus, and indirect tension tests are conducted to investigate the engineering properties of CAM mixtures at hardened stages. The scanning electron microscope (SEM) analysis is employed to determine the micro connection between asphalt membrane and the hydrated cement particles. Then, the actual dynamic response of CAM is verified through a full-scale testbed application. From the test results, it is found that the AE/C ratio imposes a substantial effect on the characteristic of CAM. The usage of high cement content not only leads to the stronger dynamic stiffness but also contributes to the lower temperature and frequency dependence of CAM mixtures. Meanwhile, the viscous-elastic behavior of CAM is prominent when using high AE levels. Overall, the laboratory and full-scale tests results suggest that the connection between CAM and ballast particles can substantially enhance the durability of railway structure, indicating a better operation of high-speed railway and stronger track foundation for sustainability development purposes.

Keywords: Railway · Track · Ballast · Cement asphalt mortar · Dynamic modulus · Full-scale · Testbed

1 Introduction

In recent years, the ballasted track structure is widely used in many countries due to its low construction cost and high performance in rutting resistance [1]. However, reports concern the great deterioration of the ballast structure due to the continuous loads from high-speed trains and environmental impacts [2, 3, 4]. Hence, many strategies have been proposed to resolve this issue. Especially, the use of cement asphalt mortar (CAM) as an

interlayer between track slab and concrete roadbed has been applied in many developed countries such as Japan, and Germany [3]. Ouyang et al. [5] states that the combined merits from both cement and asphalt in this technique will provide the riding smoothness for a high-speed train and damping ability for stress relaxation in the railway structure. However, these methods must be applied at the initial construction stage with the high-cost requirement. Hence, the need to find a feasible stabilizing solution is of importance [3].

Therefore, based on this concept, this study aims to utilize CAM in stabilizing fouled ballast [4]. The contribution of CAM as a bonding material between fouled ballast particles is expected to promote strong rutting resistance and enhance the elasticity behavior for the railway structure. In this method, high flowability CAM mixture is poured directly on top of the fouled ballast. The self-leveling of the material allows it to flow through the whole ballast structure. With the fast setting time, the maintenance project can be done at a short time for traffic reopening which adapts the strict requirement from railway maintenance projects [4, 6]. The components of CAM can also be easily provided by local company such as asphalt emulsion (AE), cement (C), water (W), and superplasticizer (SP). Therefore, it is practical to apply this technique as a sustainable solution for ballast maintenance. Prior works on the CAM stabilized ballast shows that a high AE/C ratio leads to an increase in ductility behavior of CAM mixture which improves the stress dissipation for the whole railway structure [4, 5, 6]. The damping ability from the viscoelastic characteristic of asphalt membrane can also be promoted by using the technique. However, a high AE/C ratio may lead to a remarkable drop in strength. Hence, the proper use of asphalt emulsion should be greatly considered. Therefore, the main aim of this study is to evaluate the effect of different AE/C ratio on the mechanical properties of CAM, especially the dynamic modulus and cracking resistance. To achieve this target, three AE/C ratios are used in this research including 100%, 125%, and 150% by weight of cement. The dynamic characteristic of varied mix conditions is evaluated by conducting the dynamic modulus test, meanwhile, the durability of the CAM mixture are investigated by performing the indirect tensile strength test at 28 days. Then, the microstructure of different conditions is analyzed from the SEM test. The optimized mixture is then applied in the full-scale testbed to evaluate its performance in actual application compared to the untreated ballast.

2 Materials and Methods

2.1 Materials

The Portland cement Type II is used in this study. The properties of asphalt emulsion provide by Korean chemical company are presented in Table 1. The construction sand (S) is employed in this test with a specific gravity of 2.65 g/cm^3 . Based on the suggestion from prior works [4, 5, 6], the proper use of quick-hardening admixture (QA) will increase the strength gain at an early age. Hence, this admixture is included in the mix design with a ratio of 14% by weight of cement. It is well known that adding superplasticizer (SP) will improve the workability of the cement mortar and lower the use of mixing water. In this study, the SP will be used at 2% by weight of water to improve the rheology of CAM mixture. The mix design used in this research is summarized in Table 2. The mixing

effectiveness depends mainly on the initial mixing water with the dry components. The prior works [4, 5, 6] suggest that dry components (C, QT, S) should be mixed with water first for 2 min at a rotation rate of 120 rpm, then, an asphalt emulsion is added to this combination, and the whole mixture is mixed for an additional 1 min at a rate of 60 rpm. This mixing method aims to ensure the stable condition of asphalt droplets in asphalt emulsion. The water will help lower the adsorption energy of cement particles to the asphalt droplets in the asphalt emulsion and thereby prolong the demulsification process of asphalt emulsion.

Table 1. Properties of anionic asphalt emulsion [7]

Density (g/cm ³)	Storage stability 1 day (%)	Residue after distillation (%)	Residue on 1.18 mm sieve (%)	Penetration depth at 25° (0.1 mm)	Solid content (%)
1.02	0.3	50	0.01	70	50

Table 2. Mix design (by weight of cement)

No.	Cement	QT	Asphalt emulsion	Emulsifier	Sand	Water	Superplasticizer
100	100%	14%	100%	Non polymer	50%	25%	2%
125	100%	14%	125%	Non polymer	50%	20%	2%
150	100%	14%	150%	Non polymer	50%	15%	2%

2.2 Testing Methods

2.2.1 Dynamic Modulus Test

In this study, the DTS-30 device was used to measure the dynamic behavior of CAM mixture following the AASHTO TP 342-11 [8]. The DTS-30 is the 30 kN servo-hydraulic dynamic testing system. The DTS-30 can be operated in tension, compression dynamic loading and is suited to testing a diverse range of materials such as asphalt, soil, unbound granular materials. After the mixing process, the fresh samples were cast into a mold having 150 mm in height and 100 mm in diameter (Fig. 1a). The samples were cured in the laboratory conditions at 21 °C for two days before conducting the test. Based on the guidance, five temperatures (e.g., -10, 4, 21, 37, and 50 °C) were respectively selected to cure the samples for 3 h. From each temperature range, the CAM mixture was subjected to sinusoidal axial compressive stress having 6 frequency levels (e.g., 25, 10, 5, 1, 0.5, and 0.1 Hz). The dynamic modulus ($IE^* I$) result of 1 condition is calculated based on the average value of three replicates.

2.2.2 Indirect Tensile Strength Test

The cracking resistance property of CAM is investigated by conducting the IDEAL-CT test [9]. The cylindrical IDT samples (150 mm in diameter and 62 mm in height) are subjected to the equivalent curing conditions as mentioned above. Before performing the test, the samples were cured in the chamber at 25 °C for two hours. The DTS-30 machine was employed to apply a vertical force across the specimen's diameter with a loading rate of around 50 mm/min. As suggestions by Fujie et al. research [9], the cracking tolerance index (CT index) is computed by using stress-strain data in the IDT test (Eq. 2) and this factor is very prominent to evaluate the crack performance of asphalt mixture. The author mentions that a mixture obtaining higher CT will show a better cracking resistance.

$$CT_{Index} = \frac{G_f}{|m_{75}|} \times \left(\frac{l_{75}}{D} \right) \quad (1)$$

Where,

$$m_{75} = \left| \frac{P_{85} - P_{65}}{l_{85} - l_{65}} \right|, \text{ slope at 75\% Post peak load point (PPL)}$$

G_f (J/mm²), fracture energy

l_{65}, l_{75}, l_{85} (mm), displacement at 65%, 75%, 85% PPL

P_{65}, P_{75}, P_{85} (N), displacement at 65%, 75%, 85% PPL

D (mm), diameter of specimen

2.2.3 Scanning Electron Microscope (SEM)

The SEM analysis test is conducted to investigate the microstructure organization of CAM mixture. It is expected that CAM mixture with sand will exhibit a dense structure which promotes a strong pressure bearing ability for the whole structure. The SEM test is conducted by using Hitachi FE-SEM S-4700 under a high vacuum condition (Fig. 1b). As stated before, three replicates of each condition will be scanned, and the proper image will be selected to analyze.

2.2.4 Full-Scale Testbed

In this study, the fouled ballast was used for both controlled and stabilized sections to evaluate the actual maintenance efficiency. The ballast layer was also compacted by using a vibration device to achieve the initial stability. Regards to the size of the testbed developed in this study, the two track-bed options share the same dimension of 4 m in width, 6 m in length, and 0.3 m in depth. Regards to the application process of stabilized ballast, the optimized mixture with 125%AE was used in this test. The previous works on CAM suggest the wet-mixing method for the full-scale test-bed application. In the mixing process, cement, quick-hardening admixture, and sand were first mixed together with the combination of superplasticizer (2% by weight of cement) and water for around 2 min and a shearing rate of 120 rpm. The asphalt emulsion was then added to the slurry, and the mixture was stirred at the same rate for an additional 1 min. These mixing steps will ensure the homogenous distribution of asphalt emulsion and eliminate the coalescence phenomenon. The prepared fresh mixture was then directly poured onto the

ballast surface, thanks to the high flowability of CAM (Fig. 1c). Regards to the proper volume of CAM for stabilizing ballast, the laboratory trial experiments suggest a CAM content of 7.5% ballast volume to ensure a homogenous coating of CAM on the ballast. This volume will ensure a sufficient flow of CAM through 30 cm of the ballast layer. Due to the ideal workability of cement asphalt mortar of around 30 min, the production of 1 m³ of cement asphalt mortar is suggested for each batch. This content may be varied from the requirements of each projects. The CAM stabilized zone was cured for 1 day before conducting the test. Along with the sleeper, rail and ballast layer, the instrument systems (e.g., LVDT, pressure gauges) were installed to record the roadbed pressure and track displacement (Fig. 1b). Then, the controlled and CAM stabilized track-beds are subjected to the repeated 400,000 sinusoidal dynamic loads of 1 Hz. Based on the KRL-2012 standard trainload [10], the passenger and cargo train having a speed of 140 km/h will impose a maximum dynamic load of around 165 kN. Based on preliminary research and the author's team experience, this is a critical central force that can properly be applied in the full-scale testbed. Hence, a sinusoidal wave load of 95 kN \pm 70 kN was applied in this study to investigate the dynamic performance of the stabilized method [10].



Fig. 1. Dynamic modulus test (a), full-scale testbed application (b), and CAM section (c).

3 Results and Discussions

3.1 Laboratory Experiments

3.1.1 Dynamic Modulus

The dynamic modulus test results are shown in Figs. 2 and 3. As regards the first, the temperature plays a very strong role in the dynamic modulus of CAM mixture. The higher the dynamic modulus, the lower the cured temperature. The cement asphalt mortar mixture behaves as an asphalt concrete mixture since asphalt binder is prone to the heat. Under high temperature, the dynamic modulus of higher asphalt emulsion mixtures (150AE) reduced noticeably from nearly 7000 MPa to around 1500 MPa. Meanwhile, the mixture having small asphalt emulsion content still maintain the value of around 7000 MPa. It may be attributed to the higher volume of cement hydration products established in the lower AE mixture. The cement hydration product is less sensitive to heat impact compared to the viscosity characteristic of asphalt emulsion. This finding

is also verified through the log dynamic modulus and frequency relationship shown in Fig. 3. For example, the 100AE mixture achieves the log dynamic modulus ranging from 3.4 to 4.3 while this value of mixture with 150 AE is varied from 2.3 to 3.8. The test results suggest that temperature is a critical factor in the applicability of cement asphalt mortar in the railway maintenance project.

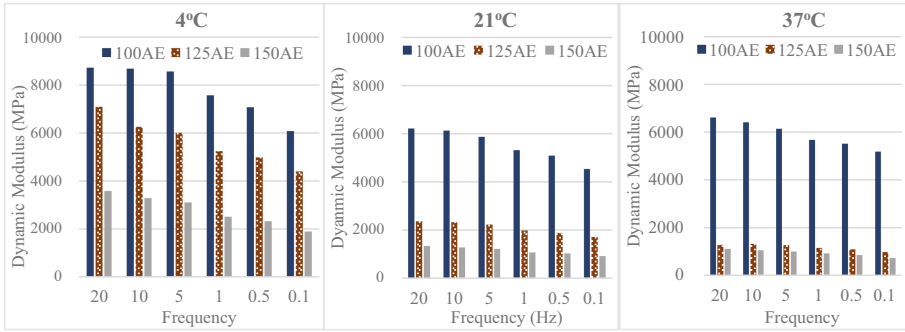


Fig. 2. Dynamic modulus test results (Dynamic modulus vs Frequency)

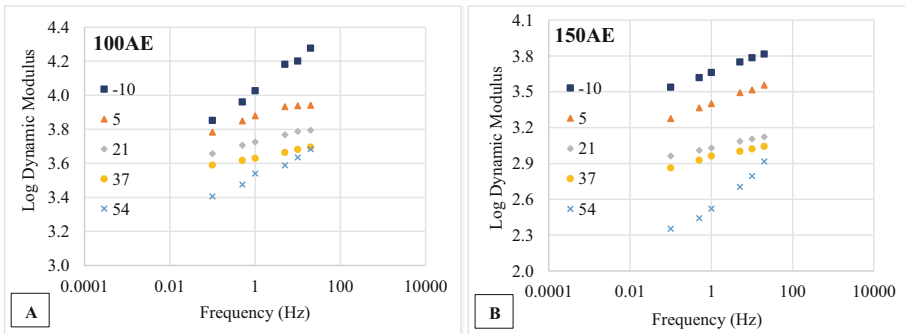


Fig. 3. Dynamic modulus test results (Log dynamic modulus vs Frequency)

3.1.2 CT Index Test

The IDT test result and the cracking index property of CAM mixtures are presented in Fig. 4 and Table 3, respectively. Among three types of AE conditions, the 100AE mixture obtains the highest IDT load of around 8kN. It may be due to the contribution of high cement hydration products. However, this mixture showed a sudden brittle failure phenomenon after reaching peak stress. Meanwhile, although mix 150AE achieve the lowest peak IDT load of around 2.5 kN, it showed very ductile behavior, indicating the visco-elastic behavior of the asphalt emulsion component. By conducting proper design and modification, this characteristic may contribute to the damping ability and smoothness of track users, promoting a better train operation. The test results also reveal

that the cracking index of mix 150AE has the highest value. This result can be explained by the high fracture energy and low m75 slope of mix 150AE.

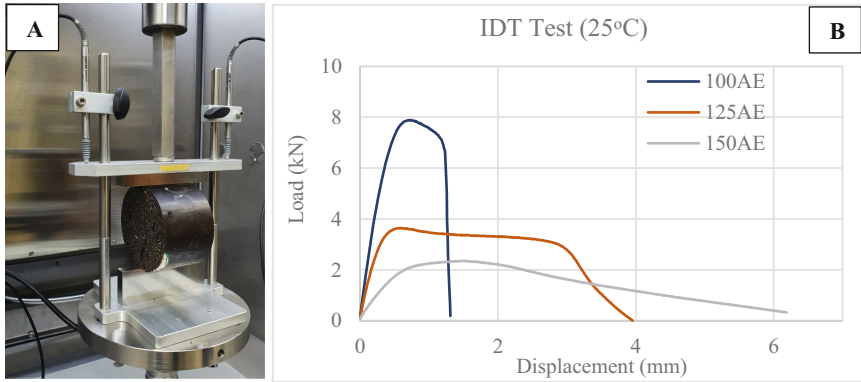


Fig. 4. ITD test apparatus (a) and IDT Test results (b).

Table 3. Summary of CT index test results

Condition	Work of fracture (kN/mm)	m75 slope	CT Index
100AE	22.15	53.00	1.90
125AE	900.37	2.00	18.20
150AE	2728.85	0.60	49.98

m75 slope: slope at 75% Post peak load point (PPL).

3.1.3 SEM Test Results

The SEM results indicate that mixture with high asphalt emulsion content exhibited poor connection between cement hydration product and asphalt membrane (Fig. 5a). This may be attributed to the coalescence phenomenon of high asphalt droplets volume, creating a dense asphalt layer that prohibits the formation of cement ettringite. Meanwhile, mix AE100 receive a homogenous distribution of the asphalt layer among cement particle with obvious ettringite structure development (Fig. 5b). The dense structure shows the good merging between the asphalt membrane and the cement hydration product. This strong bonding may lead to the good stress-bearing ability of CAM structure, as found in the dynamic and IDT test results. Interestingly, the SEM results also suggest that the cement ettringite can develop through the thick asphalt membrane covering.

3.2 Full-Scale Testbed

The plastic displacement of the controlled track and CAM stabilized track is illustrated in Fig. 6. Under the first 1000 cycles, the two sections displayed a very fast settlement

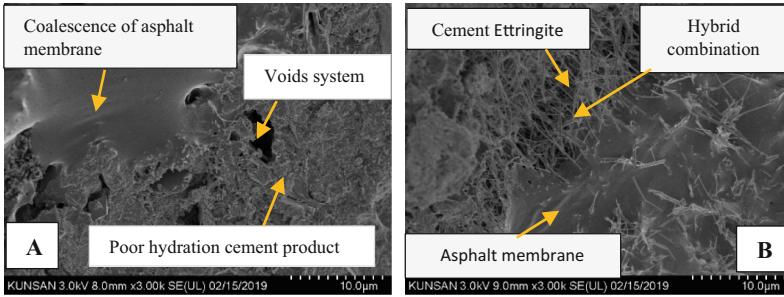


Fig. 5. SEM test results.

from 0 to approximately 2 mm. In the following 390,000 cyclic dynamic loads, both track-bed zones showed a gradual increment in settlement value. However, the treated section (Fig. 6b) remained stable after 300,000 repeated loads, while the normal section (Fig. 6a) has a tendency to increase with time. The CAM stabilizing method help improve the rutting resistance of the track system, contributing to the greater track stiffness. For instance, the maximum plastic displacement recorded in the stabilized zone is around 3 mm while this value of the controlled section is up to 5mm. Therefore, the actual performance of CAM is very promising for actual application in practice.

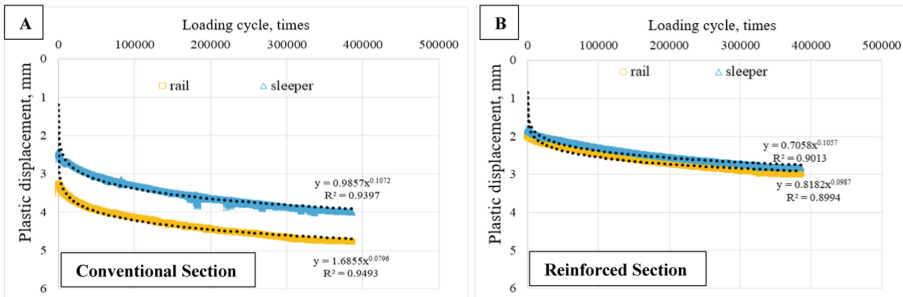


Fig. 6. Plastic deformation of full-scale track-bed.

After 400,000 times of dynamic load test with a load speed of 165 kN and a load speed of 6 Hz, the earth pressure of the CAM layer remained stable with a value of around 70 kPa (Fig. 7). This is attributed to the strong connection between ballast particles by CAM, which ensures the stress transferring during the service life of the ballasted track system. Meanwhile, the average earth pressure of the conventional layer reduced significantly after applying dynamic loads. This dynamic load created the holes and separating of underlined ballast particles (Fig. 8). This issue leads to a reduction in the stress transferring ability of the track system.

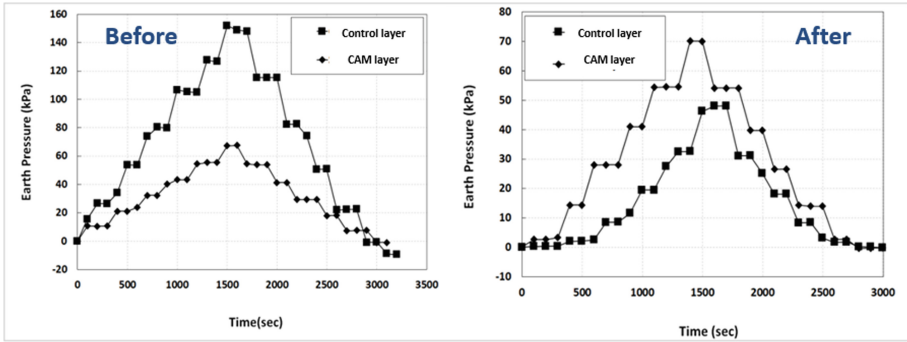


Fig. 7. Full-scale testbed results.



Fig. 8. The holes and separating of underlined ballast particles.

3.3 Life Cycle Cost Analysis

The cost-effectiveness is one of the most important factors which lead to the potential application of CAM in railway project. Hence, the life cycle cost is applied in this research to evaluate the profit provided by this ballast stabilization method. The full-scale testbed results (permanent deformation, pressure) were incorporated in a 60 years performance of a 1 km railway to cope with this objective. Based on the Microsoft Excel, Real Cost 2.5 Program [11], and Visual Basic for application code, the economic efficiency (net present value) was calculated by the below equation:

$$NPV = \sum_{k=0}^N (\text{Agency} + \text{Operationcost})_k \frac{1}{(1+i)^k} \quad (2)$$

where:

- Agency costs that refer to the construction, maintenance, and reconstruction.
- Operation costs cover to the cost of delays in the pavement service caused by maintenance and reconstruction.

- i , is the discount rate.
- estimated for year k , $N = 10$ is the number of years.
- In this analysis, the discount rate is selected at 3.5% [10]
- Based on Korean Railway Institute, the average operation cost of \$90000 per train-hour is used for this life cycle cost analysis [10].

Table 4. Agency cost for a single operation [10].

Solution	Agency cost for 1 km (\$)	
New construction	KRW	489500
Tamping fouled ballast	KRW	89000
Stabilizing ballast by Cement Asphalt Mortar	KRW	189570

Overall, due to the better rutting resistance property of the CAM section, the reinforced railway track-bed requires lower rehabilitation efforts and long-terms operation costs (Fig. 9). Also, the stabilized section having stronger durability offers lower reconstruction times throughout 60 years of operation. The life cycle cost analysis indicates that the total cost of the conventional railway can be saved up to 60% when using the new CAM stabilizing technique. Besides, it should be noted that the cost analysis is conducted based on the simplified input data, and this may be varied between projects.

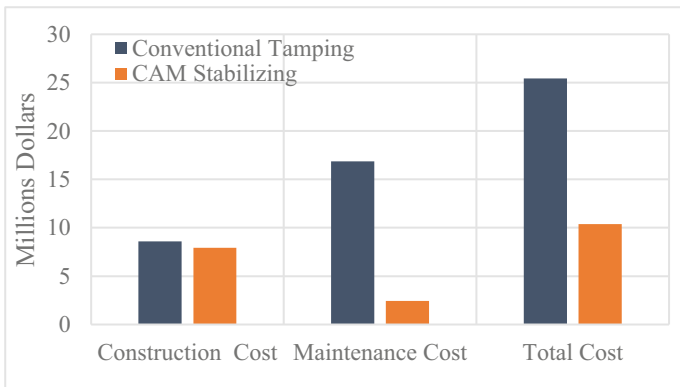


Fig. 9. 60 years of life cycle cost analysis.

4 Conclusion

This research aims to develop a new material having the novel characteristic of both cement and asphalt mortar to stabilize the fouled ballast of railway structure. Various asphalt emulsion/cement ratios are designed in this study to evaluate its dynamic

response and cracking resistance. The test results suggested that cement content has a strong contribution to the dynamic modulus of cement asphalt mortar. The dynamic modulus of higher cement content CAM mixture remains the proper value under the high-temperature impact, meanwhile, the high asphalt emulsion samples show a significant drop in dynamic modulus value. However, the CT_{index} reveals that mixture with greater asphalt emulsion content received better CT value, indicating a better cracking resistance. It is reasonable since the viscous elastic property of this condition dominates the brittle trait of cement hydration products. Regards to the SEM analysis, it should be noted that the thick formation of asphalt membrane may interrupt the development of cement ettringite, especially in a mixture having superior asphalt emulsion level. The full-scale testbed confirmed that the incorporation of cement asphalt mortar in the ballast track-bed would reinforce the rutting resistance and the whole track structure system, promoting a potential rehabilitation and maintenance solution for fouled ballast track.

Acknowledgment. This research was supported by a grant (18RDRP-B076564–05) from the Regional Development Research Program funded by the Ministry of Land, Infrastructure, and Transport of the Korean government, and also partially supported by a grant from R&D program of the Korea Railroad Research Institute, Korea.

References

1. Selig, E.T., Waters, J.M.: Track Geotechnology and Substructure Management. T. Telford (1994)
2. Brown, S.F., Kwan, J., Thom, N.H.: Identifying the key parameters that influence geogrid reinforcement of railway ballast. *Geotext. Geomembr.* **25**(6), 326–335 (2007)
3. D'Angelo, G., Thom, N., Presti, D.L.: Bitumen stabilized ballast: a potential solution for railway track-bed. *Constr. Build. Mater.* **125**, 118–126 (2016)
4. Le, T.H.M., Park, D.W., Seo, J.W.: Evaluation on the mechanical properties of cement asphalt mortar with quick hardening admixture for railway maintenance. *Constr. Build. Mater.* **206**, 375–384 (2019)
5. Ouyang, J., Tan, Y., Li, H.: Factors influencing rheological properties of fresh cement asphalt emulsion paste. *Constr. Build. Mater.* **68**, 611–617 (2014)
6. Le, T.H.M., Lee, S.H., Park, D.W.: Evaluation on full-scale testbed performance of cement asphalt mortar for ballasted track stabilization. *Constr. Build. Mater.* **254**, 119249 (2020)
7. KS M 2203. 2018. Emulsified Asphalt
8. AASHTO-T342–11. 2019 Standard Method of Test for Determining Dynamic Modulus of Hot-Mix Asphalt Concrete Mixtures
9. Zhou, F., Im, S., Sun, L., Scullion, T.: Development of an IDEAL cracking test for asphalt mix design and QC/QA. *Road Mater. Pavement Des.* **18**, 405–427 (2017)
10. Korean Railroad Research Institute. <https://www.krri.re.kr/html/en/>. Accessed Aug 2020
11. Life Cycle Cost Analysis (LCCA)
12. <https://www.fhwa.dot.gov/infrastructure/asstmgmt/lccasoft.cfm>. Accessed Aug 2020

Author Index

B

Bairgi, Biswajit, 89

C

Chakravarty, Hillol, 110

Chandak, Piyush G., 25

D

Dafalla, Muawia, 140

Darzins, Tom, 67

Das, Subrata, 110

Du, Wenbo, 150

G

Gallage, Chaminda, 166, 176

Garg, Ankit, 118

Ghani, Abdul Naser Abdul, 140

GuhaRay, Anasua, 118

H

Hossain, Zahid, 89

J

Jayalath, C. P. G., 176

K

Kadam, Digvijay, 1

Kumar, Pramanand, 110

L

Le, Tri Ho Minh, 187

Lee, Jeffry, 166

Lee, Seong-Hyeok, 187

Liu, Jinyan, 78

M

Mao, Boyu, 150

Michael, Bißmann, 41

O

O'Rear, Edgar, 89

P

Park, Dae-Wook, 187

Patil, Nagendra, 1

Patil, Nanasaheb E., 25

Patil, Omkar D., 25

Patil, Ravindra P., 1, 25

Q

Qiu, Hangyu, 67

S

Sayyed, Sabir S., 1

Seo, Jung-Woo, 187

Shaker, Abdullah, 140

Shan, Zhigang, 150

Shelar, Ajay, 1

Shen, Kanmin, 150

Shi, Jinjin, 78

Sinha, Sanjeev, 110

Syed, Mazhar, 118

T

Tapase, Anand B., [1](#), [25](#)

W

Wang, Kuanjun, [150](#)

Wang, Mingyuan, [150](#)

Wimalasena, Kasun, [166](#)

Wu, Yingbiao, [78](#)

X

Xue, Jianfeng, [67](#), [166](#)

Z

Zaman, Musharraf, [89](#)

Zhang, Yu, [78](#)